A SEARCH FOR TRANSITING EXTRASOLAR PLANETS IN THE OPEN CLUSTER NGC 4755

by

Bandupriya S. Jayawardene

A thesis submitted in satisfaction of

the requirements for the degree of

Doctor of Astronomy

in the Faculty of Science, Technology and Engineering

June 2015

James Cook University

JAMES COOK UNIVERSITY
AUSTRALIA

Townsville - Australia

STATEMENT OF ACCESS

I the undersigned, author of this work, understand that James Cook University will make this thesis available for use within the University Library and, via the Australian Digital Thesis network, for use elsewhere.

I understand that, as an unpublished work, a thesis has significant protection under the Copyright Act and; I do not wish to place any further restriction on access to this work.

STATEMENT OF SOURCES

DECLARATION

I declare that this thesis is my own work and has not been submitted in any form for another degree or diploma at any University or other institution of tertiary education. Information derived from the published or unpublished work of others has been acknowledged in the text and list of references is given.

Signature Date

ACKNOWLEDGMENTS

There are number of people without whom I would not have been able to achieve my childhood dream of studying astronomy, and I would like to thank them here.

Firstly, I would like to thank Dr Graeme White, who willingly gave the opportunity to me to work for a Doctorate of Astronomy in my spare time. This work would not have been possible without the guidance of my supervisor from mid-2006, Dr David Blank for sparing a great deal of time answering my questions and acquiring NGC 4755 data.

I would like to thank A. Prof. Andrew Walsh, Professor Ian Whittingham, Alex Hons, Dr Wayne Orchiston of JCU and other JCU staff for their support and encouragement for finishing this thesis.

I do not forget to thank the members involved in REST, who have given me the hard-earned sky data, and Arie Verveer and James Biggs of Perth Observatory for giving me sky data of open cluster NGC 4755.

This publication makes use of data products from the Two Micron All Sky Survey, which is a joint project of the University of Massachusetts and the Infrared Processing and Analysis Centre/California Institute of Technology, funded by the National Aeronautics and Space Administration and the National Science Foundation. This search has made use of the SIMBAD database, at CDS, Strasbourg, France and Kepler database of NASA.

Finally, I thank my family, D, I and Y, who have perhaps unintentionally, conspired to make my life interesting.

ABSTRACT

The search for ESP (extra-solar planets) has become a very popular astronomical research activity since the first discovery of ESP in 1995. Although, there are many ways of finding these exotic bodies, the transit method has become a widely used method; even amateurs have their opportunity to become planet hunters. This requires high precision time-series photometry and light curve analysis of large numbers of stars. When a planet transits, its radii ratio with the primary star can be determined accurately. Thus, combining this ratio with radial velocity data, the mass and radius of the planet can be realized, assuming the primary star's radius is known. The information gained from the transiting planets makes it possible to unravel the structure and composition of ESPs, understand the formation and the evolution process, and find the physical properties of the planet.

The detection of a weak, short, periodic transit signal in noisy light curves is a challenging task. As large numbers of light curves are to be analyzed, automation and an optimization of the search and analysis process is a necessity. The fluxes of stars on CCD (Charge Coupled Device) images are measured and the de-trended flux is used to draw the light curve. Normally, the search is done by a ground based detection system; hence the light curve is contaminated with noise components coming from atmospheric variations and systematic errors. To obtain high precision data without atmospheric noise, space based CCD cameras are already active.

Based on the above transit theory, this search was first done by using REST (Really Embarrassing Small Telescope) at JCU for field stars in the solar neighbourhood, GL 581, HD 13445 and HD 27894. The CCD images of the stars were subjected to CCD data reduction, pre-processing, differential photometry and analyzing by transit identification algorithms. Differential photometry, the ratio of the target star flux and reference star flux was used to nearly nullify the atmospheric variations.

The target open cluster for the main search is NGC 4755, which is widely known as the Jewel Box, in the constellation of the Southern Cross. The Perth Automatic Telescope, which can be remotely controlled, was used to obtain the data for the open cluster. 176 cluster stars brighter than 14th magnitude with published 'B' and 'V' magnitudes and another 994 faint stars in the

cluster frame have been analyzed. Several analytical signal-processing methods have been used to process the light curve to get the best light signal, having a SD (Standard Deviation) less than 5 milli-magnitudes. Later, fast wavelet transform was used to remove high frequency noise components and to produce an approximate signal which shows the long-term trend of the light curve and contain a possible transit. While no planetary transits have been identified in this cluster before, the ability to get light curves with standard deviation less than 5 milli-magnitudes is a significant achievement. The approximated light curves (using wavelets) are almost flat indicating that there are no signals with cycle time of 90 minutes or more.

The PSD (Power Spectral Density) of the light curve gives the frequency components associated with the curve. As there is a limitation of using this FFT based method, the Lomb-Scargle method was used to generate PSD.

This data was compared with 2MASS data to find closer brown dwarfs and a dozen possible candidates were found.

Variable stars in the cluster can also be studied with the light curve of stars. As there are at least 19 known variable stars in the NGC 4755; this is an opportunity to study the known variable stars in the cluster as well as to discover additional ones.

Table of Contents

Table of Figures

Table of Tables

Chapter 1

Introduction

The search of planets outside the solar system has become one of the most interesting topics in astronomy since 1995 as the first planet was discovered orbiting a main-sequence star (Mayor et al, 1995). However, the first exoplanet discovery was made by Aleksander Wolszczan in 1992 (Wolszczan et al 1992), around pulsar PSR 1257. As it is obvious that there is no other Earth-like advanced life in planets around the Sun, the quest of finding extra-terrestrial life has expanded beyond our solar system. Since our Sun, an average yellow star has a planet, which harbours life; there must be life somewhere in the other billions of stellar systems. Finding these ESP (Extra Solar Planets) is the first step of finding extra-terrestrial life. As the distances to these stellar bodies are beyond current capacity for direct viewing except for the cases of few giant planets, indirect search methods have become the popular way of identifying the existence of ESPs. For the first time in history, humans are now in a position to identify other habitable worlds at far distances.

The first detection of an ESP orbiting a main-sequence star was found by the radial velocity (to be explained later) method by Mayor et al (1995). Though there were disputes, confirmation came within 12 days from Marcy and Butler (Marcy and Butler, 1995). This discovery of 51 Peg b, a Jupiter sized planet in a 4.2 day orbit, showed that ESPs indeed exist and prompted more ESP searches. Following this, theoretical models of Jovian-mass planets were built up. These models predicted that Jupiter-mass planets orbiting close to their primary star would be significantly larger than Jupiter (e.g.: Seager et al, 2007). These other planetary systems can have a structure that is completely different to that of the solar system.

Many ESPs discovered are orbiting stars of multiple star systems. Most of them are binary systems with a separation of a few hundred AUs (Astronomical Units). However, in few cases, this separation is about 10 AU. In 2005, Konacki et al (2005) claimed that planets exist in tight triple star system (HD 188753a). In 2007, a team at the Geneva Observatory (Eggenburger et al, 2007) challenged that they couldn't detect that planet though they had the required precision and sampling rate sufficient to have detected the planet. Konacki replied that the precision of the follow-up measurements was not adequate and he was planning to release an update in 2007. Apparently, no update appears to have been published yet.

The ESP lists are available at J. Schneider's Extra-solar Planet Encyclopedia[1] (The California and Carnegie Planet Search Almanac[2] and International Astronomical Union working group on ESPs[3]. The number of confirmed ESPs continue to grow past 1918 (as on 29th April 2015), and majority of them were first identified as transiting planets. The transit photometric method is one that has proved to be very useful for finding ESPs and it is the primary scope of this thesis. As on 29th April 2015, more than 1200 planets have been confirmed as transiting (Interactive Extra-solar Planets Catalog[4]). On July 12, 2012 NASA published the first ESPs in an open cluster; Pr0201 b and Pr0211 b in Beehive open cluster which is about 175 light years away.

The transit method for detecting ESPs was first proposed by Otto Struve (1952), who anticipated the discovery of Jupiter mass planets at orbital distances as small as 0.02 AU and he also proposed to search for these objects with high-precision radial velocity measurements. This former possibility was further developed by Rosenblatt in 1971 (Rosenblatt, 1971) and later by Borucki and Summers in 1984 (Borucki and Summers, 1984). The discovery of transits from the ESP HD 209458b (Charbonneau et al, 2000), already known from radial velocity work, proved that Earth based transit planet detection is possible. The first ESPs discovered by the transit method were from the OGLE project in 2002 (Udalaski et al, 2002). The detection of TRES-1 (Alonso et al, 2004) was the first of an ESP around bright stars from a wide field star survey.

Most of these transiting ESPs have been found by wide field transit surveys, such as TRES, Super WASP (Lister et al, 2007) and HAT (Bakos et al, 2007); nearly all of them are focused on detecting Jupiter sized planets. Most of these wide field surveys use instruments with apertures smaller than 20 cm. Some searches use a more targeted approach and monitor stars with high metallicity content.

Although ESP searches are mainly conducted by ground-based telescopes, some space based transit search missions have been launched and have been successful in finding ESPs e.g. COROT (Deleuil et al, 2008) and Kepler (Borucki et al, 2011). These two missions have already

[1] http://www.obspm.fr/encycl/encycl.html
[2] http://exoplanet.org
[3] http://www.dtm.ciw.edu/boss/IAU/div3/wgesp/planets.shtml
[4] http://exoplanet.eu/catalog.php

contributed by finding many dozens of ESPs. As on April 2015, Kepler has discovered over 1000 confirmed planets, while COROT has discovered 29 planets (Cabrera et al, 2015). Although COROT is currently de-functioning due to a computer break down, the Kepler mission was approved for an extension through to 2016, i.e. four more years. As on April 2015, Kepler has over 3000 unconfirmed planetary candidates.

1.1 What is an extra-solar planet?

The historical definition of planets applies to the known ‘wandering stars’ Mercury, Venus, Mars, Jupiter and Saturn. The discoveries of the large bodies of Uranus and Neptune, controversial Pluto with similar sized Plutoids and large number of smaller bodies in the Kuiper belt region demonstrates that there is need of a clear definition for the term ‘planet’.

There may be variety of objects outside the solar system that share characteristics with solar system planets but may differ in important ways. Hence a planet is defined as an object which fulfills following criteria (Cassen et al, 2006):

- A planet is an object in orbit around a star or a multiple star system. This excludes free-floating planet-mass objects.
- A planet is not in an orbit around another planet. This excludes moons.
- A planet has a minimum mass of 10^{22}kg. This value is arbitrary; this value separates Pluto from the minor bodies of the solar system but it distinguishes planets from planetesimals, asteroids, and comets.
- A planet has a maximum mass of $10M_{Ju}$, adopting the definition of Working Group of ESPs of International Astronomical Union (IAU). This sets the boundary between planets and brown dwarfs. The value of $10M_{Ju}$ has been chosen to roughly coincide with Deuterium burning minimum mass limit (Chabrier et al, 2009). Size is not a good way to discriminate since a celestial body having a radius similar to that of Jupiter could be a Jupiter like planet (with mass M_{Jup}) up to a M-dwarf (~ 80 M_{Jup}).

The ESPs found at the beginning were Jupiter sized and many orbit very close (less than Sun-Mercury distance) to the parent star, they are thus subject to extreme hot conditions and are called hot Jupiters. Due to this proximity, the orbital period of these ESPs are very short relative to that of the Earth.

1.1.1 Classification of Extra-Solar Giant planets

Planets can be classified according to their temperature and their albedo, the measurement of the reflection of radiation. The atmospheric chemistry and stratification have a dramatic influence on the wavelength dependent albedo of giant planets and therefore on their detectability in reflected light (Cassen et al, 2006). Cloud-free atmospheres are quite dark at wavelengths longer than 0.6 μm, but water clouds and other condensates can be very reflective.

Sudarsky et al (2000) defined five different classes of planets based on temperature:

Class I: "Jovian" planets,

At T_{eff} <150 K, the albedo spectrum is determined mainly by reflection from condensed NH_3, and absorption from molecular CH_4. At longer wavelengths, the molecular absorption cross sections tend to become larger, which leads to an increased probability of absorption above the cloud deck, and therefore a lower albedo.

Class II: "Water cloud" planets,

At $T_{eff} \approx 250$ K, very strongly reflective H_2O clouds develop in the upper atmosphere. These clouds form higher than NH_3 clouds. The albedo of class II is higher than that of class I.

Class III: "Clear" planets,

At 350 K $\leq T_{eff} \leq$ 900 K, the atmosphere is free of condensates. Albedo is determined by atomic and molecular absorption and Rayleigh scattering. The photons can penetrate to depths where sodium and potassium absorption is done.

Class IV: "Roasters",

At 900 K $\leq T_{eff} \leq$ 1500 K these temperatures are expected in planets with small orbital radii. Silicate clouds deep in the atmosphere can exist. Hence these ESPs are very dark in the visible spectrum and IR spectrum.

Class V: "Hot roasters",

At T_{eff} > 1500 silicate clouds can exist very high in the atmosphere. This means these ESPs have a much higher albedo than those of class IV.

1.2 Formation of gas giant planets

There are two main distinct modes by which giant planet formation may occur, core-accretion and gravitational collapse. Planetary migration happens after their formation.

1.2.1 Formation by core-accretion

This method is based on planetesimal growth in a proto-planetary disk. As a planetesimal grows, it is capable of retaining an increasing mass of gas in its atmosphere. In fact, upon reaching a critical mass, it can induce the collapse of all the gas available in its neighbourhood, limited only by finite reservoir, or by dynamical effects associated with rotation. The planetesimal becomes the core of a gas giant planet. This mechanism is frequently called the "core instability" model. This process can last about 10^7 years, the lifetime of proto-stellar disk (Cassen et al, 2006).

Pollack et al (1996) have constructed quantitative models of the formation of Jupiter and Saturn based on this core accretion model. This model is "tuned" to achieve the maximum core mass allowed by the data, so the planet can be formed within the lifetime of the nebula.

The mass of the solid core of the Jupiter is uncertain, it could be large as $15M_e$, (Gulliot et al, 1997) but data constraining its size also permit models with no core. The question occurs, "Can a core of $15M_e$ at the Sun-Jupiter distance grow before the gas of the proto-planetary disk has disappeared?". The Pollack et al (1996) models show that Jupiter and Saturn could form massive gaseous envelopes on timescales similar to the lifetime of the solar nebula. But the time needed to Uranus and Neptune is longer than the time of the solar nebula, thus these two planets are unable to accrete a substantial envelope.

1.2.2 Gravitational collapse

This method is based on direct gravitational collapse of gas and dust together, the mechanism is fast and efficient taking only several orbital periods to isolate the planetary mass. Furthermore, it does not prevent the formation of terrestrial planets from planetesimals. Gravitational instability is unlikely to form planets of 1 M_{Jup} or less and cannot account for close-in giant planets without invoking orbital migration. Gravitational instabilities in the dust component of a disk may also play a significant role in the initial formation of the planetesimal. This process and the problems are described in Boss (2000).

1.2.3 Planet migration

Planetary migration is the most likely explanation for ESPs with orbits of only a few days. Migration occurs when a planet or other stellar object interacts with the proto-planetary disk or planetesimals, the torque from the inner and outer parts of the disk cause the size of the planet's orbit to change. In most cases, the orbital migration due to the gas disk is believed to occur towards the central star and thus is frequently used to explain the existence of hot Jupiters.

Types of planet migration (Based on Goldreich and Tremaine, 1979 and Lin and Papaloloizou, 1979)

- Type I migration

  Terrestrial mass planets cause spiral density waves in the surrounding gas or planetesimal disk which create an imbalance in the strength of the interaction with the spirals inside and outside the planet's orbit. In most cases, the outer wave exerts a greater torque on the planet than the interior wave. This causes the planet to lose angular momentum and the planet then migrates inwards. This is typical when the planet in not massive enough to clear a gap around itself.

- Type II migration

  Planets of masses more than about 10 Earth masses clear a gap in the disk, stopping type I planet migration. However, material still continues to enter the gap of the larger accretion disk, moving the planet and gap inwards. This is presumably how the hot Jupiters form. This process is slower than the type I migration.

- Gravitational scattering

  The gravitational scattering by larger planets moves planets over large orbital radii.

Results of Trilling et al (1998) show those planets with initial mass less than 3.36 Jupiter masses migrate towards the star. His simulation results show that planets with initial masses around 3.36 -3.41 Jupiter masses migrate to distances at which they lose mass to the star, but are saved by the disappearance of the disk.

1.3 General Properties of known ESP systems

The discovery of very first ESP 51Pegb has opened a new field of observational astrophysics: the systematic study of planetary systems, their dynamical properties, formation and evolution. Unexpected discoveries have stimulated new theoretical developments (Cassen et al, 2006). These discoveries showed that our solar system is not unique, but other planetary systems can be quite different. The existence of hot Jupiters cannot be explained by the standard theory of the formation of our Solar system.

There are many ESPs whose size resembles Earth i.e. having masses ranging between Earth and Neptune (Known as super Earth). On April 17, 2014, a Kepler Mission[5] announced the discovery of Kepler 186f, the first nearly earth size ESP candidate orbiting a red dwarf in the star's habitable zone and possibly a good candidate to host alien life. In April 2013, NASA announced the discovery of three new Earth-like ESPs: Kepler-62e, Kepler-62f, and Kepler-69c, in the habitable zones of their respective host stars. These new ESPs are considered prime candidates for possessing liquid water and thus potentially life. Before that, there are only few known super Earths Kepler 69c, GJ 1214b, 55 Cnce and HD 97658b. Fressin et al (2013) suggest that Kepler survey indicates super Earths are more common than previously anticipated.

1.3.1 Properties of the planets

The systems so far found are hot Jupiter systems: Some giant (or several) planets orbit the star. As on 29th April 2015, there are known 1211 planetary systems[6]. The lowest mass planet known is PSR 1257 12b with a mass about $7*10^{-5}$ M_J [7] which is less than four Earth masses. Although the expected masses of ESPs are on the scale of Jupiter mass, there are many ESP's having a mass between a super Earth (a planet which is heavier than the Earth and having a mass less than ten Earth masses) and Jupiter. Orbital characteristics of these planets are measured by the radial velocity method (described in section 1.4.2). Giant planets have mostly been detected due to the sensitivity of the radial velocity method. In most cases the eccentricity of hot Jupiters (tidally relaxed) are zero[8], indicating that they have circular orbits and their planets have periods on the scale of a few days.

[5] http://kepler.nasa.gov
[6] http://exoplanet.eu/catalog.php
[7] http://exoplanet.eu/catalog.php
[8] http://exoplanet.eu/catalog.php

Several spectroscopic studies attempted to analyze atmospheric environments of transiting planets. The study of HD 209458b during a transit shows neutral sodium absorption (Fortney et al, 2003). Absorption due to hydrogen, oxygen and carbon are found in this planet. As the mass and the radius of some planets are known, the average density and the state (Gaseous/Solid) of the planet are known. Some ESPs also show different behaviour: e.g. evaporating exosphere (Vidal-Madjar et al, 2004).

1.3.2 Properties of the parent stars

The stars harboring hot Jupiters are more metal-rich on average than the stars without planets. Thus, the probability of finding a giant planet increases with metallicity ([Fe/H]) (Valenti and Fischer, 2005) though there are some cases where metal poor M-dwarfs have giant planets. This high metallicity is believed to be a property of the proto-stellar cloud from which the stellar system originated. Santos et al (2003) find no significant correlation between host star metallicity and orbital parameters, but they found a tendency for the host star of short period planets to have a higher metallicity than the host star of longer period planets. They also point out that although there is an apparent lack of massive planets around metal poor stars, it is not statistically significant. It can be expected that up to 25 - 30% of the more metal-rich stars ([Fe/H]> 0.2 - 0.3) host a close-in giant planet (Da Silva et al, 2006).

There is little known about the relative frequencies of planets in various new stellar environments. Even today, transit searches on open clusters have not been very successful. However there was success for the constellation Hyades, The ESP host star, Iota Horologii has been proposed as an escaped member of the primordial Hyades Cluster (Vauclair et al, 2008).

1.3.3 Planets in multiple systems

At least 467 multi planetary systems[9] have been found, including at least eight systems with three planets, two with four planets, one with five planets and one with seven planets. Some systems are locked in orbital resonance (Cassen et al, 2006). The two giant planets of star GJ 876 are not only locked into a 2:1 ratio, their axes appear to be nearly aligned. The three planets in υ Andromeda have apsidal lock (Marcy et al, 2001). Resonances may be common in these planetary systems. Kepler search has already detected three ESP candidates with radii smaller than that of the Earth in a single system (Muirhead et al. 2012).

[9] http://exoplanet.eu/catalog.php

There are at least 18 planets having more than one stellar companion and one planet is a member of a triple system. 55Cancri b is the first planet known to be orbiting a double star system. The ESP 6 Cyg b is orbiting a triple system (Chochran and Hatzes, 1997). This indicates planets can survive in multiple stellar systems, with binary separation of about 20 AU. This evolution method must be very different to other systems as gas giants orbiting very close to the parent star(s) while parent stars orbiting each other closely experiencing a gravitational pull from each star. In October 2013, Schmitt et al 2013, announce that Kepler search has found a seven planet candidate KOI 351.

1.4 Extra-solar planet search methods

1.4.1 Direct imaging

As the name suggests, this is the most obvious method of finding ESPs, via the radiation they emit or reflect, by taking high-resolution image of the host star and its immediate surroundings. Given the distance to the star and the faintness of the planet, this method is an extremely difficult method. However, it can be utilized in space-based observations where atmospheric influences are minimal, or by using adaptive optics which reduce the effect of seeing. Direct images can also been taken by using destructive interference nulling, the combining of beams from multiple telescopes to cancel out the light of the target by destructive interference. This search can be done at infra-red wavelengths, where thermal emission from the planet may reduce the planet to star brightness ratio.

Planets can be imaged in two ways. The first way is using the visible starlight reflected by the planet from its parent star, which depends on a planet's albedo, its size and distance from the parent star. This is mainly applicable to the giant planets, and the reflected light from the planet is measured as it follows the orbit. The other way is to detect the thermal radiation that the planet itself emits in the infrared, which includes internal heat generated by its contraction under gravity and the decay of radioactive elements, and re-radiation of starlight. The biggest difficulty is the large contrast between the planet and the parent star at a very small angular separation (Cassen et al, 2006). Many planets are strong infrared sources. In our solar system, the outer planets Jupiter to Neptune actually emit more radiation than they absorb from the sun (Smith, 1995).

In July 2004, a group of astronomers used the European Southern Observatory's Very Large Telescope array in Chile to produce an image of planet 2M1207b, a companion to the dwarf 2M1207 (Chauvin et al, 2004). The planet is believed to be several times more massive than Jupiter and to have an orbital radius greater than 40 AU.

The first multi-planet system, announced in November 2008, was imaged in 2007 using telescopes at both Keck Observatory and Gemini Observatory. Three planets were directly observed orbiting star HR 8799, whose masses are approximately 10, 10 and 7 times that of Jupiter (Marios et al, 2008). In 2010 the fourth orbiting planet was found (Marios et al, 2010).

On November 2008, the discovery of an ESP Fomalhaut b was announced. This was the first ESP to be seen with visible light, captured by the Hubble Space Telescope. The mass of the planet is less than three times the mass of Jupiter and at least the mass of Neptune. There are some indications that the planet's orbit is not apsidally-aligned with the dust disk, which may indicate that additional planets may be responsible for the dust disk's structure (Kalas et al, 2008). Some recent observations find a very eccentric orbit ($e \sim 0.8$), indicating that Fomalhaut ‘b” cannot be the planet that is constraining the system's eccentric debris ring. This Fomalhaut “b” could be a transient dust cloud produced by a catastrophic collision between planetesimals in the disk (Lawler et al, 2015).

The difficulty of employing direct methods has given rise to several indirect methods, which rely on the gravitational effects of the orbiting ESPs on the star.

1.4.2 Radial velocity

The radial velocity or “Doppler Wobble” method, which has been the most successful method so far for the detection of ESPs, measures the periodic shifts of the spectral lines due to the star’s reflex motion. After obtaining a time series of high-resolution spectra of the target star, the spectra is searched for periodic variations of absorption lines due to the motion of the star around the centre of mass of the star-planet system. This method is most sensitive to high mass planets in close orbits around low mass stars. This yields orbital parameters of the planet as a function of orbital inclination, which is indeterminate, hence mass cannot be determined unambiguously. Since the target star must have a sufficient number of narrow absorption lines, the stellar photosphere must be sufficiently stable so radial velocity surveys have concentrated mostly on F, G and K main sequence stars (Cassen et al, 2006). For most of the existing telescopes, these radial velocity surveys are not able to search large numbers of stars fainter than V~8 magnitude.

1.4.3 Pulsar timing

The millisecond pulsars rotate very fast and are particularly very stable. The pulses arrive with a regularity which compares with the accuracy of the best atomic clocks. The detection of planets around such pulsars relies on the gravitationally induced wobble, to and away from the Earth. When the pulsar is at its furthest point from the Earth, the pulses have a slightly greater distance to travel, and arrive later than the average; when the pulsar is at its nearest point, they arrive slightly earlier. If the periodicity in the pulse arrival times is observed over a long period, the wobble can be measured. Since pulse arrival times can be measured very accurately and very small changes can be observed, this method so far has been a successful method of finding two planetary systems. The planets are the three planets of pulsar PSR B1257+12 (Wolszczan, 1994) and the planet around pulsar PSR B1620-26 in the globular cluster M4 (Arzoumanian et al, 1999).

1.4.4 Gravitational micro-lensing

This method measures the temporary magnification of a background star when a foreground planet passes in front of it and its gravitational potential bends the light emanating from the source. The monitoring of gravitational micro-lensing events is the only current method that is capable of detecting Earth-like planets from the ground unless the star is late M dwarf which, being a small star, means that a small planet can be found via the transit method (section 1.4.6). The drawback of this system is that the observations cannot be repeated. By 2009, a total of five ESPs have been detected in micro-lensing events, including OGLE 2003–BLG–235, OGLE-2005-BLG-071Lb, OGLE-2005-BLG-390Lb, OGLE-2005-BLG-169Lb, and two ESPs in OGLE-2006-BLG-109 (Bennet et al, 2009). By 2011 this increased to seven with two ESPs in MOA-2007-BLG-192Lb.

1.4.5 Astrometry

Although the stars seem fixed, they are orbiting the Galaxy, and gradually appear to move from their fixed positions in the constellations. If no planets are present, the star should appear to move linearly if oscillations about the galactic plane are neglected, but if the star does have a planetary system; it must show a "wobble". As the gravity of the star pulls on the planets and maintains them in their orbits, the gravity of the planets pulls on the star. Being far more massive, the star's attraction is easily the stronger, but the pair is orbiting a common centre of gravity. Thus, as the star itself orbits the Galaxy, its planets cause a noticeable wiggle in its motion. In astrometry, the size of the “wobble” is measured, which can give the orbital element and the mass without an ambiguity. This method is applicable to all types of stars, and more sensitive to planets with larger semi-orbital axis (Cassen et al, 2006). In 2009, VB 10b became the first planet discovered by this method (Pravado and Shaklan, 2009) though this planet was suspected to exist in 1983 (Harrington et al, 1983).

1.4.6 The transit method

The transit method is based on the observed decrease of luminosity from a star when a planet passes in front of it (Figure 1.1). Since planets are small compared to their parent star and emit no light of their own (note: Jupiter is about the same size as a late M-dwarf), such a phenomenon is not observed except when the planetary orbit is near or at edge-on as seen by the observer. As the planet crosses the star (Figure 1.1), it will block some of the light from the star, making it dimmer (brightness decreases) and then brighten again when the planets orbit carries it towards the far side of the star.

There are four named "contacts" during the transit - moments when the circumference of planet touches the circumference of the star at a single point (Price, 2000).

1. First contact (external ingress): Planet is entirely outside the disk of the star, moving inward
2. Second contact (internal ingress): Planet is entirely inside the disk of the star, moving further inward
3. Third contact (internal egress): Planet is entirely inside the disk of the star, moving outward
4. Fourth contact (external egress): Planet is entirely outside the disk of the sun, moving outward

A planetary transit is described by three parameters:

1. The period of the transit, which can be verified by the radial velocity method, if the star is sufficiently bright and the planet is sufficiently massive
2. The duration of the transit, including time of ingress and egress
3. The fractional change in brightness of the star

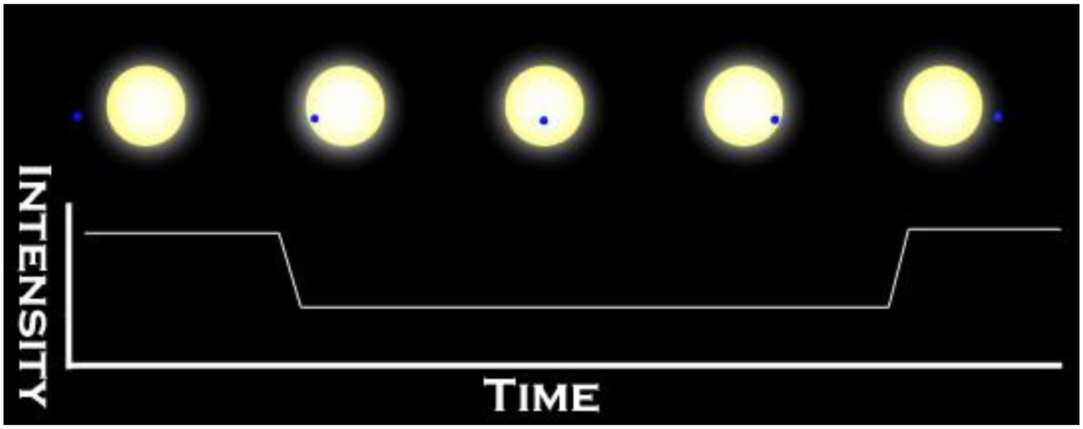

Figure 1.1 Transit method

(From ESP Project- **http://www.psi.edu/esp/process.html**)

For circular orbits, the duration of the transit reveals the orbital period while the flux decrement, ignoring the limb darkness, represents the size of the planet relative to the star. For a star with known mass and size, the maximum transit duration is constrained by the orbital period and the size of the parent star (Jenkins et al, 2002).

The physical relationships and laws describing transits are:

(a) Orbital period of the planet (P), which is given by the Kepler's third law:

The square of the orbital period of a planet is proportional to the cube of the semi-major axis of its orbit,

$$P^2 M_* = a^3 \qquad (1)$$

where 'a' is the semi-major axis of the orbit and M_* is the stellar mass in solar masses.

(b) The transit duration, τ_c (in seconds) of a planet on a circular orbit of radius 'a' (in meters) around a star of mass M*(in kg) and radius R* (in meters) is given by Loeb in 2009

$$\tau_c = 2\, R^*(1 - p^2)^{1/2} / (GM^*/a)^{1/2} \qquad (2)$$

where, p is the minimum separation between the planetary trajectory and the stellar disk centre on the sky, with same units as R*.

(c) The variation of the flux during a transit is given by (excluding limb darkening, a falloff in brightness of the disk of a star from the centre to the edge),

$$\text{Flux}_{\text{transit}}/\ \text{Flux}_{\text{before}} = 1 - R^2{}_p/R^2{}_s \qquad (3)$$

where R_p is the radius of the planet and R_s is the radius of the star.

The magnitude of the drop depends on the size of the parent star as well as the planet. The fractional drop is a simple ratio of the area of the star to the planet with the assumption that there is no limb darkening.

(d) The a priori probability that a planet transits its parent star as seen from the line of sight from Earth, $P_{transit}$ is given by,

$$P_{transit} = 0.0045\ (1_{AU}/a)\ (R_s/R_o)(1- e * \cos(\pi/2 - \omega))/(1-e^2) \qquad (4)$$

where 'a' is the semi-major axis, 'e' is the orbital eccentricity and ω is the argument of periastron reference to the plane of the sky (Seagroves et al, 2003).

(e) For circular orbits and solar sized stars, the following approximate relationships are valid. The transit probability, p_{tr} is given by (Barnes, 2007)

$$p_{tr} = (R_s/a) \qquad (5)$$

And the transit duty cycle T_d is given by

$$T_d = (R_s/\pi * a) \qquad (6)$$

Based on detecting analogues of 51Pegb, a hot Jupiter, the characteristics of the signal of a transit and the difficulty of transit method are: (1). The amplitude of the flux decrement $(R_p/R_s)^2$ in a transit is roughly equal to 0.01, implying that no planet is larger than 10% of the star. (2) Hot Jupiter type of transits can occur once per 3-7 day orbital period and last 2-4 hours (Charbonneau et al, 2007). Present systems can find Neptune sized planets and lower mass planets such as super Earths (planets are in size of the Earth or bigger) to late M-dwarfs.

The estimated value of the rate of occurrence of hot Jupiters for Sun like stars is about r = 0.0075 (depends on the metallicity of the star), and the likelihood of hot Jupiter system with a semi-major axis 'a' presenting a transiting inclination is $p \sim (R_s/a) \sim 0.1$ (for a uniform distribution of orbital inclinations). Assuming that complete transit coverage is achieved, the number of stars that must be examined to find one transiting hot Jupiter system is n = 1300/g, where 'g' is the fraction of stars examined that are "good" targets. If 'g' is 1%, statistically 130,000 stars have to be observed (for 2-4 hours) in order to find hot Jupiter-type ESPs (Charbonneau, 2003).

Photometric surveys for transiting ESP are well suited to find objects with periods of order less than 10 days but have difficulty detecting longer period transits due to the requirement of longer time-baselines and the possibility of not seeing the whole transit at any one location. The required maximum photometric sampling interval is determined by transit durations that generally last several hours. In order to be convincing, the photometric cadence must be sufficiently high for either the planetary ingress or egress (with each extended for approximately 1/6 of transit duration) to be well sampled. Poisson statistics indicates that the significance of a transit detection increases in proportion to $N^{1/2}$, where N is the number of independent photometric samples within the transit interval (Castellano et al, 2004). This result does not consider red noise which can be the dominant noise source.

The rings around exo-planets (exo-rings) would be the next breakthrough of research in exo-planets. Zuluaga et al (2015) introduces a novel approach of identifying exo-planetary rings by searching anomalous deviations in the residuals of a standard transit light curve fit.

A ground-based wide field photometric search for ESP transits represents an alternative and complements other search techniques. Transit-based detections favour the detection of giant planets in short-period orbits. With this method, planets orbiting stars of a wide range in spectral class (F and later type dwarfs) are detectable. For some systems, photometric information alone may be complicated by confusion between planets and white dwarfs or brown dwarfs. This problem may be eliminated if the mass is determined from the radial velocity data and is found to be compatible only with that of a planet (Howell, 2000).

There are different types of transit searches active. These types can be classified as: (As Charbonneau (2003) and Horne (2003))

- <u>Shallow, wide angle transit surveys</u>

  These are small aperture (~10cm) and wide-angle (~10˚) transit surveys targeting bright stars. The main challenge is to achieve 10^{-2} magnitude accuracy in differential photometry over wide field of view. If the accuracy is achieved, these surveys may find Jupiter sized planets around nearby bright main sequence stars of stellar types of F, G, K and M stars. STARE - STellar Astrophysics & Research in ESPs (Brown, 2000) and Vulcan (Borucki et al, 2001) projects are these shallow, wide-angle transit surveys. In recent times, some wide-transit projects like SuperWASP (Lister et al, 2007), TrEs (Alonso et al, 2004) and

HATNet (Kovacs, 2005) have been successful in finding transits. Another survey around is QES (Bryan et al, 2012).

- Intermediate galactic plane transits surveys

  Transit searches in the direction of the galactic disk at distances of 2-4 Kpc belong to this type. The galactic plane provides a high density of stars in the long narrow volume. E.g. OGLE III project (Udalski et al, 2002)

- Deep galactic plane surveys

  Low luminosity transit surveys targeting K and M stellar type stars in the direction of galactic plane using large telescopes with wide field CCD cameras belongs to this type. Project EXPLORE (Mallen-Ornelas et al, 2003) is one of these galactic plane surveys.

- Open cluster surveys

  These surveys need larger telescopes, and field stars usually dominate these surveys. This is discussed in more detail later since this is directly related to this thesis.

- Globular cluster transit surveys

  These surveys target the main sequence stars in the crowded core of globular clusters. The Hubble Space Telescope (HST) has the ability to resolve main sequence stars in the crowded cores of the closer globular clusters. Project SuperLupus on 47 Tucanae (Bayliss et al, 2008) is one currently active globular cluster survey.

- Special target transit surveys

  Some surveys target specific stars to enhance the chances of planet discovery. Project TEP, Transiting ESPs[10], targets low-mass eclipsing binaries and the transit search directs amateur observers to target stars with known planets. High-precision multi-band photometry is used to find transiting planets in young M1Ve debris disk star AU microscopii (Hebb et al, 2007). Project Mearth targets nearby M dwarf stars in search of new Earth-like exoplanets (Berta et al, 2013).

[10] http://www.iac.es/project/tep/tephome.html

1.4.6.1 Constraints in transit method

The principal challenge facing transit surveys is to attain adequate photometric precision in the face of spatially varying atmospheric extinction (dimming of light in its passage through the atmosphere) and instrumental effects. One needs efficient methods for rejecting the many false alarms that appear in the photometric light curves. These false alarm results are from eclipsing binary systems, small stars transiting large stars, and eclipsing binaries diluted by the light of a third star (Alonso et al, 2004). Some false alarms are due to second order refraction, absorption effects and blending of nearby stars due to the atmosphere. Stellar spots, pulsating stars and stellar flares may also cause false alarms. The resolution of the transit depth in the stellar light curve at data reduction state is a main factor for successful transit search. Other restrictions also come from intrinsically low transit probabilities and small transit duty cycles (Seagroves et al, 2003). Accuracy of the transit detection method is affected by interstellar scintillation caused by the clouds in interstellar space and this can be periodic and may affect the measured magnitude.

1.4.6.2 Sky coverage of transit search

In theory, planetary transits can be found in any direction in the sky. Analysis of 1918 ESPs already found (as at 29th April 2015), shows that the stars of spectral types F, G, and K and stars with super solar metallicity (property of having more relative metal content that the Sun) have a high probability of having hot Jupiter type planets, while type M stars are not known for having hot Jupiters (Bonfils et al, 2013). For a wide field search, the higher the density of the stars in the field, the closer the angular separation of stars which may blend stellar images, so that extra work is needed to identify the transit.

1.4.6.3 Factors which affects the visibility of a transit

There are many factors which determine the success of transit method; with the amount of sky noise present in the light curve governing the possibility of identifying the transit. The others are:

- Ratio of the size of the planet to the star - As the ratio increases, the probability of finding a transit gets higher.
- Stellar variability – This is the inherent noise of the star, which causes dips in the light curve on the time scale of a transit so the absence of variability is preferred.
- Brightness of the star – Too bright stars may saturate the CCDs, thus contaminating the flux of the neighboring stars.
- Photometric aperture – Too small aperture will increase the noise.

- Duration of the transit – Typical hot Jupiter transit is less than 4 hours and there is no optimum. If it takes too long, chances are higher that any transit will be missed.
- Instrument noise – The lower the noise the better the SNR.
- Detection efficiency – Measure of false alarm rate and SNR and depends on the identification method.

1.4.6.4 Science from transit searches

Once an ESP is found, there is other information that can be obtained from transit searches. Some examples of using transit results are:

- Derivation of planetary parameters

  Radius, mass and period allows calculation of average density of the planet and the internal structure state, and provides possible hints about the formation of the planet. A transit search allows direct determination of the planets radius relative to the parent star, orbital inclination and, provided more than one transit is observed, the orbital period (Aigrain et al, 2004). The period of the planet is confirmed by radial velocity (RV) data. A bright parent star allows highly accurate orbital parameters to be deduced from RV measurements (Bodenheimer et al, 2003). Unless RV data is present, it is impossible to say that a given transit is due to a giant planet, a brown dwarf, or a very low mass star.

  The resultant ESPs of the first three OGLE searches (detected by transit method and confirmed by RV data) had very low periods and low masses. Their density was markedly higher than that of less close in hot Jupiters found later in other surveys, and their predicted mass loss rates through evaporation up to four times higher than that of HD 209458b. The transiting ESPs TrEs-1 and OGLE-TR-111b have orbital characteristics more similar to the hot Jupiters discovered via the RV method and have been presented as the missing link between RV and transiting planets. Their derived radii are closer to those of the very close-in OGLE planets than transiting ESP HD 209458b. These lower radii imply higher densities and they may cause shallower transits and hence be harder to detect (Aigrain and Pont, 2007).

- Analysis of peculiarities of planets

Some planets are larger than expected. HD 209458b has estimated radius of $1.35R_{Jup}$ and a mass estimated to be 0.69 M_{Jup}. The mass is much less than expected while the size is 20% greater. This can happen only if the deep atmosphere is unrealistically hot (Charbonneau et al, 2006).

There are four possibilities have been suggested to explain the anomaly.

1. HD 209458b might be tidally heated through orbital circularization (Bodenheimer et al, 2003). The heating effect of the star does increase the predicted radius over that of an isolated planet but only by about 10%, not by 30-40% as observed for HD 209458b (Laughlin et al, 2004).
2. Strong insolation-driven weather patterns on the planet are envisioned to drive the conversion of kinetic energy into thermal energy at a pressure of tens of bars (Guillot et al, 2002). This theory predicts that other transiting planets with similar masses and at similar radiation levels should be similar in size to that of HD 209458b (Laughlin et al, 2004).
3. The effective radius of a hot Jupiter observed in a transit is significantly larger than the photosphere's radius reported by planet evolution codes. The large effective optical depth of the upper atmosphere viewed obliquely at the planetary limb causes a larger photometric depth than if the planet were simply an opaque sharp-edged sphere (Burrows et al, 2003).
4. According to the competing gravitational instability hypothesis these gas giant planets condense directly from spiral instabilities in proto-stellar disks on a dynamical timescale of $\tau < 10^3$ yrs. Solid particles of the newly formed planet can precipitate to form a core during the initial contacting phase. Only 1% of the matter in the planet is condensable, hence in a Jovian-mass planet a core, even if it does form, will be much less massive than in the core accretion scenario (Boss, 1998).

Some planets are smaller and heavier. The ESP in HD 149026 has estimated radius of $0.725R_{Jup}$ (Charbonneau et al, 2006) which is anomalously small for its mass and, if it is transiting, the derived mass M = 0.36 M_{Jup} is too high for a Jupiter type planet and it is a hot Saturn in size. Indeed, it has a large core. This type of planet is easier to form when a proto-planetary disk is metal rich. Indeed, the parent star HD 149026 is an inactive metal-rich solar type star. Another suggestion is that the planet may have migrated inward when it was less massive than present, and became stranded at the

2:1 resonance with the X-point of the proto-stellar disk (Shu et al, 1994). Some of the planetesimals would accrete on to the stranded planet, increasing its compositional fraction of heavy elements. An alternative theory suggests that this kind of planet can be formed through a giant impact scenario between two isolation-mass embryos (Winn et al, 2005).

1.4.6.5 Follow up observations of ESPs

Once a transiting planet is confirmed, possible follow up work includes:

- High precision photometry in other bands can exploit colour dependent limb darkening (a falloff in brightness of the disk of a star from the centre to the edge) of the star. Furthermore, it may be possible to observe colour-dependent variations in the observed planetary radius since the planet would appear slightly larger when observed at wavelengths where the atmosphere contains strong opacity sources (Brown and Charbonneau, 2000). The effect of limb darkening is wavelength dependent and its impact on the light curve can be significant because a model of the planet determines the orbital inclination and radius.
- If successful, observations of reflected light would yield the planetary albedo directly, especially at infrared wavelengths. Predicted values for the albedo are highly sensitive to the atmospheric chemistry and condensates (Brown and Charbonneau, 2000). This method has been used with the IR based Spitzer telescope (Burrows et al, 2008).
- Observations at wavelengths longer than a few microns may also detect the secondary eclipse as the planet passes behind the star, allowing measurement of the planet’s daytime temperature and quantifying the net energy deposition in the planetary atmosphere (Brown and Charbonneau, 2000). This has been done in infrared space missions, e.g. Spitzer. Using Spitzer in infrared (8µm), Deming et al (2007) found a transit and secondary eclipse of the hot Neptune ESP, GJ 436b. The nearly photon-limited precision of these data allow them to measure an improved radius for the planet, and to detect the secondary eclipse.
- By taking the ratio of high precision spectra in and out of transit, it is possible to see additional absorption features due to absorption of light passing through the limb of the atmosphere of the planet (Brown and Charbonneau, 2000). For HD 189733b, this has been done with the Spitzer telescope (Grillmair et al, 2008).

- Changing time intervals between successive transits can be an indication of other planets(s), giving the opportunity of finding low mass planets. If both planets transit then both mass and the radius can be determined and radial velocity measurements are not necessary (Holman et al, 2005). There is a possibility of finding other transiting planets, assuming approximately coplanar orbits (Brown and Charbonneau, 2000).
- If photometry processes can achieve 0.1 milli-mags, then it may be possible to detect planetary rings and/or large rocky satellites (Brown and Charbonneau, 2000).
- Using Spitzer telescope, Gillon et al. (2010, 2012) have ruled out transits for the super-Earth HD 40307b and characterize the properties of the transiting super-Earth 55 Cnce.

1.4.6.6 Transit search from space

Already, there are three small spacecrafts that have been sent to the orbit for transit observations, the Canadian MOST, French/ESA COROT and NASA Kepler. The first two were initially conceived with the primary objective of studying the internal structure of stars through astroseismology. With the discovery of hot Jupiters, observations of ESPs have therefore been added to their scientific goal. COROT had two different modes possible: a survey mode, which used a wide-field camera to search for new transiting planets, and a targeted mode to get detailed light curves of stars that were already known to host planets. COROT could monitor 6000 - 12000 stars in magnitude range of 11 to 16.5, if the orbital period is no longer more than 50 Earth days (Cassen et al, 2006). COROT was the first mission capable of detecting rocky super Earth type planets (1.7 to 4.8 Earth masses), which are several times larger than Earth, around nearby stars. It has a 30-centimetre space telescope.

COROT was launched in December 2006. It detected its first ESP, COROT-Exo-1b, in May 2007 (Deleuil et al, 2008). This planet is a hot Jupiter, orbiting a sun-like star 1,500 light years away. COROT found 29 transiting ESPs (Cabreara et al, 2015) and, in 2012, it suffered a major computer failure[11].

The Kepler satellite was launched in March, 2009, and it explored the structure and diversity of ESP systems with 12˚ field with a 0.95-meter diameter telescope. The FOV is the region of the

[11] http://smsc.cnes.fr/COROT/

extended solar neighbourhood in the Cygnus region along the Orion arm centered on galactic coordinates (76.32°,+13.5°) or RA=19h 22m 40s, Dec=+44° 30' 00'[12] .

The objectives of Kepler mission are:

1. Determine the percentage of terrestrial and larger planets there are in or near the habitable zone of a wide variety of stars;
2. Determine the distribution of sizes and shapes of the orbits of these planets;
3. Estimate how many planets there are in multiple-star systems;
4. Determine the variety of orbit sizes and planet reflectivity, sizes, masses and densities of short-period giant planets;
5. Identify additional members of each discovered planetary system using other techniques; and
6. Determine the properties of those stars that harbor planetary systems.

Transits by terrestrial planets around solar type stars will produce a small change in a star's brightness of about 1/10,000 (100 parts per million, ppm), lasting for 2 to 16 hours. Kepler looked at close to 200,000 stars so that if Earths are rare, a null or near null result would still be significant. By the end of April 2015 Kepler produced over 1000 ESPs[13].

On August 15, 2013, NASA announced that Kepler would not continue searching for planets using the transit method due to mechanical failures. In May 2014, a new mission plan named *K2* "Second Light" was started. K2 involves using Kepler's remaining capability, photometric precision of about 300 parts per million, compared with about 20 parts per million earlier, to collect data for finding and studying more exoplanets. On December, 2014, NASA announced that the K2 had detected its first confirmed exoplanet, a super-Earth named HIP 116454 b[14]. In early 2015, nearby M dwarf with three transiting super-earths discovered by K2 data (Crossfield et al, 2015).

Canada’s only satellite MOST, Micro variability and Oscillations of Stars was launched in 2003[15]. This measures changes in the brightness of the light emitted by nearby stars.

[12] http://kepler.nasa.gov
[13] http://kepler.nasa.gov
[14] http://kepler.nasa.gov
[15] http://www.space.gc.ca/asc/eng/satellites/most.asp

In 2017, the TESS (Transiting Exoplanet Survey Satellite) space telescope of NASA will begin an all-sky survey of bright, nearby FGKM dwarf stars[16].

The success of Spacecraft based transit searches pushed ground based transit search projects to a side. However, in August 2014, HAT project announced a finding of a warm Saturn transiting an early M-Dwarf star (Hartman et al, 2015).

1.5 Search in open clusters

Open clusters (OC) are excellent laboratories for many different aspects of astrophysics. They can contain several thousand stars, and thus should yield at least a handful of transit detections when complete phase coverage is obtained (Charbonneau, 2003). The open clusters provide samples of stars with a common age, metallicity and distance. Project PISCES (Mochejeska et al, 2002), project STEPSS on open cluster NGC 1245 (Burke et al, 2004), search on NGC 6791 (Montalto et al, 2007), NGC 2099 (Hartman et al, 2009) and project KELT on open cluster M44 (Pepper et al, 2008) are some examples of open cluster transit surveys.

Observing members of open clusters is difficult and time consuming due to the large angular size (Burke et al, 2004). The use of wide field camera reduces this difficulty. One disadvantage is that follow up is difficult for relatively faint stars in the cluster. Most of the projects searching ESPs in open clusters use the transit method, which is somewhat well suited to dense stellar environments.

A benefit of searching for transiting planets in open clusters is that the interpretation of transiting candidates is greatly simplified since the stellar radius and mass can be reliably assumed from the cluster colour-magnitude diagram (Charbonneau, 2003). Open clusters form a coeval set of stars with homogeneous properties. This homogeneity makes it possible to determine with relative ease their age and metallicity from spectroscopy. Owing to their relatively low relaxation times, open clusters provide an opportunity to study stellar systems in various stages of dynamical evolution. Characterizing the fraction of cluster members that have companions with stellar to planetary masses in comparison to the field stars provides valuable insight into how these processes affect stellar and planetary formation (Burke et al, 2004).

[16] http:// web.mit.edu/newsoffice/2013/nasa-selects-tess-for-mission-0405.html

The planet frequency might be higher for open clusters with super solar metallicities. For [Fe/H] between +0.2 and +0.4, the planet frequency around field stars is 2-6 times higher than at solar metallicity. However, only a few clusters have been reported to have metallicities above [Fe/H] = +0.2 (Montalto et al, 2007).

The main challenges for open cluster transit surveys are (Von Braun et al, 2005):

- The number of monitored stars - This number is generally lower than in rich Galactic fields due to the smaller field size, which reduces the statistical opportunity of detecting transits.
- Cluster Contamination – Clusters are typically concentrated and determining a cluster member is difficult without proper motion data because of the contamination by galactic field stars.
- Differential reddening – Differential reddening across the cluster and along the line of sight can make cluster parameter determination difficult.

Careful cluster selection can help maximize the number of stars, maximize the probability of transits detection and reduce line-of-sight and differential reddening. Open cluster selection depends on (Von Braun et al, 2005):

- Cluster richness and observability – Cluster richness is a measurement of the number of cluster stars and field stars which contaminate the cluster view.
- Cluster distances – Cluster must be sufficiently distant to ensure that it fits into the FOV.
- Cluster Age – If the cluster is young, many stars could be of spectral types O, B and thus there may be many variable stars; unless spectral types are known there will be an overlap of variable stars and stars with transiting planets.
- Range of metallic ties – Current surveys based on the radial velocity method on our solar neighbourhood indicate that stars with higher metallicities are more likely to have planets than metal poor ones, hence it is better to have selected a metal rich open cluster.
- Position in the sky – If the open cluster is closer to the Galactic disk, then the higher the contamination due to Galactic field stars.
- Cluster radius and number of member stars - Cluster should not be too crowded.

Since the aim is finding hot Jupiters, open clusters with Sun like stars (stellar type G) would give better results.

In September, 2012 two planets; Pr0201b and Pr0211b which orbit separate stars were discovered in the Beehive Cluster. The finding was significant for being the first planets detected orbiting stars like Sun in an open cluster (Quinn et al, 2012). Using ESO's HARPS planet hunter in Chile, along with other telescopes around the world, three planets orbiting stars in the cluster Messier 67 was found (Brucalassi at al, 2014). Interestingly, one of these exoplanets is orbiting a star which is almost identical to the Sun in all respects.

Using Kepler data, Meibom et al (2013) , announced the finding of two ESPs in open cluster NGC 6811, Kepler-66b and -67b of three-fourths the size of Neptune, are the smallest planets to be found in an open star cluster, and the first cluster planets seen to transit their host stars, which enables the measurement of their sizes. This confirms that transit method can find mini-Neptune sized planets, if a space telescope is used.

1.6 Variable Stars

Many stars vary in brightness. This variation could be periodic. Depending on the type of the variable star, the brightness changes in these stars can range from a thousandth of a magnitude to as much as few magnitudes over periods of a fraction of a second to years. The reason for the variability could be one of the many reasons; the well-known variable star Algol has eclipses due to one star orbiting around it. As the transit planet search depends on the variation of the intensity of emitted star light, wide field transit search may find new variable stars. Transit surveys of star clusters also give updated information about the closest variable stars.

In most young clusters many of the bright stars are variables and often they are hot blue stars. These stars have started to evolve away from main sequence and have entered one of the “instability strips” that can be found in Colour - Magnitude (HR) diagrams. Lower mass stars can become RR Lyrae variables while the high mass stars can become Cepheids (Freedman et al, 2002).

Variable stars are classified according their photometric variations. The most common kind of variation is a change of luminosity but other types of variations can occur, in particular changes in the spectrum. There are two basic kinds of variable stars; intrinsic in which variation is due to physical forces of the stellar system, or extrinsic, in which variability is due to the eclipse of one star by another in a multi star system or to the effects of stellar rotation. The intrinsic group has three main classes of variable stars, pulsating, eruptive and cataclysmic while the extrinsic group has two main classes of variable stars, eclipsing binary and rotating stars.

1.6.1 Pulsating variables

These stars show periodic expansion and contraction in their surface layers, which may be radial or non-radial. While the non-radial pulsations cause deviations from the spherical form of the star periodically, the radial pulsations keep the variable star in its spherical shape. The changes in these pulsating variables are determined by the pulsating period, the evolutionary status of the star and the characteristics of the pulsations of the star.

There are many pulsating stars. Some pulsating variable star types which may affect transit search are[17] ;

- Cepheid and Cepheid-like:

  Cepheids: (Period: 1 -70 days, Amplitude variation: 0.1 to 2.0 mags)

  These yellow giant or super-giant stars having high luminosity, belong to F spectral class at the maximum and G to K at the minimum. They have short periods (days to months) and their luminosity cycle is very regular. Cepheids have a strict period-luminosity relationship. (Freedman et al, 2001).

- Beta Cepheids:

  Beta Cepheids (BCEP) are one of the principle variable types in young open clusters. BCEPs have sinusoidal periods over 0.1 to 0.7 days and show changes in luminosity of 0.1 to 0.3 magnitudes. Spectral classes of BCEPS are often found between O9 and B3. Beta Cepheids are the predominant variable stars in the NGC 4755 cluster (see A.1), which has been selected as the target cluster for this thesis.

Other pulsating variable star types:

RR Lyrae stars: (Period: 0.2 to 1.0 days, Amplitude variation: 0.3 to 2 magnitudes), Mira variables (Period: 80 -1000 days, Amplitude variation: 2.5 to 5.0 magnitudes), Semi-regular:

[17] http://www.aavso.org/vstar/types.shtm

(Period: 30 -1000 days, Amplitude variation: 1.0 to 2.0 magnitudes), and RV Tauri Stars: (Period: 30 -100 days, Amplitude variation: up to 3.0 magnitudes)

1.6.2 Eruptive variables

These objects experience eruptions on their surfaces like flares or mass ejections. Flare Stars and Wolf-Rayet variables of main sequence and S Doradus stars of Giants/Super-Giants belong to this type.

1.6.3 Cataclysmic variables

These stars show an outburst of the surface, accretion disk or a stellar explosion caused by thermonuclear processes either in their surface layers or deep interiors. Many Novae are prime examples for this type.

1.6.4 Eclipsing binary stars

These are binary systems with the orbital plane lying near or at observer's line-of-sight. The stars periodically eclipse each another, causing a decrease in the apparent brightness of the system as seen by the observer. The period of the eclipse, which coincides with the orbital period of the system, can range from hours to years. "Algol star" is the famous type, which shows this behavior.

1.6.5 Rotating stars

When stars rotate, they show small changes in light that may be due to dark or bright spots, or patches on their stellar surfaces. Bright spots also occur at the magnetic poles of magnetic stars. Stars with ellipsoidal shape can show changes in luminosity as the viewer sees different projections.

1.6.6 Other types of variable stars

There are Irregular variable stars which don't show any periodicity.

From the light curve of a variable star, the following derivations are possible:

- The luminosity variations of the system: periodical, semi-periodical, regular or unique
- The period of luminosity fluctuations
- The expected shape of the light curve (symmetrical, angular or smoothly)

1.7 Thesis outline

This thesis is about finding transiting ESPs in the open cluster NGC 4755 and also possible variable stars in the cluster as both depend on light curve variability. In chapter two, the CCD data reduction process is described while chapter three is about transit identification methods, detailing the different methods and giving emphasis on de-noising methods using fast wavelet analysis. Description of simulation work, cluster observing process details and the details about NGC 4755 are presented in chapter four. In chapter five, the results are presented; the observationally determined probability graphs, the light curves and the Power Spectrum graphs of the cluster stars. Chapter six concerns the analysis of the results, and chapter seven explains possible future work. Finally, the conclusions of the thesis are given.

Chapter 2

CCD Data Reduction Process for Transit Method

Since 1980, Charge Coupled Devices (CCDs) have been the main signal detector in many areas of observational astronomy; imaging, astrometry, photometry and spectroscopy. The transit method is based on analysing sky images taken by CCD cameras. Before and after the images are taken, the CCD image capturing process has to undergo a specific set of steps. These steps are:

1. Pre-processing

   In this stage, the standard CCD reductions steps are carried out; i.e. bias subtraction and the removal of dark current from the raw frame using the bias and dark frames, followed by flat-fielding using flat field frames.

2. Stellar photometry

   This refers to the accurate determination of the apparent brightness of an astronomical object. Although there are several methods to mark the aperture and obtain the brightness, the main requirement in the process is uniformity among all the CCD images.

3. Post-processing

   Post Processing is the stage at which light curves are produced from the output of stellar photometry. If absolute photometry is used, the results of step 2 from numerous different frames are combined and calibrated to fundamental magnitude scales by comparison with (or without) similar observations of other stars having known brightness. This calibrated magnitude scale is used for light curve analysis. All analytical and statistical analysis is then applied to the light curve.

2.1 Pre-processing

Pre-processing is done for all image files: bias (zero exposure darks) frames, dark frames, flat field frames and image frames. i.e.

$$\text{Clean Image} = \text{Raw Image}\,[i,j] - \text{bias}\,[i,j] - \text{dark}[i,j] / (\text{Normalized master Flat Field}\,[i,j] * \text{Illum}\,[i,j])$$

Where [i,j] refers to the pixel point. Illumination frames may not be available for all the cases.

Normalized Master Flat = (Raw – Flat Dark)/Flat

(Howell & Everett, 2000)

To achieve high precision calibration frames are averaged or median combined (preferred) to produce combined master bias, dark and flat frames.

2.1.1 Photometry

The accuracy and precision of the photometry process depends on the flux from the star, the sky background, atmospheric extinction, telescope optics, filter used and exposure time. Most of the above factors are dependent on the wavelength observed and they vary with time and with location, temperature, humidity and altitude.

Aperture photometry

For isolated stars on flat backgrounds, usually aperture photometry is the best method to obtain the intensity and magnitude of a star. The intensity of the stellar image is integrated over a circular aperture, with a radius of a few times the full-width-half-maximum (FWHM) value of the star. The background is usually estimated from a ring shape surrounding the star with large radius. The radii are chosen by counting pixels that are filled to half the dynamic range between the background and the brightest pixel in the star's image.

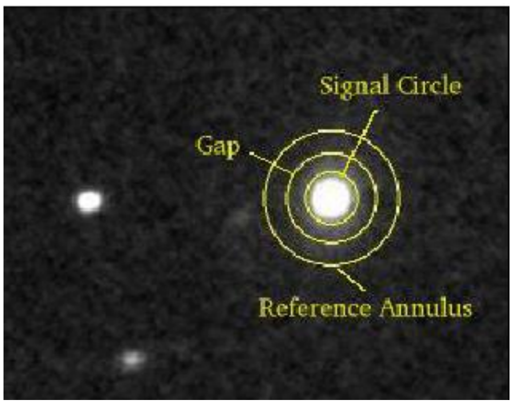

Figure 2.1 Annulus rings

To estimate the background level, first annuli are selected around the stars, random points of intensity are selected between inner and outer annuli, and an average is taken. The intensity is the sum of signal circle pixels counts with background subtracted. The middle annulus is a gap that allows the reference annulus to be unaffected by the star's Gaussian edges, while allowing the signal circle to be small.

Aperture photometry is fast, simple and accurate, if the field is not crowded. It can still give reliable light curves even for moderately crowded fields, if the atmospheric variations are removed from the star flux.

Stellar Point-Spread Function (PSF) fitting

If the search is of crowded fields, aperture photometry is not a good choice. A method of iteratively re-analyzing data to search for global minima in the distribution of the residuals and errors is needed, hence the use of the PSF.

The two-dimensional shape of a stellar image given by the point spread function (PSF) is a strong indicator of the location and intensity of the star at the local plane with the colour depending on the atmospheric conditions and telescope optics. A perfect PSF for a star will contain ~100% of the light within an inscribed circle of 3.0 times the FWHM of the PSF.

Nyquist's theorem for critical sampling can be applied to a PSF image on a CCD for pixel sampling; the sampling parameter 'r' is given by,

$$r = FWHM / P \qquad (7)$$

where P is the pixel size and both FWHM and P are given in same units, usually arc seconds. For $r <= 1$, the data are considered to be poorly sampled data, while $r > 1.5$ is considered well-sampled data (Howell & Everett, 2000).

PSF profile fitting techniques are done by matching the theoretical PSF to the actual data. This means that a normalized pattern is fitted to a star in the image to obtain the intensity and the magnitude using non-linear techniques. The idea is that the spread of the image on the CCD and the number and distribution of counts with the image should confirm to a standard pattern, which will be the same for stars of all magnitudes. The only difference will be the scale of that standard profile. For each star, some fundamental parameters must be determined, the position, in 'x' and 'y' coordinates, of the centroid of the star within the frame and the amplitude of the star's profile above the local diffuse sky brightness.

A number of mathematical functions can model PSFs; the most common is:

Gaussian,

$$G(r) \; \alpha \quad \exp\,(r^2/2a^2) \qquad (8)$$

where 'r' is the radius of the point source, and 'a' is the fitting parameter (Howell, 2000).

The scaling of the model PSF to match the amplitudes of stellar profiles provides a very precise measure of the relative brightness. However, since each data frame has its own PSF that may be quite different from those found in another frames, profile-fitting photometry does not necessarily guarantee accurate comparisons from one exposure to another.

2.1.2 CCD data reduction

2.1.2.1 Back ground level

The mean of the background sky B_{sky} is given by (Howell, 2000),

$$B_{sky} = \left(\sum_{i=1}^{n} B_i\right)/\,n \qquad (9)$$

where B_i is the background level of the annulus region of the i^{th} sample and n is the total number of samples in the annulus region.

The variance of the background V_b is given by (Howell, 2000),

$$V_b = \sum_{i=1}^{n} \;(B_i - B_{sky})^2\,/(n-1) \qquad (10)$$

2.1.2.2 Intensity

After selecting an arbitrary window containing the star, the FWHM is calculated for each frame and 1.5*FWHM or any suitable radius is taken as the radius of the star to calculate intensities. Some experts advise (Howell, 2000) using 0.8*FWHM as the limit of the radius.

The mean intensity of the star M_{mean} is given by,

$$M_{mean} = 1/N) \sum_{i=1}^{N} (I_i - B_{sky}) \qquad (11)$$

where N is the number of points with intensity higher than the background level within the selected (1.5*FWHM) radius and I_i is the intensity of i^{th} the pixel in the signal circle.

According to Howell (2000), if the radius of the source is 3 * FWHM, then it would contain 100% of the flux from the object. However, that will decrease the SNR. To increase the precision, a signal circle has to encompass at least 80% of the FWHM.

Selecting source aperture is arbitrary. To find the centre, the marginal distributions of the PSF are used. For well-sampled, relatively good images, simple (x, y) entraining provides a very good determination of the centre position of a PSF.

2.1.2.3 Image centering of PSF

Howell (2000) advised that the simplest and most widely used centering approximation for a PSF is that of the marginal sums of first moment distributions. Starting with a rough pointer to the position of the centre of the star, the intensity values of each pixel within a small box centered on the image and of size L x L (say L equals 2) are summed in both x and y directions. The marginal distributions of the PSF are found from (equations 12-17 are from Howell (2000))

$$I_i = \sum_{j=-L}^{j=L} (I_{i,j}) \qquad (12)$$

$$J_j = \sum_{i=-L}^{i=L} (I_{i,j}) \qquad (13)$$

where $I_{i,j}$ is the intensity (in Analogue Data Unit - ADU) at each(x, y) pixel: The mean intensities $\mathbb{I}$ and $\mathbb{J}$ in x and y directions are determined by

$$\mathbb{I} = (1/(2L+1)) \sum_{i=-L}^{i=L} (I_i) \qquad (14)$$

and,

$$\mathbb{J} = (1/(2L+1)) \sum_{j=-L}^{j=L} (J_j) \qquad (15)$$

Finally, the intensity-weighted centroid is determined using

$$x_c = \left(\sum_{i=-L}^{i=L} (I_i - \mathbb{I})\right) x_i \Big/ \left(\sum_{i=-L}^{i=L} (Ii - \mathbb{I})\right) \text{ for all } (Ii - \mathbb{I}) > 0 \qquad (16)$$

$$y_c = \left(\sum_{j=-L}^{j=L} (J_i - \mathbb{J})\right) y_i \Big/ \left(\sum_{j=-L}^{j=L} (Jj - \mathbb{J})\right) \text{ for all } (Jj - \mathbb{J}) > 0 \qquad (17)$$

2.1.2.4 Magnitude of point source

The apparent magnitude (or instrumental magnitude), M_{inst} of the star is given by

$$M_{inst} = -2.5 \log_{10}(I) + C \qquad (18)$$

where

$$I = S - N_{pix}B \qquad (19) \qquad \text{(Howell, 2000)}$$

I is the source intensity, N_{pix} is the total number of pixels contained within the considered area, B is the sky back ground signal strength, S is the total integrated photometric source signal and C is an appropriate constant, usually ~23.5 -26 for most observing sites and determined by calculating when source magnitude is placed on a standard magnitude scale such as that of the Johnson or the Stromgren system (Howell, 2000).

2.1.2.5 Calibration

Calibration without a colour correction is appropriate when the instrumental system is well matched to the target standard system.

The calibration equation is:

$$m_{calib} = m_{inst} - A - Z + k{*}X, \qquad \text{(20) (Castellano et al, 2004)}$$

Where m_{calib} is the calibrated magnitude, m_{inst} is the instrumental magnitude, A is an arbitrary constant which is often added to the instrumental constants, Z is the photometric zero point between the standard and instrumental systems, K is the atmospheric-extinction coefficient and X is the air mass (likely to range from low to high) correction.

The first order extinction for the 'V' band is given by

$$v_0 = v - a_v * X \qquad \text{(21) (Castellano et al, 2004)}$$

where v_0 is the true extinction-corrected apparent magnitude, X is the air-mass, a_v is the V band first order extinction coefficient in magnitudes per unit air mass, and v is the measured V-band magnitude. For the other bands, similar equations can be derived by using band specific first order extinction coefficients.

Second-order extinction depends on the colour difference between the target star and a comparison star and is defined by

$$v_0 = v - a_v*X - b_v*(B\text{-}V)*X \qquad (22)$$

where b_v is the second order extinction coefficient in units of magnitudes per air-mass per unit difference in B-V colour in magnitudes (Castellano et al, 2004). Although this equation is for band 'V", this can be generalized for the other bands using band specific coefficients.

For a small zenith angle (z), X = sec z is a reasonable approximation.

A more refined equation for the mass: as defined by Howell & Everett, (2000);

$$X = \sec z - 0.0018167 (\sec z - 1) - 0.002875 (\sec z - 1)^2 - 0.008083 (\sec z - 1)^3 \qquad (23)$$

The above equation implies the use of z_t, the true zenith angle, that is, the zenith angle to the observed object in the absence of the atmosphere, as opposed to the apparent zenith angle z_a affected by refraction effects.

Air mass remains quite low for $z < 45^\circ$, reaches 2 at $z = 60^\circ$ and increases rapidly thereafter.

If zenith distance is not given, it can be calculated from.

$$\text{Sec } z = 1/(\sin\varphi \; \sin\delta + \cos\varphi \; \cos\delta \cos h) \qquad (24)$$

where, φ is the latitude of the observations, δ is the declination of the object observed and *h* is the hour angle of the object observed.

The hour angle is simply:

$$h = s - \alpha \qquad (25)$$

where α is the right ascension of the object observed and *s* is the local sidereal time.

Once the final magnitude is found, a light curve (graph of magnitude vs. time) can be obtained.

For calibration without colour, the following equation is used (Palmer and Devanhall, 2001).

$$M_{calib} = M_{inst} - A + Z + k*X \quad (26)$$

where,

M_{calib} - calibrated magnitude

M_{inst} - instrumental magnitude

k - atmospheric-extinction coefficient

Air mass depends solely on the zenith distance, which can be calculated from the celestial coordinates of the object, the location of the observatory and the time of observation. If the star is observed throughout the night then the M_{inst} can be plotted against the air mass. Such a plot should be a straight line with a slope of "k". On the other hand, if suitable standard stars are in the FOV, then each observation of standard stars M_{calib} is known in addition to M_{inst}. Using least squares, A, Z, k and Z can be obtained. The main assumption of a constant extinction coefficient may not be valid for longer hours (> 3hours) of search duration. The extinction can be changed significantly on many time scales due to conditions of the air, particularly the amount of dust in the air.

2.1.2.6 Differential photometry

Differential photometry requires no reduction to a magnitude system tied to standard stars. The differential extinction arises from differences in air mass between the object and comparison star in a single exposure and increases with air mass. The closer the object and comparison stars, the lower the differential extinction. In the optical region of the spectrum, the extinction drops as the wavelength increases. The choice of similar colour comparison stars can minimize the second-order extinction, which varies with the product of air mass and the difference Δ (B-V) in colour between the stars. If the stars to be compared are near one another on the celestial sphere and are similar in colour, or if the observations are limited to low values of air mass, the first-order (air mass difference dependent only) extinction and the second-order (colour difference dependent) extinction corrections are generally small compared to the expected photometric transit depth. Furthermore, CCD differential photometry allows the simultaneous measurement of the brightness of all stars in a given field through virtually identical values of air mass (Castellano et al, 2004). Differential photometry is largely unaffected by small changes in atmospheric transparency such as thin clouds. If the zenith angle is zero, the absorption in the sky is at the minimum.

For best results in differential photometry, every star under observation needs a reference star, which should be similar in colour to the star under observation. This star must not be a variable star. Castellano and Laughlin (2001) defined the precision as the SD of the measurements of a constant brightness star. In addition, they advise to select a reference star within a half a degree and to minimize systematic errors due to poor tracking, focus changes or telescope light throughput changes.

In differential photometry, the measurement of the difference in brightness between two stars is well suited to the detection of planetary transits. Superior results are obtained if light curves containing obvious systematic effects are removed or the systematic variations reduced before they are submitted to the search algorithm.

2.2 Conditions to detect a transit from a light curve

For the absolute magnitude, the air mass is calculated and the extinction coefficient can be obtained from a published air mass chart. The extinction coefficient increases with decreasing wavelength and the air mass can vary 50% over the time and can change during a night.

Once a de-trended light curve is drawn, the SD (σ) of the flux counts gives an indication of the quality of the light curve. For a hot Jupiter around a solar type star, about 10 to 20 milli-magnitude signal amplitude difference is typical. To be suspicious, the SNR must be greater than 3 and to be absolutely sure the SNR must be more than 5. If σ is about 5 milli-magnitudes, it is considered enough to find a transit of an ESP. However, radial velocity data is still needed for the verification since small stars or grazing eclipsing binaries give similar transits to ESP.

For a sub-metre telescope and a commercial CCD, a typical hot Jupiter transit observation will have a SNR of 4 (20 milli-magnitudes/5 milli-magnitudes). Accordingly, with this σ, some event can be seen and be verified by re-observation. If a light curve with 30 seconds time sampling interval is smoothed by using a moving average of 20 points, the SNR is increased by a factor of $\sqrt{20}$ and σ is reduced by $\sqrt{20}$, giving the desired σ of 5 milli-magnitudes after processing. In this case, time resolution is 30 * 20 = 600 seconds or 10 minutes under the assumption that the only noise present is the random noise. Since the transit time of a hot Jupiter around a solar-type star transit time is about 90 minutes, ten minutes time sampling gives nine points for the light curve, which is adequate to determine the transit.

If the SNR is relaxed, say from 4 to 3, a moving average of 10 points can be taken, thus giving a time resolution of 5 minutes. This can find a close-in transiting ESP around a very low mass star, which typically has a transit time of 45 minutes.

The main constraint is the ability of the camera, which measures the transit depth of the light curve, and the precision of the photometric process. The combined effects of transit probability and duration imply that, with a given observation strategy, the probability of obtaining any in-transit observations of a given planet decreases rapidly with orbital period, thus more observing time is necessary (Aigrain, 2002). The brightest limit is set by CCD saturation and the faintest side is limited by the minimum SNR needed to detect the ESP.

The shape of the light curve depends on (Bissinger, 2004):

- The immediate environment surrounding the ESP
- The inclination of the orbit of the planet to the star
- The environment surrounding the parent star
- Earth's atmosphere
- Optical paths of the telescopes and CCD camera
- Position of the star at time of detection
- Photometric aperture
- Brightness of the star and stellar variability
- The noise present at the telescope and the camera
- CCD integration time

2.3 Noise present in the photometry

The noise in the transit signal is mainly caused by following noise spectral components.

- White Noise – Signal with flat frequency spectrum in linear phase, being un-correlated in time.
- Brown (or red noise) – Ideally, this has decreasing power density of 6dB per Octave with increasing frequency (density proportional to $1/f^2$ (roughly)) over a frequency range. Nearby values are correlated with each other. This is concentrated in low frequencies. This is commonly known as Brownian noise.

Photometric system noise is a combination of:

1. Photometer noise - CCD, Telescope errors
2. Background noise - Stray light, atmospheric, background stars, cosmic ray hits
3. Shot noise ($1/\sqrt{n}$) - Errors arising due to stellar magnitude, aperture areas, white light Quantum efficiency, transit duration
4. Processing noise – Errors from calibration, flat fielding

Some CCD noise sources, like output amplifier noise, camera noise and clock noise are independent of the signal level. These CCD noise sources are combined into a single noise source called readout noise. They are characteristic of the camera. Noise from the CCD output amplifier depends on thermal noise and flicker noise, which is frequency dependent. All these errors are combined in photometer errors.

Not all noise components can be removed by averaging the data. Pont (2006) showed that this systematic noise is correlated in typical hot Jupiter transit time scales, cannot be ignored and could be the dominant noise. Systematic noise can usually be eliminated (or at least reduced) by calibration, if the reason for the noise is known.

If there is a systematic noise component in the combined noise, the SD value of the average of 'n' points will be greater than the theoretical value ($\sigma/\sqrt{n}$).

Transit signals are weak ($\Delta F/F$ is about 10^{-2}) and are concentrated in a small fraction of the total signal. The change in magnitude, Δm, can be significant, given the uncertainty of the magnitude estimate σ. If only one magnitude measurement was made during the transit, a relatively large deviation from the mean magnitude would be required to identify the transit (perhaps $\Delta m >= 5\sigma$) (Howell et al, 2000).

There are different ways of calculating the SNR (signal to noise ratio) of the light curve.

The Generic CCD equation for SNR (Howell, 2000, p. 54) is

$$SNR = N^* /\sqrt{(N^* \, n_{pix} (N_S+N_D+N^2{}_R)} \qquad (27)$$

where N* is the total number of photons (count multiplied by gain) while N_{pix} is the number of pixels under consideration of SNR calculations. N_S is the total number of photons per pixel from the background sky, N_D is the total number of dark current electrons per pixel and N^2_R is the total number of electrons per pixel resulting from the read noise.

For sources of noise that behave under the auspices of Poisson statistics (which includes photon noise from the source itself), for a signal level of N, the associated 1σ error is given by $\sqrt{N}$. If the total noise is dominated by N*, once the sky background has been subtracted then the CCD equation becomes SNR = $\sqrt{N^*}$, yielding the expected result for a measurement of a single Poisson behaved value. This is good approximation for stars much brighter than the background.

The term bright source refers to the case for which the SNR errors are dominated by the source itself (i.e. SNR ~ $\sqrt{N^*}$), and a faint source is the case in which the other error terms are of equal or of greater significance compared with N* and therefore the complete error equations are needed (Howell, 2000). The Standard Error (SE) will obtain its maximum when SNR is at its minimum (i.e. at the faintest star).

For error calculations, the full flux of the star is necessary. The slope and the intercept of log10 SD vs. magnitude (- 2.5 *log10 (Flux)) graph give an estimate of other parameters/error of the photometry process. Regression fitting can determine the slope and the intercept. This intercept represents variations in the flux count.

Images can be stacked in order to increase SNR. It could be the sum, average or median of several frames. If the final image is the average of N frames then as defined by Howell (2000),

Effective gain = N*gain

Effective read out noise = √(N) * readout noise

Resultant Noise = Previous Noise/√(N)

If there are at least two flat field images and two bias images, then the readout noise can be calculated.

Photometric errors will not be all Gaussian. However, the non-Gaussian form of the errors has no practical impact on the analysis as there are so many data points that the central limit theorem guarantees that the combined behaviour in each phase bin will be Gaussian (Pepper et al, 2003). Howell et al (2000) suggested that it is better to limit the entire data reduction process to a small sub-section of the CCD with the assumption that differential photometry will eliminate the systematic errors that neighbouring stars (those in the same CCD) appear to have in common.

The best ways to assessing the precision of the whole reduction process is to plot a graph of the SD of the magnitude measurements for each star against the mean instrumental magnitude (Castellano and Laughlin, 2001). The post processing procedure has to be designed to maximize signal to noise and decrease the SD as much as possible. The SNR is related to SD by SNR= $1/\sigma$, where σ is SD of the measurement. The relationship between the various sources of uncertainty and the SD expressed in terms of magnitude is (as in Howell and Everett, 2000);

$$\sigma \text{ magnitude} = (1.0857 * \sqrt{(N_{ph} + P)}) / N_{ph} \quad (28)$$

where N_{ph} is number of photons, $P = N_{pix} (N_{sky} + N_{th} + N_{2rp})$ is the noise term,
where, N_{pix} – number of pixels
N_{sky} – number of photons per pixel from the background sky
N_{th} - number of dark current per pixel
N_{2rp} – number of electrons per pixel resulting from the noise source

The constant 1.0857 is the correction term between an error in flux and the same error in magnitude. Lower SD value indicates better reduction.

If the noise is low compared to the total photons, the equation (28) reduces to

$$\sigma = 1.0857/\sqrt{N_*} \quad (29)$$

where, N_* is he total number of photons detected from the star and P the noise term , the number of photons or electrons contributed by all sources of noise (Howell and Everett, 2000). Using a CCD, the best obtainable precision will occur if all of the collected photons are from the star and no other noise source contributes. Poisson statistics require 10^6 photoelectrons per pixel in the flat field frames in order to achieve a final photometric precision of 0.001 of magnitude.

The SNR can be improved by choosing the right sizes for the 'signal circle' and sky annulus. A larger sky area is always better, but they also produce a greater percentage uncertainty on the total count vote. The exact boundary of the star and its neighbourhood cannot be easily determined due to other stars. The uncertainty of the signal circle is proportional to the square-root of the number of pixels in the signal circle, whereas the uncertainty of the sky annulus is inversely proportional to the area of the sky annulus. Hence, the SNR is maximum when the signal circle is small, but not smaller than the FWHM, and when the sky annulus is large.

Close visual analysis of light curves reveals that approximated curves (Described in Chapter 3) have the shapes of typical red noise, while the original curves have pink noise (red plus white noise) characteristics (Pont, 2006). Simulations (see chapter 5) show that the approximate curve must show very little deviation or no deviation at all unless there is an anomaly like a transit event or a flare. There are two distinct behaviours of red noise depending on the survey. In some surveys the red noise is independent of magnitude; in others it is proportional to the photon noise. The surveys using large telescopes show the first behaviour while the ones using small cameras show the second (Pont, 2006).

As the SD of the approximated light curves gives the red noise component present, we can use the SD as the signal to red noise ratio of the light curve after normalizing the signal to a unit magnitude. This calculation is simpler than S_{red}, the ratio of the best-fit transit depth to the Root Mean Square (RMS) scatter when binned on the expected transit duration, and gives a measure of the reliability of the transit detection (Collier Cameron et al, 2006).

$$S_{red} = \delta\sqrt{N_t} / \sigma L^b$$

where,

- L - Average number of data points spanning a single transit, b is the power-law index that quantifies the covariance structure of the correlated noise,
- N_t - The number of transits observed
- δ - The transit depth and
- σ - The weighted RMS scatter of the un-binned data.

Chapter 3

Algorithms for the Analysis of Light Curve

Differential light curves can be analyzed by simple visual, statistical, or analytical methods. A transit identification algorithm (TIA) is a mathematical tool that examines the light curves for the presence of transits. Once an algorithm is developed, the algorithm is tested by simulations to verify that the algorithm produces a result within the desired confidence level. This is done by generating a test static for each set of free parameters in some method or another. If test statistics exceed a certain value determined by the desired level of confidence then the event is not a chance occurrence of noise and it could then be determined whether there is a transit-like event in the light curve.

Detecting transits from a light curves is a classical signal-detection problem for deterministic signals in coloured noise. An essential component of signal detection is the characterization of the light curve noise which may also include stellar variability. The result is a time series of test statistics representing the likelihood that a transit was occurring at each point in time.

Generally, the differential light curve (the signal) consists of equally spaced pulses of duration much shorter than the expected orbital period. If the orbital period is less than twice the sampling interval, a transit cannot be identified (Nyquist Sampling theory). This light curve needs filtering to extract a transit waveform hidden in it as noise overlaps the signal. Filtering always has two related aims, to reduce noise, and to compress data. If the signal can decomposed into different frequency blocks known transit frequencies can be searched in the blocks (this method is used in wavelet analysis, to be discussed later). As filtered signals may be different to the original, the statistical properties will also be different.

3.1 Transit identification algorithms

Statistical analysis and analytical signal processing methods are used to analyze the differential light curve. Two statistical methods used are the Bayesian algorithm (Aigrain and Favata, 2002) and the Box fitting Least Square algorithm (Kovacs et al, 2002). For analytical signal processing, the light curve is considered as a normal signal contaminated with noise, and general signal processing methods are applied. One method is the matched filter algorithm (MFA), which is based on frequency domain convolution and which can be implemented by correlation in the time domain, between the differential light curves and the expected transit shape curve. Tingley (2003a) compared several of these different techniques and concluded that none are superior. Moutou et al (2005) have done blind tests for five planetary transit algorithms and concluded that specialized algorithms can detect transit signals down to the noise limit.

The noise present in the light curve can have a significant effect on the results. For ground-based surveys, systematic noise in the photometry affects the ability to detect planetary transits, and a detection threshold based on white Gaussian noise is insufficient since the noise in the light curve is quite red, with a low frequency component (Pont et al, 2006). Statistical methods and running average depend on the assumption that the long run noise mean becomes zero, which is not realistic in practical situations. Moreover, MFA (described in the section 3.1.1) only gives the optimum performance when the noise is pure white Gaussian. To remove noise and smooth the signal, the simplest filters are moving average and median filtering while the folding technique enhances the signal in the folding time length, if the folding length is closer to the orbital time.

Details of the algorithms are as follows:

3.1.1 Matched filter algorithm (MFA)

First suggested by Jenkins et al (1996) for transit detection, the idea behind the matched filter is correlation, and convolution is used to perform the correlation. The amplitude of each point in the output light curve is a measure of how well the filter kernel matches the corresponding section of the input light curve. The matched filter is optimal in the sense that the top of the signal peak is farther above the noise than can be achieved with any other linear filter.

The matched filter is the linear filter, *h*, that maximizes the output signal-to-noise ratio. For a linear shift-invariant system x(n), and the output y(n), the matched filter convolution sum is given by,

$$y[n] = \Sigma\, h[n-k]\, x[k], \text{ where } k \text{ changes from } -\infty \text{ to } +\infty$$

The method as implemented assumes a simple square-well transit model, which is a valid assumption when searching for a signal very close to the noise level, for which the shape of the short ingress/egress phase of the transit is essentially unresolved. This method searches for multiple transits spanning a large range of periods and transit start times within a transit parameter space determined by characteristics of the dataset.

3.1.2 Approach of Hans Deeg

This approach is based on the idea of analyzing the data with a series of test signals spanning parameter spaces of time and magnitude and includes a time-based weighting. This time-based weighting is necessary to account for the difference in time increments of the observations from different telescopes. This was specifically designed for the complex circumstances found in a data set of several years of observations of CM Draconis (Deeg et al, 1998).

In this approach, a test signal with transits included is subtracted from the light curve for each individual night of observations and a parabolic fitted to what remains. A parabola is fitted to each individual night of observations, which is intended to model the residual nightly extinction variation. These fits are then compared to the original data and the residuals determined, and test statistics calculated from the residuals (Tingley, 2003b, using Deeg et al, 1998).

3.1.3 Bayesian Method

An alternative to the conventional MFA is the Bayesian approach (Bayes' theorem) in statistics and was designed for the COROT project. This approach maximizes the use of whatever information is available on the phenomenon one is trying to detect and is relatively flexible, incorporating new information into the detection process as it becomes available. It estimates an unknown parameter through the maximization of a likelihood function, invoking as much a priori information as possible in order to improve the estimation. WGN (White Gaussian Noise) is assumed, and the signal can be represented as a Fourier series. By finding the most likely period of the signal, the coefficients of the Fourier series can then be determined (Defay et al, 2001).

In the Bayesian method, Bayesian parameters like prior distribution are evaluated first. This is closely related to the field of data modeling. The strength of this approach is the ability to deal with nuisance parameters via marginalization. The other strength is the asymptotic distribution of the likelihood function.

3.1.4 Box search with low pass filtering

This method searches for box-shaped signals in normalized, filtered and unfolded light curves which were designed to detect single and periodic transit events (Moutou et al, 2005). For the detection of transit-like events, a general search tool is used. All data points deviating from the average signal by 3σ are identified and the neighbouring deviating points are combined into a single detection. Further investigation is done for where the depths and duration of events are determined.

3.1.5 The box-fitting technique

The Box fitting Least Square method described by Kovacs et al (2002) is essentially a χ^2 fit of a square-well transit model to the observation. Through minimization, the depth of the transit can be removed as a free parameter, reducing the computational load. They have examined the statistical characteristics of the Box-fitting least square algorithm to detect periodic transits in time series of stellar photometric observations. This algorithm relies on the anticipated box-shape of the periodic light curve, and assumes a strictly periodic signal, with a period P_0, that takes only two discrete values, H and L (L is the transit phase and H represents values outside the transit) with an expected transit depth of H-L. This method ignores all other features that could be in a transit. The time for ingress and egress is assumed negligible compared to the transit.

The time spent in the transit phase L is qP_0, where the fractional transit length q is assumed a small number (~0.01 -0.05). For any given set of data points, this algorithm aims to find the best model with estimators of five parameters – P_0, q, L, H, and t_0, the epoch of the transit. If a zero average signal is assumed, $H = -Lq/(1-q)$, then the number of parameters is reduced to four. For several data sets, the maximum of the average squared deviation of the fit is related to the average variance of the noise

3.1.6 Correlation

Correlation is a statistical tool used to measure how well two samples resemble each other. Since correlation is not designed primarily for transit identification, it can be used as a benchmark to measure the effectiveness of the statistics behind the various statistical detectors (Tingley, 2003a). The correlation method is not affected by gaps in the coverage of the data. Missing blocks do not contribute to the correlation function.

Mandel and Agol (2002) describe an algorithm for a sliding transit template that can be used in correlation. Moutou et al (2005) used this for their transit comparison experiment. Previous filtering of the long-term variations is not crucial in this case, because the template covered only a small part of the light curve (the observed period) at a time.

3.1.7 Approach of Aigrain and Collaborators

Aigrain and Favata (2002) employed a Bayesian method which consists of calculating the likelihood of the data given a certain number of parameters, varying the parameters over a given range and identifying the value of each parameter whose probability is maximized according to Bayes' theorem.

Two great strengths of the Bayesian approach are the ability to deal with nuisance parameters via marginalization, and the use of the evidence or Bayes factor to choose models. This approach is based on the more general period-finding method of Gregory Loredo (described in Aigrain and Favata, 2002).

Aigrain and Irwin (2004) suggest another optimum filter based on the following maximum likelihood algorithms:

1. Maximum likelihood approach in the Gaussian noise
2. Gregory –Loredo Method
3. Optimum ^{2} calculation (By directly maximizing the likelihood or minimizing ^{2})
4. Making use of the known characteristics of planetary transits
5. ^{2} minimization with a box-shaped transit.

Aigrain and Irwin (2004) have introduced a box shaped transit finder and they suggest that MFA and cross correlation gives the best results compared to other methods.

3.1.8 Whitening, matched filter and Bayesian reconstruction - COROT mission

The COROT mission uses a Fourier domain whitening filter, which divides the signal by its own spectral power density function, thereby whitening the noise (Carpano et al, 2003). There is no prior knowledge; hence this acts as an adaptive filter. Once this is coupled with a matched filter, it becomes an optimum filter. In the multi-transit case, both the matched filter and any other detection method based on the Bayesian approach combined with the decomposition of both data and the reference signal into their Fourier coefficients were investigated. Carpano et al (2003) stressed that, in the multi-transit case, the matched filter was found to perform better than the Bayesian method. However, the Bayesian method can be used post-detection to re-construct the real transit signal.

3.1.9 Wavelet domain adaptive filter - Kepler Mission

The filter developed by Jenkins et al (2002), is based on an optimal filter, but takes into account the fact that the some characteristics of the noise such as stellar variability, are likely to change significantly over the duration of the observations (Kepler has spent its entire operating lifetime of 4 years continuously observing the same field). Hence, a Fourier domain filter cannot account for this, and a wavelet based approach was therefore devised. Dividing the data by its spectral density can be crudely approximated by dividing it by its variance in a number of separate frequency band passes. Instead of frequency filters, this filter measures the dependence of the noise variance on both frequency and the time by using wavelet decomposition (see section 3.2). Bootstrap simulations are supposed to test the performance of the combined wavelet and matched filter on simulated light curves (Carpano et al, 2003). These simulations concluded that solar levels of variability do not prevent the detection of Earth sized planets around a bright star (V<12),

3.1.10 Fast Fourier transform (FFT)

The most popular signal processing method can be used to analyse light curves if the light curve has no discontinuities, otherwise it has to be applied separately to the segments.

The FFT is an efficient algorithm to compute the discrete Fourier transform (DFT) and it's inverse. Let x_0, x_{N-1} be complex numbers. The DFT is defined by the formula,

$$X_k = \sum_{n=0}^{N-1} x_n e^{-\frac{2\pi i}{N} n k} \qquad k = 0, \dots, N-1.$$

Evaluating these sums directly would take (N^2) arithmetical operations. An FFT can compute the same result in only (N log N) operations. The FFT transforms the signal from the time domain to the frequency domain, thus if the light curve has a recurring transit like feature then it will be indicated by a vertical line in the frequency domain if the frequency is plotted along the horizontal axis.

As many time discontinuities occur in ground base observations, the FFT can only be used for segments of data which have no discontinuities. Light curves of space based transit searches are generally longer and continuous thus better for FFT. However, the average Power Spectral Density (PSD) can be taken over all time segments, providing that number of points used for FFT remains constant. The advantage of PSD is it enhanced common frequency components is all time segments and reduces any random frequency components. Thus it is a very good tool to find frequent frequency components in a non-continuous signal. Since the Fourier transform of a random signal is itself random, any prominent frequency lines are suspicious, because it indicates a hidden signal with no randomness.

3.1.11 Lomb- Scargle algorithm

This least-square fitting method gives a periodogram analysis of a non-periodic and discontinuous signal. This method can be used where the traditional FFT is limited. (Press et al, 1992)

3.1.12 Folding

In the folding method, data is re-grouped and plotted against the assumed period. This transforms a signal which originally looked like pure noise to a periodic series with a modest amount of additional remaining noise. If the period of the recurrent pattern is not known, it is very difficult to identify unevenly timed, transit like patterns in noisy data. If it is possible to transform the data to a period that is very close to the correct one, then a signal may be seen (Templeton, 2004).

3.1.13 DST (Detection Specialiee de Transits) algorithm

This analytical algorithm aims at a specialized detection of transits by improving the considerations of the transit shape and the presence of transit timing variations. Cabrera et al (2012) use BLS algorithm (Kovacs et al, 2002) to generate the DST. Cabrera et al (2012) apply COROT de-trending and transit tool to published Kepler data to find new transit candidates.

3.1.14 TRUFAS algorithm

This algorithm was developed to analyze COROT data. This uses continuous wavelet transformation of the de-trended light curve with posterior selection of the optimum scale for the transit detection. This algorithm needs the presence of at least 3 transit events in the data (Regulo et al, 2007).

3.2 Wavelet analysis in TIA

Wavelet analysis can be used to analyze time series that contain non-stationary power at many different frequencies (Daubechies, 1990). It makes it possible to determine periodicities and the time at which these periodicities exist. The wavelets are scaled and translated copies of a finite-length or fast-decaying oscillating waveform. Wavelet transforms have advantages over traditional Fourier transforms for representing functions that have discontinuities and sharp peaks.

In formal terms, this representation is a wavelet series representation of a square integratable function with respect to either a complete, ortho-normal set of basis functions, or an over complete set of frame functions, for the Hilbert space of square integratable functions.

If the wavelet transform is regarded as a filter bank, wavelet transforming can be considered as passing the signal through this filter bank. This is the Fast Wavelet transform (FWT) algorithm (Mallat, 1989) and is known as a two-channel sub-band coder in the signal processing industry. Every band is divided into two bands; the low frequency band and the high frequency band. The outputs of the different filter stages are the wavelet and scaling function transform coefficients. In implementation, a filter bank "sub-band coding algorithm" is widely used in wavelet analysis. Figure (3.1) shows the basics of sub-band coding where in each level of decomposition, the previous lower sub-band is split into two halves to get two-channels.

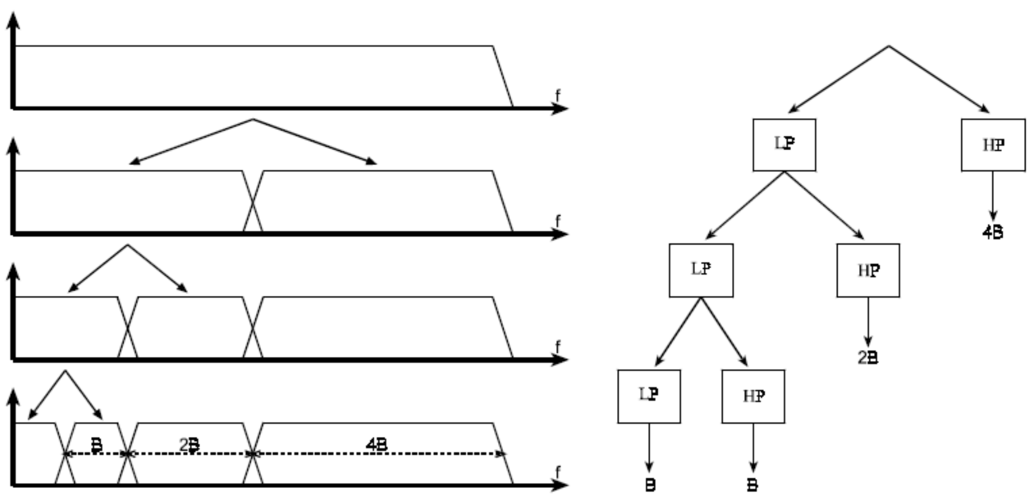

Figure 3.1 Splitting the signal spectrum with iterated filter bank

For many signals, the low frequency components are the most important. It is what gives the signal its identity. The high-frequency components impart finer features and noise. In wavelet analysis, approximations (A) are the high-scale, low-frequency components of the signal, while details (D) are the low-scale, high-frequency components. This down sampled decomposition can be iterated using iterated filter banks, with successive approximations being decomposed in turn, so that one signal can be broken down into many lower resolution components. This will be done up to suitable decomposition level depending on the expected transit duration. Successive approximations possess progressively less high frequency information. With the higher frequencies removed, what is left is the overall trend, the slowest part of the signal.

In the real world, there is no signal without noise. De-noising is not necessary for all practical purposes, especially if signal to noise ratio is very high. Unfortunately, more often this noise corrupts the signal and must be removed in order to recover the original signal. This noise removal can be done in the time-space domain of the original signal or in a transform domain. If the latter is chosen, it can be done in the Fourier transform time-frequency domain or the wavelet transform time-scale domain.

Wavelet de-noising is not smoothing the signal. In smoothing, high frequencies are removed and the low frequencies are retained. In de-noising, regardless of the frequency content of the signal, the approach is to remove whatever noise is present and retain whatever signal is present. Wavelet de-noising is considered a non-parametric method and due to the nonlinear shrinking of coefficients in the wavelet transform domain, wavelet de-noising is strictly distinct from other de-noising methods, which are linear (Coifman and Donoho, 1995).

Wavelet decomposition in FWT can be used to remove a large part of the noise of the signal, thus making a de-noised signal. The normal de-noising procedure involves three steps.

1. Decompose - Select a wavelet, select a level N. Compute the wavelet decomposition of the signal to level N.
2. Threshold detail coefficients - For each level from 1 to N, select a threshold and apply soft thresholding (described in next paragraph) to the detail coefficients.
3. Reconstruction - Compute wavelet reconstruction using the original approximation coefficients of level N and the modified detail coefficients of levels from 1 to N.

Hard thresholding is the simplest method and can be described as the process of setting to zero the elements in the wavelet domain whose absolute values are lower than the threshold. Soft thresholding is an extension of hard thresholding, first setting the elements whose absolute values are lower than the threshold to zero, and then shrinking the nonzero coefficients towards zero. The hard procedure creates discontinuities while the soft procedure does not. For these two threshold methods, the corresponding theoretical results are available in Donoho (1995).

Relationship of threshold in mathematical notation:

If thr denote the threshold,

if $|x| > thr$,

hard threshold of the signal = x ;

soft threshold of the signal = sign(x) (|x| - thr);

else

hard threshold of the signal = is 0, (provided that $|x| < thr$);

soft threshold of the signal = 0;

end

To determine significance levels for wavelet spectra, an appropriate background spectrum has to be chosen. For light curves, the possible background can be white noise that has a flat power density spectrum or red noise in which power is concentrated in low frequencies. It is then assumed that different realizations of the differential light curve will be randomly distributed about this expected background, and the actual spectrum can then be compared with this random distribution. The original signal can be reconstructed from the coefficients of the approximations and details.

The wavelet de-noising does not require any assumptions about the nature of the signal. It allows discontinuities and spatial variation in the signal, and exploits the spatially adaptive multi-resolution features essential to the wavelet transform. Furthermore, this method exploits the fact that the wavelet transforms map white noise in the signal domain to white noise in the transform domain. Thus, while signal energy becomes more concentrated into fewer coefficients in the transform domain, noise energy does not. It is this important principle that enables the separation of signal from white noise (Taswell, 2000).

De-noising with orthogonal wavelet transforms sometimes exhibits visual artifacts near singularities. In the neighbourhood of discontinuities, wavelet de-noising can exhibit a Gibbs-like phenomena, alternating undershoot and overshoot of a specific target level, because the curves in question are partial reconstructions obtained using only terms from a subset of wavelet basis (Coifman and Donoho, 1995). Although these phenomena are much better behaved than the Fourier based de-noising, in which Gibbs Phenomena are global rather than local, they are still visually annoying.

The threshold level named as the universal threshold corresponds to a minimum risk. This threshold is defined as $\sigma*(2*\log(n))^{1/2}$, where n is the signal length and σ is the SD of the noise (Donoho et al, 1995). Wavelet de-noising based on hard thresholding consists of taking the wavelet transform of the signal, multiplying the wavelet coefficients by the multi-resolution support and applying the inverse wavelet transform.

The FWT increases the possibility of finding ESPs transits in noisy light-curves as the process isolates the signals in the frequency bands of interest. The selection of the right wavelet is important for this process; the optimum setup for an ESP transit search can be obtained by comparing signature data generated from a simulation against the data from a real ESPs search. From the simulations (presented in next chapter), the best decomposition levels have been identified as seven to eight as the last approximate signal containing the signals corresponds to frequencies of possible transits which are typically longer than 1 hour (See Appendix F). The FWT can de-noise white Gaussian noise effectively. De-noising of red noise and finding a transit depends on the magnitude of the red noise and the characteristics of the red noise at the time of transit. Since red noise and ideal transit signals (noiseless) are in close low frequency bands, an estimate of the red noise present is useful to identify low frequency signals. The Fourier power spectrum shows that typical transit signal has a roughly similar spectrum to red noise and practically all the energy is concentrated in very low frequency band, i.e. frequency less than 5 cycles per day (this will be illustrated in Chapter 7 when analyzing the results).

Chapter 4

Simulation, Observations and Validation

4.1 Simulations

Simulations give the basis for validating the theoretical concepts used for describing the transit and the process used in the data handling. This gives an idea of the limits of the theory, possible outcomes and the conditions of the input data.

4.1.1 Search algorithms for Simulations

To evaluate the performance of TIAs and to also get confidence over detected transit level photometric excursions, a light curve simulation is necessary. Unlike the real data, simulated data can cover all the possibilities that may occur. A light curve containing 1% diminution in light, with 2 hours duration similar to a known transit curve would serve this purpose. For simulation for multi transits, different diminutions with different durations are added to the light curve.

The standard way to construct a synthesis light curve is to use a random number generator, which produces white Gaussian noise (WGN) for the virtual observations. While the study of individual light curves might be instructive on a case-by-case basis, a Monte Carlo (MC) simulation is truly needed to reliably compare the different detectors. More events yield more reliable results. The detection of planets via the transit method needs a thorough search through planet parameter space by varying the period and phase, and sharing a detection statistic obtained at each trial point in the parameter space.

The general steps of light curve simulation are:

1. Making a noise free light curve
2. Adding random Gaussian noise
3. Inserting coloured noise

Most of the transit search projects use MC techniques (Wall and Jenkins, 2003) to simulate the performance of the telescope network, performing simulations with different configurations of observations in order to optimize coordination of an actual campaign.

Anomalies are often present in light curves and more rigorous testing is necessary to determine whether any are statistically significant. There are numerous known and unknown sources of errors and variability even in a well-controlled photometric process and particularly so when using multiple data sets from multiple observers.

The setting of the transit detection threshold is often considered as a minor component in the simulations. The threshold is generally modeled as a minimum SNR of the transit detections assuming uncorrelated noise in the photometric data (Pont et al, 2006).

4.1.3 How to get limiting depths in a filtered light curve

The figure 4.1 shows that removal of higher frequency noise components in the light curve even keeps the original depth of the box the same as the depth of the filtered box shape. Hence it can be assumed that the depth of the signals in the approximated light curve gives the transit depth of the original system. The depth of the signal is proportional to the ratio of the planet radius and the host star radius (Equation. 3 section 1.4.6).

For all these calculations, the limb darkening is not considered. If limb darkening is considered the depth of the transit will be higher; hence calculations of the stellar parameters will be different. Generally, transits are generally 'U' shaped due to limb darkening, while grazing binaries give 'V' shaped transit curves.

4.1.2 Simulation with wavelets

Light curves with transits containing white Gaussian noise and red noise were simulated and then sub-band coding was applied. For the sub-band coding, different wavelets and different levels were used and the results were used for making a signature database.

For simulations, typical transit scenario curves were generated, and then the magnitude was normalized to 1000 for easy viewing (and resembling milli-magnitudes). To satisfy a typical observation environment, this light curve had 720 sample points representing a six-hour observation period with a 30 second cadence.

In wavelets, when the decomposition level increases it would affect the signal shape depending on the frequency components being filtered out. To show this effect, a square well shaped signal is used and its behaviour in removing higher frequency components for level 2, 5 and 7 is given in Figure 4.1. As high frequency contents are filtered out, the square wave shape becomes a half sine wave. It can be noticed that the depth of the signal remains almost unchanged up to level 7, at which further filtering is stopped. If a half sine wave signal is used instead of square wave signal input, the filtered sine wave shape remains, but the depth of the signal is reduced.

The use of a box shape test pattern for the transit shape is justified because most of the transits show a flat bottom with much less time in egress and ingress. The box-fitting technique (Section 3.1.5) and the correlation (Section 3.1.6) can be used in these last level approximated signals (also in last level detailed signals) provided that the pattern searched is a sine wave.

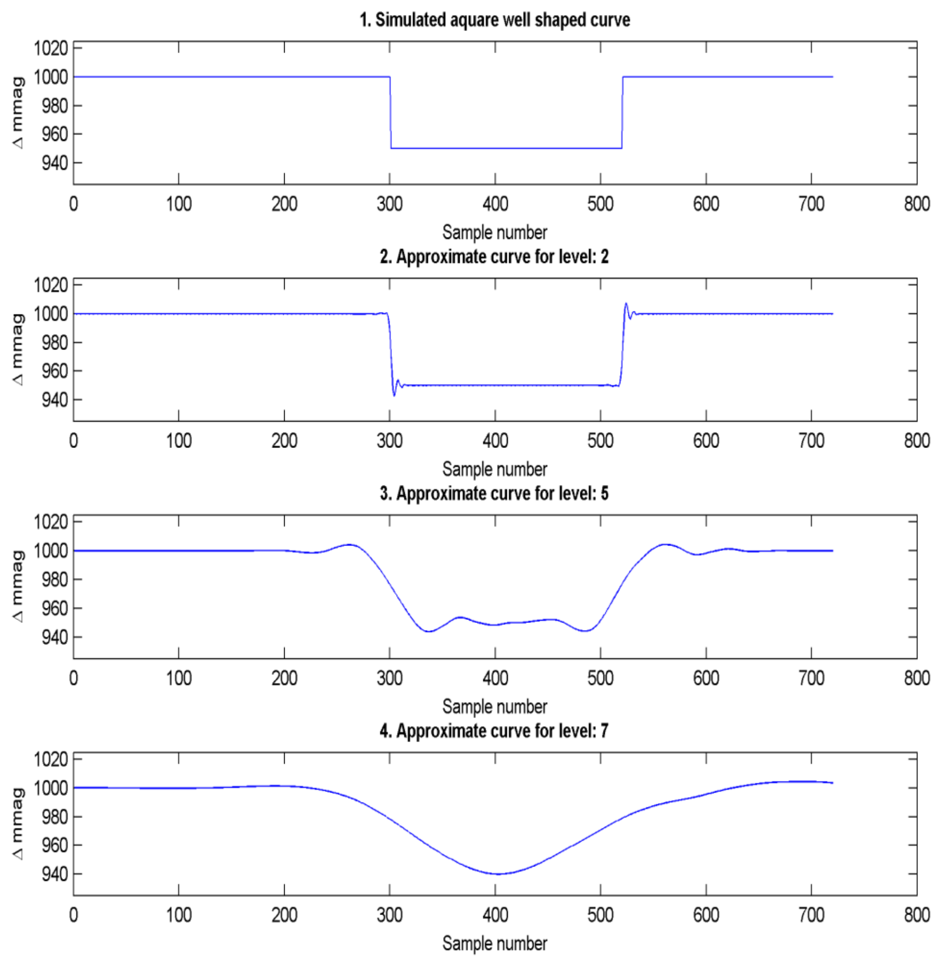

Figure 4.1 Illustration of behaviour of a square wave under FWT

To illustrate the behaviour of removing higher frequencies and approximation in a transit type signal, simulation was done with the transit depth set to three values, 5-15 milli-scales, where 5 milli-scale could be a grazing (lower R_p/R_*) transit while 15 milli-scales represents a typical value of a transit signal for a hot Jupiter around a solar-type star. White Gaussian noise with SD of 15 milli-scales(the same size of the full transit in order to hide the transit) and red noise are then added to the transit light curve assuming additive noise, so the resultant light curve has a hidden transit (see Figures 4.2a to 4.2c). If the depth of transit is d, and the SD of noise is σ, (considering white Gaussian noise only) then for this scenario d/σ indicates Signal-to-Noise ratio (SNR), which has nearly a unit value for Figure 4.2c. For a selected wavelet (e.g. Doubechies 7) and for different decomposition levels, the approximated signal was reconstructed using the MATLAB wavelet toolbox with the MATLAB default settings (see the Appendix G). This gives the signature signals for a transit for different wavelets at different decomposition levels. The increase of decomposition level of wavelets was stopped when the approximation signal (result from the wavelet analysis) at the last tested level contains the transit signal (See Appendix F for details). Figure 4.2a.1 is the ideal transit signal with transit depth of 5 milli-scales, while Figure 4.2a.2 has white Gaussian noise of SD of 15 milli-scales. Figure 4.2a.3 has simulated red noise and Figure 4.2a.4 is the combined signal of the transit, the Gaussian noise and the red noise. Figure 4.2a.5 shows the approximated signal at level 7. Figures 4.2b and 4.2c shows the behaviour when the transit depth is 10 and 15. Figures 4.2b.5 and 4.2c.5 show the existence of the transit of a half sine wave but for Figure 4.2a.5 the transit is too shallow to be visible.

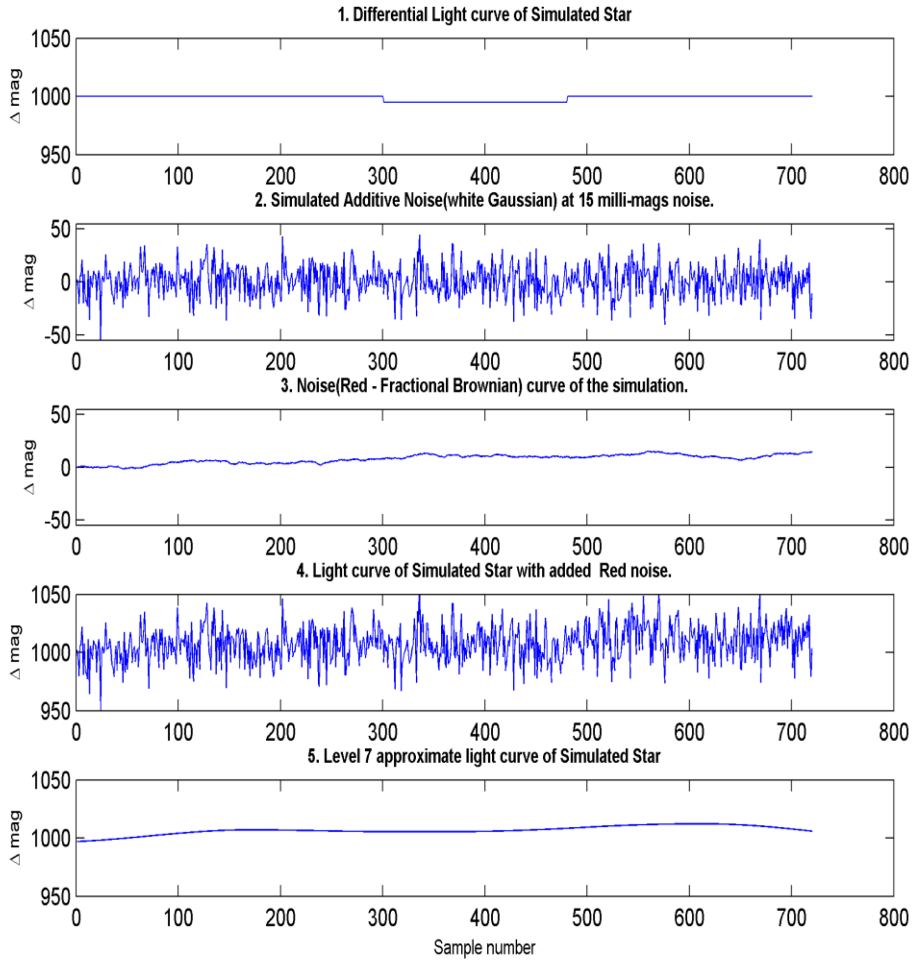

Figure 4.2a Behaviour of a square wave transit signal (5 milli-scales depth) with white Gaussian noise and red noise

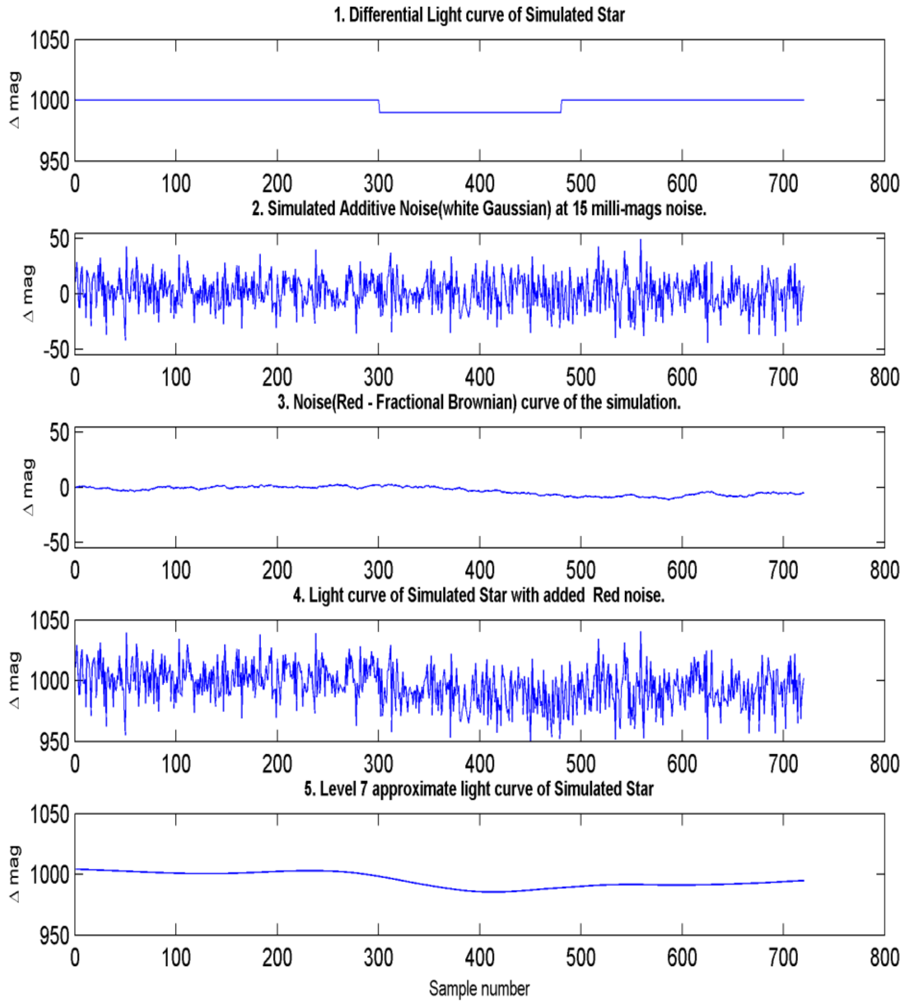

Figure 4.2b Behaviour of a square wave transit signal (10 milli-scales depth) with white Gaussian noise and red noise

Red noise is generated by Fractional Brownian motion using the algorithm proposed by Abry and Sellan (1996). In MATLAB, the Fractional Brownian motion (fBm) is a continuous-time Gaussian process depending on the Hurst parameter H ($0 < H < 1$) and length L. The Hurst parameter H is a measure of the level of self-similarity of a time series that exhibits long-range dependence. It generalizes ordinary Brownian motion which corresponds to H= 0.5 and whose derivative is the white noise. A value of H = 0.5 indicates the data is uncorrelated or has only short-range correlations, whilst the closer H is to 1, the greater the degree of long-range dependence. As stated before, Brownian walks can be generated from a defined Hurst parameter. If the Hurst exponent is $0.5 < H < 1.0$, the random walk will be a long memory process by definition. For simulations, red noise with H = 0.5 was generated by using MATLAB functions. This red noise component gives SD of 5.3 milli-scales.

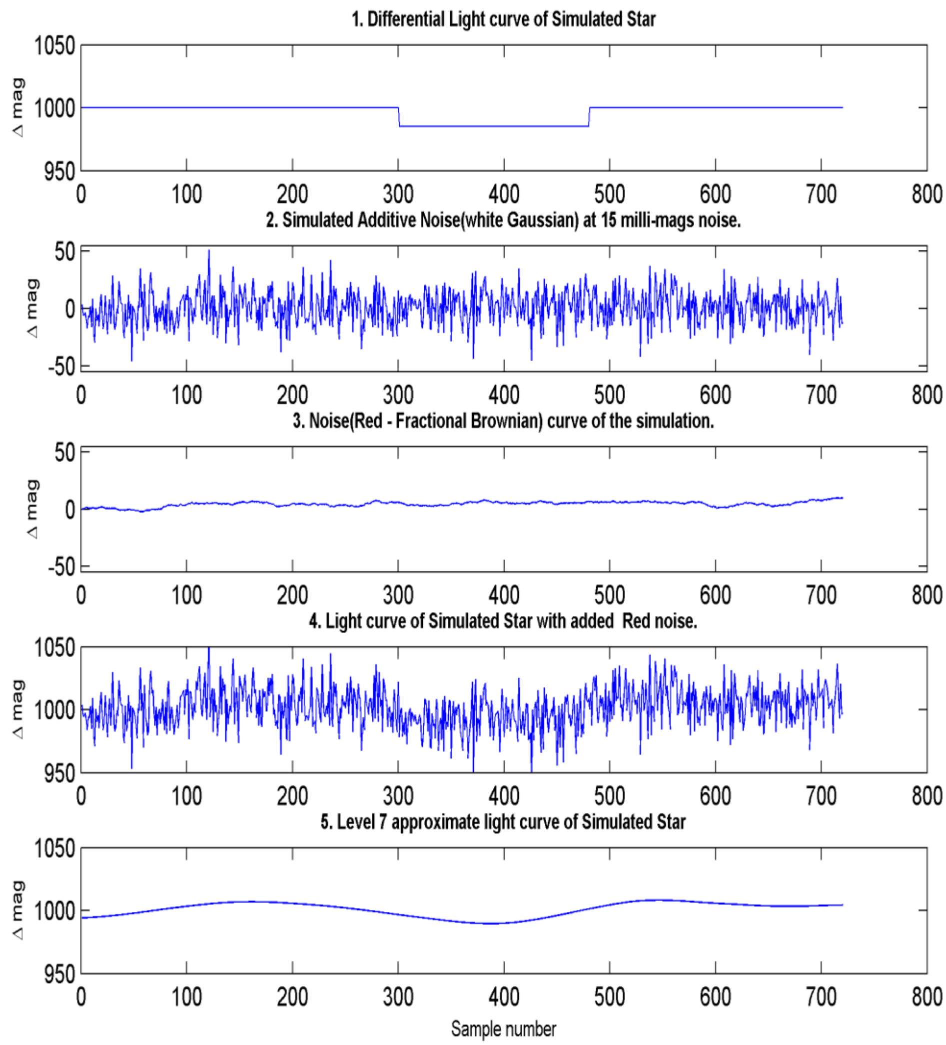

Figure 4.2c Behaviour of a square wave transit signal (15 milli-scales depth) with white Gaussian noise and red noise

The last simulation result shows that wavelet approximation based on filtering can recover a transit signal in the presence of red noise and white Gaussian noise (WGN). Since red noise is in the lower end of the frequency spectrum, a higher decomposition level is needed to remove it significantly. If the frequency components of the transit are higher than the band width of the selected decomposition level, this process will remove the sine shaped transit from the approximated signal of the chosen level but it will be retained in the detailed signal of a lower level. The approximated signal still can show a transit for different simulations of red noise while showing that a part of the fBm red noise has been filtered out. The approximated signal may have a visible transit, if the SD of the noise is less than the amplitude dip of the transit signal.

The Power Spectral Density (PSD) using FT of the signals of Figure 4.2[a-c] is given in Figure 4.3[a-c]. The peak of the combined signal varies toward the right with the input of the signal. The unit of x-axis is the frequency in dB (1/days). It can be seen that frequencies of red noise is concentrated at the lower end and frequencies of white noise is distributed over the frequency range considered (0 to 20 cycles per day). Since, the considered frequency range (-15dB to +10dB or 0.03 to 31 1/Days) is very short, PSD of the added Gaussian noise does not show the flat spectrum lines, however with a longer frequency range, PSD shows the standard flat spectrum lines. The sampling rate is 30seconds, i.e. 2880 times a day. The original signal mean has been removed from the input to the PSD calculations. As level 7 decomposition retains signals with periods more than 1 hour, all signals less than 24 cycles per days remain after filtering. The Lomb-Scargle (LS) periodogram gives similar PSD diagram.

fBm or red noise has relatively higher frequency components at very low frequencies and has the 6dB/octave decrease with increasing frequency. Though the magnitude of red noise is low in time domain, the energy in frequency domain is high; almost the same scale as the signal magnitudes in frequency domain. White noise in other hand has comparatively less energy in time domain as well as the frequency domain. For the signal, its mean has been removed to show the signal frequency components. Once red noise is added, for PSD mean cannot be removed from the final signal as is removes the red noise component. Hence, PSD of the final signal, red noise frequency components are dominated at the lower end and frequency components of the signal are dominated in the higher end of the plot. For the same reason, PSD of the approximated signal suffers from same red noise at the lower end. LS periodogram does not suffer from mean of the signal (DC value) and thus practically better analytical for getting periodograms, if one is interested in lower end frequencies.

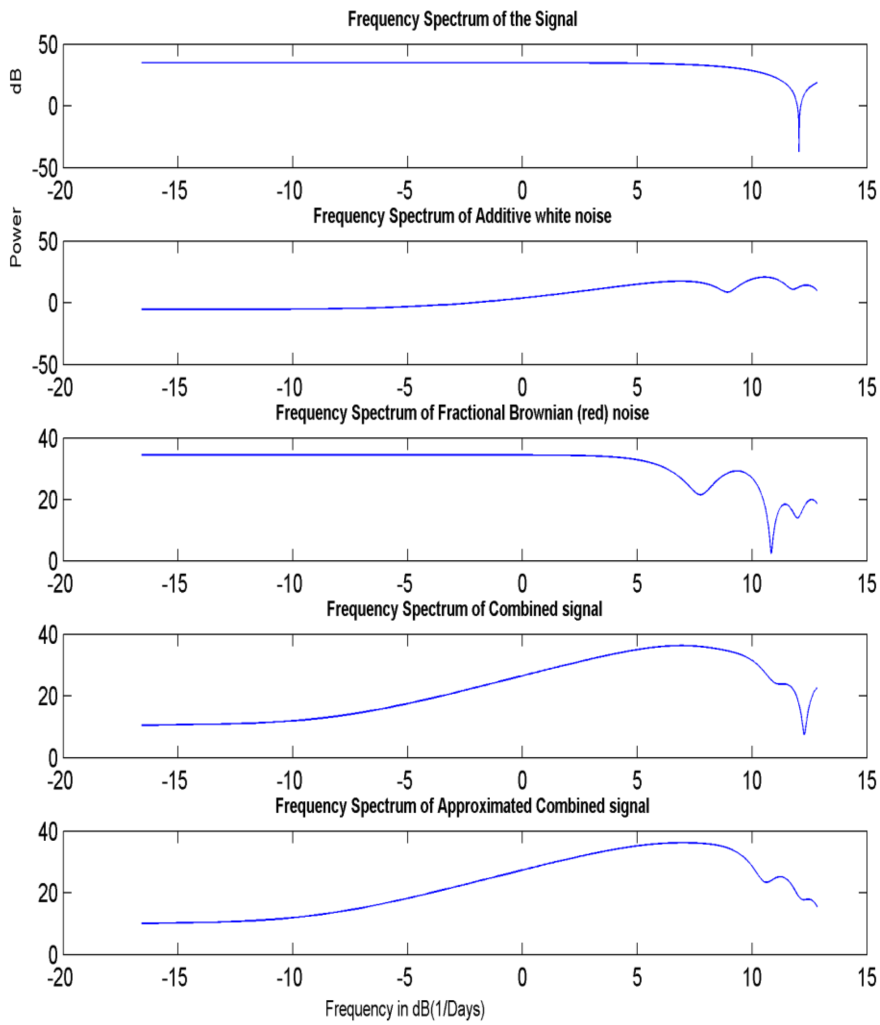

Figure 4.3a The PSD graphs of the signal of Figure 4.2a

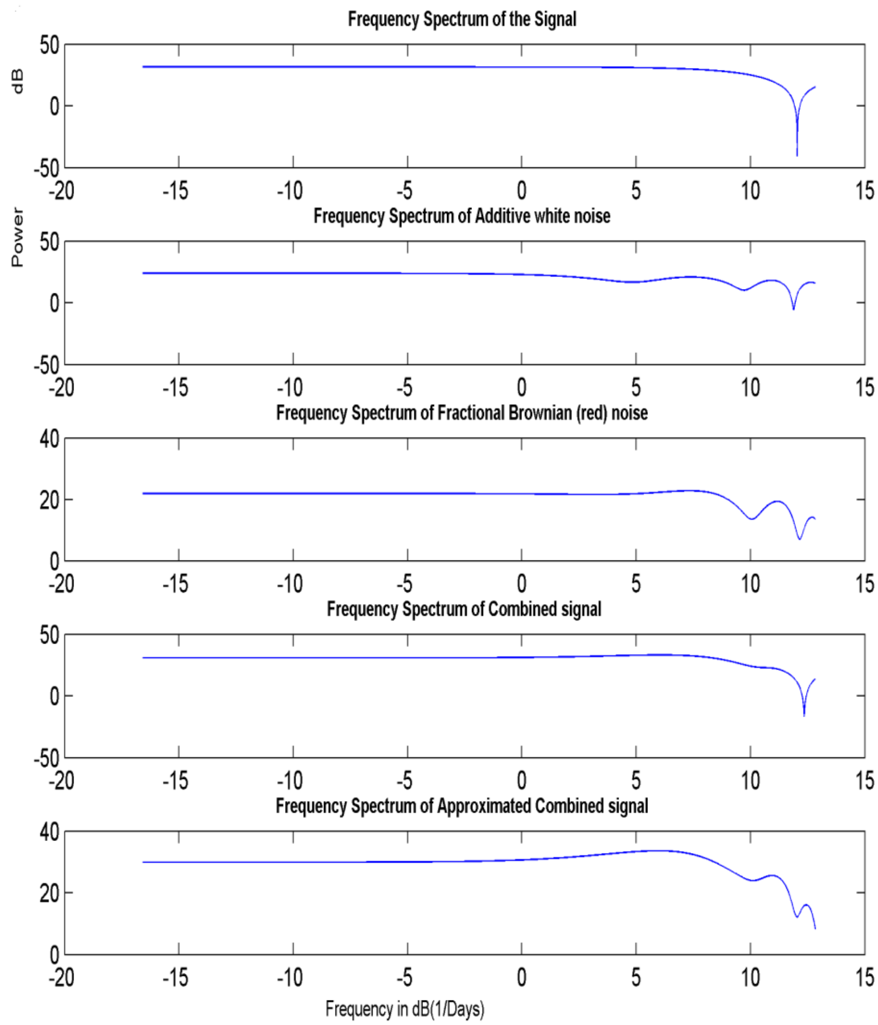

Figure 4.3b The PSD graphs of the signal of Figure 4.2b

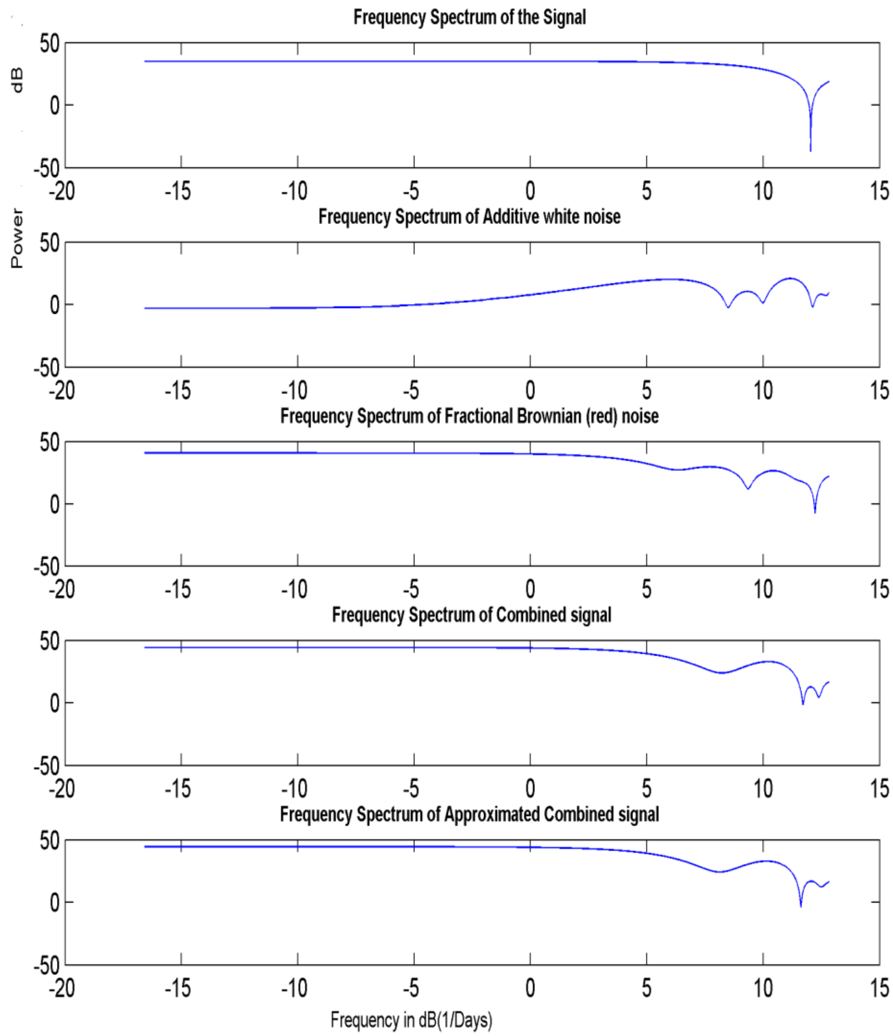

Figure 4.3c The PSD graphs of the signal of Figure 4.2c

Figure 4.3a frame 1 (Figures 4.3b frame 1 and 4.3c frame 1) clearly shows the FT of a square wave, the sync function (distorted under log scale) and Figure 4.3[a-c] frame 4, the combined signal shows the addition of sync function with other frequency components and this complicated form doesn't indicate existence of transit clearly.

The next figure (Figure 4.4) shows the behaviour of a recurring transit signal (with 15 milli-scales) simulation. Figure 4.4 frame 5, the approximated signal at decomposition level 7 shows traces of transits.

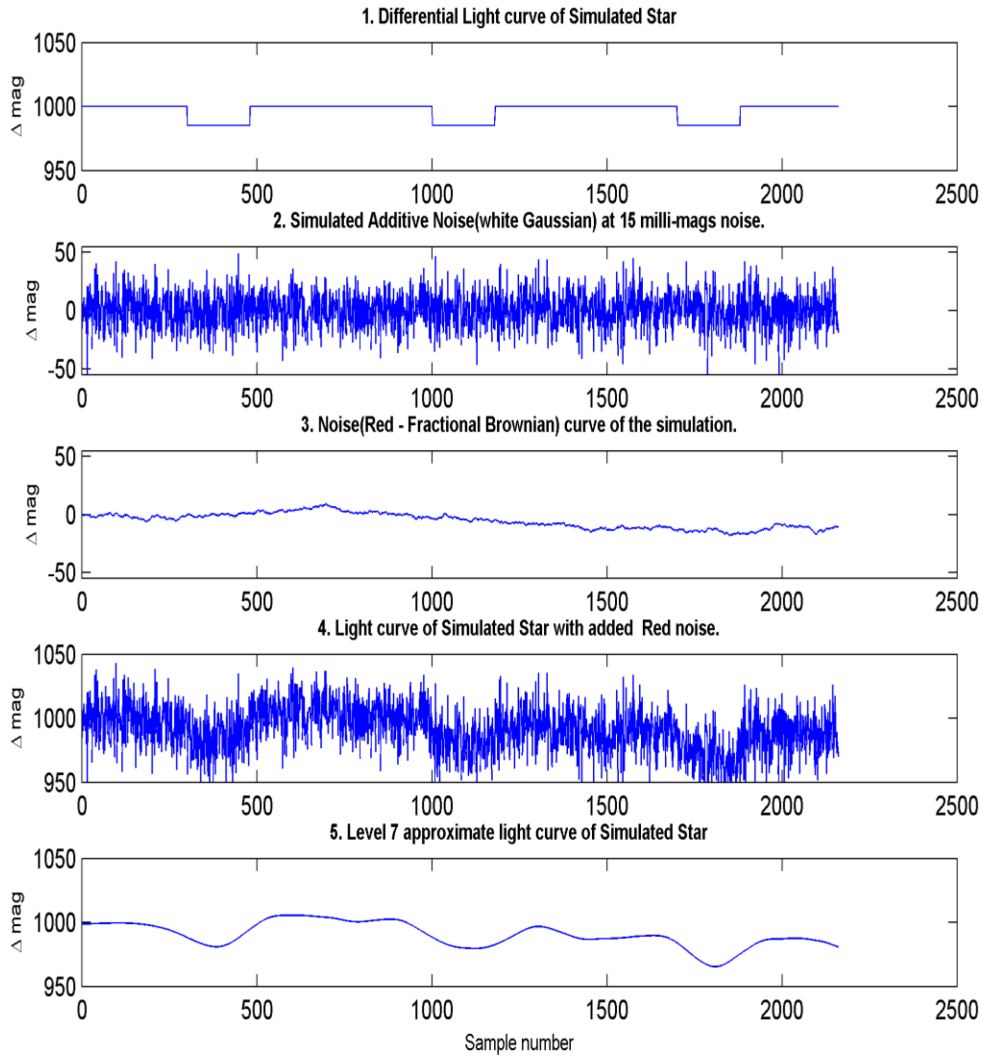

Figure 4.4 Behaviour of a multi transit signal with white Gaussian noise and red noise (15 milli-scales)

Figure 4.5 shows the PSD diagram of the Figure 4.4. It is similar to the PSD graphs of the Figures 4.3[a-c] with a sync function in Figure 4.4.1. The simulations show that the approximated signal is dependent on the behaviour of the red noise component while this component is effectively free from white Gaussian noise. If the red noise component does not change more than few milli-scales during the observation window of a transit of 15 milli-scales, then a transit dip can be identified easily. Decomposition level of 7 is the optimum for finding the transit of more than one and half hour (See the Appendix F).

When the red noise is present at the 5 milli-scales or higher level, simulations show that it is hard to detect a transit by using FWT approximation. When the amplitude of the red noise exceeds the transit depth, false alarms can appear.

Since the red noise (due to the systematic changes) can change quicker than the re-occurrence of the transit signal, the red noise then has higher frequency components (approximately Figures 4.3.4 and 4.3.5) than the transit signal.

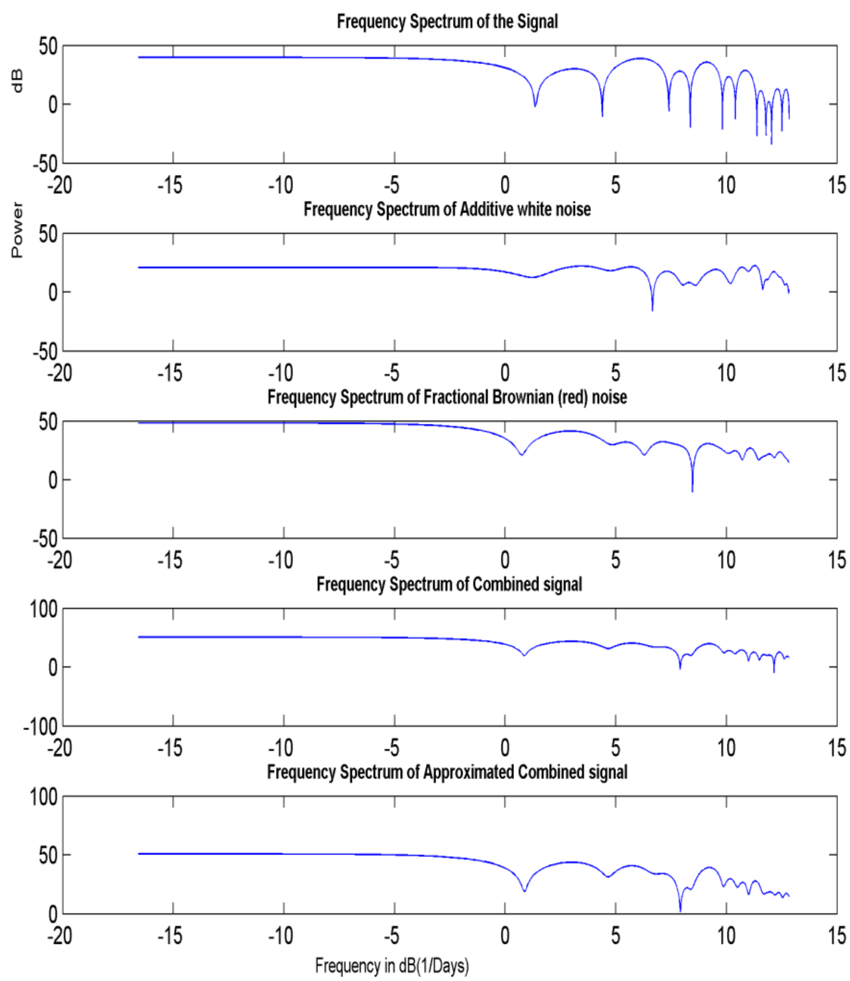

Figure 4.5 The PSD graphs of the signal of Figure 4.4

For these simulations, it was assumed that SNR is less, i.e. SNR < 3. If SNR is more than 3, the transit can be seen from naked eye, and as transit is obvious there is no need to do de-noising.

4.1.2.1 Simulations for variable stars

Since our target is an open young cluster, the cluster must have plenty of variable stars; hence we simulate light curves for variable stars (Figure 4.6). With all other similar conditions as in Figure 4.2, the approximated curve does not show any clear signal with variability as it has been filtered out.

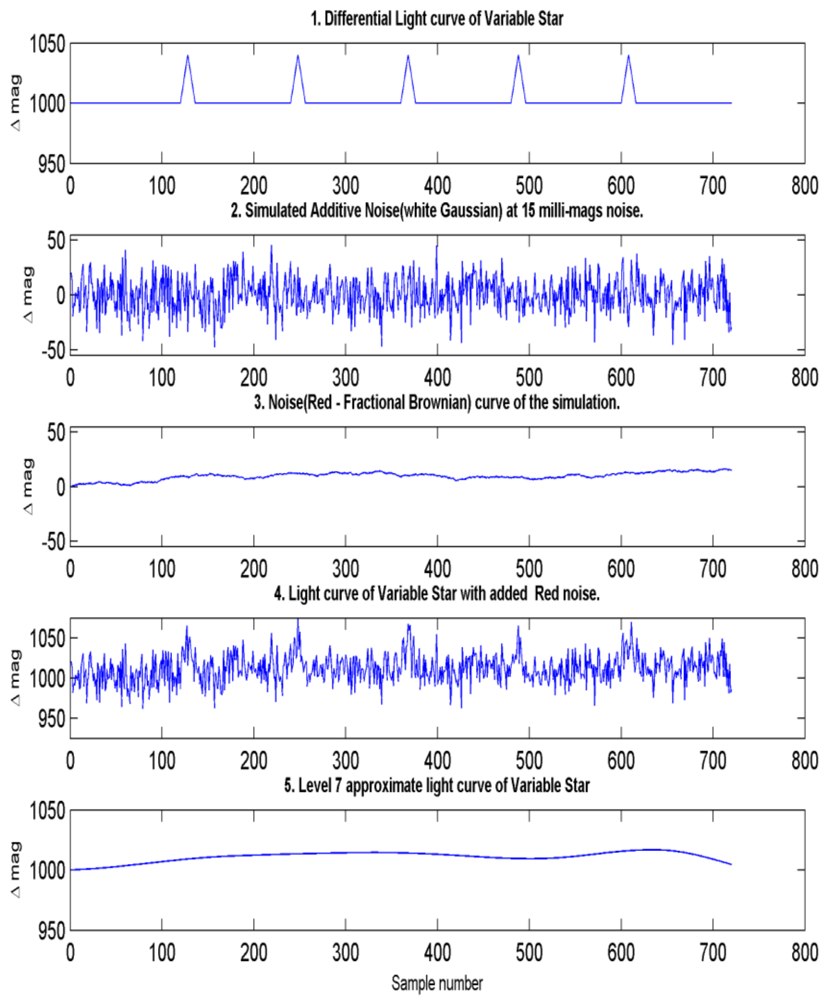

Figure 4.6 Behaviour of a variable star light curve with white Gaussian noise and red noise

The PSD graphs of the signals of Figure 4.6 are shown in Figure 4.7. The PSD of the original signal shows the repeating frequency patterns. The invisible signal traits in Figure 4.6 are visible in Figure 4.7 in the frequency domain (before de-noising). De-noising may remove pulse if the cyclic time is very small and if the pulse is very narrow (like impulse function) there is a good chance FT detects the signal. The stellar patterns of variable stars are different to each other and they are unique to the star. The simulations for a pure sinusoid and two beating sinusoids (simulating possible Beta Cepheids) are given in Figure 4.8 and Figure 4.10 respectively.

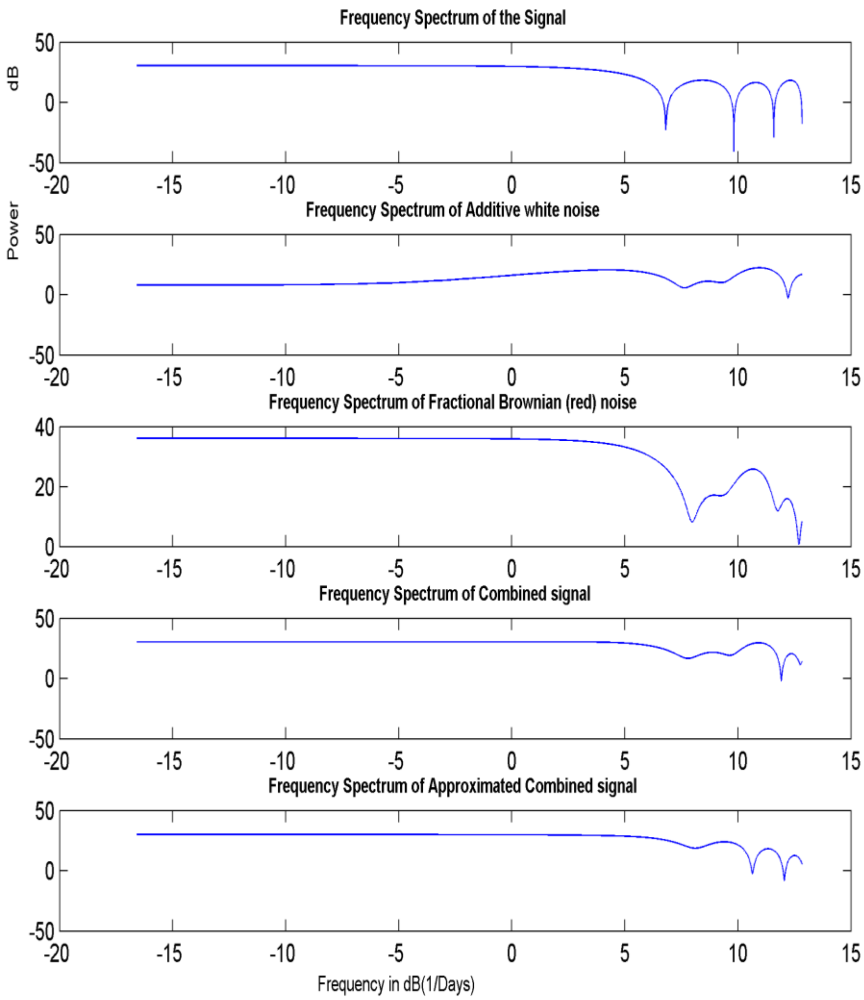

Figure 4.7 the PSD graphs of the signal of Figure 4.6

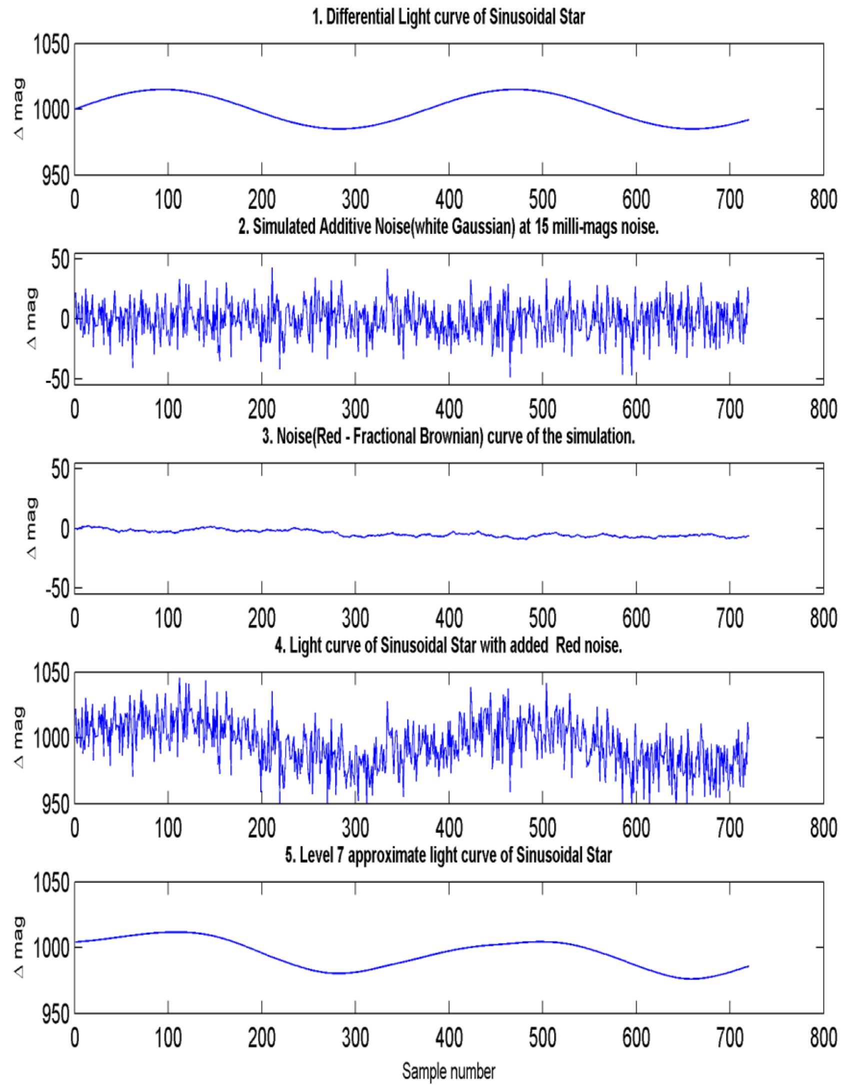

Figure 4.8 Behaviour of a variable star (sinusoid) light curve with Gaussian noise and red noise

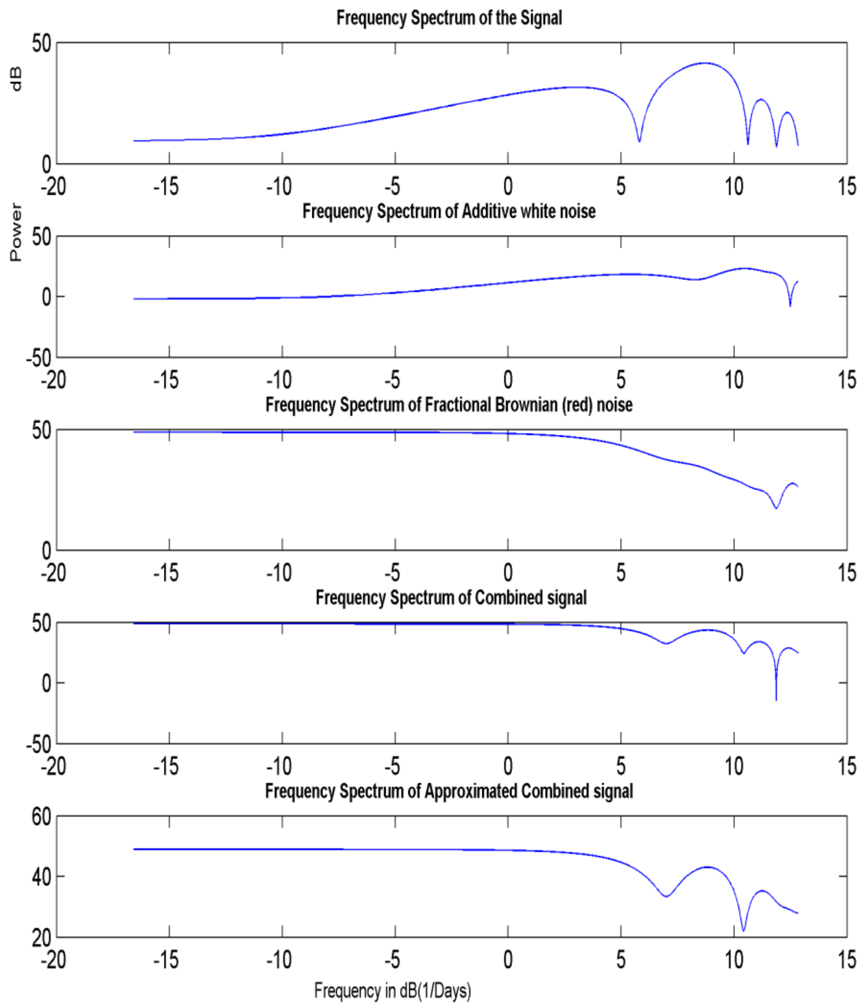

Figure 4.9 The PSD graphs of the signal of Figure 4.8

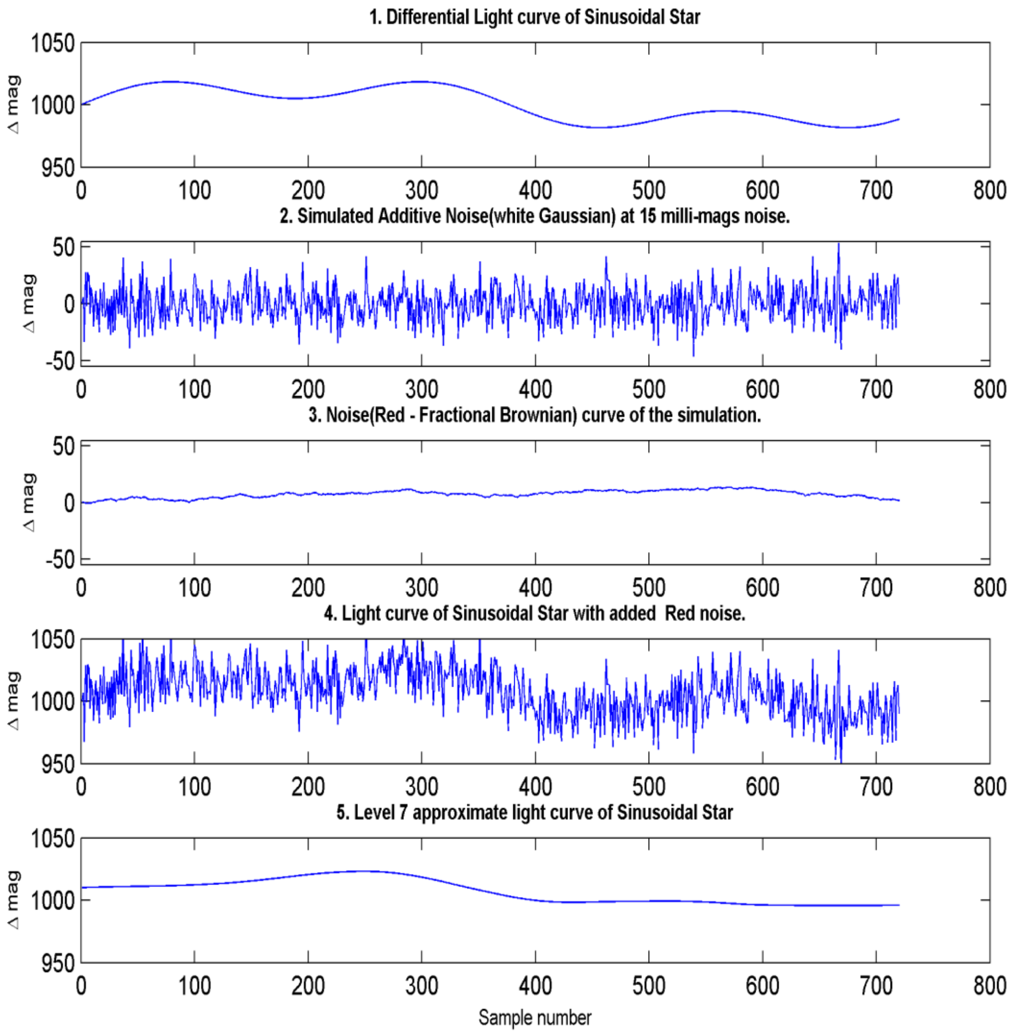

Figure 4.10 Behaviour of a variable star (two beatings) with Gaussian noise and red noise

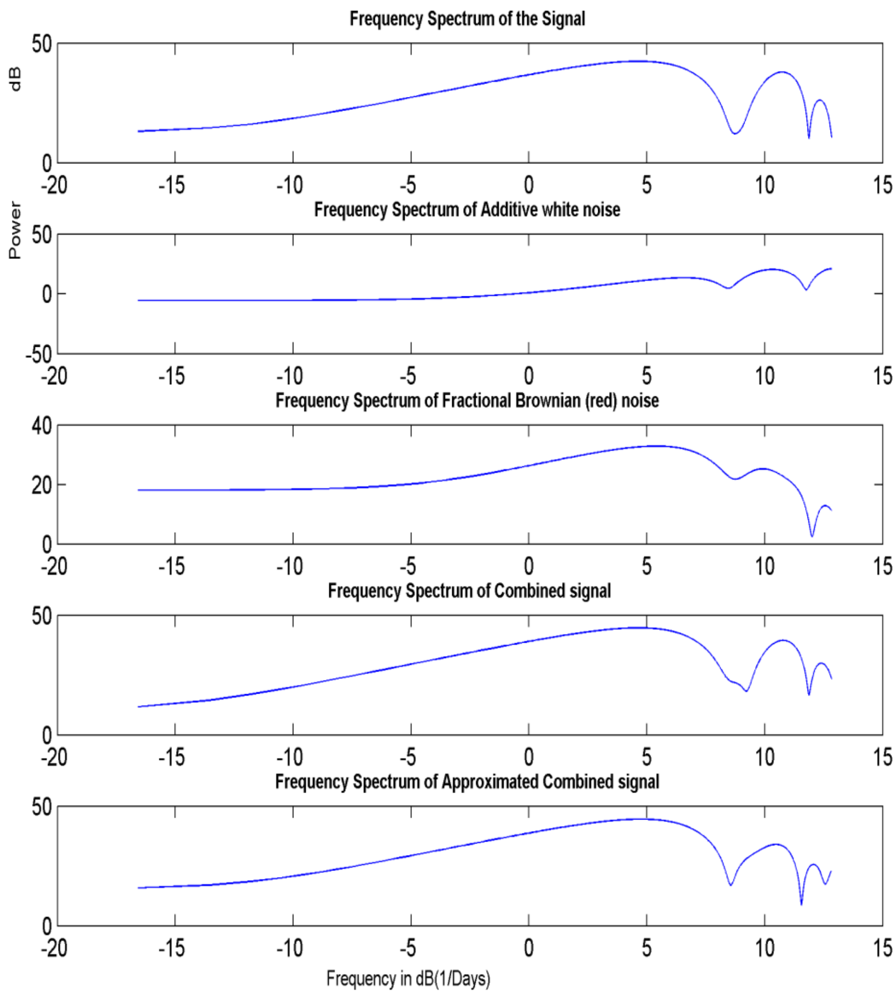

Figure 4.11 The PSD graphs of the signal of Figure 4.10

Transit depth milli-scales	depth/SD of WGN (σ = 15 milli-scales)	Red noise with H=0.5	Results
5	1/3	Yes	Transit is hidden
10	2/3	Yes	Transit is visible
15	1	Yes	Transit is visible

Table 4.1, Summary of the results of simulations under different transit depths at level 7

Variable star trait in Red noise and Gaussian noise	Time series- De-noised	Frequency domain
Periodic pulse	Not clear	PSD[18] clearly shows
Sinusoid	Clear (depend on noise level)	PSD clearly shows
Two beatings	Can be seen, depends on noise level	PSD clearly shows

Table 4.2, Summary of the results of simulations for variable stars at level 7

Using different de-noising methods listed next, a signal with combined Gaussian noise and red noise (the signal in Figure 4.8 frame 4) is de-noised. The software routines used are available in the MATLAB wavelet tool box. This de-noising generally works with a signal model of $s(n) = f(n) + \sigma\, e(n)$, where time n is equally spaced. In the simplest model, suppose that e(n) is a Gaussian white noise N(0,1) and the noise level is supposed to be equal to 1. The de-noising objective is to suppress the noise part of the signal s(n) and to recover f.(n)

De-noising methods used;

1. The principle of Stein's Unbiased Risk Estimate. (SURE) - An estimate of the risk for a particular threshold value (Coifman and Donoho, 1995).
2. The universal threshold in the fixed form
3. Minimax thresholding - an estimator that realizes the minimum, over a given set of functions, of the maximum mean square error.

Minimax and SURE threshold selection rules are more conservative and are more convenient when small details of function ‘f ‘ lie in the noise range[19] .

---

[18] Power Spectral Density

[19] http://www.mathworks.com/access/helpdesk/help/toolbox/wavelet/wavelet.html?BB=1

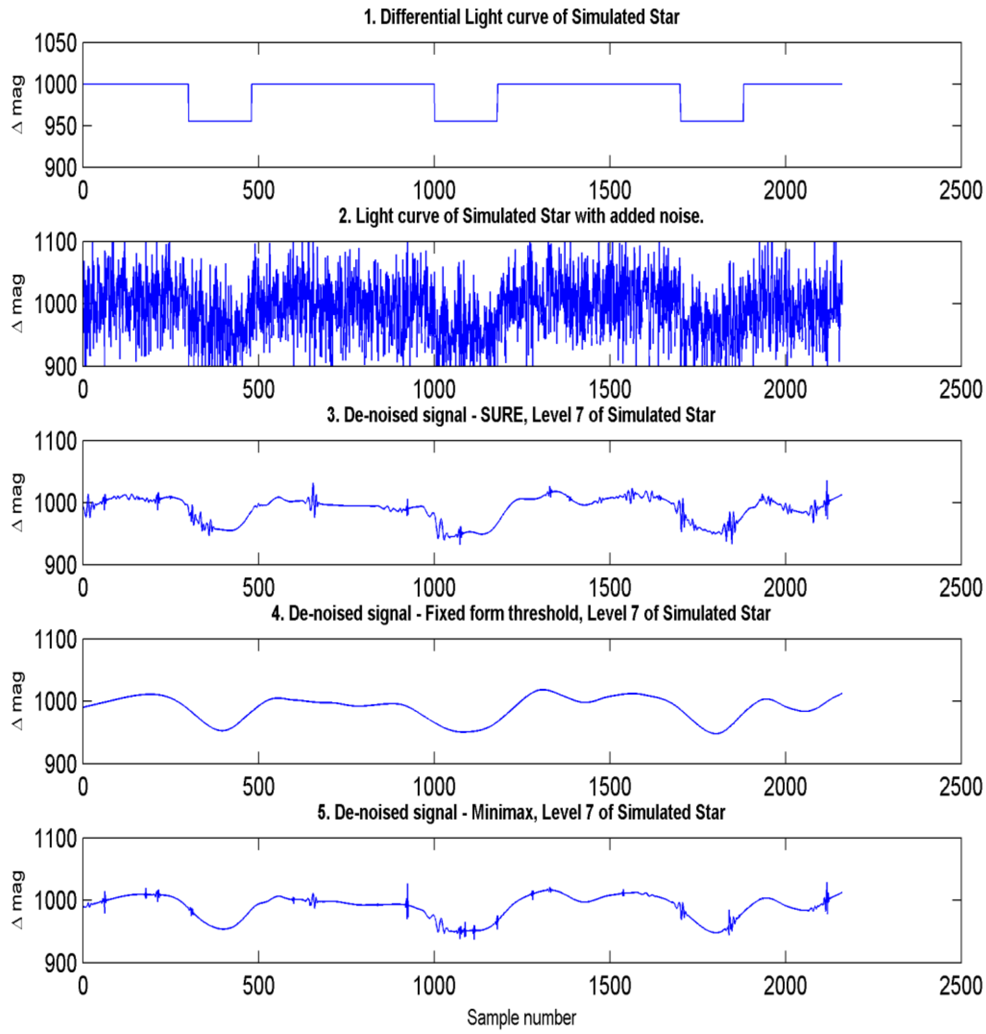

Figure 4.12 Time domain illustration of de-noised method.

Figure 4.12 shows the time domain de-noised signal while Figure 4.13 shows the PSD graph of the signals in Figure 4.12.

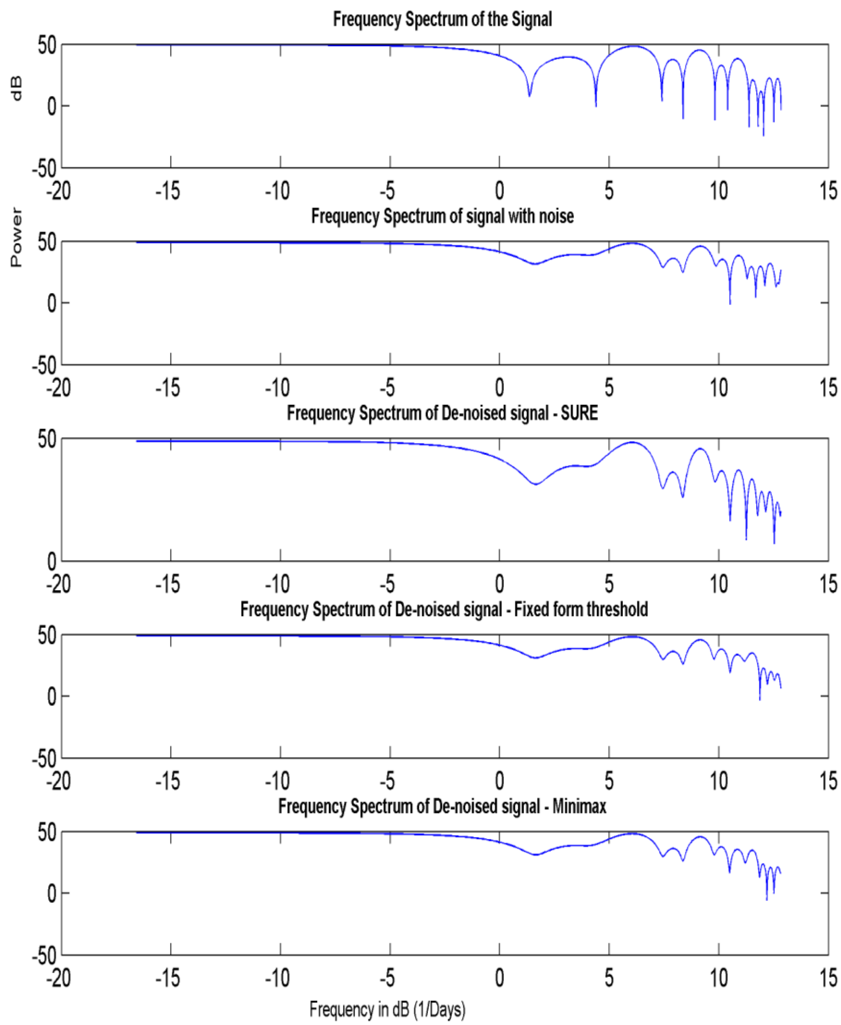

Figure 4.13 Frequency domain representations (PSD) of de-noised methods.

4.1.4 Probability of Transit finding

An observing schedule is necessary when conducting transit surveys to maximize the chances of observing transits. The factors which determine the length of the schedules are:

1. Number of observing hours available per day
2. Minimum duration of expected transits
3. If one night (or more) of scheduled time is missed, provisions are needed to recover data in the missing observing window(s)

The observing hours per day depends on the human resources available and time of the year. Six hours of observing period is assumed for this simulation.

The algorithm for finding the length of the observing period needed to cover ‘N’ number of full days is based on the assumption that multiple orbital periods of planets fit-in at least one of the observing windows (Figure 4.14). If the ESPs have orbital periods of multiples (or very close to) of one Earth day, there is a possibility that these transits will never be caught because the transit dip occurs in the day time. The observing season is important since in summer less observing time is available.

Figure 4.15 gives the probability of finding a planet with known period and Figure 4.16 gives the probability coverage of all transits less than a given transit period (or an observation time span). The logic of the calculations is based on a random variable representing the phase of the planet where the phase represents the relative position of the planet with respect to the star as seen from Earth. For each value of period, the total probability is calculated using a big number (say one thousand, a compromise between resolution and computational time) of random phase values. If the sum of the phase and the beginning of the first observation window, minus the period falls into an observation window, a transit occurred. The probability per period is defined as the ratio of the number of successful transit events found and the number of iterations (for different phases).

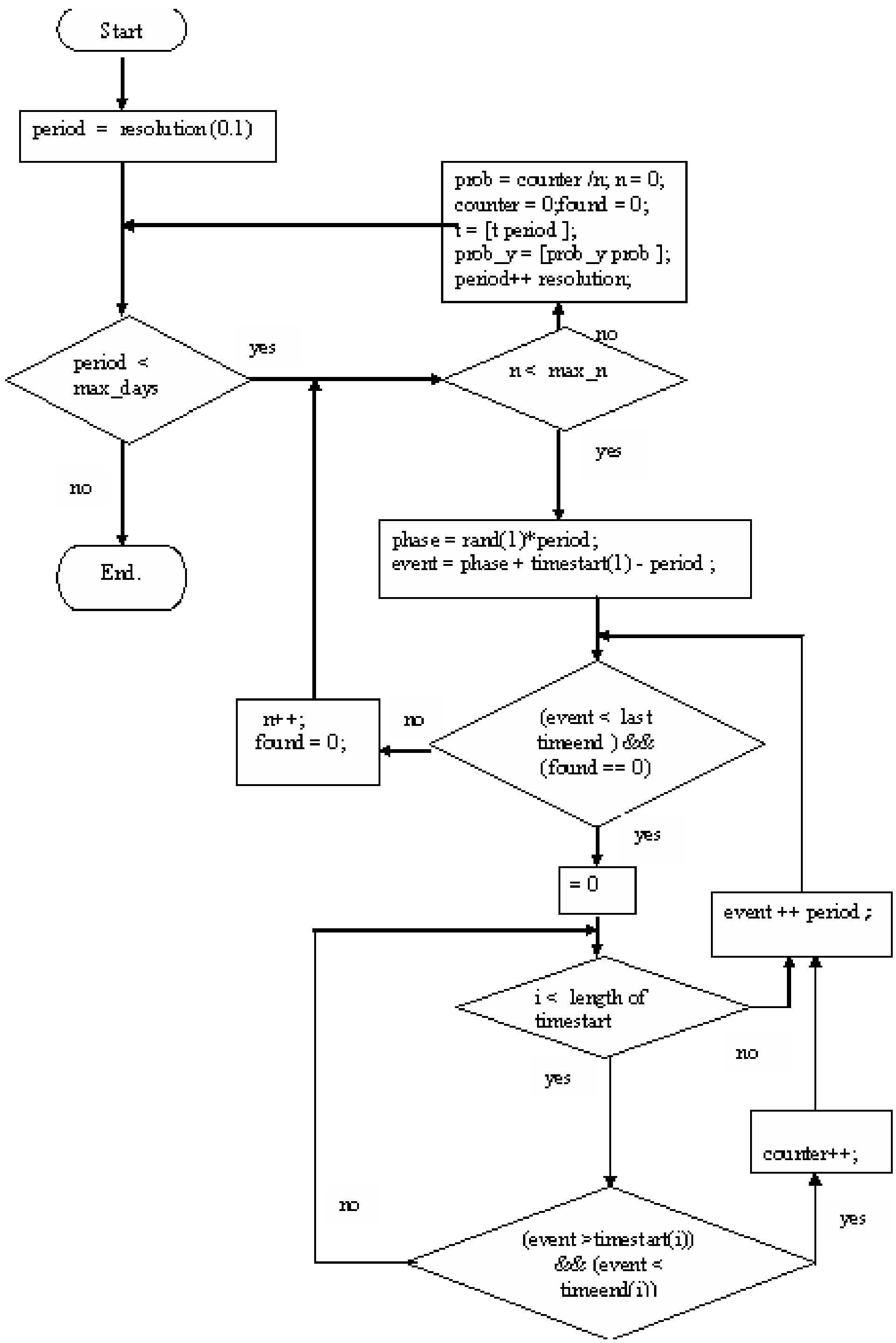

Figure 4.14 Logic used in calculating probability of transit

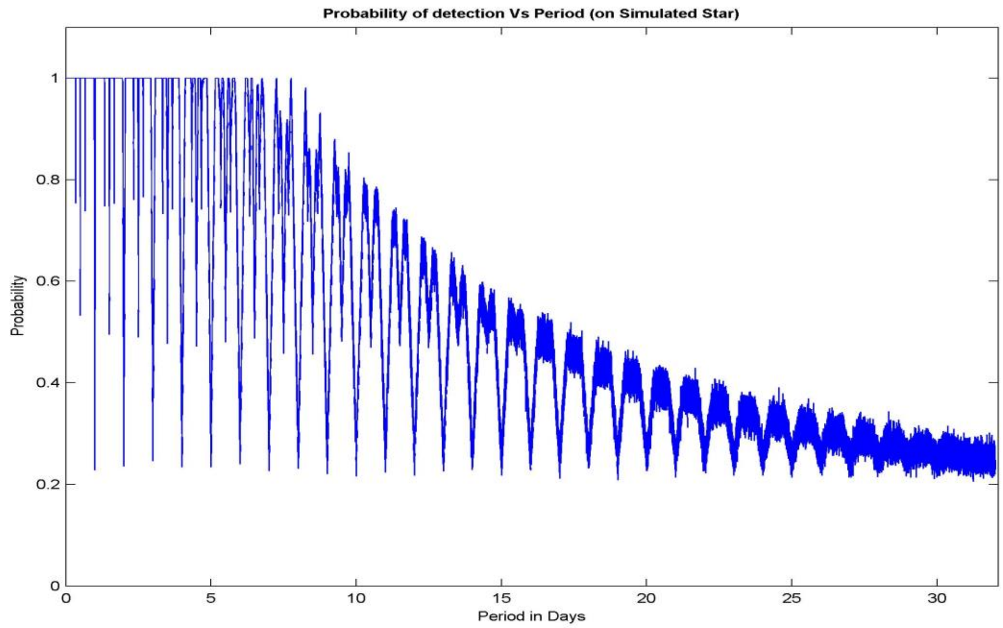

Figure 4.15 Probability of finding a planet with known period using simulated data

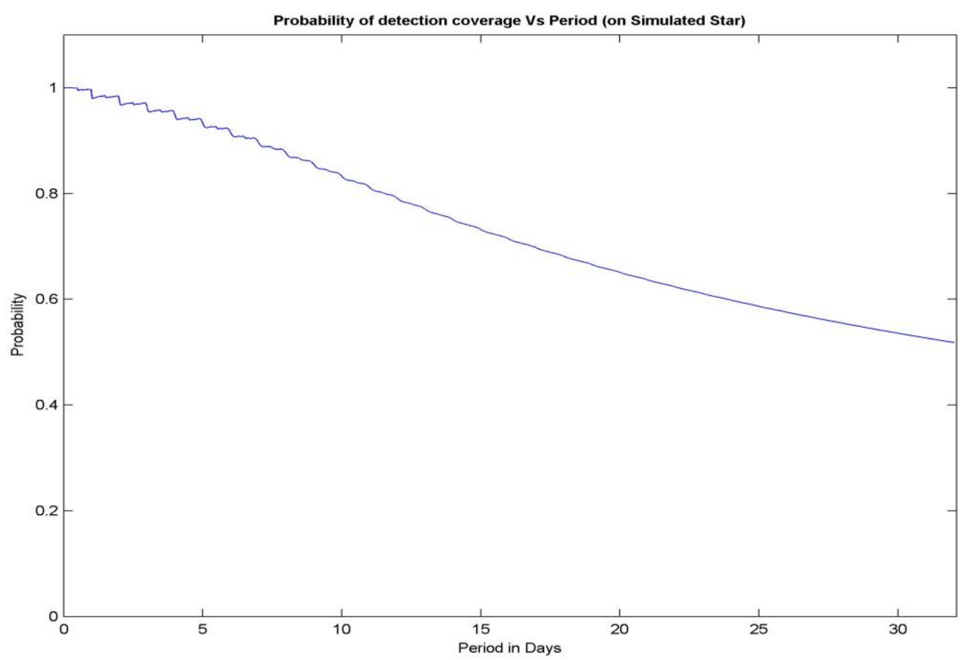

Figure 4.16 Probability of coverage of transits of known period for data used for Figure 4.15

4.1.5 Probability of Missing Transits

For a given set of data, there is a possibility that a transit can still exist, but the process missed the identification of that incident. This possibility was calculated by the method developed by LaFreniere et al (2007). This method uses following statistical equation,

$$F_{max} = \ln(1 - \alpha)/N\langle p \rangle$$

When N is sufficiently large, we assume that using Poisson statistics is valid, so the probability of having transiting ESP is smaller than Poisson statistics.

F_{max} is the maximum percentage of transiting ESPs that could still be there given a sample size of N stars with the probability of a detection per star being <p> and α is the certainty. Setting $\alpha = 0.95$, it can be determine the maximum number of transiting ESPs that could have been missed with a certainty of 95%. <p> is determined by Monte Carlo simulation for a given orbital period (Section 4.1.4) and N is found by the number of light curves with RMS noise value less than pre-determined threshold. Once <p> and N is determined, a value for F_{max} can be found.

Baraffe et al (2003) models on brown dwarfs and ESPs, indicates that 7 million year old hot Jupiter could have a radius of $2.0R_{Jup}$ if it has a mass of $10.0M_{Jup}$ and a radius of $1.7R_{Jup}$ if it has a mass of $1.0\ M_{Jup}$. A transit by Jupiter over the Sun would produce a transit depth of 0.0105 (Zombeck, M, 1990). The transit depths for a 2.0 and 1.7 R_{Jup} ESP would be 0.0067 and 0.0048.

ESP transit depths for different spectral types and radii are given in table 4.3.

Spectral type	1.7 R_{Jup}	2.0 R_{Jup}
A0	0.48%	0.67%
A5	1.0%	1.4%
F0	1.5%	2.1%
F5	2.1%	2.9%
G0	2.8%	3.9%
G5	3.5%	4.8%
K0	4.2%	5.8%

Table 4.3 Transit depths with Spectral types.

Using these depths of the spectral types, a box shaped transit is induced into the light curves of faint stars of the NGC 4755 vicinity. These stars are of type A or latter spectral types. The resultant curve is checked for possible transits and later by de-noising.

4.2 Observations

A transit search requires milli-magnitude photometric precision of time scales of weeks to months. Simulations are needed to determine possible results that would be obtained and to tune the observation process for better results.

4.2.1 Preliminary Studies

The transit search at JCU was first performed by using REST data for the nearby stars, GL 581 (Jayawardene et al. 2007) and HD 27894, before moving on to observe open clusters. None of these field searches found a transit, but it was an opportunity to test the algorithms and to tune the systems. GJ 581, a small M2.5 dwarf (R^{*}= 0 .299 R_s von Braun et al. (2011)), is known to host up to 6 planets.

4.2.2 The Distance to the object

This transit search is originally based on the assumption that 3% change of the magnitudes can be determined for stars of 'V' magnitude of 14 on the camera. As young hot Jupiters can have a radius of more than R_{Jup} (Chabrier et al, 2006) and the young parent star radius is not much different from that of a mature star, the transit depths can be bigger than those for older stars; making a bigger change in the flux (Cassen et al, 2006).

Assuming the stars being observed are those that are solar-like (i.e. from F5 to K5), the maximum distance can be computed from

$$m - M = 5*\log(d) - 5$$

Assuming a limiting magnitude m = 14 for band R, and assuming an absolute magnitude M_R for F5 star = +3.4, M_R for G5 star = +5.1 and M_R for K5 star is +7.3, the maximum distances that the search can detect a star with limiting magnitude of 14 are:

F5 = 1320 pc

G5 = 600 pc

K5 = 220 pc

If M_R is 12, then the distances are:

F5 = 530 pc

G5 = 240 pc

K5 = 90 pc

For those calculations, NGC 4755 is little too far away (1976 pc). If an accurate star tracking is available and if the photometry process can still identify a 4% change of the magnitudes (as COROT does[20]), then finding a transit is still possible by going deeper. This cluster is still young (8-10 million years old) and, having younger hot Jupiters, there is still a possibility of finding a transiting planet. Since the magnitude 14-distance limit of a F5 spectral type star is 1320 pc; it is unlikely to find any cluster F5 stars brighter than magnitude 16.

If M_R is 16, then the distances are:

F5 = 3310 pc

G5 = 1510 pc

K5 = 550 pc

If cadence is increased to 5-10 minutes, we can go deeper up to magnitudes 15-16. Interstellar reddening affects the stars brightness, thus affecting the distances calculated.

4.2.3 The telescope

The FITS images of NGC 4755 were obtained from the RAE Perth Internet Telescope at Perth Observatory. In 2005, the Perth Observatory acquired a fully robotic Internet Telescope from the Real Astronomy Experience (RAE) of the Lawrence Hall of Science at the University of California at Berkeley. This telescope is mounted in the "University Dome" of Perth Observatory at longitude 116^o East and latitude 32^o South. The RAE telescope is a Celestron C14 on a Paramount mount and has an Apogee AP7 CCD camera with no anti-blooming and a selection of filters. This has a focal length of 40 cm. The RAE telescope at Perth Observatory can be operated remotely utilizing the Internet.

The CCD images capture information and Telescope parameters given in Table 4.4.

[20] www.corot.com

Exposure time:	30 seconds
Image size:	512 Pixels wide X 512 Pixels high
Pixel size:	24.0 x 24.0 microns
Exposure state:	ABG-Low Rate DCS - Yes DCR – No
Temperature:	Approximately -20˚ C
Response factor:	2000.00, 1.00 e-/ADU
Focal length:	4.1 m
Aperture diameter:	0.4 m
Optical filter:	R [J-C std] Standard color band of image

Table 4.4 CCD Parameters

Figure 4.17 The RAE Robotic telescope at the Perth Observatory

4.2.4 Data acquisition and reduction of the images

The telescope was programmed remotely via observer submitted schedule files. The sampling interval of consecutive FITS frames is about 42 seconds. MaxIm Dl version 4.58 was used to process CCD images with bias, dark and flat corrections. The telescope was refocused in every 100 images. While observing, the telescope would point somewhere along the meridian, take a brief exposure and return to the target for every 100 images. This was done to correct the track which slowly drifts over time. Hence, having the telescope take a meridian image resets the tracking. As turning the telescope off was tried during a meridian crossing, there are gaps of 10 to 20 minutes in each night's data. Since the camera is fixed for every 100 frames before it was re-centered, as time passes and the apparent sky positions move westward, stars at the edge of the reference frame (stars at the Western side of the cluster) move out of the FOV. The drift of the center of the frame towards the eastern edge at the 100th image was less than 1/3 of the width; hence nearly almost all stars selected were in the all frames. Upon completion of observing, and after bias, dark and flat file correction, the data sets were backed up on DVD and posted to the author. Telescope programming, dark and flat file corrections were done by Dr. David Blank and Arie Verveer of the Perth Observatory. The rest of the data reduction process was semi-automatic using a Linux version of IRAF and C++ routines developed for this search. IRAF routines (daofind, tvmark and phot) were used to do the data reduction using aperture photometry. For given photometric values, e.g. aperture, SD, image-centering algorithm, minimum flux count, etc., IRAF identified the point sources in the FITS image.

CCD temperature:	-20°C, +/- 0.1°C Stable during all observations
Read out Noise	7-11e
Air Mass:	1.33E0 (multiple of zenithal air 8mass)
Bias Subtraction:	Bias 2, 512 x 511, Bin1 x 1, Temp -20C, Exp Time 0ms
Dark Subtraction:	Dark 7, 512 x 511, Bin1 x 1, Temp -20C, Exp Time 300s
Flat Field:	Flat R 1, R, 512 x 511, Bin1 x 1, Temp -20C, Exp Time 50ms

Table 4.5 FITS header Parameters

Moon light affected the light flux as the full moon was inside the observing window. Since differential photometry was used for the reduction, it is assumed that this issue has minimum effect for the calculations. As the camera uses anti-reflection coated silica windows and forced air-cooling, seeing errors have been made minimized.

A quick look at the CCD images reveals that some bright stars (NGC 4755 1-4 and BU Cru) have been saturated in all frames and blended into the nearest stars, this is worst for the stars at the centre of the cluster, where many stars are concentrated. This not only made the bright stars unusable but it created diffraction spikes around nearby stars of the CCD frame, thus making the other faint stars near the saturated star unusable. However, the blended light curve can also be caused by an eclipsing binary.

For each data set per day, a master frame was selected, stars were marked and the master frame was used to generate coordinates of the stars in the other frames of the set. In this selection, all blended stars were avoided. These coordinate marked frames were directly used with IRAF 'phot' utility to get the flux of each star. Twelve pixels were used as the aperture radius and the aperture circle was taken as 20 pixels. All data sets were subjected to a pre-validity-test (check for zeros, infinity and the upper limit of the flux count) to make sure the flux was reasonably valid. The combined routines gave an ASCII file with all-star parameters. These parameters were extracted as per star data for later processing using MATLAB routines (wavelet related routines are in Appendix H) in differential photometry, signal processing, plotting and archiving. The aperture size affects the precision of the differential photometry, thus the best aperture was selected for stars by trials on a few stars of the data set through empirical testing of several different aperture sizes. Since all stars of the cluster are chosen as a group for semi-automated reduction process, this aperture is not the optimum for all the stars of the cluster. An aperture which is too small will give pixelization of the detector and possible centering errors, while a larger aperture will generally have noise associated with unwanted sky pixels.

The data was de-trended before it was plotted and used for further analysis. For de-trending, there are two types of problems any trend filtering algorithm must tackle (Kovacs et al, 2005)

- Increase the detection probability by filtering out trends from the composite signal.
- Restore the signal form by filtering out trends from periodic signals, assuming that period is known

To remove systematic trend, there are several algorithms which have been already published, such as TFA for MACHO (Szulagyi et al, 2009) and Sys-Rem (Mazeh et al, 2006). Wavelet de-noising was selected to remove the trend.

To identify stars in the cluster, the SIMBAD database was used as the prime catalogue source. For fainter stars, 2MASS, DSS catalogues and WEBDA cluster catalogues were used to obtain position and photometric data.

The original and the approximated light curves were tested using correlation with a simulated light curve having a one hour dip. A square dip has been used as the correlate signal as illustrated in Figure 4.1. If the correlation finds a match, it would be amplified. Nine points (6.3 minutes) and fifteen points (10.5 minutes) moving average were used to smooth the light curve to improve the SNR, expecting a visible transit type signal. It was noted that the light curves from de-noising are more effective for reducing noise components than smoothing (see section 6.1). As the high-frequency components have been suppressed in the de-noised signal, PSD of the approximated signal has less energy (typically, at least ten times less) in high frequencies.

176 stars were identified and nearly all of them were type B stars. As we need to go deeper for type F or G stars, the second reduction batch was done by lowering the pixel threshold value (by 50%) while other parameters remain constant. The stars were searched for with 4 arc minutes radius from the centre of the cluster. This constant area is the area used for the differential photometry of the cluster. This gave 994 additional stars which are not listed in SIMBAD and 473 of them have equivalent coordinates as in the WEBDA data base, which uses the Arp et al (1958) notation. As there are no published 'R' magnitudes for these stars, expected R magnitudes were extrapolated from the known 'R' magnitude values. More details of these stars are in sections 4.2.6 and 4.2.7.

4.2.5 Data processing

MATLAB routines were used for further processing of the reduced data. At first, five reference stars were selected to make a super composite reference star using the proportional weight of their flux. Next, the differential data was obtained and these data points were tested for primary data validation and removal of bad data and outliers. For normalization and other statistical analysis, the median was used as the statistic because it was less affected by extreme values than the use of an average. Before the conversion to magnitude values, this data was next subjected to de-trending, the process of subtracting the mean or a best fit line of the data in each segment, which enables the analysis to focus on the fluctuations in the data about the trend. Once magnitudes were calculated, then all the data were shifted by the mean of the magnitude values towards zero. The resultant curve was considered as the final light curve, which was then subjected to the wavelet analysis to get the approximated curve which showed the long term behaviour. Results of the detailed analysis obtained by wavelet decomposition were separately analyzed for any visible discrepancies.

To remove systematic errors from the light curve, the light curve was subjected to a trend filtering algorithm (de-trending) available in MATLAB. This de-trend algorithm computes the least squares fit of a straight line (or composite line for piecewise linear trends) of the data and subtracts the resulting function from the data, thus removing systematic errors.

In addition to the wavelet decomposition, the differential light curve was cross correlated with a signal with one hour dip implementing the matched filter algorithm in time domain. The selection of one hour signal is arbitrary as there is no baseline, although it is the shortest transit time expected. Any value could be chosen, as the result does not depend on the transit duration (a property of correlation). The intention was to find a possible correlation between two signals and if there is a dip in the light curve, there would be an amplified dip in the cross correlated output. One good way to detect the orbital period (or frequency) is to analyze the light curve with FTs. The FT used was the built in MATLAB routine; FFTW library (Cooley and Tukey, 1965). As the light curves had missing data, the entire light curve could not be directly applied to FFT. Hence, the segmented light curves have been used for FFT. The FFT was applied with a fixed number of data points (64K) and then the PSD was summed up for all days (or all segments) and the average was taken in order to minimize noise components. As none of the segmented data has 64K points, the idea behind using large numbers of FFT points is to increase frequency resolution and to obtain the sharpest possible frequency components in the signal. The limitation occurred in FFT was the maximum length of a segment of continuous data, which was 100 samples covering 70 minutes. This can find a signal with minimum frequency of 20.54 cycles/Day. The requirement is to find frequencies much less than this value. I.e. if a Beta Cepheid variable star is considered, a 3 cycles/Day frequency must be detected. This needs about 7 hours of continuous data. This limitation was verified by adding sine signals to the light curve and analyzing the PSD. The PSD frequency line was correct only when the sine frequency is more than 20.54 cycles/day.

The LS method is superior as it doesn’t suffer from frequency limitations and DC values present for lower frequencies and is preferred over FFT. Unfortunately, LS method couldn’t apply for data of an entire day because of the computing memory limitations.

For stars with known variability, folding is a very useful tool for analyzing light curves. All light curves were tested for folding cycles of 1 hour to 10 days with step size of 30 minutes. The thirty minutes step size was arbitrary, but it is a good compromise. A smaller step size would be more accurate but would increase the number of plots to be analyzed. Variable stars with known variable cycles were further folded into the published variable cycle time obtained from AAVSO**.**

Using multi-point data averaging, the precision of the data can be increased by reducing the noise. To make a light curve with lower sample rate, data can de binned, such as combining four 42- second frames to make 168 seconds frames, thus reducing the processing load. Binning the individual data sets also reduces the noise, which is inversely proportional to the square root of the number of data sets used, a technique which increases the SNR (Bissinger, 2004). This may help to identify any hidden signal in noise environment.

Short Time Fourier transform (STFT) was used to find possible localized frequency components in both, the normal and the approximated light curves. For STFT, 256 points of windows were considered with 128 point overlapping (the MATLAB built in function for spectrogram needs overlapping to minimize the sharper edge effects between successive block samples). These STFT graphs gave different strengths of frequencies in different segments, and it is limited to the high end of frequencies as this also suffers from the limitation of 100 sample points per segment. The frequency components in the PSDs have some similarities in various stars.

As in Figure 4.2a, fixed threshold and minimax level methods were used to de-noise the signal. The de-noised signal of decomposition level of seven was used for the analysis.

Establishing transit candidate selection criteria:

The selection criteria of a transiting planet must be robust enough to eliminate false transits. These parameters are:

- Transit shape – Although the theoretical shape is a dip with semi-circular shape or a flat bottom, in practice this is extremely hard to achieve, unless observation is from a satellite. Practically, a 'V' shape signature is searched for, although it can indicate grazing eclipsing binary. If the reference star is brighter than the target, transit will be shown as a pulse, instead of a dip.
- Depth of the light curve – Generally planet/stellar radii are about 0.2% for a typical hot Jupiter around a F type star and about 25% for a Saturn type planet around a M dwarf

star, which could also be a case for a fore-ground star. When limb darkening is ignored, the transit depth is proportional to the square to the depth. Hence any depth outside this range will be readily rejected.

- Duration-Period of the transit – For hot Jupiters around solar-type stars, this may not exceed 3 hours and any transit which lasts more than 3 hours may be rejected for transit search. These will be preserved for further analysis on variable stars.
- Transit periods - Folded curves having periods less than twenty four hours are searched for transit like signatures.
- Orbital frequency - From PSD versus frequency (cycles/day) graphs, peaks having frequency less than 8 cycles/day are searched. These peaks represent cyclic events (possibly transits) of cyclic period more than three hours.
- SNR - As SD (error term) of the curve is known, the SNR can be calculated.

4.2.6 NGC 4755 – The Jewel Box, the selected open cluster

The open cluster under investigation is NGC 4755, also known as the Jewel box or Kappa Crux. Lacalle discovered this fine southern open cluster in 1751-52 AD which is famous for its multi-colour, blue, yellow and red stars. The name Jewel Box was given because one of the bright stars appears extremely red (B-V = 2.2) while the others are apparently blue (B-V < 0.3). This is one of the youngest open clusters with age of 7.1 million years. In the Shapley/Melotte classification, this cluster belongs to group 'g', the considerably rich and concentrated compact clusters (Archinal and Hynes, 2003). The hottest star is of type B0 and the three brightest stars are blue giants of magnitude 5.75 and type B9, magnitude 5.94 and type B3, and magnitude 6.80 and type B2, while the fourth brightest star is magnitude 7.58 M2 super-giant.

NGC 4755 is in a very bright portion of the Southern Milky way. The CCD images are centered on the middle of the cluster and each CCD image covers the sky of 10.4' X 10.4'. Situated close to the cluster there is huge dark area of the sky, called as 'the Coal Sack' right within the band of the Milky Way. This is a huge dark nebula, at about a distance of 500 to 600 light years, and 18.39 to 21.46 seconds in diameter.

Feature	Value
Right ascension	12:53.6 (hours: minutes)
Declination	-60:20 (degree: minutes)
Distance from Earth	1.98 k parsecs (6.4 kly)
Visual brightness	4.2 magnitudes
Apparent diameter	10 arc-minutes
Galactic longitude	303.208
Galactic latitude	2.503
Metallicity	-0.21 and (0.02 Sanner et al (2001))

Table 4.6 Basic data of NGC 4755[21] (Paunzen et al, 2010)

The selected open star cluster must be more or less fit in the FOV of the CCD camera and that meant cluster tended to be more distant than otherwise desirable. That's the main reason NGC 4755 was selected though it was further than the expected.

Arp and van Sant (1958) published the first paper on this cluster using modern photometric data. Data was obtained for the brightest stars by photometry for fifteen stars, plus two others for dimmer photometry. They placed fifty seven stars in Quadrant 1 (North West), forty one in Quadrant 2 (North East), forty two in Quadrant 3 (South West) and sixty two in Quadrant 4 (South East) (see Appendix A). This star nomenclature was used to find magnitudes of some selected stars. The main source to find magnitudes of the stars of the cluster was the CDS SIMBAD astrophysical database, which uses the notation of Sanner et al (2001). The other sources for magnitudes were Sagar and Cannon (1995), although there are total of 12 or more different sources now available.

The brightest stars are at the western part of the cluster. Brighter than eighth magnitude are the brightest members of the 'A' shaped asterism. Bedelman (1954) was the first to recognize that the principal stars in the NGC 4755 are super giants. NGC 4755 is famous for its principle variable stars, the beta Cepheids with spectral types of B0 to B3. There are also two known E-II eclipsing binaries, BU Cru and CN Cru. Currently there are 19 known (see Appendix A) or suspected variable stars in this cluster.

[21] https://www.univie.ac.at/**webda**/

As NGC 4755 is a young open cluster with population 1 stars, stars in this cluster have high probability of having planetary systems. According to current definition of metallicity, this is a metal poor cluster as and the value of the metallicity is -0.21. Sanner et al (2001) give metallicity as 0.02 thus making the cluster marginally metal rich.

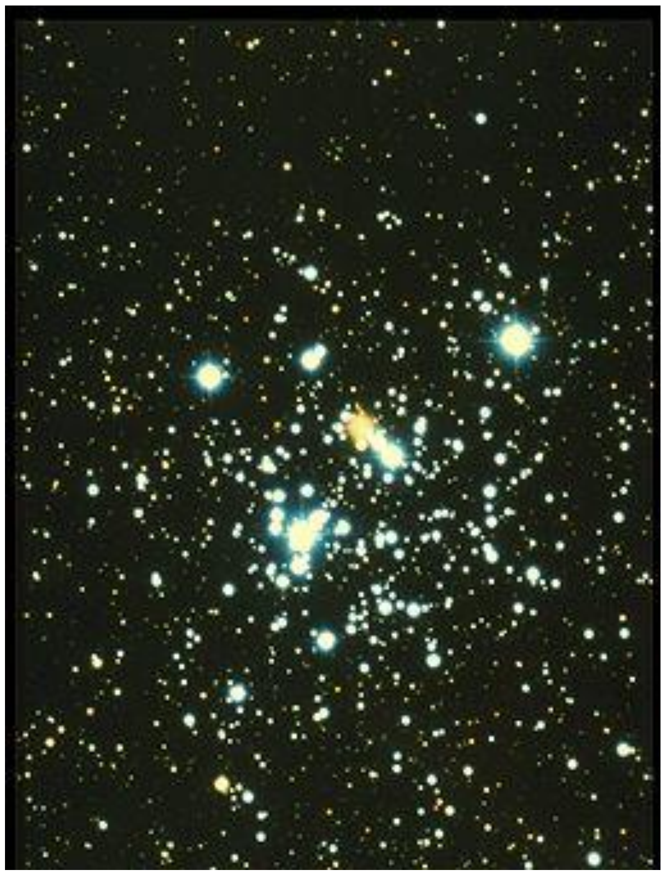

Figure 4.18 Open Cluster NGC 4755 taken by AAT

The observations were done from 18th May 2007 to 21st of June 2007 for 17 nights and 176 stars with known magnitudes ('V' magnitude range considered was 5.77 to 14.12) were selected for the first set for reduction although 256 stars were in the 10 arc-minute circle region of NGC 4755. The majority of stars considered were type B0 with published magnitudes and the magnitudes of stars were stretched up to 14+. There are some stars with extrapolated R magnitude possibly belonging to spectral type A or F. The second data set consists of 994 fainter stars of unknown spectral type with extrapolated 'R' magnitudes of 8.84 to 18.89 in the same FOV.

Although binary pairs are known to exist in open star clusters, none are usually listed. For NGC 4755, only four pairs can be found in the Washington Double Star Catalogue (WDS), and these are B 805, JSP 561, JSP 563 and JSP 562 / HDS 1808 (See Figure A.3).

4.2.7 Reference stars

Reference stars are necessary to get the magnitudes of the stars. Some bright field stars are generally needed for this purpose. For the stars with known magnitude and stellar type, it was easier to find reference stars with similar magnitude and spectral type which belong to the cluster within 3 arc-minutes distance. To minimize noise, five non-variable stars in the cluster were selected to make a composite super reference star by applying weighted averages based on the proportions of median flux value.

Star Name	V – magnitude (from SIMBAD)	Spectral type
NGC 4655 SBW 19	10.17	B2.5V
NGC 4755 SBW 31	10.89	B2.5Vn
NGC 4755 SBW 33	10.99	B2V
NGC 4755 SBW 22	10.22	B1V
NGC 4755 SBW 18	10.14	B1V

Table 4.7 Stars for the composite reference star

(Star magnitudes are from SIMBAD)

The light curves of reference stars of NGC 4755 are given in Appendix C. The SD is in the range of 0.005 and 0.010 magnitudes.

As these cluster reference stars all belong to stellar types 'O', 'B' or 'A', a composite reference star using the field stars on the FOV was used for the calculations. There were only three possible foreground field stars (As in SIMBAD) found to be in the all the CCD frames (Table 4.8) with known magnitudes. Unfortunately, these stars have unknown spectral types. As there were higher SD (0.010 to 0.015 magnitudes) for the differential light curves than the stars in Table 4.7, this composite field reference star was not used for the final calculations.

Star Name	Magnitude (As in SIMBAD)	Spectral type
CPD 594569	B - 10.30	-
SAO 252071	V - 10.0	-
CPD 594539	B - 9.85	-

Table 4.8 Stars for the composite field reference star

(Star magnitudes are from SIMBAD)

4.3 Validation Algorithm with data of known transiting ESPs

4.3.1 Using a Space Probe – Kepler

As many of the ongoing ESP searches release data to the public, it was possible to validate algorithms with known transiting ESPs. Light curves of many Kepler transiting planets were analysed with de-noising and the results with Kepler 4b, 32b and 70b are given below. These three known transiting planets were selected as they demonstrate three different types of results. As Kepler ESPs are not directly related to this research, results have been put into Appendix J.

Kepler light curves show many instrumental trends (as the spacecraft makes a quarterly roll to align its solar panels to the Sun) in the light curve, hence data was de-noised and de-trended as segments; the de-noising method shows very positive results. Other than the transits, de-noised curves show unavoidable edge-effects and many recurring characteristics, possibly transits from other orbiting planets (e.g. Kepler 32).

De-noising and LS method work well if the orbital period is in the range of many days, that means there are enough samples for the calculations. The use of Kepler light curves justifies the ability of de-noising, combined with PSD to find orbital time of a transiting planet.

4.3.2 Using same Telescope on Transiting Exo-Planet

Using the same Perth Telescope, relatively closer star was monitored for transiting planets since 2007. Since the observation conditions are similar, this is a good test for Perth Telescope; whether it can detect a transit and whether de-noising can actually find transiting planets. The data obtained on 8th June 2007 was analyzed by de-noising algorithm and results are listed below. Subsequent observations show that there is enough evidence for a transiting planet (Blank, D, et al (2015)). Dips at the ends (the edge-effect of de-noising) of de-noising frames were discarded and the middle dip is sufficient enough for suspecting transit.

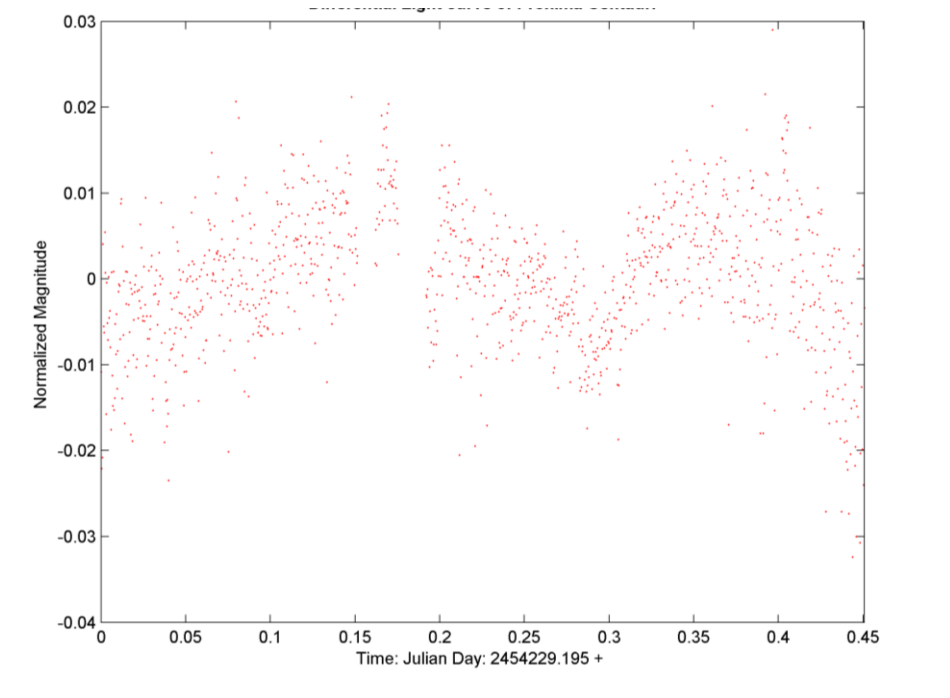

Figure 4.19 Light curve of transiting exo-planet (on 8th June 2007)

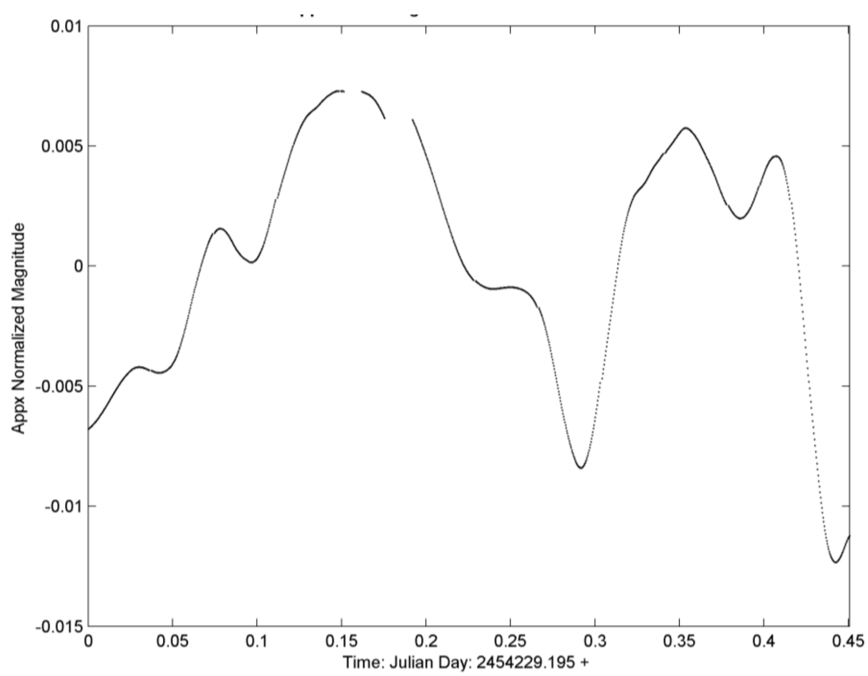

Figure 4.20 De-noised Light curve of transiting exo-planet

There is a transit of 2 hours. The big dips at the ends are not the transits; they are there since MATLAB based de-noising algorithm suffers from edge effects and must be discarded. The real transit is at 2/3 from the left. As there is only one instance of transit, there is not enough data for LS periodogram. This transit has SNR of 1.24.

Chapter 5

Results

In this section, the output of real data of the transit search and freely available satellite data is presented. For consistency, negative magnitude values are running down the y-axis.

5.1 Estimation of probability of detection

For all observation windows, the graph of probability of detecting ESPs vs. orbital period is given in Figure 5.1 and the probability of total transit coverage vs. orbital period is given in Figure 5.2. Figures 5.1 and 5.2 are similar to the graphs of the simulations given in chapter 4 (Figures 4.15 and 4.16), but the upper limit of the probability of detection is less for the observational data due to the use of shorter observational intervals than the observation time intervals expected in the simulation. This makes finding a transit much harder than predicted in the simulations. ESPs with orbital times with multiples of twenty-four hours or close to 24-hours have lower probability of being detected by the search and, if these ESPs make transits in daytime, they will never be detected.

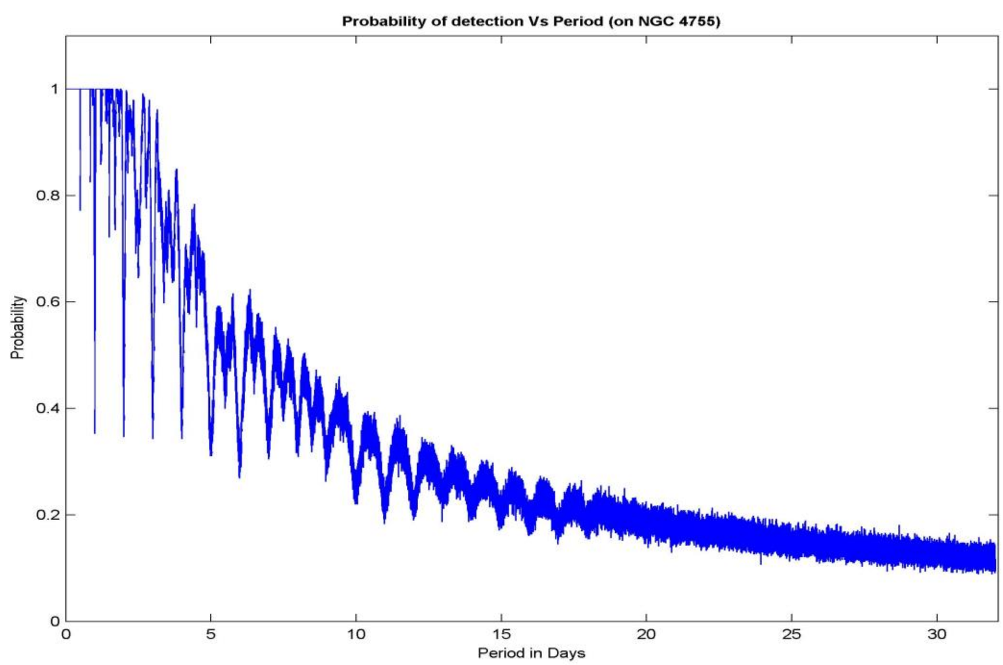

Figure 5.1 Graph of probability of detection vs. orbital period

However, the lower limit of these 24 hour (or closer) probabilities is higher than the simulated (Figures 4.15 and 4.16). The higher simulated values may be due to non-consideration of the earth's orbital motions and the difference in 24 hour standard day and sidereal day data overlapping.

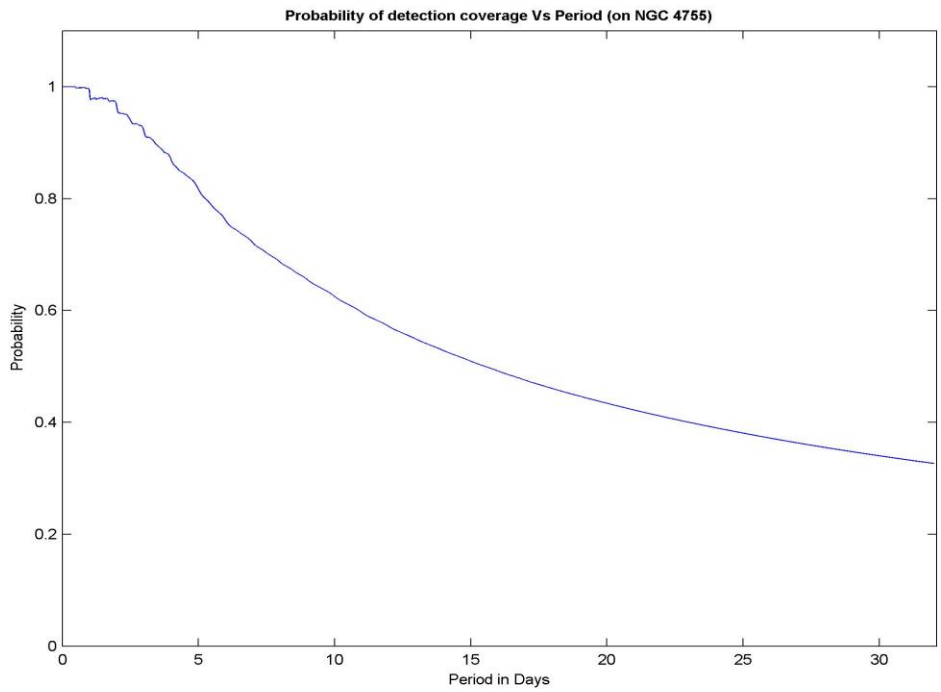

Figure 5.2 Graph of probability of detection coverage vs. orbital period

5.2 Obtaining R magnitudes

To get calibrated 'R' band magnitudes, $\log_{10}$ (light intensity counts) vs. known 'R' band magnitudes are plotted for known stars (Figure 5.3). The approximated straight line for calibrated 'R' magnitude (plotted in red) is a curve with the gradient of -0.4022 and the intercept of 9.3212. Once the curve parameters; the gradient and the intercept, are known, 'R' magnitudes of stars are obtained by using the points on the straight calibration line.

The 'R' magnitudes of the 1169 stars in the FOV vary from 6.5 to 18.9. 'V" magnitudes are available from previous studies of the cluster, such as Arp and Van Sant (1958). As V-R values can be calculated for these stars, their spectral types can be determined.

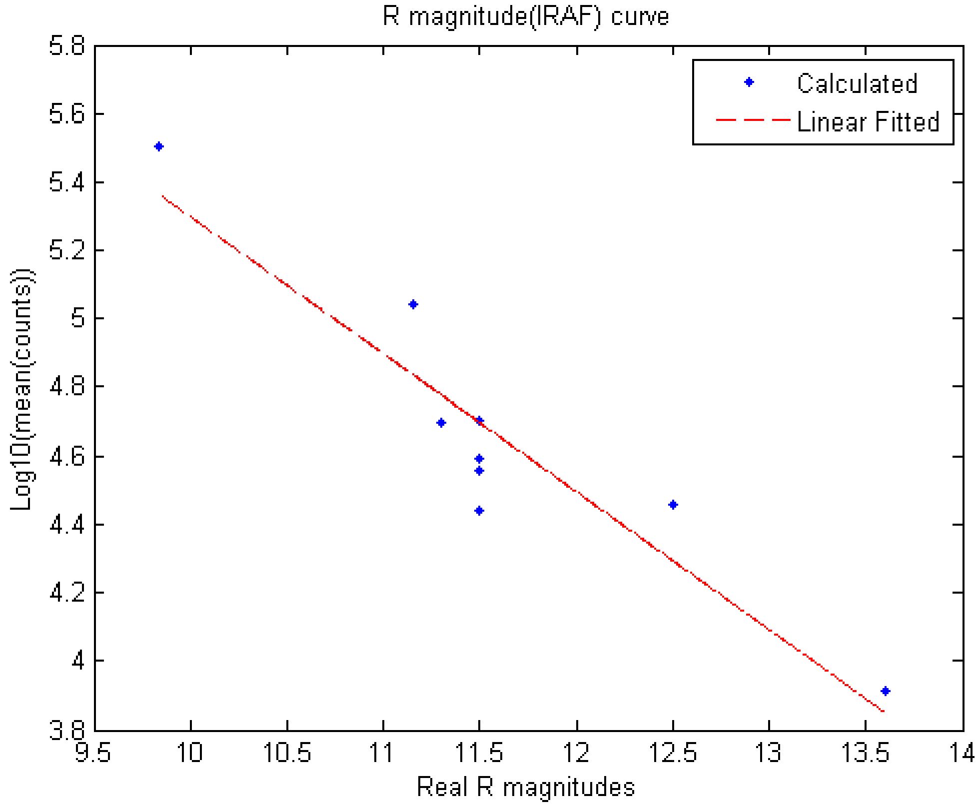

Figure 5.3 Log_{10} (counts) vs. published ‘R’ Magnitudes. Red curve is the approximated curve

5.3 Light curves and application results of selected stars of NGC 4755

In this cluster, most of the known stars are brighter than V=12, and belong to the spectral types of B and O. These stars are too bright and not considered for transit search. The summary of the photometric results of the cluster are tabulated in two tables; Table D.1 (Appendix D) consists of stars with known identifiers, and most of these stars have published spectral types in the SIMBAD database. Table D.2 (Appendix D) consists of fainter stars, and 473 of them have found references in the WEBDA[22] database. The published spectral types of these faint stars are not known but, for some, after interpolating for the position, approximate spectral types were estimated from 2MASS data.

The convention of star naming used in this thesis is that; if a reference was available in the SIMBAD star catalogue, the SBW notation ‘NGC 4755 SBW XXX’ (after Sanner et al, 2001) was used while preserving the common star name. When the SBW notation was not available, the

[22] http:// www.univie.ac.at/webda/

ESL (Evans et al, 2005) notation was used. If none of the above notations are available, the first available SIMBAD star notation was used. Magnitudes of fainter stars (Table D.2) are not available in the SIMBAD database and these stars are given project specific numbers (JC_1, 2…).

The format of the brighter star table (Table D.1) is

Star # WEBDA Data Base	Star name Sanner et al (2001) or Evans et al (2005) or SIMBAD preference	RA (ICRS 2000)	Dec (ICRS 2000)	Spectral type	R magnitude	Std dev	15pt Std Dev	Comments

Where the format of fainter star table (Table D.2) of the FOV of the cluster NGC 4755 is

JCU Star #	WEBDA Db #	RA	Dec	Rmag	Std Dev	15ptStd Dev

The results table also has a column of fifteen point average for the entire span of the experiment. For variable stars with known periods, folded light curves were also drawn for two multiples of the given periods.

To remove common noise at any frequency, a notch filter was used (See Appendix I for details of this filter). The aim was to find a weak signal close to stronger signal. This filter effectively removes the frequency component, but no hidden frequency component was observed around this frequency.

De-noising is for removing the noise in the signal. De-noised data has been plotted with demarcation line between each day and since noise has been removed, de-noised curves look like continuous line though the light curves have discontinuities.

The idea of using frequency domain of experiment data is to find variable stars in the cluster since series of impulse pulses can be translated to frequency domain by FT successfully. This may help to find a transit though the probability is extremely low.

5.3.1 Standard deviation Vs. R magnitude of stars

The SD of each light curve was plotted against the 'R' magnitude for every star as in Figure 5.4a and was zoomed for smaller scale noise in Figure 5.4b. This graph uses 1169 stars in the cluster FOV. The graph shows that up to the magnitude of 15, the minimum SD is usually less than 0.2 magnitudes, which is just enough to find a transit. These low SD stars are already known and they are the non-variable brighter set of the cluster. High SD is not good light curves for transit search. For many stars, the SD is still too high to find a transit; hence there is a need of alternative techniques to reduce the SD. For stars of spectral types of F, G and K, which reside in the area where the magnitude is more than 14, the minimum SD is much higher than expected for transits. This high SD confirms the calculations in section 4.2.2, where the limiting distance was estimated to observe a transit for a F5 star. The distance to this cluster (1976pc) is higher than the calculated (1370pc) thus giving a SD higher than wanted. Hence, to go deeper for F, G and K stars, SD has to be reduced and de-noising is needed.

There are some stars having magnitude less than 14 with a significantly higher SD than the rest. This could be an indication of variable stars (Pepper et al, 2008). Under the assumption that stars having 'R' magnitude less than 14 with SD of 0.5 or more are possible variable stars (possible beta Cepheids), the number of possible variable stars was calculated to be 40 out of 1169.

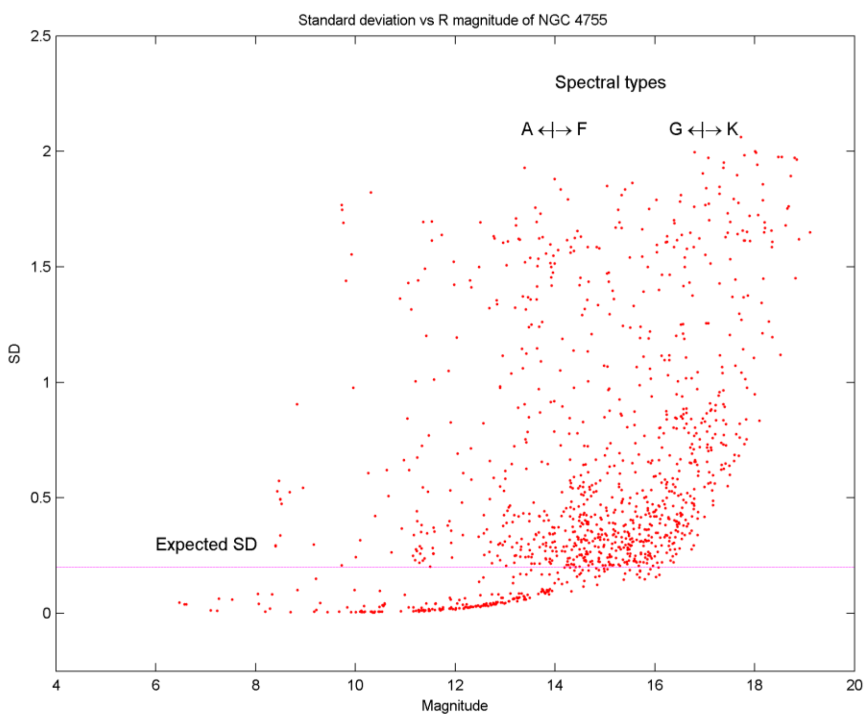

Figure 5.4a Graph of SD of the light curve vs, magnitude of the cluster stars, y axis is in units of magnitude.

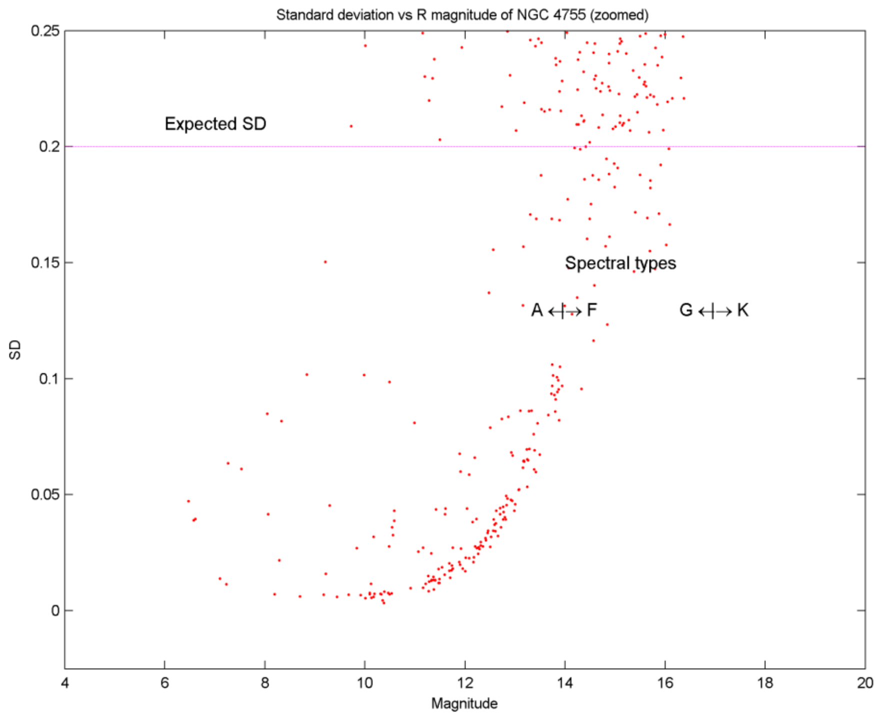

Figure 5.4b Graph of SD of the light curve vs, magnitude of the cluster stars (zoomed for smaller scale), and y axis is in units of magnitude.

5.3.2 Light curves of a comparison star and 14th magnitude stars

Light curves of NGC 4755 SBW 22, NGC 4755 SBW 200, NGC 4755 SBW 222 and NGC 4755 SBW 225 are given in Figure 5.5. NGC 4755 SBW 22 is a star of B1V spectral type with 'V' magnitude of 10.22, while the other three stars have magnitudes closer to 14. Figure 5.6 is the zoomed approximated version of the light curves where differential magnitudes were plotted against the frame number instead of Julian time. Figure 5.7 is the Power Spectral Density (PSD) graphs (LS method) of these stars and Figure 5.8 shows the PSD graphs (using LS method) of the approximated signal at the decomposition level of 7. The approximate signal at the wavelet decomposition level of 7 contains the signals of 90 minutes or longer orbital period. This approximate signal is about 100 times lesser in magnitude than the original.

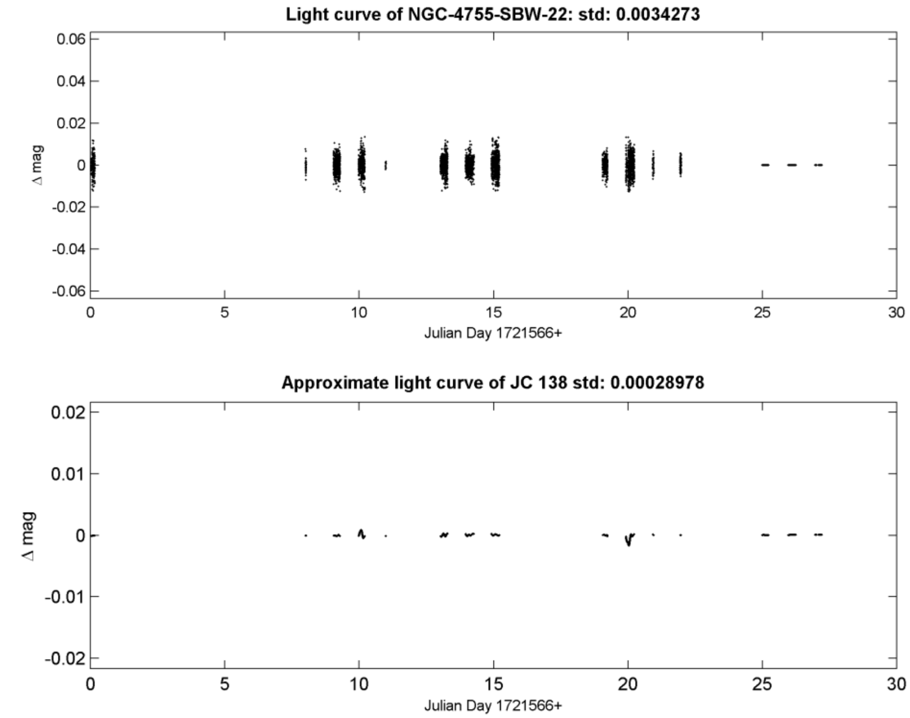

1. NGC 4755 SBW 22 , B1V, V=10.22

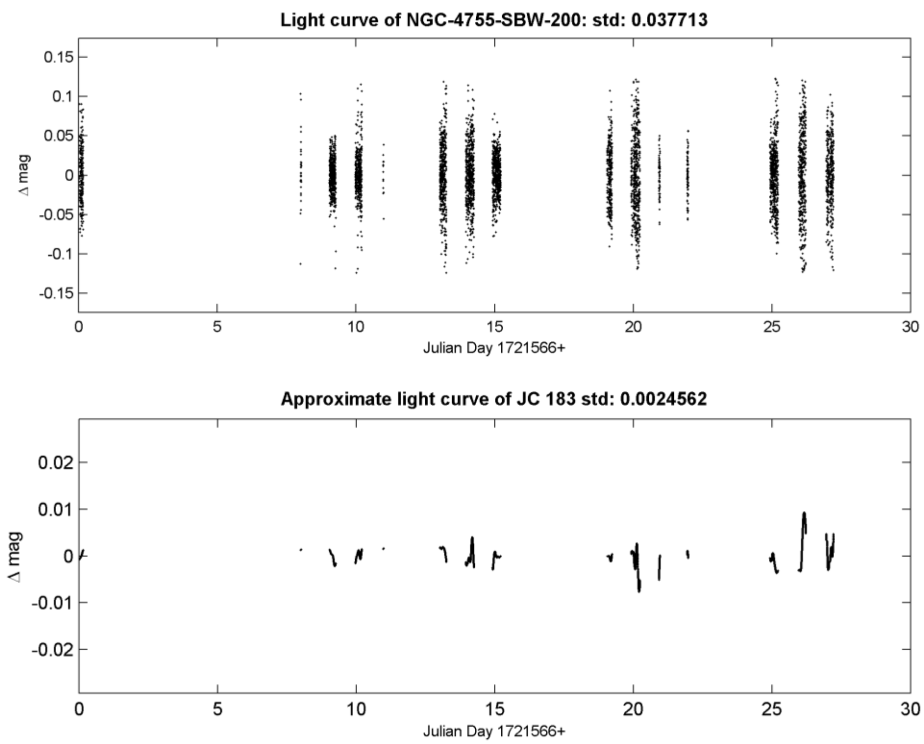

2. NGC 4755 SBW 200, V= 13.50

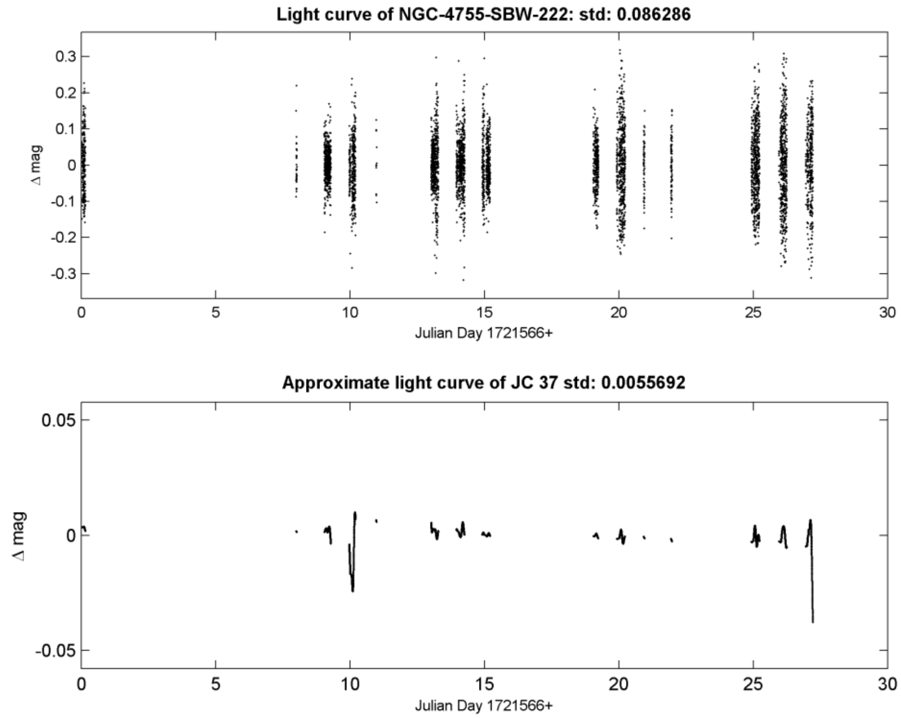

3. NGC 4755 SBW 222, V=14.00

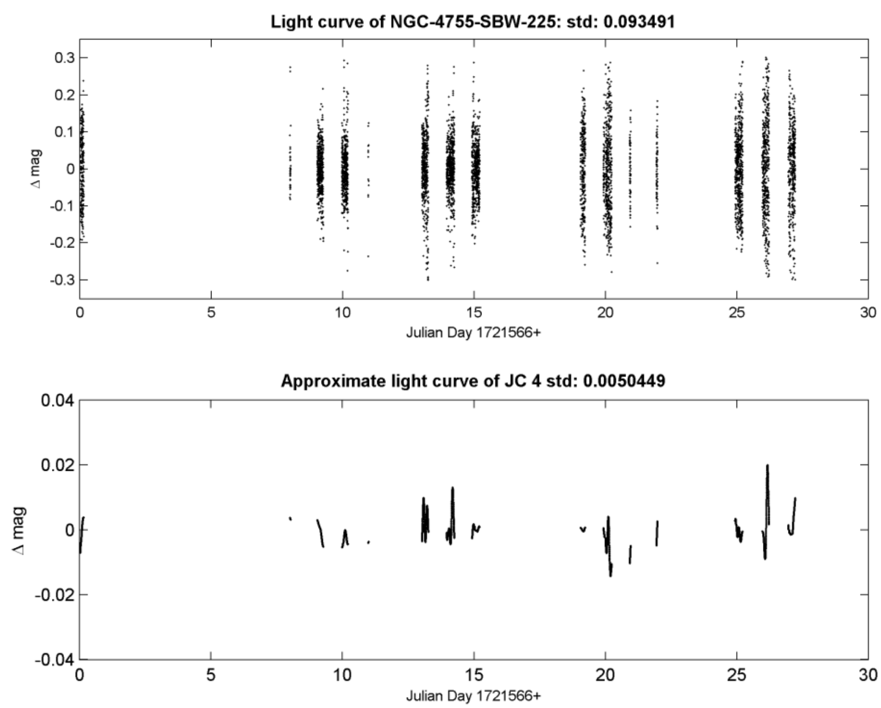

4. NGC 4755 SBW 225, V=14.06

Figure 5.5 Full light curves of a comparison star and three stars of magnitude 14

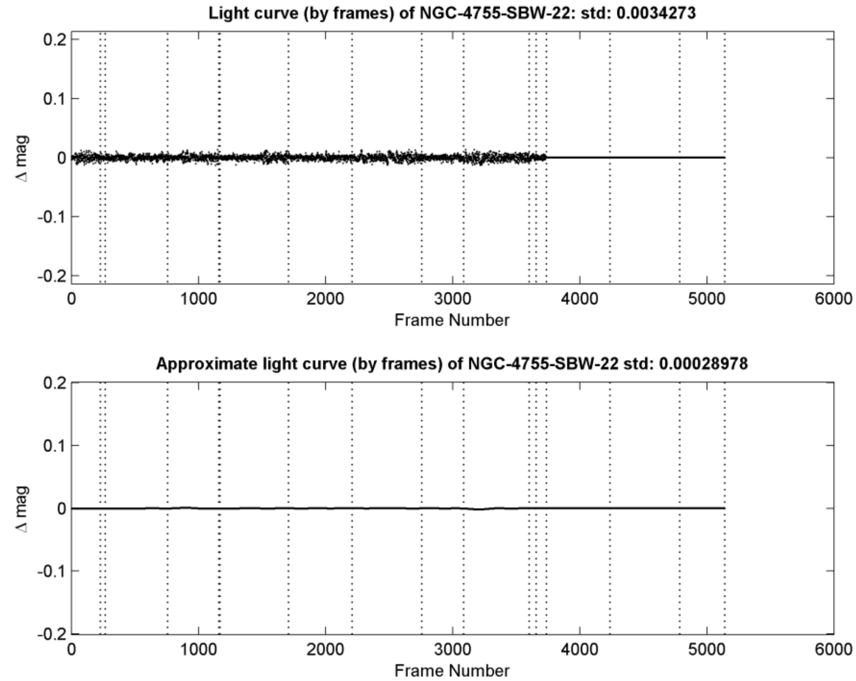

1. NGC 4755 SBW 22

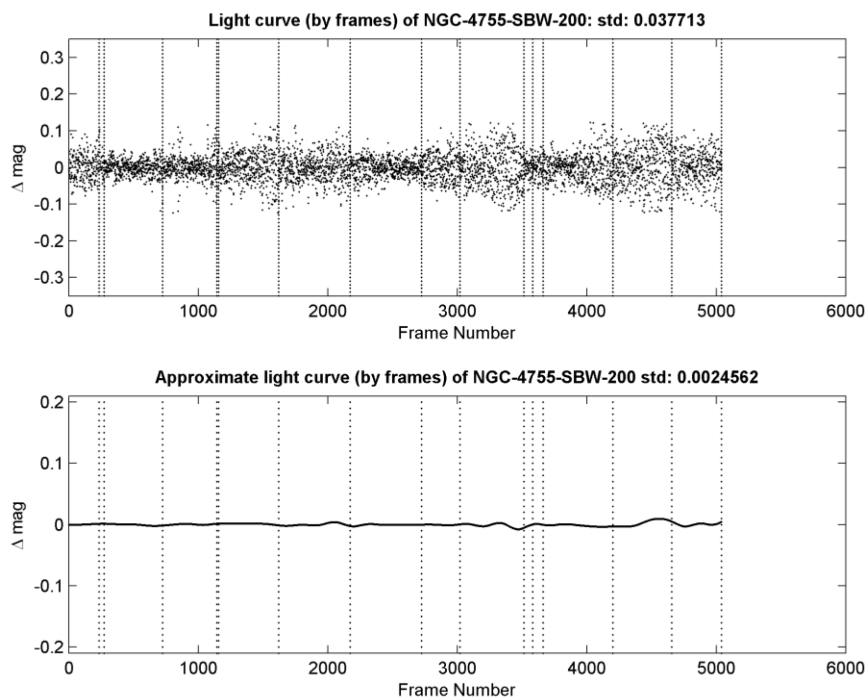

2. NGC 4755 SBW 200

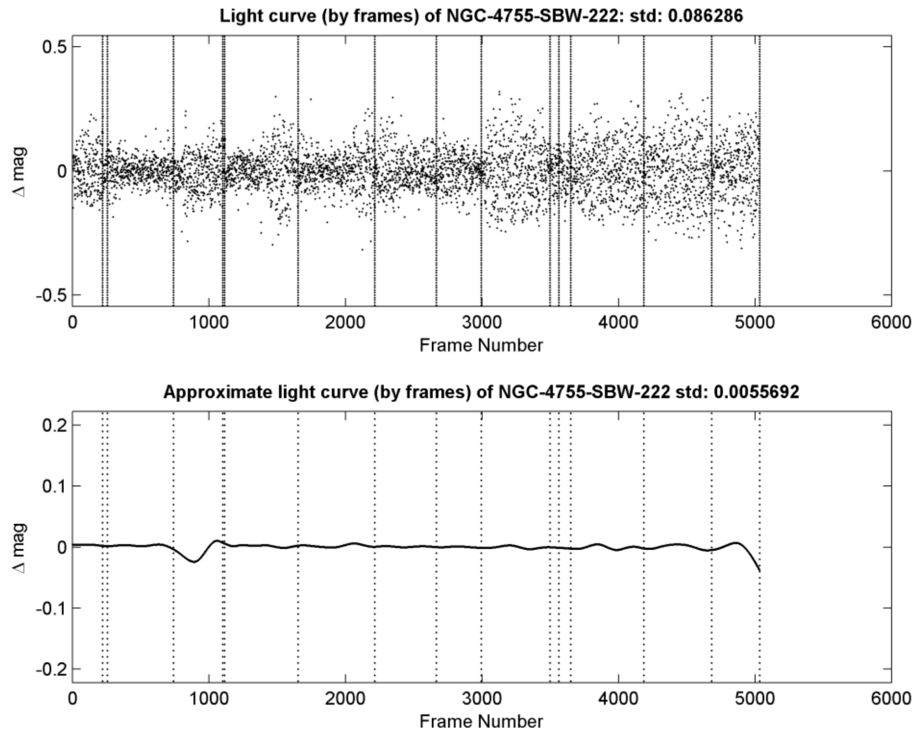

3. NGC 4755 SBW 222

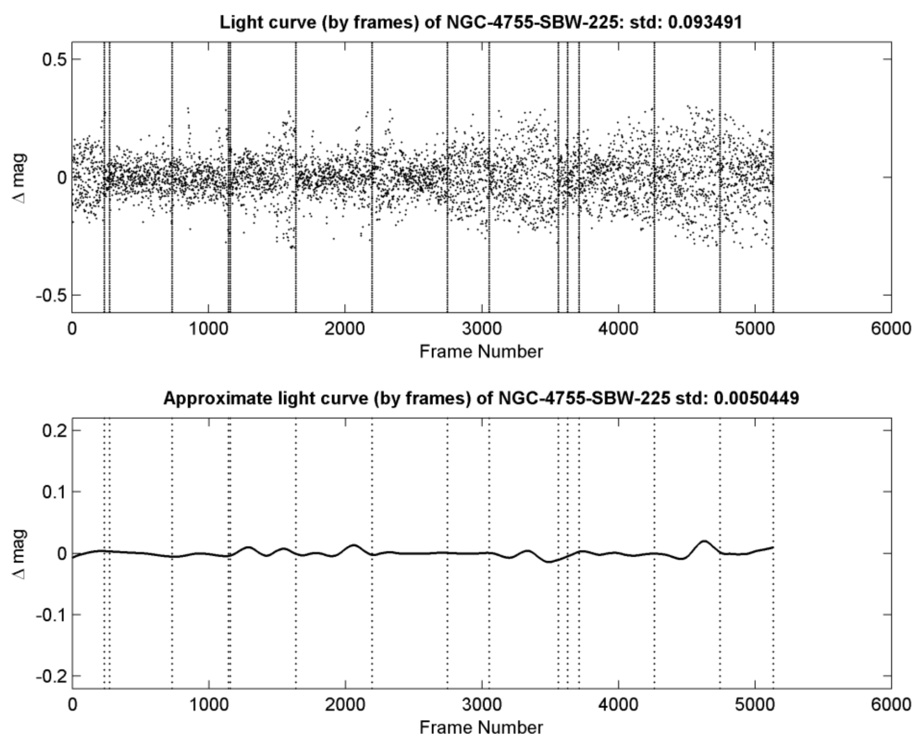

4. NGC 4755 SBW 225

Figure 5.6 Zoomed approximated curves of stars of Figure 5.4

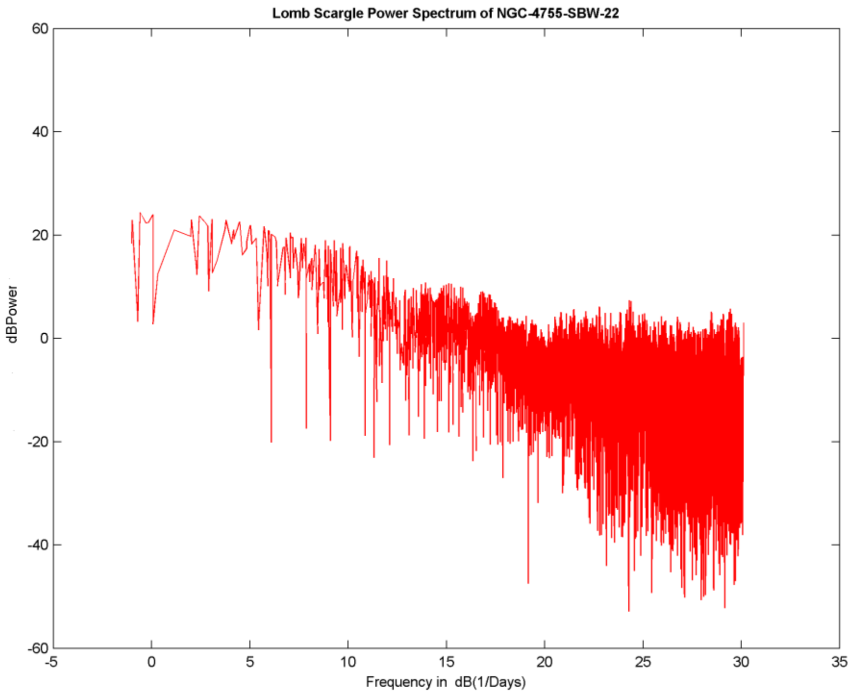

1. PSD of NGC 4755 SBW 22

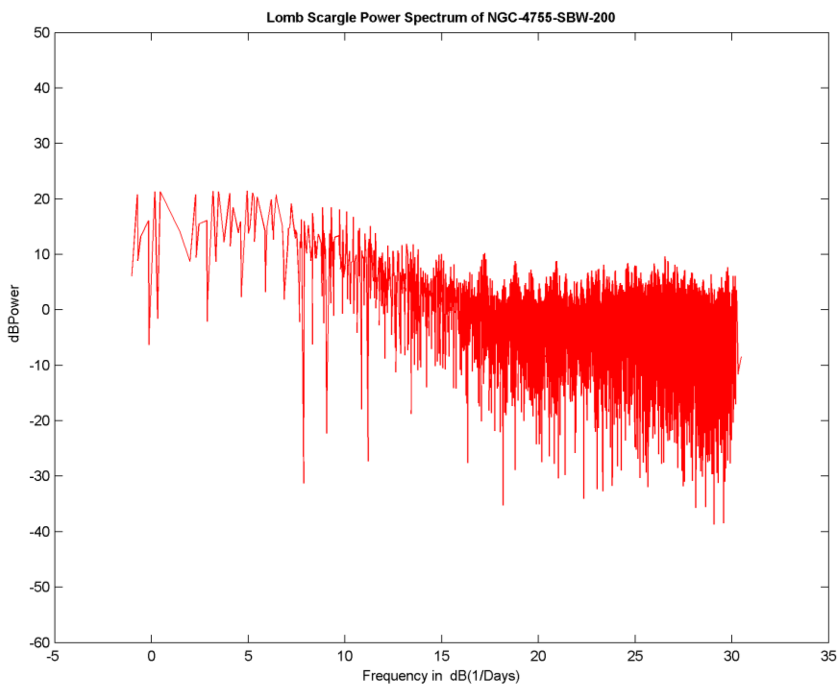

2. PSD of NGC 4755 SBW 200

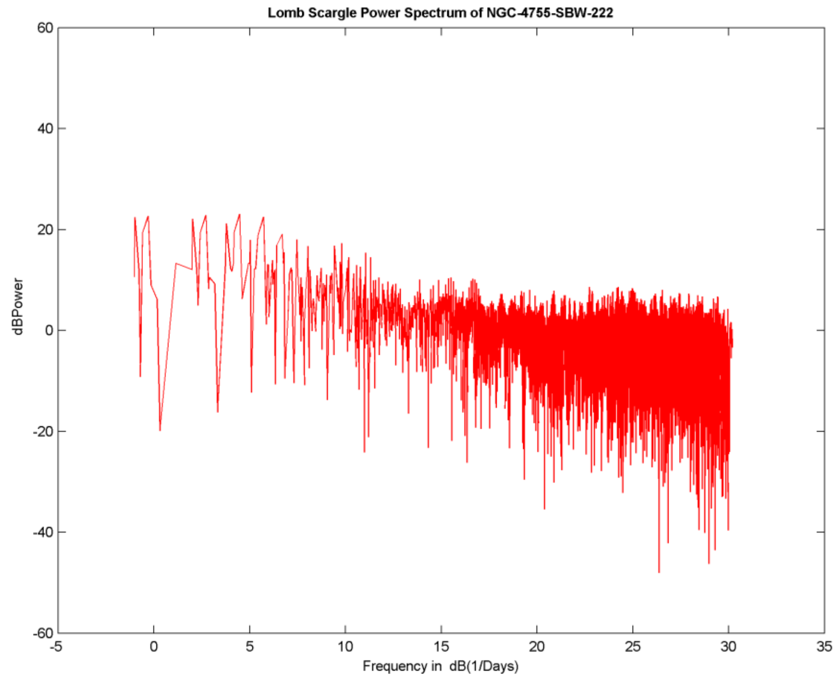

3. PSD of NGC 4755 SBW 222

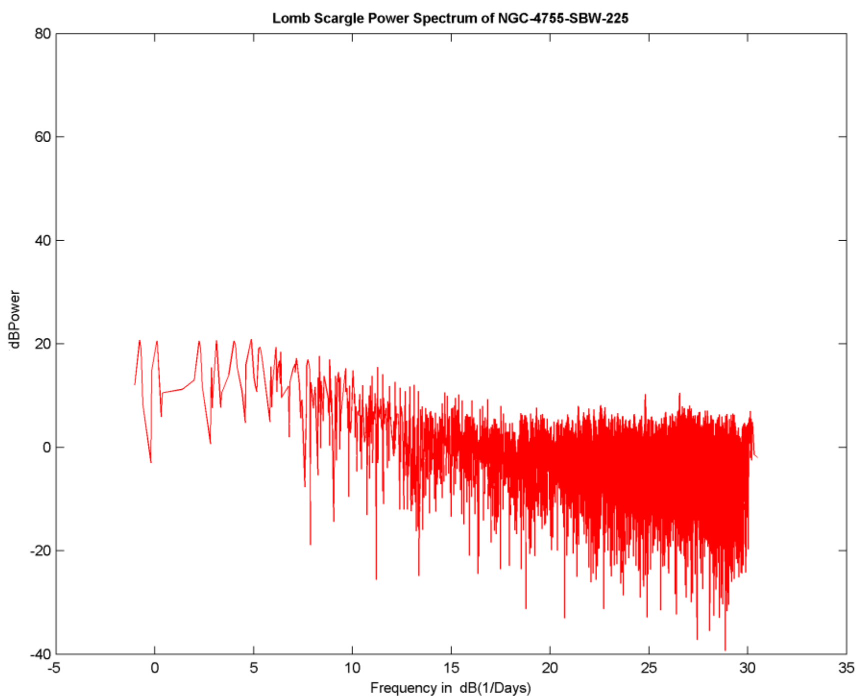

4. PSD of NGC 4755 SBW 225

Figure 5.7 PSD diagrams of stars of Figure 5.5

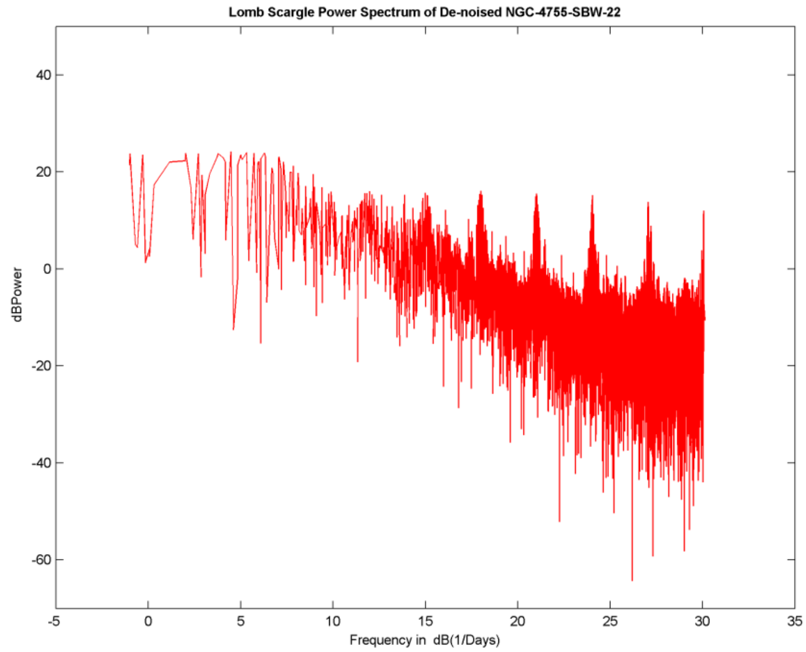

1. Approximated signal, NGC 4755 SBW 22

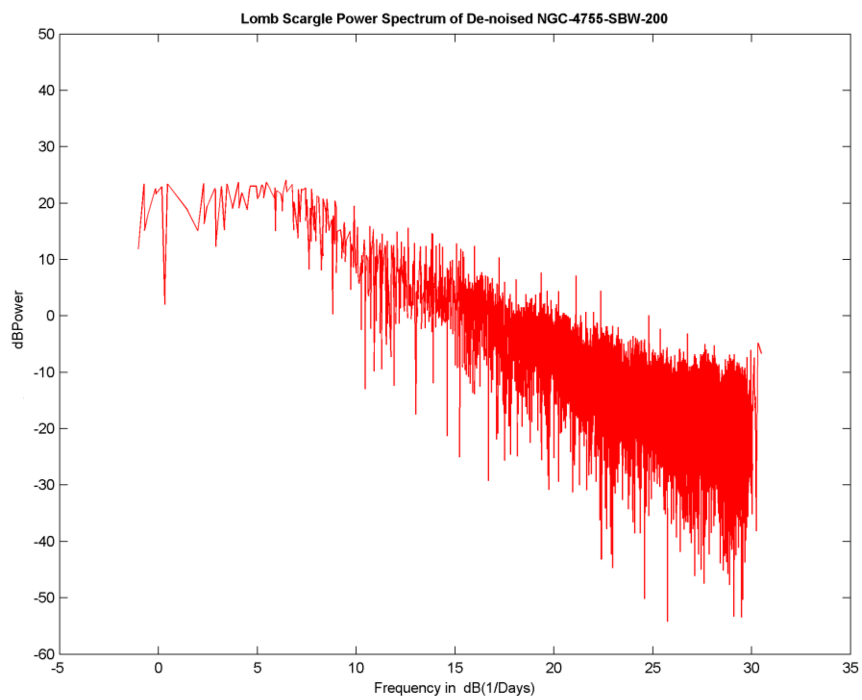

2. Approximated signal, NGC 4755 SBW 200

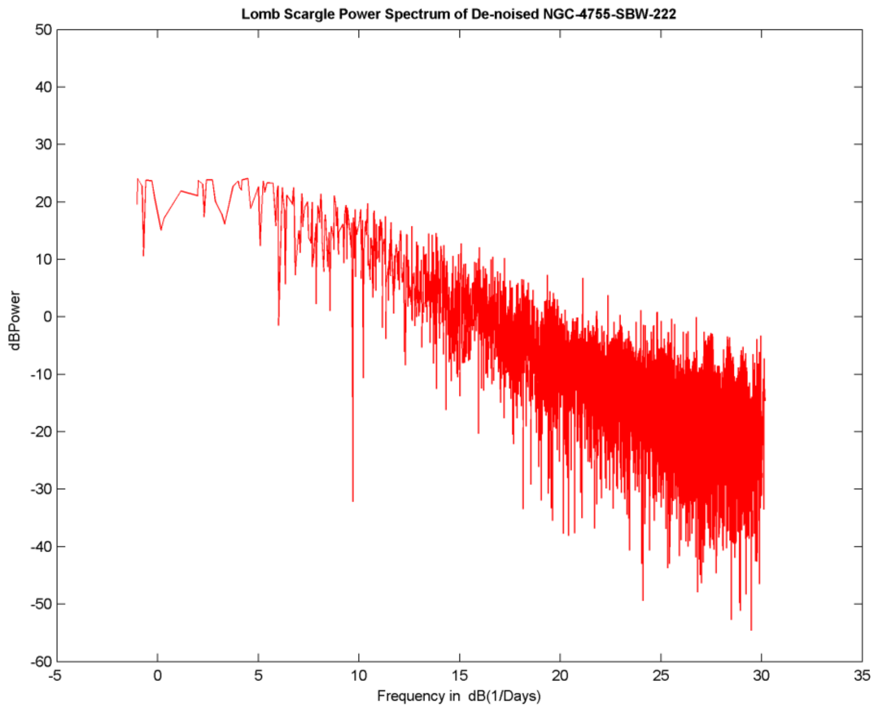

3. Approximated NGC 4755 SBW 222

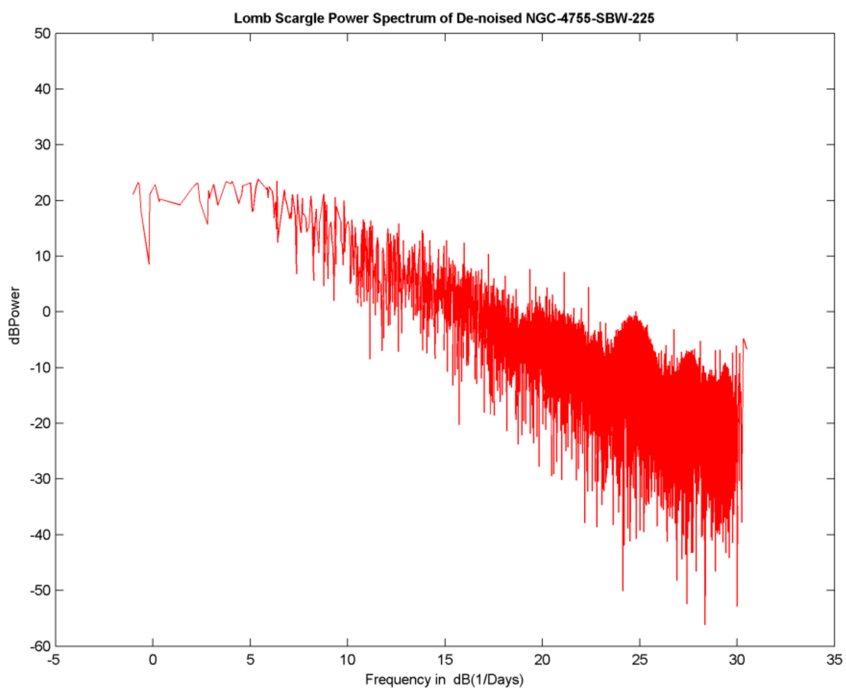

4. Approximated signal, NGC 4755 SBW 225

Figure 5.8 PSD diagrams (Approximated to decomposition level 7) of stars of Figure 5.5

PSD diagrams are good tools to find common frequency components of non-continuous signals like these light curves. The FFT based PSD diagrams suffer from the limitation of continuous samples per a segment (a maximum of 100), so it cannot show valid frequencies below 20 cycles/Day. Hence, LS method based PSD diagrams were used as LS is not suffered from discontinuities of the light curves. Though LS show peaks around frequency ranges of 0-5cycles/day, there are not enough points to get smooth curve tip and gives trouble for finding peaks accurately. In approximated PSD, the frequency component strength is further reduced as filtering has been done; typically by a factor of 10^3. Approximated signal is mostly free from white noise, but contains low frequency ‘red’ noise, which is probably a systemic frequency component added by thermal drift of the detector or atmospheric effects.

5.3.3 Light curves of some known variable stars

NGC 4755 has twenty three known variable stars (see. Appendix A, Table A.1). Light curves of NGC 4755 SBW 4 (EI Cru), NGC 4755 SBW 7 (CY Cru), NGC 4755 SBW 49 (EG Cru) and NGC 4755 SBW 15 (CX Cru) are given in Figure 5.9 and Figure 5.10. Figure 5.11 gives the PSD diagram of stars in Figure 5.9. Some bright variable stars ($V < 7.0$) are saturated, and they were not considered for data reduction.

Light curves of CY Cru and CX Cru have double band structure for three days. This must be due to be misalignment of the calculated centre of the star to the actual, thus making blending effect with the neighbors, there is not much difference in these FFT periodograms with LS periodograms in section 5.3.2. The fundamental of these peaks will give the possible period of the variable star.

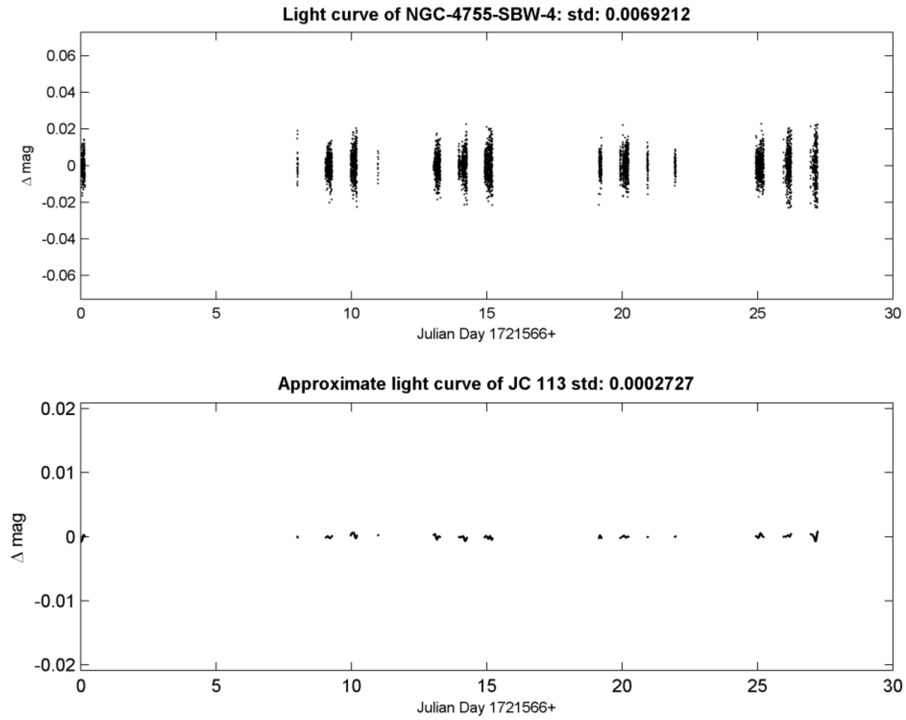

1. NGC 4755 SBW 4, (EI Cru), BI, V=9.38

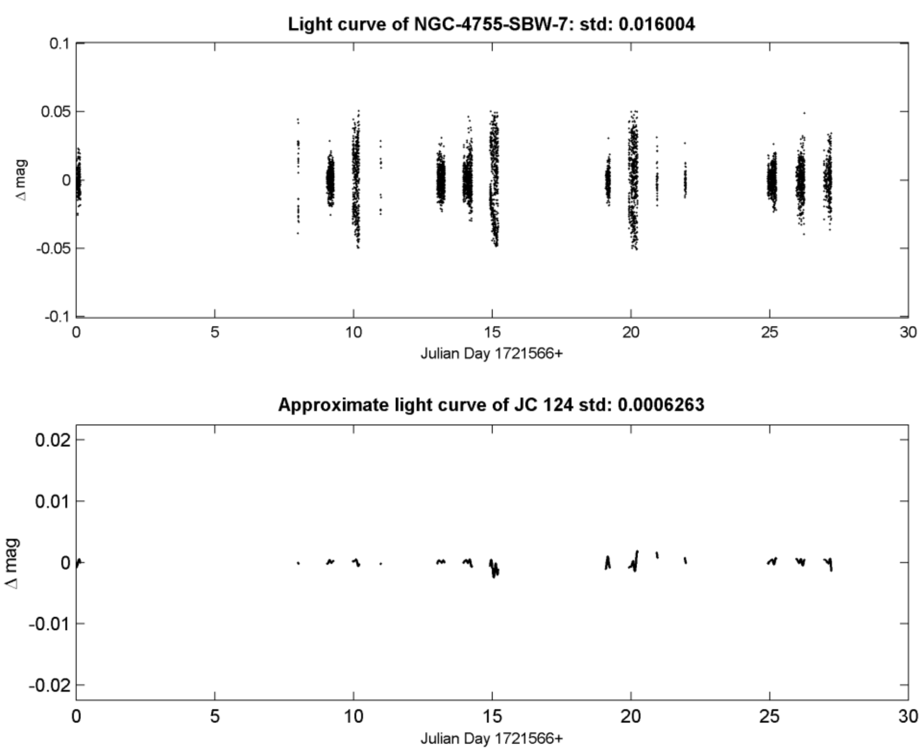

2. NGC 4755 SBW 7 (CY Cru), B1.5, V= 9.6

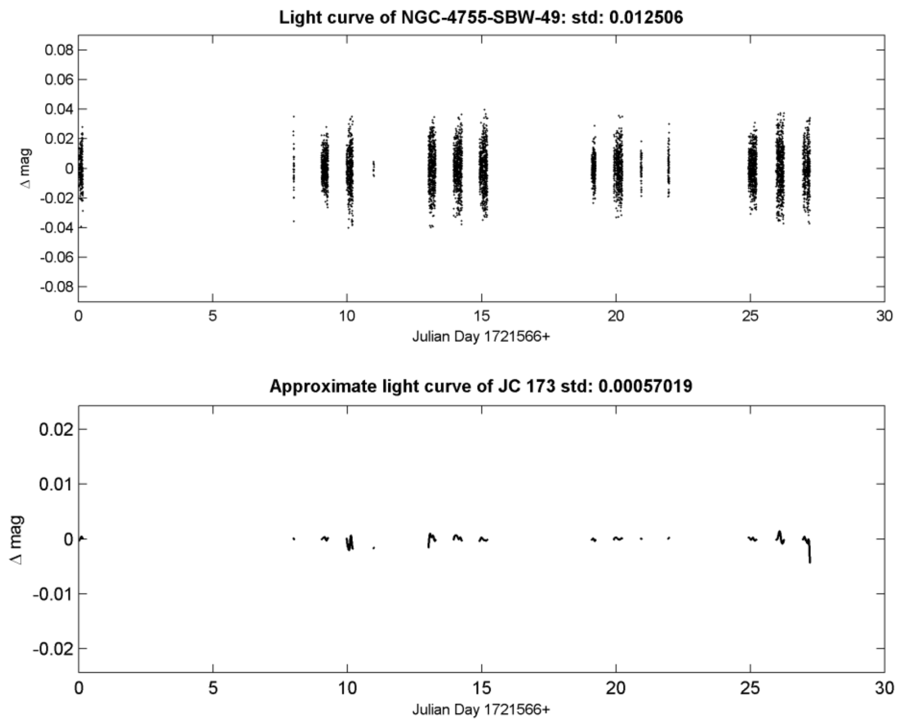

3. NGC 4755 SBW 49 (EG Cru), B3Vn, V=11.45

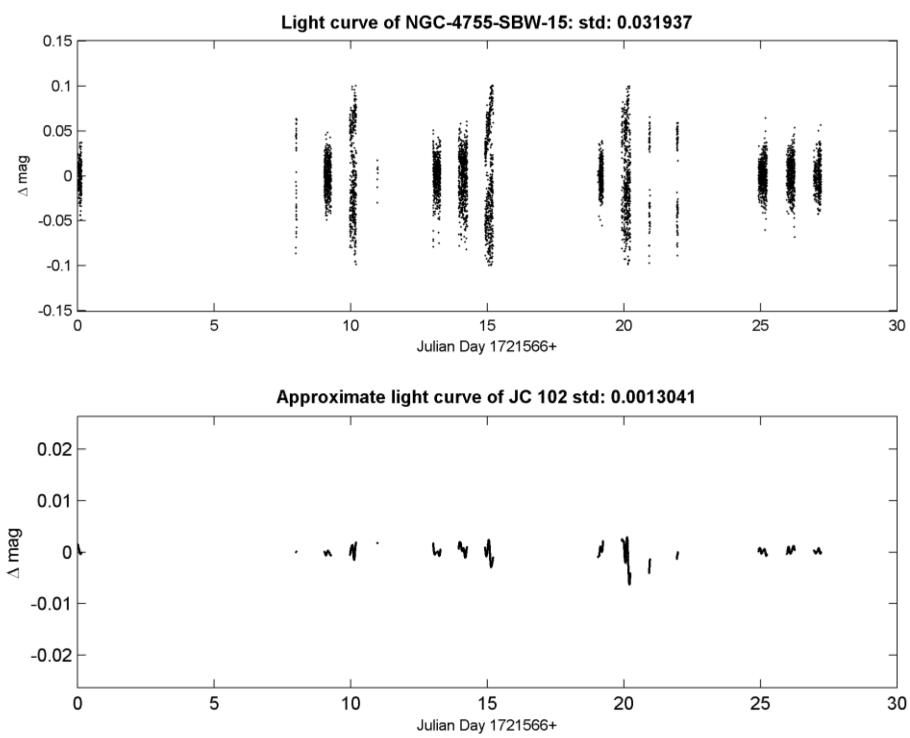

4. NGC 4755 SBW 15 (CX Cru)

Figure 5.9 Full light curves of some known variable stars

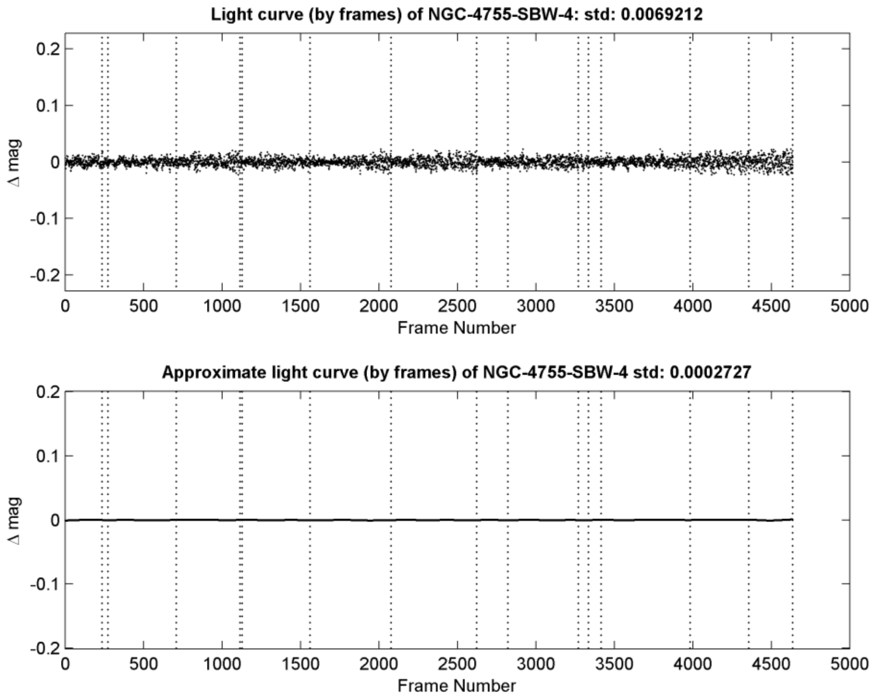

1. NGC 4755 SBW 4 (EI Cru)

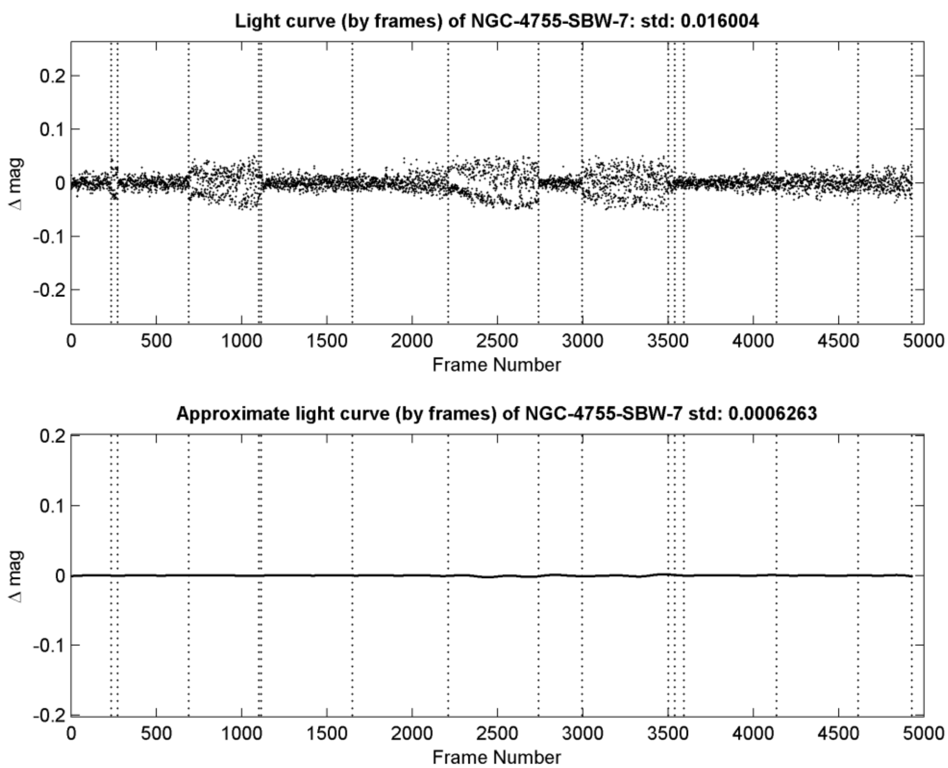

2. NGC 4755 SBW 7 (CY Cru)

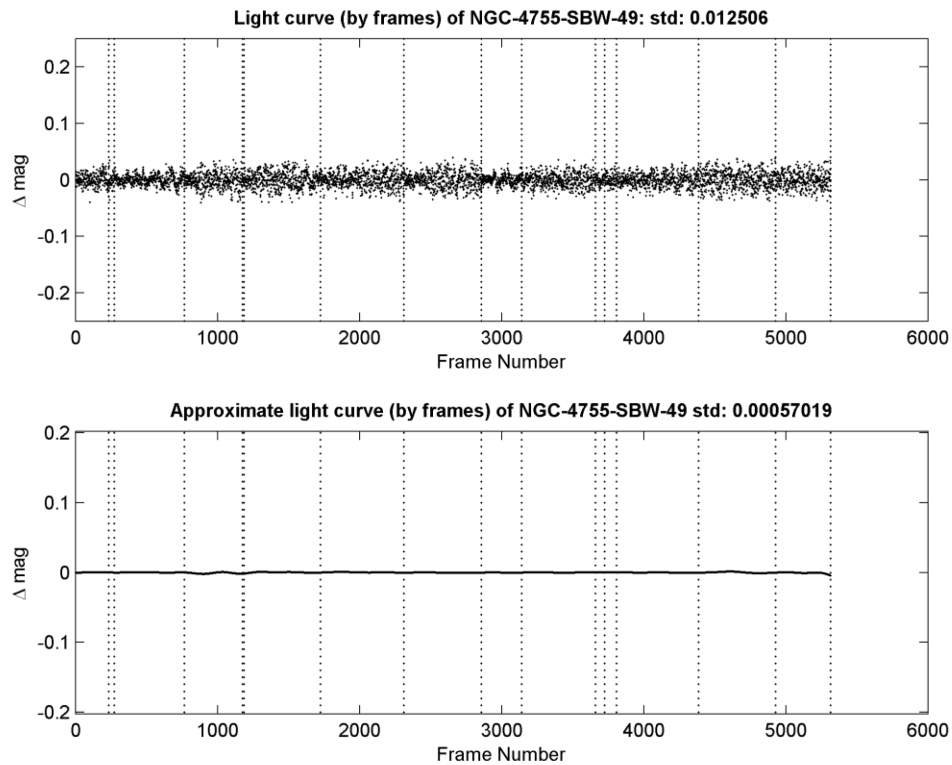

3. NGC 4755 SBW 49 (EG Cru)

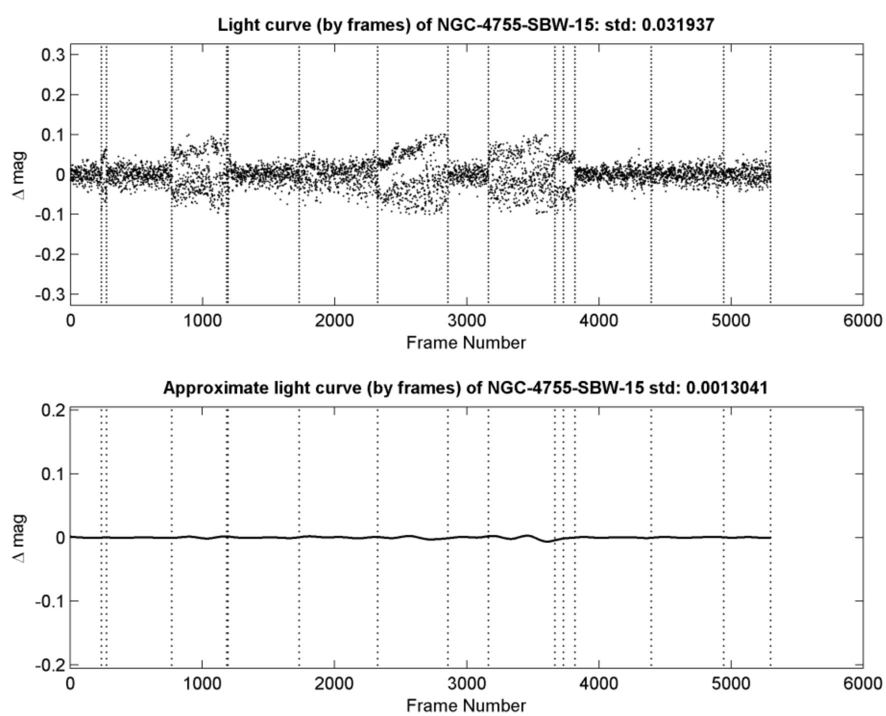

4. NGC 4755 SBW 15 (CX Cru)

Figure 5.10 Full light curves (with frames) of some known variable stars

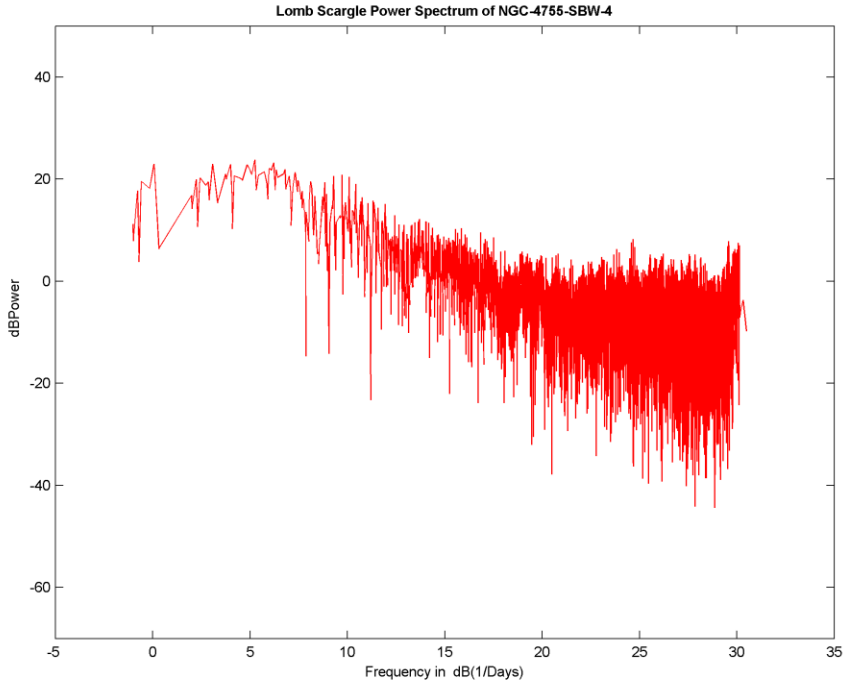

1. NGC 4755 SBW 4 (EI Cru)

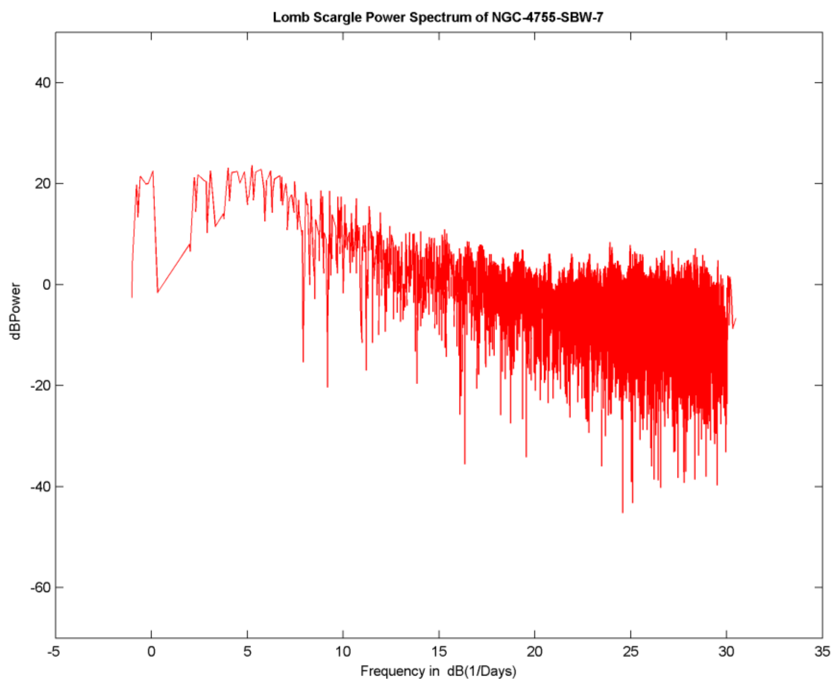

2. NGC 4755 SBW 7 (CY Cru)

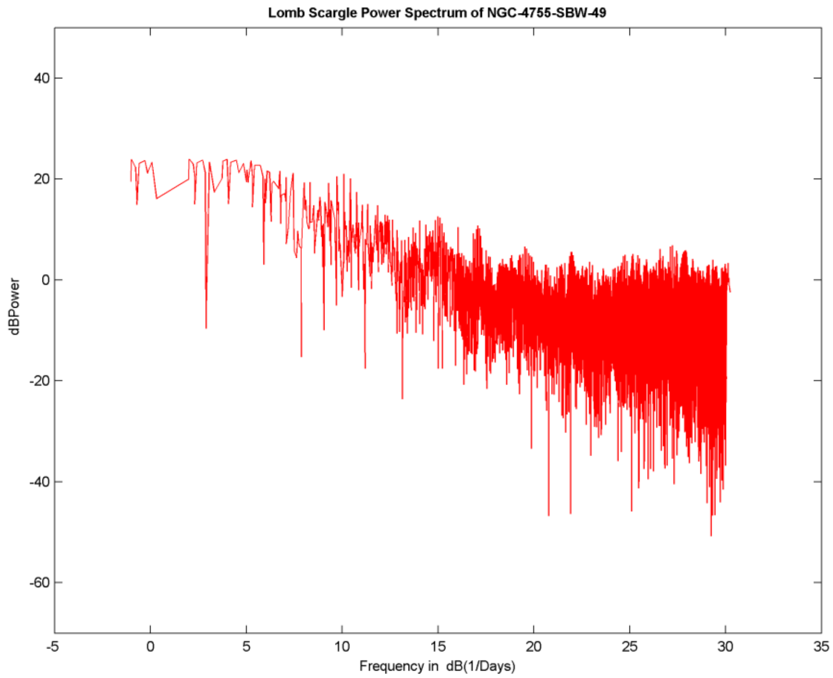

3. NGC 4755 SBW 49 (EG Cru)

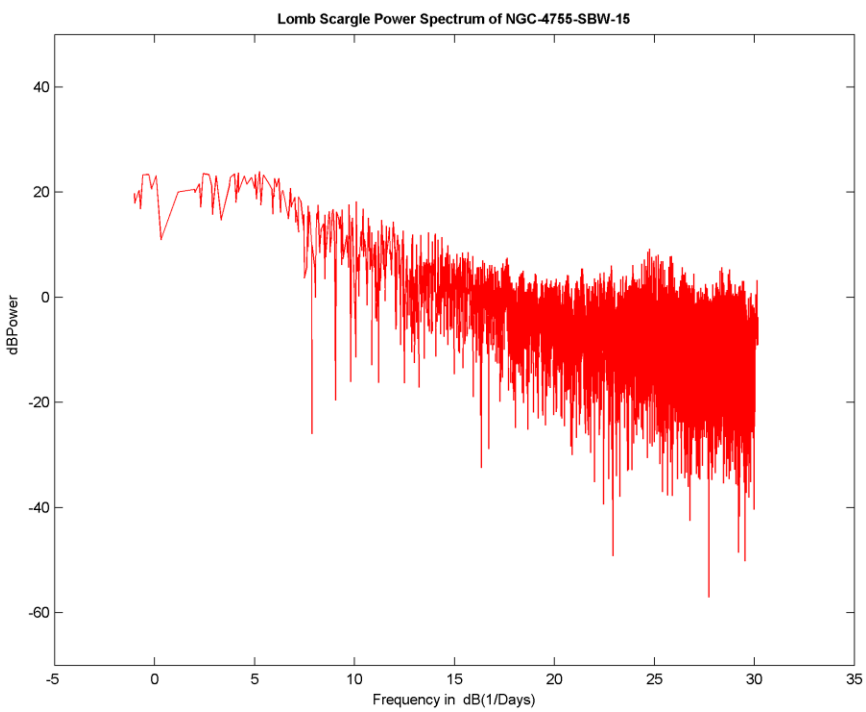

4. NGC 4755 SBW 15 (CX Cru)

Figure 5.11 PSD diagrams of stars of Figure 5.8

5.3.4 PSD diagrams of variable stars in NGC 4755 with known cyclic times

PSD diagrams of variable stars (Table 5.1) with known cyclic times (They are listed in AAVSO) from the cluster are given in Figure 5.12.

Star name	Published cyclic time (days)	Variable star type	Peak frequencies (Cycles/ day) as in the PSD	Period found in this search (days)
NGC 4755 SBW 3 (BW CRU)	0.203 (4.9 cycles per day)	Beta Cepheid	5.0 dB	0.316
NGC 4755 SBW 8 (BT CRU)	0.133 (7.5 cycles per day)	Beta Cepheid	5.5 dB	0.28
NGC 4755 SBW 9 (BS CRU)	0.275 (3.6 cycles per day)	Beta Cepheid	3.5 dB	0.446
NGC 4755 SBW 27 (BV CRU)	0.16 (6.25 cycles per day)	Beta Cepheid	3 dB	0.5

Table 5.1 Summary of the variable stars with published cycle time

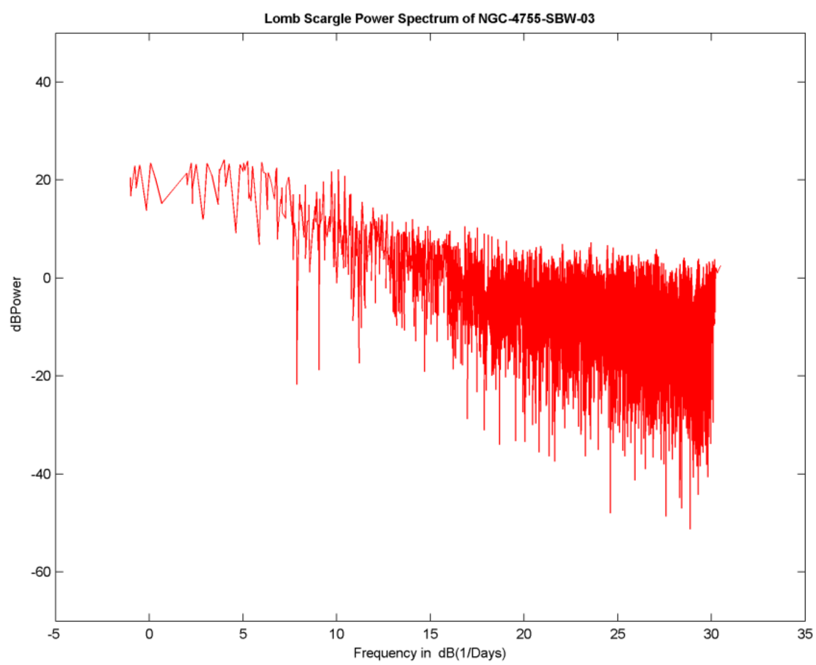

1. NGC-4755-SBW-3 (BW CRU)

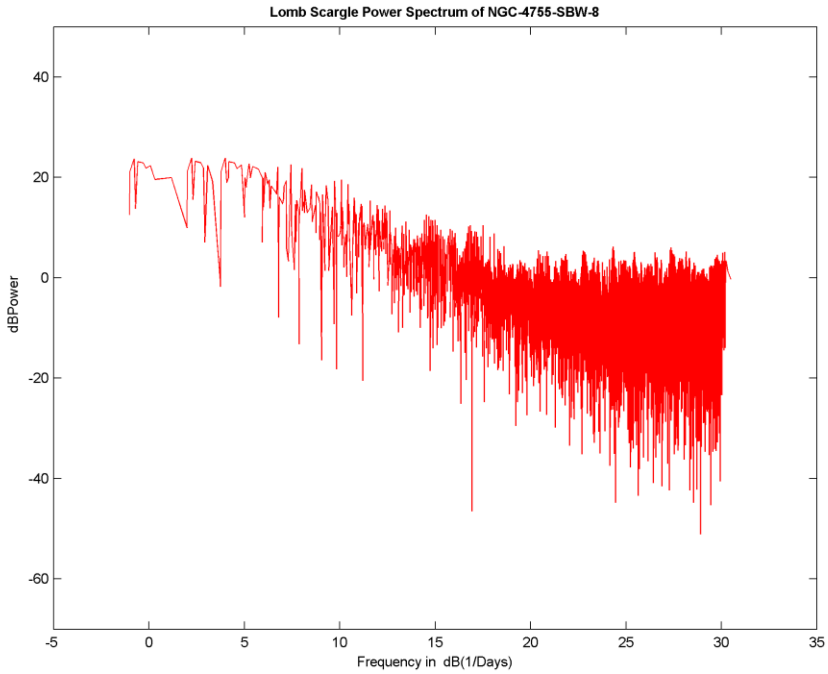

2. NGC-4755-SBW-8 (BT CRU)

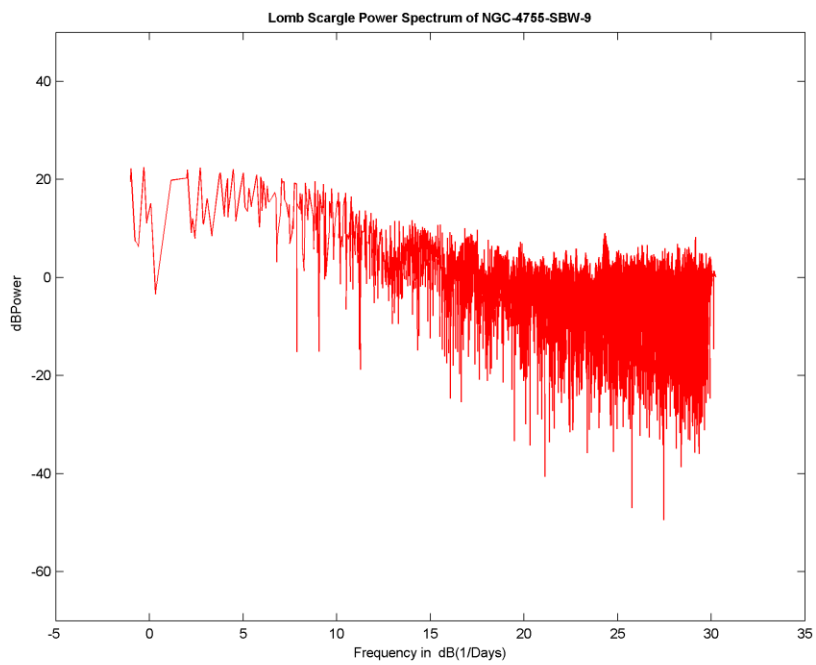

3 NGC-4755-SBW-9 (BS CRU)

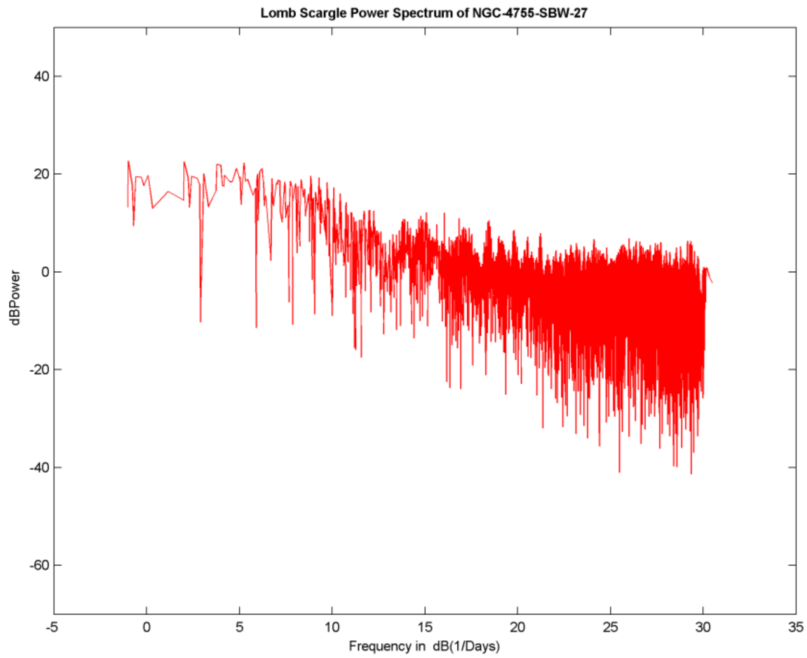

4. NGC-4755-SBW-27 (BV CRU)

Figure 5.12 PSD graphs of variable stars of NGC 4755 with known cyclic times

There is a significant difference of values of calculated periods and the published periods of variable stars. Apparently, the selection of main peaks in PSD diagrams is very difficult as the PSD curve is not a smooth-curve at the main peak and the adjacent peaks to the main. The difference of frequency value to the published value could be the error of selection of the main peak. At least the calculated periods are in range of the expected period. There are other peaks in the diagram, caused by being the harmonics of the fundamental or effects due to blending with nearby stars. The results suggest that there is lot of noise in the data and there is a need of data in a longer time segment; current 100 samples (50 minutes) are not adequate.

About 30 faint stars showed the possibility of them being variable stars. But the estimated spectral types of some of these stars are of type M or K; hence they cannot be variable stars. The question is; are they having closer transiting planets with orbital period of couple of hours? Table E.1 gives a summary of these stars; it shows only the stars having entries in the Arp and Van Sant (1958) tables. The given frequency is an extrapolated value as all suffer from limits introduced by 70 minutes continuous sampling time limit. All the known variable stars which have given deviation free light curves show some kind of harmonics in their PSD diagrams.

The PSDs of the simulated curves (Figure 4.22) follows the PSD of the real. The magnitude of red noise in time domain is much less than the signal but in the frequency domain, energy of the red noise is in the same range of the energy of the signal. Simply, the red noise is significant in the frequency domain though white noise is not as white noise is mainly in higher frequencies.

5.3.5 Folded light curves of variable stars with known period

Folding a light curve may show a pattern of transit which may not be seen in the original light curve. To some extent, it is the time domain alternative for PSD. However, the selection of required folding interval is challenging. If the periods are known, multiples of the periods can be selected as the folding interval for different trials. The folding method was applied for all known nineteen variable stars from one hour to fifteen days with 30 minutes increments to find possible orbital periods. This method works only if the possible periods of the variable stars are multiples of 30 minutes. For variable stars with published periods, BW Cru (0.203 days), BS Cru (0.275 days), BV CRU (0.16 days) and BT Cru (0.133 days), folding was done for double of the published variable period value and is given in Figure 5.13.Unfortunaely, variability was not observed. That could be due to high noise content present in the light curve.

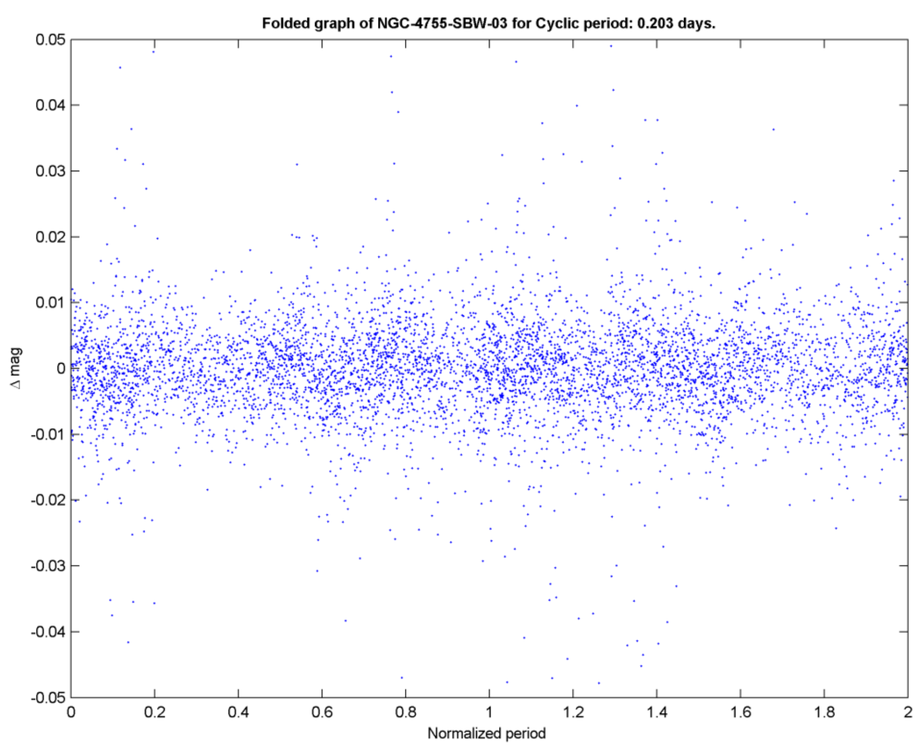

1. For double periods of BW CRU (NGC-4755-SBW 3)

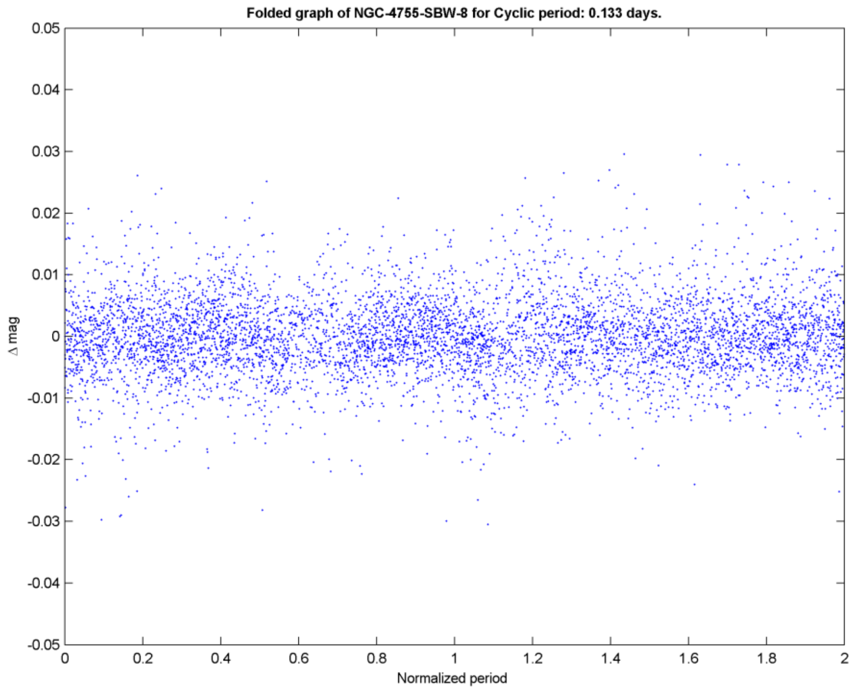

2.For double periods of BT CRU (NGC-4755-SBW-8)

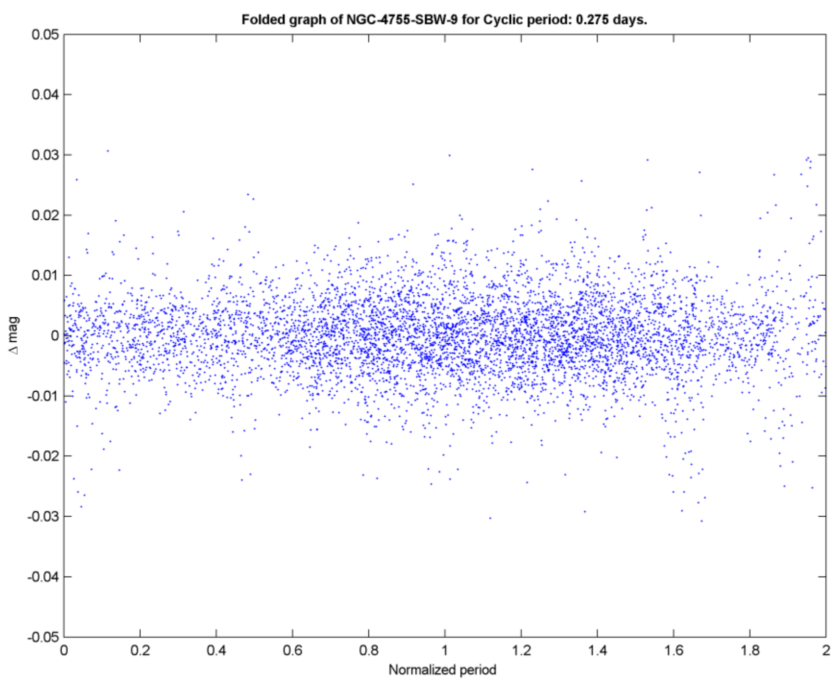

3. For double period of BS CRU (NGC-4755-SBW-9)

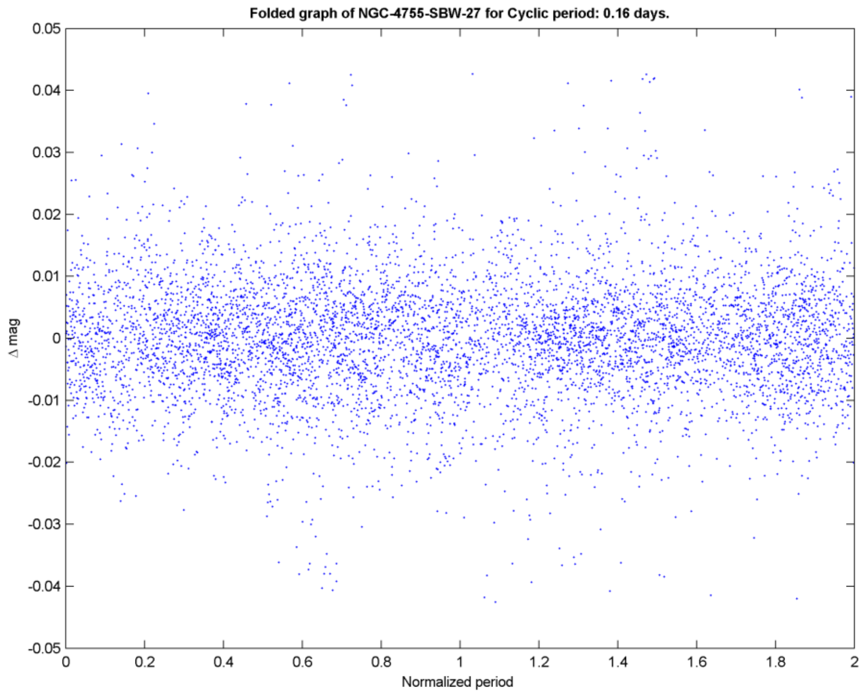

4. For double period of BV CRU (NGC-4755-SBW-27)

Figure 5.13 Folding curves of BS CRU, BW CRU, BT CRU and BV CRU

5.3.6 Validating variable stars with NASA periodogram service

Using tools given by NASA Exoplanet Archive Periodogram Service[23], the light curves of published variables stars were validated. Periodograms of LS and BLS methods were selected. The results are in Appendix K. It shows that BLS method is giving more realistic values over LS method. However, to determine actual cyclic time there should be a light curve showing variability.

5.3.7 H-R diagram

H-R diagrams are used to deduce star characteristics (e.g. temperature, age etc...) from its color, i.e. magnitudes form different color bands. It gives at what stage it is in now in life cycle. As B-V values are available for 473 stars in the FOV of the cluster, H-R diagrams are drawn (Figure 5.14). These B and V magnitudes were taken from the WEBDA astronomical database. Figure 5.14.b, H-R diagram of R Vs V-R roughly follows Figure 5.14, V Vs B-V, drawn from the published data, except the left-end. This diagram shows that most of the stars in cluster are yellow

[23] http://exoplanetarchive.ipac.caltech.edu./cgi-bin/Periodogram/nph-simpleupload

(0.5 < B-V < 1.5); there are blue stars (B-V< 0.5) and some red stars (B-V closer to 2.0). The H-R diagrams in Figures A.4 and Figure 5.14 are matching well, thus verifying that the star mapping from the cluster is accurate. Most of the stars of the cluster follow the main sequence. When the R magnitude is less than 15, the stars in Figure 5.14.b have magnitudes little higher than the expected; thus making the H-R curve to become a nearly vertical segment to the left of the figure, rather than being a left to right downward arc, representing the main sequence. It is suspected that the interstellar reddening and the interfering from the nearby Coal Sack have affected the 'R' magnitude.

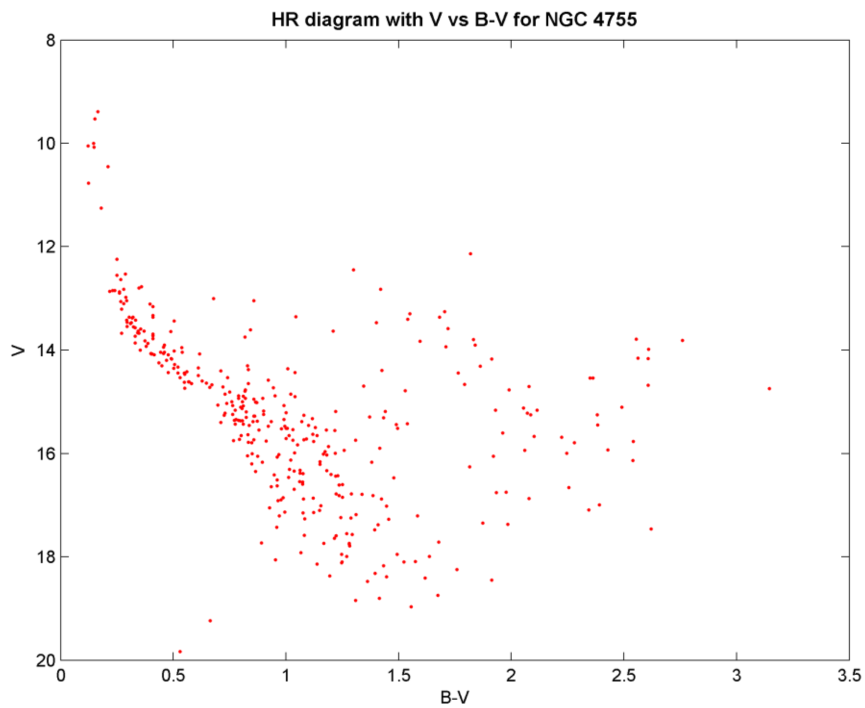

(a) V Vs B-V from Webda data

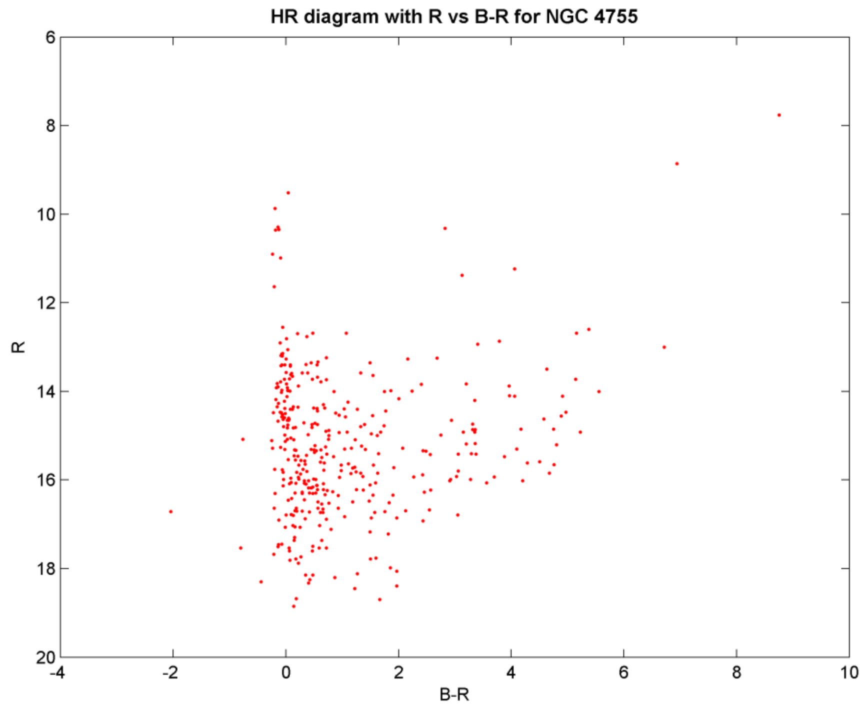

(b) R Vs B-R

Figure 5.14 HR diagrams of cluster stars

5.4 Missing Transits

There were 256 faint stars with calculated spectral types of A0-K0 that had matched ARP (Arp and Van Sant, 1958) coordinates. Table 5.2 presents count of stars whose light curves showed they could give transit like curves for ESPs having radii of 2.0 R_{Jup} or 1.7R_{Jup}.

Spectral Type	ARP total stars	2.0R		1.7R	
		Visible	De-noised	Visible	De-noised
A0	49	1	9	0	5
A5	28	0	11	0	6
F0	17	0	9	0	4
F5	57	6	23	0	11
G0	26	2	11	1	6
G5	37	8	15	8	15
K0	42	5	16	2	11
Sum	256	22	94	11	58
Total			116		69

Table 5.2 Summary of the simulation for the missing transits (Bad sections of the curve were neglected)

Based on the calculated spectral types, every light curve is induced with a square well shaped transit. A noisy night is selected for the injected signal as those nights have more chances to hide a transit. Results for spectral types F5 and G2 are given in Figures 5.15 and 5.16. The diagrams show that if there is a transit, it could have been observed. The red line indicates the mean of the curve and the segment in which the fake signal is injected while blue in de-noised is an indication for a bump which can occur instead of a dip.

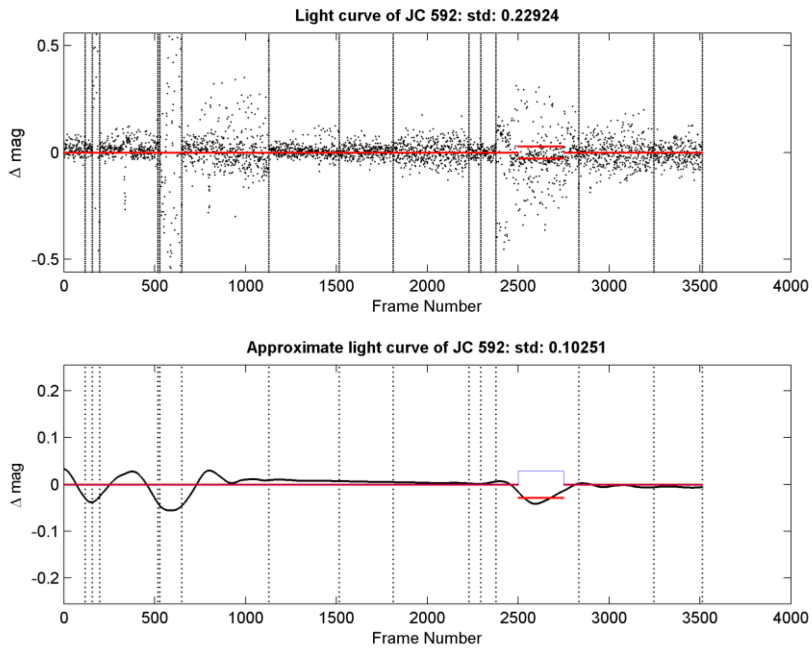

Figure 5.15 Induced transit for spectral type F5

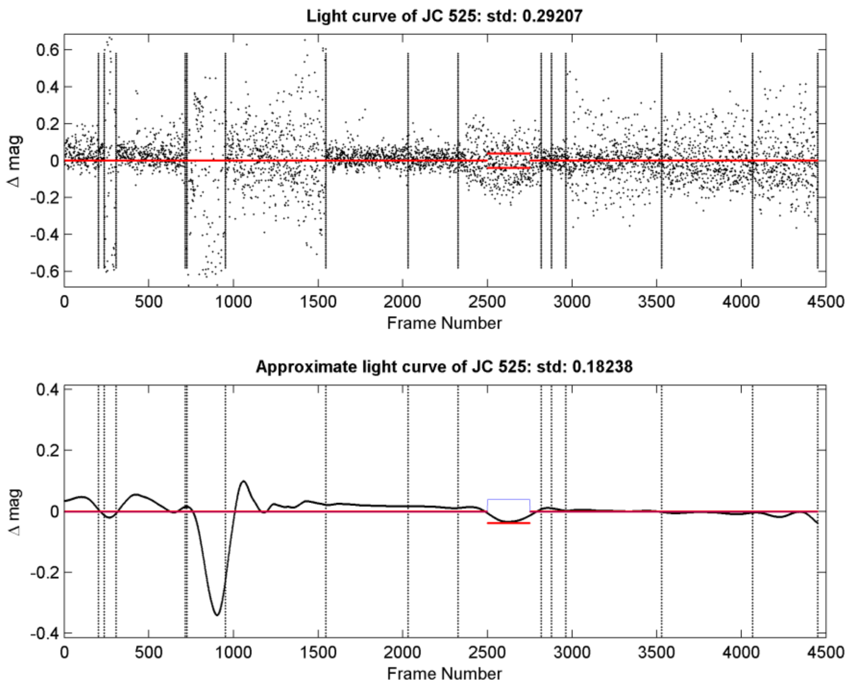

Figure 5.16 Induced transit for spectral type G2

5.5 Comparison with 2MASS survey data

2MASS (see Appendix B) data is available for the Kappa Crux region. Using J, H and K band spectral values, 2MASS data can be used for identifying M, L or T dwarfs. To identify stars in the FOV, 2MASS coordinates were compared with CCD frames for 4 arc seconds maximum error.

Conditions with Spectral value	Result
0.4 < J-K< 1.3 & R-K > 5.5	Stars are dominated by M dwarfs and Asteroids
J-K > 1.3	All 2MASS brown dwarfs
R -K > 5.5	stars are either early M dwarfs (M6-M8) or L dwarfs
R -K > 5.5 & J-K > 1.3	All L dwarfs
J-K> 1.7 & K < 15.0	2 MASS, L type dwarfs
H-K >0.7 & J-H> 0.9.	L dwarfs

Table 5.3 Conditions for brown dwarfs (Kirkpatrick et al (1999))

Table 5.3 shows the conditions for brown dwarfs (Kirkpatrick et al (1999)). The results are plotted in Color-Color diagrams to cancel the distance from the equation as the distance to the suspected brown dwarfs are not known. From these plots star characteristics like age can be deduced. Figure 5.17 gives J-K vs. R-K for stars in NGC 4755 FOV. R magnitude is obtained from this transit search and J and K magnitudes are obtained from the results of the 2Mass survey. Table 5.4 gives stars with R-K > 5 and it shows possible L or T and M dwarfs in NGC 4755 FOV. Though, there are many objects in FOV of NGC 4755 can be possible M type or brown dwarfs, only 23 have matched with 2MASS objects. In Figure 5.17, early L dwarfs are located at J-K ~ 1.2 and late L dwarfs extend to J-K ~ 2.1.

2MASS identifier	B	R	J	H	K	R-K	J-K	Comments
12534269-6022102	16.76	16.05	12.139	11.126	10.84	5.21	1.30	
12534067-6023117	17.889	16.23	10.64	9.396	8.872	7.36	1.77	Possible L or T [24]
12532862-6023219	18.251	16.90	13.469	12.272	11.87	5.03	1.60	
12540131-6021582	18.566	18.34	13.38	12.217	11.86	6.48	1.52	Possible L or T
12540106-6022276	16.57	15.41	11.569	10.576	10.18	5.23	1.39	
12540194-6022580	17.565	17.37	13.292	12.353	12.14	5.24	1.16	
12535992-6023427	16.5	17.00	12.32	11.644	11.52	5.48	0.80	Possible M dwarf
12532065-6020444	17.283	15.96	11.618	10.513	10.14	5.82	1.48	Possible L or T
12532283-6024382	20.692	17.30	12.459	11.813	11.59	5.71	0.87	Possible M dwarf
12531457-6020117	17.217	17.50	13.323	12.237	11.91	5.58	1.41	Possible L or T
12541033-6020184	17.657	16.71	11.681	11.005	10.8	5.91	0.89	Possible M dwarf
12531706-6019278	16.596	15.39	11.428	10.354	9.971	5.42	1.46	Possible L or T
12541169-6023420	17.596	16.78	12.603	11.428	11.12	5.66	1.48	Possible L or T
12541155-6020156	17.657	16.71	12.117	11.332	11.08	5.63	1.04	Possible M dwarf
12531585-6019241	17.604	16.58	12.284	11.204	10.91	5.67	1.37	Possible L or T
12530998-6020269	16.591	16.78	11.739	11.005	10.83	5.94	0.91	Possible L or T
12541786-6022392	17.97	18.29	14.01	13.117	12.86	5.43	1.15	
12541774-6022549	16.89	16.37	12.329	11.314	10.93	5.44	1.40	
12530964-6019546	16.343	15.72	11.57	10.582	10.22	5.50	1.35	Possible L or T
12530581-6021084	18.38	17.07	13.032	12.29	12.07	5.01	0.97	
12541465-6024259	15.641	15.51	9.569	8.985	8.857	6.66	0.71	Possible M dwarf
12530381-6021298	18.676	18.14	14.28	13.33	13.03	5.11	1.25	
12530373-6021215	18.858	19.11	14.582	13.994	13.86	5.25	0.73	

Table 5.4 Inspection with 2 MASS survey where R-K > 5 (2MASS All-Sky Catalog of Point Sources - Skrutskie et al, 2006)

[24] Followed up by Miroslav Fillipovic and this is a very strong L contender (private communication). Later by Jonathan Gagni.

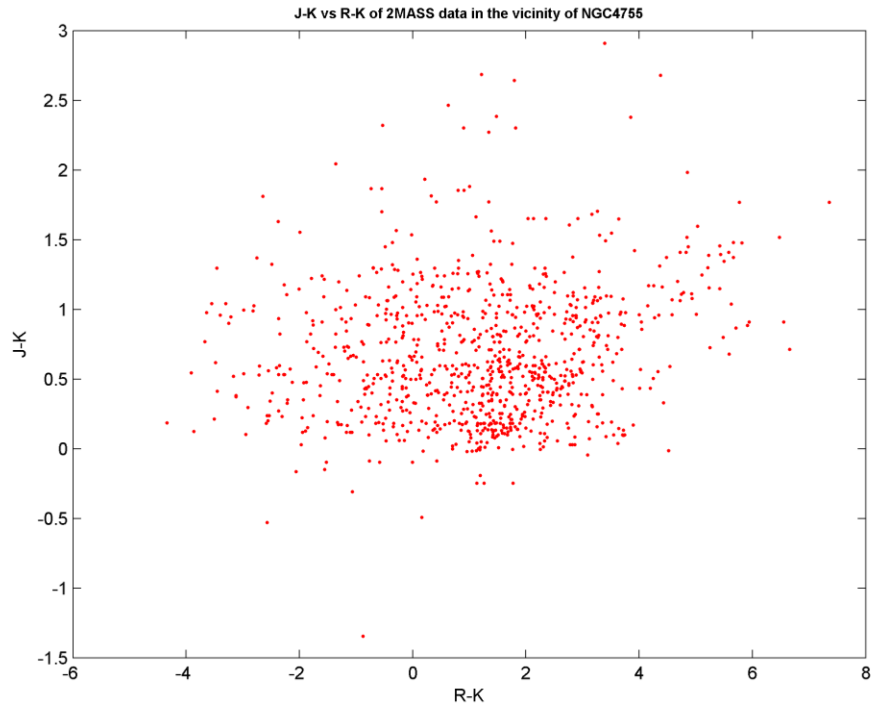

Figure 5.17 Plot of J-K vs. R-K around 4' radius of NGC 4755

A plot of J-H vs. H -K (Figure 5.18) gives possible brown dwarfs (type L and T) in the FOV of the NGC 4755. L dwarfs are in the region where H-K > 0.7 and J-H> 0.9. Figure 5.18 shows early M-types, (J-H, H-K) ~ (0.6, 0.2) and late-M dwarfs, (J-H, H-K) ~ (0.7, 0.5) as in brown dwarf classification (Kirkpatrick et al, 1999). Early T -dwarfs are seen at (J-H, H-K) ~ (0.9, 0.2). T dwarfs classification is given in Table 5.5. These J-H, and H-K, values are solely depending on the accuracy of 2MASS survey. The space positional match of 2MASS brown dwarf type objects to objects of JCU transit search is an indication that many objects in the FOV of NGC 4755 are not belong to the cluster and very closer than the cluster itself. JCU search helped to get the 'R' magnitude of these objects which is missing in 2MASS survey. The classification of these suspected brown dwarfs depends on the accuracy of 'R' magnitudes calculated. These possible brown dwarfs are to be validated by spectral analysis. Note: the object #2 of Table 5.4 was tested for spectral analysis and results indicated that this could be type L[25]). In March 2014, NIR Spectroscopy tests[26] identified this object as a very distant giant.

[25] Followed up by Miroslav Fillipovic (private communication).
[26] Done by Jonathan Gagni

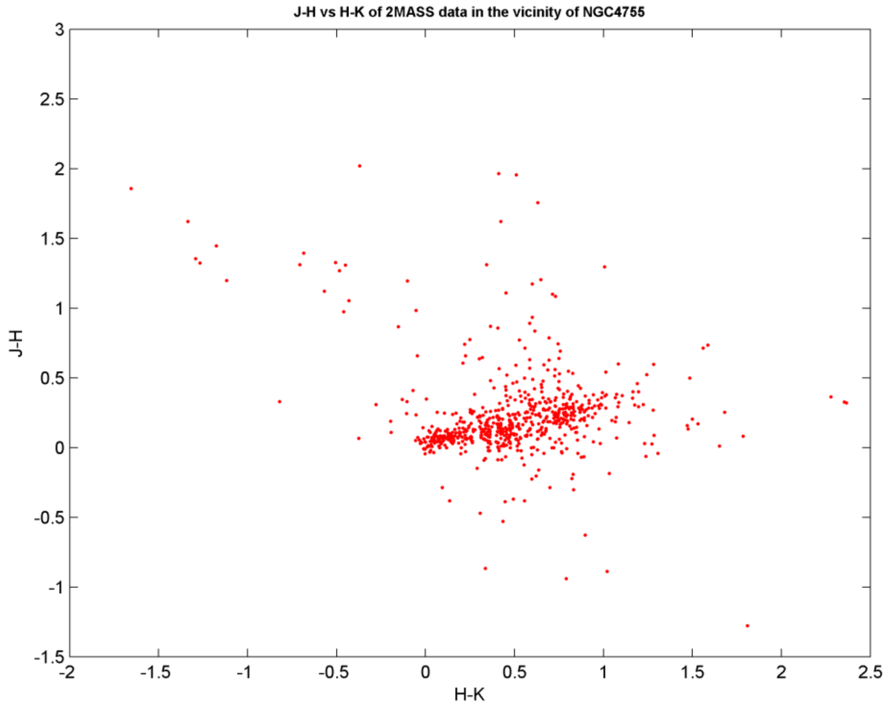

Figure 5.18 Plot of J-H vs. H-K around 5' radius of NGC 4755

Conditions for L or T dwarfs	Result
J-K > 1.3 and K <13 and R-K > 6	Nearer L dwarfs
J-K = 0 (appx)	Typical T -dwarfs (table 5.4)
H-K >0.7 and J-H> 0.9.	L dwarfs

Table 5.5 Conditions for L or T dwarfs as in Kirkpatrick et al (2000)

2Mass Identifier	B	R	J	H	K	R-K
12534417-6021537	16.315	15.363	13.105	13.301	13.111	2.252
12533938-6022398	10.174	11.0509	10.849	10.859	10.866	0.1849
12534690-6022273	9.759	10.6156	11.371	11.747	11.68	-1.0644
12533802-6022395	14.65	14.4477	9.917	9.92	9.93	4.5177
12533559-6021328	13.446	13.4235	12.958	12.773	14.303	-0.8795
12535173-6021586	13.75	12.8451	9.712	9.715	9.758	3.0871
12535302-6021572	13.158	12.8451	12.137	12.192	12.14	0.7051
12534949-6023029	13.723	9.2481	8.267	8.278	8.288	0.9601

12534492-6023236	17.336	11.9006	13.311	12.52	13.459	-1.5584
12533229-6020435	17.05	14.6604	14.012	14.833	14.503	0.1574
12534687-6020207	16.403	15.2064	13.819	13.725	14.011	1.1954
12533549-6023467	9.681	10.5712	9.379	9.356	9.387	1.1842
12532566-6022596	10.222	11.0173	9.857	9.886	9.856	1.1613
12534794-6024192	14.461	11.9332	13.831	13.525	13.995	-2.0618
12535753-6024580	9.012	9.9116	8.843	8.847	8.859	1.0526
12531057-6020501	16.99	16.0812	15.988	15.554	16.084	-0.0028
12541183-6024182	13.754	14.5474	13.039	13.011	13.031	1.5164
12530768-6019304	16.019	16.285	15.776	15.971	15.862	0.423

Table 5.6 Inspection with 2 MASS survey where |J-K| < 0.01 (2MASS All-Sky Catalog of Point Sources - Skrutskie et al, 2006)

Figures 5.17 and 5.18 shows that there are several T dwarf candidates also present in NGC 4755 FOV.

Chapter 6

Analysis of Results

Although many transit identification methods were described in Chapter 3, the analysis in this study is done by;

- Visual inspection of the original light curves and the wavelet based de-noised light curves. Looking at the LS periodogram for a possible frequency line related for a transit.
- Using software routines written for the analytical methods (correlation) in chapter 3 to unveil any transit.

6.1 Transit signatures of differential and approximated light curves

All the approximated light curves have SD less than 10 milli-magnitudes until the 'V" magnitude reaches 14, with the exception of a few stars; this is higher than the expected SD of 5 milli-mag. For example, the light curves (Figure 5.6) of the star with 'V' magnitude of 14.00, NGC-4755 SBW 222 has a SD of 86 milli-magnitudes and the approximated version has a SD of about 6 milli-magnitudes. Some light curves have very high SDs due to the possibility of these being variable stars or bad sky conditions of the observing nights. Four hours of observation data on the night 19 is bad, and once these bad data sets are excluded, the SD of the approximated curve will be reduced by two milli-magnitudes while the normal light curve can be reduced by seven milli-magnitudes. In general, for stars with 'V' band magnitudes less than 14, the photometric precision of the approximated data set is less than five milli-magnitudes.

Theoretically, averaging (continuous) of 'n' points decreases the SD by $\sqrt{n}$ for a Gaussian signal. A fifteen point moving averaging decreases the SD only by little more than a factor of 2, instead of the theoretical value which is closer to 4 (See Appendix G). This indicates that noise in light curves differs significantly from Gaussian noise; thus there could be a strong red noise component in the light curves.

De-noising reduces the SD of original differential light curves by more than 50%. Many approximated graphs show SD less than 1 milli-magnitude. For bright stars with magnitude less than 11, the improvement from de-trending is apparently higher. De-trending allows focus on the analysis of the fluctuations in the data about the trend.

Because of the apparent sky positions move westward, stars at the Western side of the cluster move out of the FOV and new star appear on the Eastern side; CCD for a star is changing. As the intrinsic CCD response may not be uniform across the FOV, this movement may cause non uniform photon capture. This also introduces differential position effects, which may contribute to the noise when the target star images are close to the edge of CCD plate.

Blends of target stars could be a prime reason for getting extra flux amount and different noise levels as some light curves show two series of light curves for some nights. This contamination of flux reduces the observed eclipses and transit depths.

In a given night, there is an approximately linear change in differential magnitudes with time. This trend is due to differential extinction, the changing sky conditions and the twilight varying over the time interval of 6-8 hours of observations. This effect is greater for the fainter stars. It was noticed that the larger the photometry aperture the larger the slope (trend). This drift could happen due to the inability of the IRAF sky fitting routines to follow changes of environment (background) level effectively. As the ratio of flux is used, it was assumed that the differential photometry cancels this drift. To minimize the drift, the effective aperture radius was trialed and changed during the data reduction phase but this had negligible effect on final magnitude values.

In the de-noised light curves of stars of spectral types of A and O, there are dips in range of 5 milli-mags lasting many minutes. These stars are not the typical stars where transits are expected. These variations could be because the star under consideration is a variable star (as in Pepper et al, 2008) although a recurrent pattern is not found.

The inserted fake transits used to find the probability of missing transits, clearly show the advantage of the de-noising of the light curves, as the results show very clear transit in the de-noised curve, while the raw light curve does not show any signs of transits.

Kepler data (Appendix J) has many recurrence type peaks and transit like artifacts. These could be transit signals of other planet orbiting the same star. As shown for Kepler 32b (Appendix J), the signatures of these other planets can be found by better BLS periodogram as in Appendix K. Many Kepler light curves also show many instrumental trends. Other than transits, de-noised curve shows unavoidable edge-effect of Matlab routine and recurring characteristics. For curves like Kepler 4b, these recurrent characteristics are not significant as SNR is very high. For Kepler 32b and Kepler 70b, this recurrent characteristic contaminates the desired data as the magnitudes are in same range as the transit signal.

6.2 Correlation with simulated light curves

The cross correlation with a simulated transit signal shows no signs of a transit in the correlated curves. The half transit like feature (like a glitch) at the end of the correlated graphs was not due to a transit but was a limitation of the MATLAB software which handles the end conditions badly. If there was a transit, the correlator must give a magnified transit type curve at the time window of the transit.

6.3 Segmented FFT and PSD by LS

For the light curve of the cluster, the meaningful lowest frequency is determined by the maximum continuous data segment which lasts about 6 hours. Thus the lowest frequency expected is about 4 cycles per day. But, as telescope realignment happened during data capture, the actual continuous segment is about 100 samples (1.17 hours); the minimum detectable frequency is closer to 20 cycles per day. As the lowest orbital time expected for a hot Jupiter is around one day, i.e. transit frequencies are closer to one cycle per day, the FFT PSD cannot detect transits as it is quite sensitive to the very short-period transiting planets. However, it can detect star variability, which is typically many cycles per day. To get over the problem of telescope re-positioning, the LS method is used to get the PSD. This shows peaks around 3-5 Cycles/day. This is generally good for many variable stars of Beta Cepheid's which are having variable frequency of that range.

The ratio of transit duration to period, or the duty cycle, varies as $P^{(-2/3)}$ (where P is the planet's orbital period) and is large as 20% for ultra-short-period planets. In this case taking FFT may be effective to find parameters (IEEE, 2014).

At the decomposition level of seven, a common minor peak appears at 23 cycles per day with about 100 times less power. This frequency is erroneous and this could be due to the discontinuities in the light curve. I.e. the homogeneity of the sampling sequence was lost when the telescope is repositioned in every one hundredth frame. Harmonics type behaviour can be seen in the known variable star, indicating variability. There could be side-lobes in the PSD diagram, but they are not visible due to the large relative bandwidth of the peaks as the average is taken out from the separate PSD curves.

As discussed earlier, the PSD curves of variable stars, NGC 4755 SBW 5 (EI Cru), NGC 4755 SBW 3 (BW Cru) and NGC 4755 SBW 27, and some other stars show prominent frequency peaks which could be harmonics (Listed in Appendix E).

The PSD of approximated light curve of NGC 4755 SBW 22 shows spikes at frequencies of multiples of 16.5 per day. This feature appears when noise is removed. This star is of type B, brighter and has good SNR for the light curve. The only possibility is; this star can be a variable star. This needs to be analyzed as a future application.

Applying LS method to known transiting planets: Kepler 4b and Kepler 32b give nearly similar orbital period. Kepler 72b has an orbital period lesser than it can be measured by de-noising. Kepler 4b is not for de-noising as SNR > 100 and de-noising is for light curves having SNR < 3.

6.4 Noise issues

For the light curves, the SD of the multi-point average of ‘n’ points is greater than the theoretical value ($\sigma/\sqrt{n}$); there is a systematic noise component (red noise) also present in the noise. Calculations show that it needs 16 - 25 samples to be binned in order to get the required SD to the de-noised light curve. This makes the new sampling interval 10.7 - 16.6 minutes and that gives only 3-6 samples per hour, giving insufficient sampling points to cover transits having transit duration less than two hours. However, it could still indicate something suspicious.

Pont (2006) suggested that if the camera is small in FOV, its red noise is proportional to the photon noise, and that can be a reason for red noise of Perth telescope. Although transits reside in the region of the red noise component, which is hard to remove, an actual transit signal can still be detected with red noise present, provided that SNR is reasonably high. Although a typical transit signal is being looked for, grazing or shallow transits (or eclipses) may pass un-noticed as the trend of the light curve is neutralized.

There are other noise sources as the observing is done through the atmosphere. Scintillation causes a stellar image to ‘dance’ rapidly and randomly with time on a scale of few arc-seconds, making a faint star smeared into disk unless observed by a high-resolution telescope. This affects greatly to the SNR as the stars in the cluster are mostly less than one arc-second in diameter. Rapid-scintillation becomes larger and this becomes a considerable noise source when the cluster moves to the horizon. When the cluster is at the zenith, it gives the best SNR and at the horizon it has highest absorption and scintillation. The nights are not completely dark as scattered moon light and sun light can be present. As this search has been done for a month, the noise due to moon light cannot be neglected for some days (Note: 1st June 2007 is a full moon day), though the differential photometry should remove this error.

This search is a wide star project and as there are thousands of stars to be looked at, the reduction process is automated. Hence, the reduction is based on some pre-set parameters to a program which finds stars in given CCD frame. Though this method worked well, the pre-set parameters are not the perfect for all the stars as stars have different stellar types; hence it can introduce noise to the system. In an automated reduction, addition of such noise cannot be avoided.

The data obtained for Kepler 4b shows very clear transits as that data was recorded in atmosphere free environment. Still this data shows gradual declining of flux level with time, similar to what being observed in ground based telescopes. SNR is clearly over the minimum expected of 3. With such a good SNR, transits are clear. As the depth of transit is getting low, the effects of artefacts in the light curves become severe as for Kepler 32b and 70b. At the end, though there is no atmospheric noise components, these light curves behaves similar to the one observed at earth; with possible instrument related noise.

The important quantity that limits accuracy and determines the faintest object that can be detected is not the signal strength, but the noise present in the signal itself.

6.5 Known variable stars in the NGC 4755 open cluster

Although the prime intention is to find transits in the NGC 4755 cluster, it has many stars of spectral class B which is unsuitable for transit search as their brightness and intrinsic variability could mask any planet which transits. However, these can be previously-unknown variable stars.

These class B star light curves generally have higher SD than normal stars of the same spectral type and same magnitude. Light variation signal due to a Jupiter sized planet in a B type star is smaller than a G or K type star. Even for the known Beta Cepheids, it is difficult to positively identify unevenly timed, short period variability in noisy data. As folding method did not give any pattern, there is possibility that the data is suffering from large noise component. Hence, it is natural to deduce that the magnitudes of the variations are smaller than the SD of the variable stars. De-trending shouldn't affect the shape of the light curve, but may have affected very long term behaviour, which is typically many number of days. Note: the published variable periods for these stars are in the range of 0.1 - 0.3 days.

Appendix K has the results obtained by using NASA tools for periodograms for LS and BLS methods. The results of LS method differ from large margin while BLS method gives values in similar range.

6.6 Field stars in the NGC 4755

There are several known field stars in the FOV of the NGC 4755 cluster; CPC 20.1 3735, CPD 594569, SAO 252 07, CPD 594539, HD 312082, HD 312073 and CCDM J1 2538-6023B (a double star). They all have magnitudes around 10.0 but, as the faint stars in the cluster, their 'R spectral type was calculated. Data reduction and transit analysis on these stars do not give any possible transit candidates (The stellar type is not correctly known, could be type F). In addition to these stars, comparison with 2MASS survey data in this FOV identified many fainter stars.

6.7 2MASS survey comparison

For H-R diagrams, Color-Color plot was used in Fig 5.14 to remove the dependency on the distance to the star. Color difference was enough to identify the stellar type and the age. The HR diagram (Figure 5.14) indicates unusual red stars. This may not belong to the cluster and this must be an indication of closer stars in the FOV of NGC 4755(Field Stars Section 6.6). These stars can be brown dwarfs or may be late 'L' type of cooler brown dwarfs. The findings for these stars listed in Table 5.3 depend on the accuracy of the 'R' magnitude and an error of 0.5 of 'R' magnitude may change the stellar type of the predicted brown dwarf.

6.8 Why are transit simulations and results different?

For the simulation work, it was assumed there was pure white noise and red noise from fractional Brownian motion. The actual data has many systematic errors than the anticipated and the random noise seems to be stronger than the simulated samples.

The cluster is too distant for the Perth telescope to get data with desired SNR for faint stars, which could be F or G stars. Even the SD of many brighter O and B stars is high. For faint stars, the binning and de-noising did not improve the signal to the desired SNR. This lower SNR also makes the error in interpolated R magnitude much higher. As sky conditions change day to day, observations on different days have different sources of errors which affect differential magnitudes. All of these issues make it better to find a statistical solution for the periods and shapes of the corresponding light curves solution for every night.

One of the main constraints is the ability of the camera, which governs the precision of the photometric process. The exposure time also set up limits for the stars, the brighter limit is set by the saturation (The brightest stars of the cluster, having V magnitude less than 7, are always saturated) and fainter limit is governed by the minimum SNR needed to detect an ESP.

A PSD curve of actual data showed some similarity with those for the simulated data, although the expected features were somewhat deteriorated indicating that actual data has high noise content. The simulation assumed that non-interrupted sampling during the entire observation. However, real data was not continuous, the maximum continuous stretch was 70 minutes and it restricted minimum frequency to be searched by using PSD using FT. Even though LS method is used to alleviate this issue, real data couldn't produce matching PSD to the simulated.

6.9 How the results are translated to project requirements

This is an attempt to find transiting ESPs in a distant open cluster using a ground based wide field CCD camera with the analysis based on signal processing algorithms. The process is similar to the other ESP searches, as it involves getting many days' differential light curves and looking for the differences of the light curves in order to find a transiting signature. Validation of data was done by comparing with simulated data, using real data from successful searches and by inducing fake transits to find missing transits. Unfortunately, like many other transit searches of far distant open clusters, no ESPs were found. However, it has been showed that this method can be used to find transits in a noisy environment. i.e. the transiting planet mentioned in section 4.3.2.

The projects original method of finding transits is by light curve analysis. As the SNR is less than the lower limit of the SNR expected, wavelet based de-noised approximated curves were used to increase the SNR. As this concept was proposed in 2006, it must be the first time that wavelet based de-noising is used in transit search by removing noise to get the long term signal by reducing SD. De-noising gives the researcher the choice of selecting the lowest orbital frequency scale in which the transit may occur. In other transit searches, smoothing the light curve is mostly done by getting a multi-point average, but this just distributes the noise and never removes it fully. Thus de-noising is far superior to noise cancellation. This also stretches the limit of magnitude to which the search can go for. Though the maximum magnitude was about 12 for the cluster, the de-noising showed that the limit can be stretched above 16 for transit search only.

As change of flux may be due to being a variable star with very short period, frequency domain use of data was considered. As FFT based PSD amplifies the common frequency components in the frequency spectrum, it helps the identification of cyclic behaviour, especially of variable stars with narrow pulses in light curve but suffers minimum frequency limit from the length of data segment of this search. LS algorithm removes the time-discontinuity issue in data.

Though it is believed that this cluster contains 200 + stars photometry was done for 1169 stars; that means vast majority of stars are field stars in FOV of 4' radius around the centre. And many of these field stars have entry in the 2MASS survey.

The ultimate goal was to find ESPs; hence in general the end result is no new ESPs. The results obtained from simulation and data validation show the ability to find transits using the existing system with de-noising: thus the current setup nicely fits into a typical transit search program and is adequate enough to find parameters. However, the data is useful to find cyclic periods of variable stars and with help of 2MASS data; it was extended to search brown dwarfs.

By adding a fake well shaped transit signal to the actual signal, it has been proven that the current algorithm can detect typical ESPs; 2.0 R_{Jup} ($10M_{Ju}$) or $1.7R_{Ju}$ ($1M_{Ju}$), which could exist in the NGC 4755. There is no reason to miss a transiting hot Jupiter in the data, provided the transit is correctly aligned to the observation field of view. To determine whether this process can detect smaller ESPs (Neptune sized), a new model is needed as the current model is not sensitive enough.

The algorithms developed here can be customised used to analyse public domain data such as Kepler and COROT, as done in validation section (section 4.3).

In summary, the main reasons of not finding transits (including optional variable stars) are the distance to the cluster NGC 4755 (section 4.2.2) and the very small samples size of the stars.

Perth Telescope does not have the capability to get the required SNR, even though de-noising is used to boost the SNR for transit search only as de-noised data is not the best for searching cyclic periods though at attempt was made. Capability of the telescope is about 3 magnitudes shorter for good light curves. The sample size of stars is about 1000 is not comparable to the sample size of stars of 130000 needed to find one transit as mentioned in section 1.4.6 (Charbonneau, 2003). Fault in calibration and analytical methods are ruled out as these methods worked well with simulated data and two sets of real data, Kepler and Transiting exo-planet data (Blank et al 2015).

Chapter 7

Future work and conclusions

7.1 Future Applications

The primary aim of this thesis was to find transiting planets in the open cluster NGC 4755. Although no transits were found; there are many other and possibly better ways this data can be used for a scientific search.

- Changing aperture photometry to PSF (Point spectral function) photometry. IRAF software supports this method but it is more complicated to run as a batch and extra work has to be done.

- Calculating false alarm rate. It is important to know the probability of a false alarm, should there have been a possible detection in order not to mistake a false signal for a real one. Vartools (Vartools is in References Web list) finds the false alarm rate for large number of light curves in one go. The alarm variability statistics are based on published work of Tamuz et al. (2006). The Matlab program used to obtain Lomb-Scargle periodogram also gives estimated significance of the power values (probability). The significance returned is the false alarm probability of the null hypothesis, i.e. that the data is composed of independent Gaussian random variables. Low probability values indicate a high degree of significance in the associated periodic signal.

- Filtering out transit like signatures hidden in normal light curves. This can be done by removing variable stars and blended stars, and by calculating the period per duration ratio and, if the ratio is not in the hot Jupiter type range, dropping the star.

- Recognize patterns or signatures. Box fitting algorithms can be used (Use successful BLS method). Online BLS periodogram facility by NASA is already available.

- Apply different de-noising methods to the data set. Assuming known or estimated noise properties for the input data derive or make use of wavelet coefficient probability distributions at each level, under a null hypothesis of stochastic input (Starck et al, 2006).

- Adopting algorithms of other fields. It may be possible to adopt algorithms that deal with processes that are slowly varying such as seismology. These algorithms may perform better with red noise.

- Removing systematic trends by reducing red noise. Normal de-noising mainly reduces Gaussian random noise or white noise; the systematic errors are from the red noise but there is no direct way to remove this noise completely unless the source characteristics are known.

- The anomalies in the light curves could be because of the present of ringed planet (Zuluaga et al (2015) and this search can be extended to find exo-rings.

Using data for variable star search:

- The harmonics of PSD data indicates that there is a possibility of the existence of un-identified variable stars in the cluster of the magnitude range of 12 -16.

This data set can be used to do the statistical analysis as described by Aigrain et al (2002) and Aigrain et al (2004). This would be a test for the success of probability statistical methods vs. analytical methods. This data can be analyzed by PSF fitting photometry using the IRAF DAOPHOT package or image subtraction using the ISIS2.2 package (Alard and Lupton, 1998). ISIS does not assume any specific functional shape for the PSF of each image. Therefore, it models the kernel that convolutes the PSF of the reference image to match the PSF of the target image. After the reference image is convoluted with the computed kernel and subtracted from the image, the photometry is done on the resulting difference image (Montalto et al, 2007). Comparison of PSF photometry with aperture photometry (with neighbouring stars subtracted and PSF fitting) by Montalto et al (2007) showed both methods have larger errors with respect to the expected error level and that the PSF fitting approach in general results in poorer photometry for the brightest sources compared to the aperture photometry. They were able to improve photometric precision by using image subtraction photometry, and suggested that image subtraction photometry is more suitable for crowded regions, e.g open clusters NGC 4755.

7.2 Conclusion

Open clusters are regarded as good planet transit monitoring targets because they represent a family of stars of the same multiplicity and distance. This process of searching ESPs is similar to other transit ESP searches, getting many days' differential light curves and looking for difference of the light curves in order to find transiting signatures. Validation was done by comparing with simulated data, Kepler project data and counting possible missing transits. Only handful of ESPs are already found in open clusters, mainly because the SD of the light curves of type F-K type stars are too high to detect a Jupiter sized planet.

This search differs from other searches by two ways. This uses a wavelet based de-noising to the light curves, which in fact removes the noise to get the long term signal, thus decreasing SD, which is better way to find a hidden transit. As no transiting planets found and the cluster is having type B stars, frequency domain analysis is used to find variable stars on assumption that these stars generate narrow pulse like signals. It uses the Lomb-Scargle algorithm: a form of Fourier Transform, taking every segment into consideration. This was a success to get frequency information but the failed to match the published data of variable stars in the cluster.

By adding a fake, well-shaped signal into the actual signal it has been proven that de-noising algorithm can find ESPs of Jupiter size orbiting "F" or "G" which may exist in the NGC 4755.

The target was to find ESPs; the end result has not contributed to expand our knowledge of ESPs. There is no officially known F, G of K stars in the cluster yet, though light curves were tested for over 1000 stars and spectral types were determined using available data of previous searches. The distance to the cluster NGC 4755 is beyond the operational capability power of telescope used to get CCD images and total number of observed stars is too-low to the statistically required number of stars to be observed to get a valid transit.

This is a good opportunity to study variable stars in open clusters; Metal poor NGC 4755 is a cluster having many variable stars, especially Beta Cepheids. Four of the known variable stars have known periods but the folding method could not match the published period. Though these stars are brighter, type B stars, still the telescope is about 2-3 magnitudes inferior to find cyclic pattern.

As the ‘R’ magnitude is available, with the use of 2MASS survey data, this photometry data is helpful to find brown dwarfs in the FOV of NGC 4755 by analyzing the spectral lines.

In future, this search will be continued to optimize our transit detection methods to search for fainter stars.

Appendix A

The open cluster NGC 4755

Star No.	Name	Type	Magnitude. Max	Magnitude. Min	Mag. Type	Period Days	Spectral Class
1	BS Cru	BCEP:	9.75	9.79	V	0.275	B0.5V
2	BT Cru	BCEP	9.8	0.032	B	0.133	B2:V
3	BU Cru	E:	6.8	6.9	V		B1.5Ib
4	BV Cru	BCEP	8.77	0.05	B	0.16	B0.5III(n)
5	BW Cru	BCEP	9.03	9.09	V	0.203	B1V
6	CC Cru	ELL:	7.97	0.08	V		B2III
7	CN Cru	EB	8.61	0.24	B		B1V
8	CQ Cru	E:	12.52	0.07 B	V		B5III
9	CR Cru	E:	11.44		V		?
10	CS Cru	E:	9.83		R		B21Vne
11	CT Cru	BCEP	9.82	0.02 B	V		B1.5V
12	CU Cru	E:	9.58		V		B1.5V
13	CV Cru	BCEP+E:	10.29	0.04 B	V		B1.5V
14	CW Cru	BE	9.98	0.02 B	V		B2Ivne
15	CX Cru	BCEP+E	10.08	0.04 B	V		B1V
16	CY Cru	BCEP+E:	9.66	0.05 B	V		B1.5V
17	CZ Cru	BCEP	10.26	0.02 B	V		B2Vn
18	DS Cru	ACYG:	5.79	5.75	V		A2Iabc
19	DU Cru	LC	7.08	7.52	V		M2Iab
20	EE Cru	Pulse	12.46		V		B3V
21	EI Cru	BCEP	9.38		V		B1V
22	EH Cru	Pulse	11.59		V		B3V
23	EG Cru	Pulse	11.45		V		B3Vn

Table A.1 Variable stars in NGC 4755

Note: Beta Cepheid stars, often abbreviated as the BCEP or β Cepheid type, others are E-II eclipsing binary

Note: These Tables are taken from Andrew James (2002)[27], and SIMBAD database[28]

---

27 www.homepage.mac.com/andjames/
28 http://simbad.u-strasbg.fr)

Star	Mag. (V)	B-V	Spectral. Class
A	5.75	0.325	B8-9 Ib
B	5.94	0.224	B5 II or Ib
C	6.80	0.243	B3-4 II
D	7.85 (7.66)	(2.28)	K5 giant (M2Iab)
E	8.35	0.118	B5II or III
F	9.09	0.153	B6 III:
G	9.79	0.195	B6 V: (B1V)
H	9.93	0.194	(B1.5V)
H	9.93	0.194	(B1.5V)
I	10.04	0.336	(B1.5Vn)
J	10.58	0.151	(B2V)
K	11.42	0.321	(B3V)
L	11.88	0.302	(B8:V)
M	12.40	0.384	(B8III-V)
N	12.76	0.739	
O	13.17	0.494	--
P	13.37	0.254	--
Q	13.38	0.587	--
R*	9.58	0.17	B1.5V
S*	9.59	0.228	B1.5Vnpe
T*	5.75	0.309	A2Iabe

Table A.2 Bright photometric stars of NGC 4755, Stars in Table A.3

[Arp, H. and C. van. Sant (1958) page 34.]

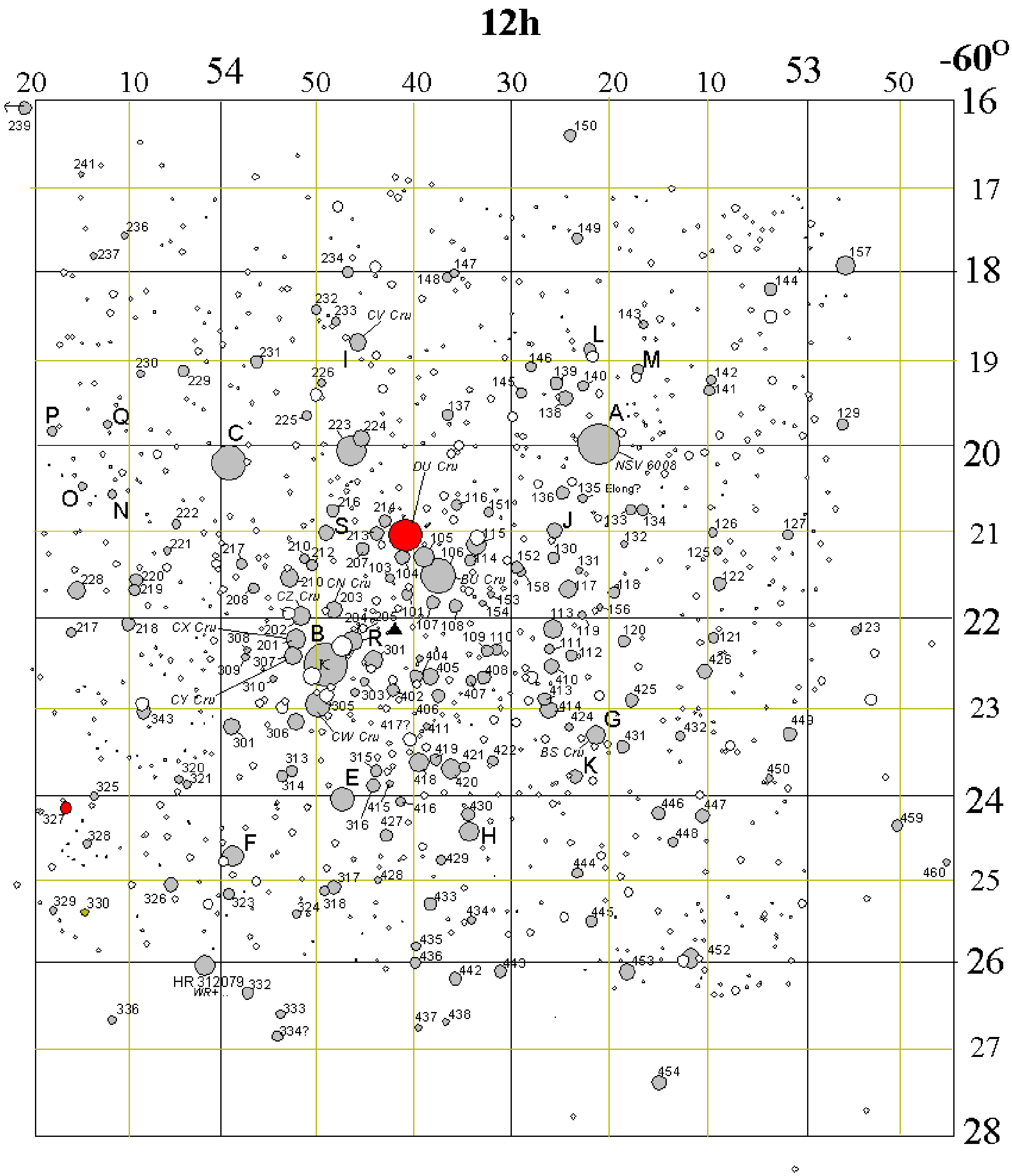

Figure A.1 ARP STARS of NGC 4755

The positions of each of the stars in the text are of NGC 4755 showing all the ARP Stars. These stars appear in the original source; Arp, H. and van Sant, C; “Southern Hemisphere Photometry IV: - The Galactic Cluster NGC4755.”, Astron. J., 63, 341-346. (1958)

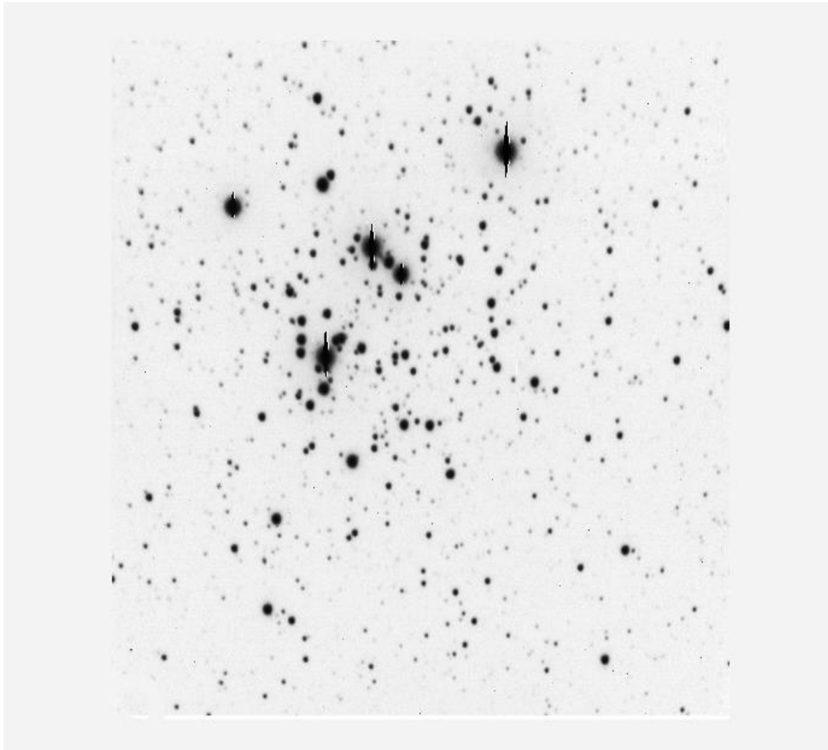

Figure A.2 Open Cluster NGC 4755 as in an FITS image taken by Perth Automated Telescope

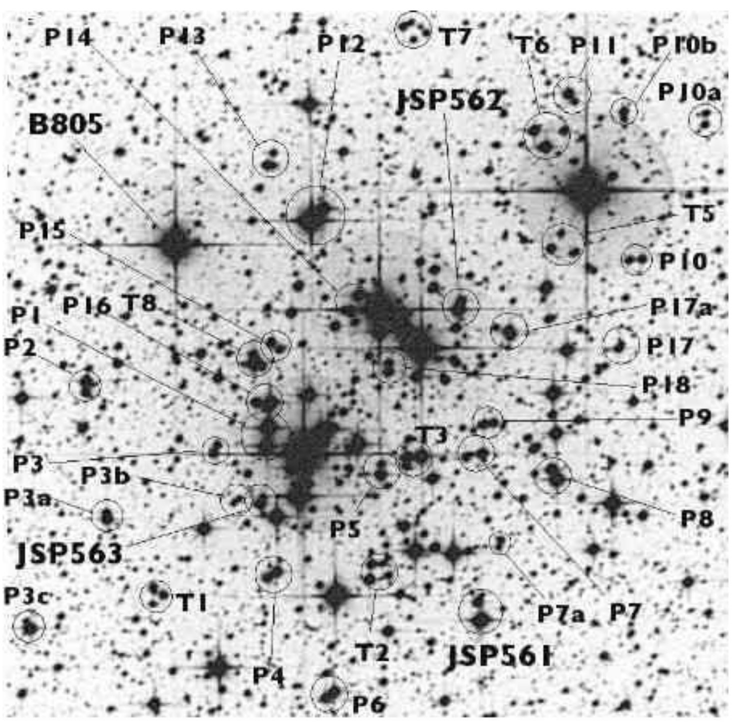

Figure A.3 Double and triple star systems in NGC 4755

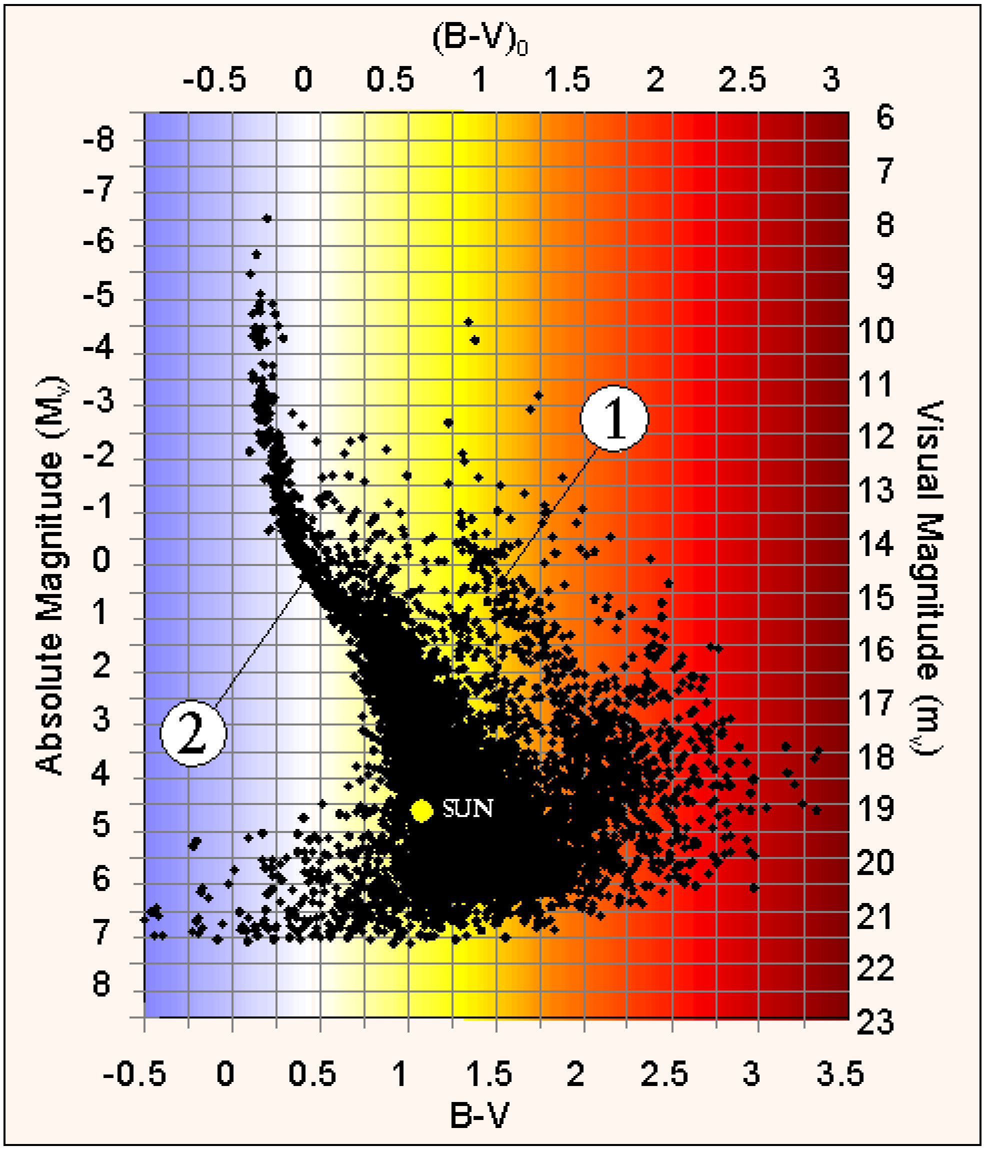

Figure A.4 Colour - Magnitude diagram of NGC 4755

(From Andrew James (2002)[29])

[29] www.homepage.mac.com/andjames

Appendix B

The Two Micron All Sky Survey (2MASS)

The Two Micron All Sky Survey (2MASS) project is a ground-based project for studying the near-infrared sky. Before this project, the only other infrared survey was the Two Micron Sky Survey (TMSS; Neugebauer & Leighton 1969) which scanned 70% of the sky and detected about 5,700 celestial sources of infrared radiation.

The 2MASS has already uniformly scanned the entire sky in three near-infrared bands (I, J and K) to detect and characterize point sources brighter than about 1 mJy in each band, with signal-to-noise ratio (SNR) greater than 10, using a pixel size of 2.0". This work has achieved about 80,000 -fold improvement in sensitivity relative to previous surveys. This utilizes the near-infrared band windows of J (1.11 - 1.36 µm), H (1.50 - 1.80 µm) and K_s (2.00 - 2.32 µm). (Jarret et al, 2000).

2MASS used two automated 1.3-m telescopes, one at Mt. Hopkins, AZ, USA, and one at CTIO, Chile. Each telescope was equipped with a three-channel camera, with each channel consisting of a 256×256 array of HgCdTe detectors, capable of observing the sky simultaneously at J (1.25 microns), H (1.65 microns), and K_s (2.17 microns). The northern 2MASS facility began in 1997 June, and the southern facility in 1998 March. Survey operations were completed on 2001 February 15[30].

The following are the Survey's Level 1 requirements although the actual performance achieved in many cases surpassed these requirements.

- Magnitude Limits

  For unconfused sources outside of the Galactic Plane (|b|>10°), and outside of any confusion-limited areas of the sky outside of the Galactic Plane

[30] http://www.ipac.caltech.edu/2mass/overview/about2mass.html

		Magnitude Limits	
Band	Wavelength (μm)	Point Sources (SNR=10)	Extended Sources
J	1.25	15.8	15.0
H	1.65	15.1	14.3
K_s	2.17	14.3	13.5

Table B.1 Magnitudes

Note: At SNR=10, sigma (mag) = 2.5 / ln 10 = 0.109.

.

- Completeness and Reliability

For unconfused sources outside of the Galactic Plane (|b|>10°), and outside of any confusion-limited areas of the sky outside of the Galactic Plane

	Galactic Latitude Range			
Parameter	>|30|°	|20|-|30|°	|10|-|20|°	<|10|°
Differential Completeness				
Point Sources	0.99	--	--	--
Extended Sources	0.90	--	--	--
Differential Reliability				
Point Sources	0.9995	0.9995	0.9995	0.9995
Extended Sources	0.99	0.99	0.80	--

Table B.2 Locations

- Photometric and Positional Accuracy

Photometric precision	
Unconfused point sources (for sources with SNR >> 20)	5%
Unconfused extended sources (for isophotal magnitude at 20 mag/sq. arcsec.)	10% (H < 13.8)
Photometric spatial uniformity	
Point sources	4%
Extended sources	10%
For Brightest measurable stars	
Photometric bias (for Ks>4)	<2%
Repeatability	5% for K_s=8
	10% for 4<K_s<8
Position Reconstruction Error	0.5"

Table B.3 Positions

- Sky Coverage

The sky coverage will be >>95% for galactic latitude |b|>10° and ~95% for |b|<10°. The overall coverage will have no gaps > 200 square degrees. (Jarret et al, 2000)

Appendix C

Reference stars

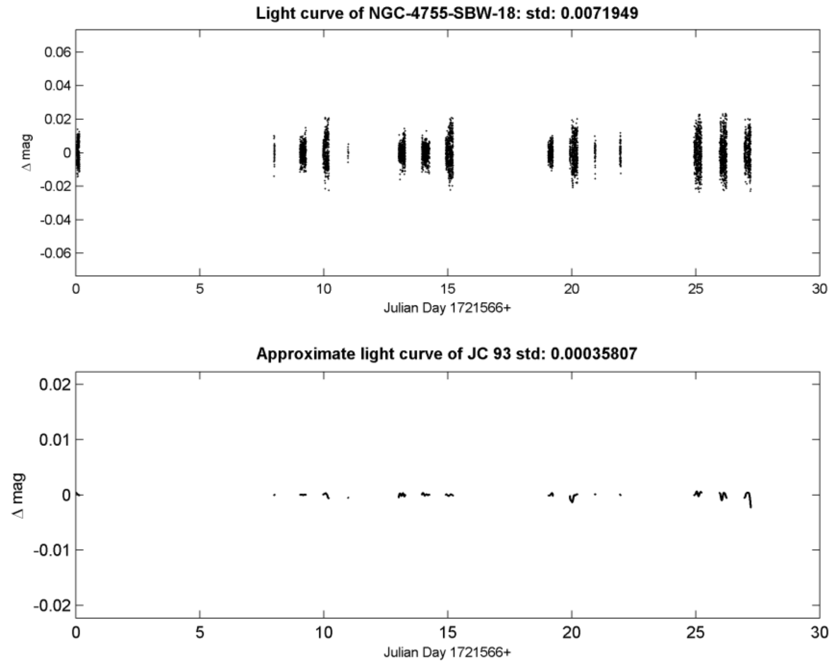

Figure C.1.1 Reference Star NGC 4755 SBW 18

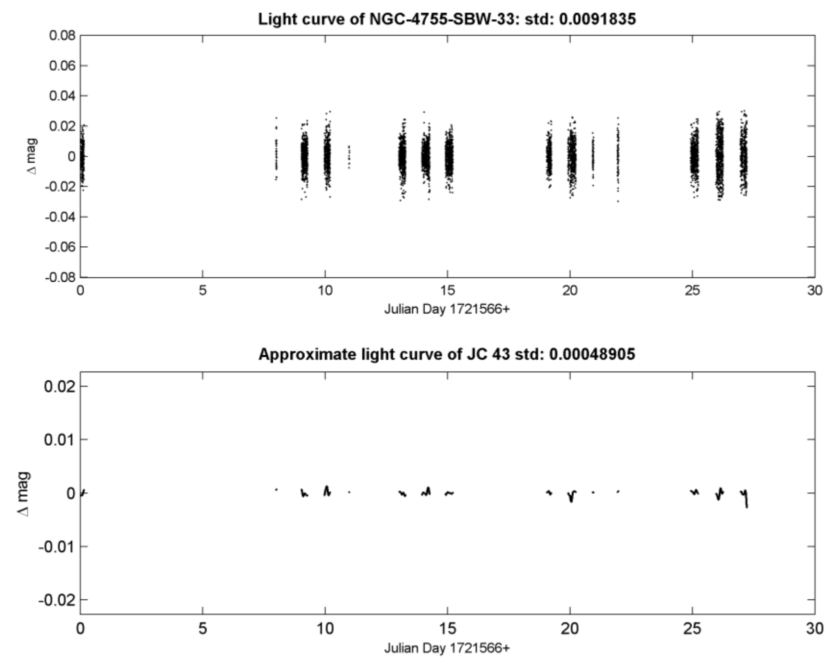

Figure C.1.2 Reference Star NGC 4755 SBW 33

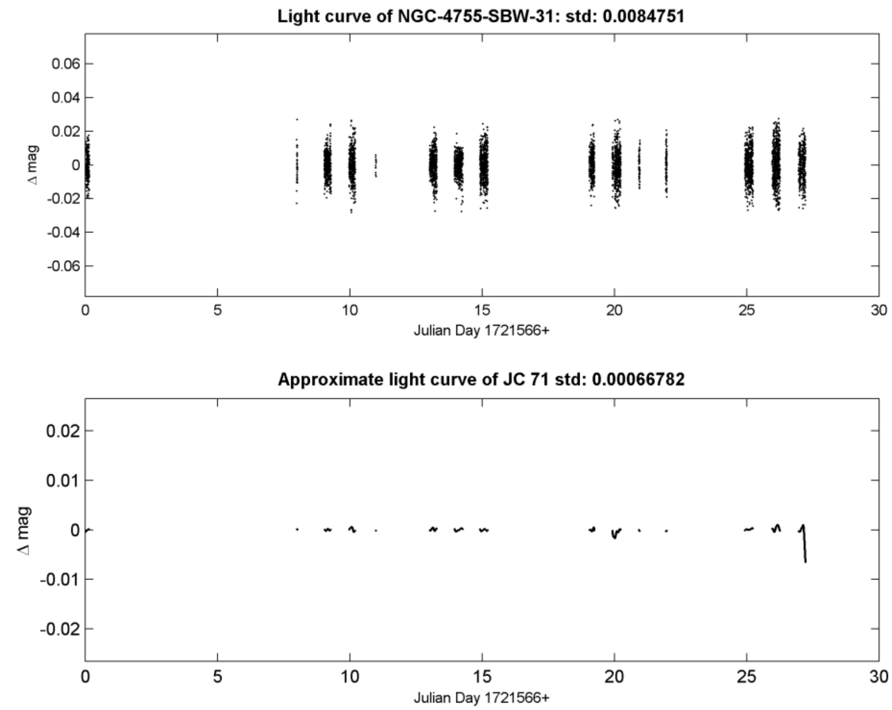

Figure C.1.3 Reference Star NGC 4755 SBW 31

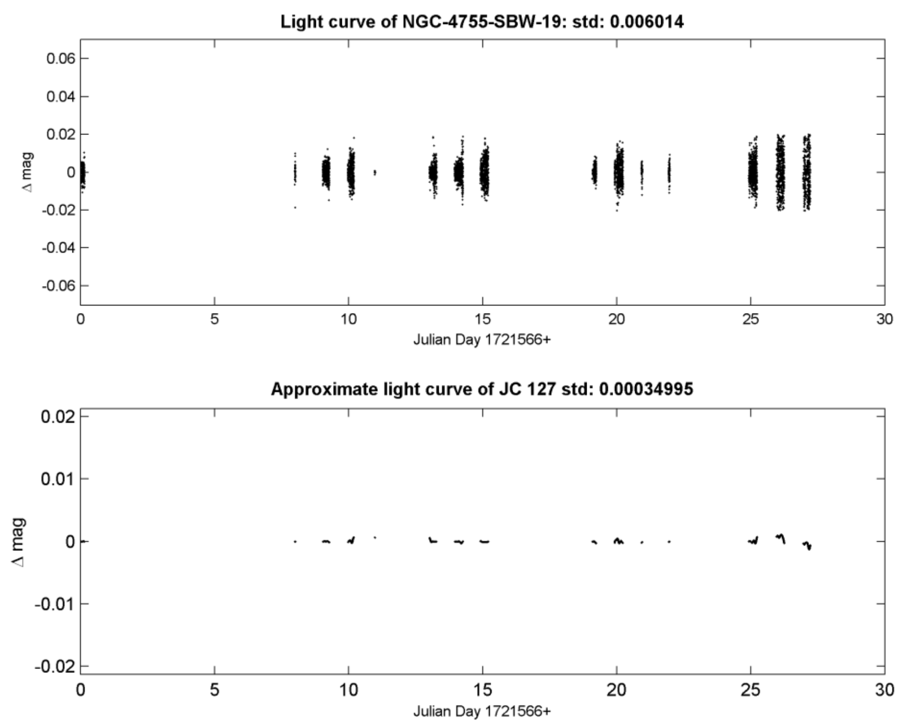

Figure C.1.4 Reference Star NGC 4755 SBW 19

Figure C.1 Light curves of Reference Stars NGC 4755

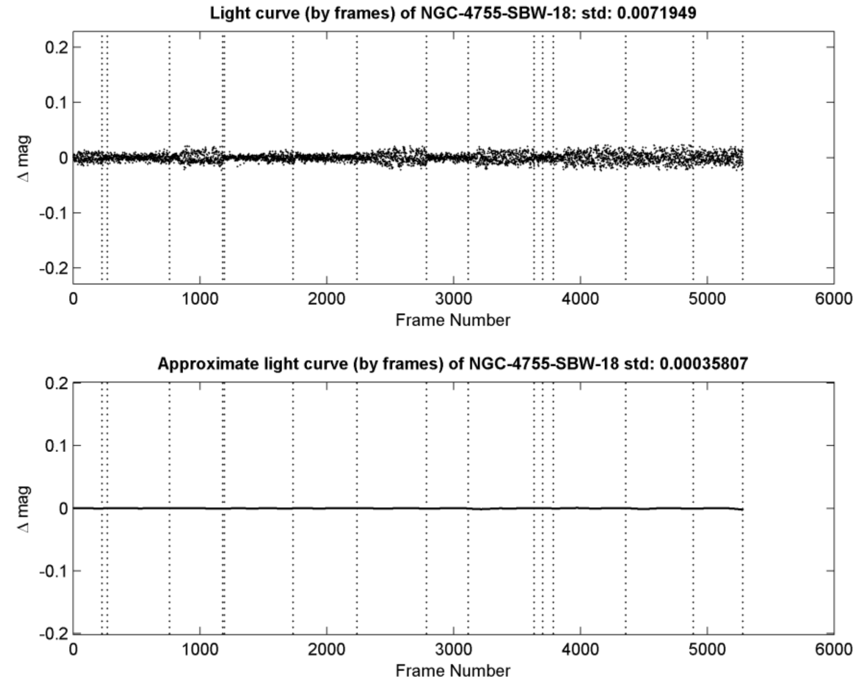

Figure C.2.1 Reference Star (frame base) NGC 4755 SBW 18

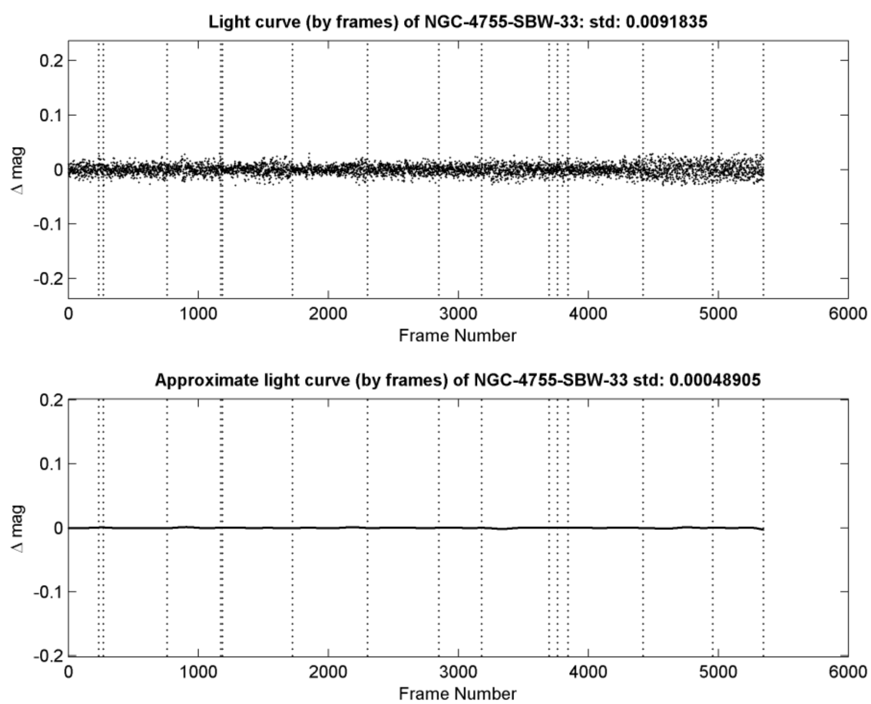

Figure C.2.2 Reference Star (frame base) NGC 4755 SBW 33

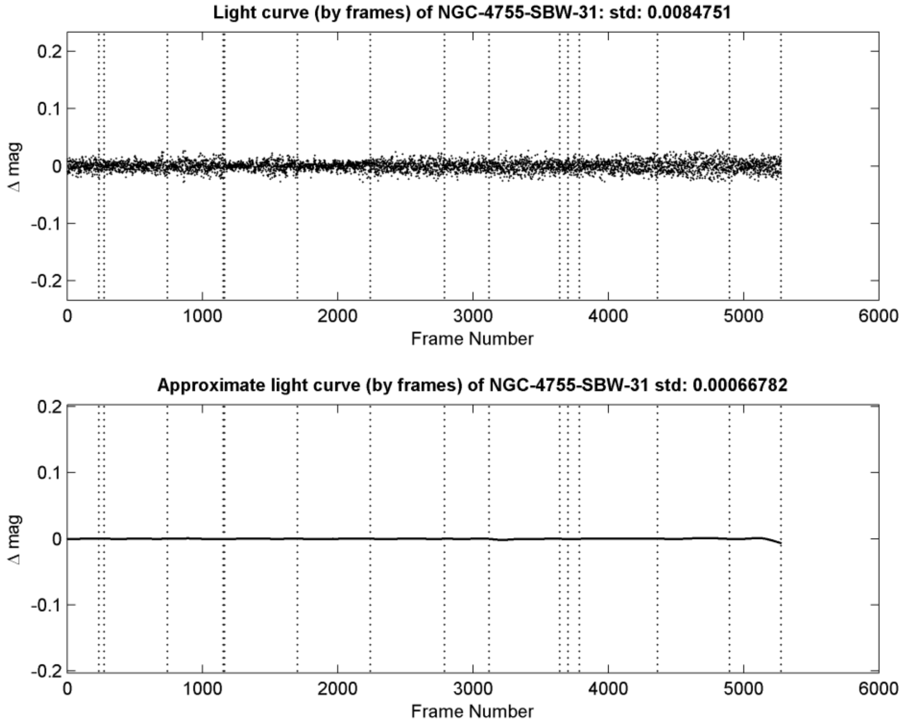

Figure C.2.3 Reference Star (frame base) NGC 4755 SBW 31

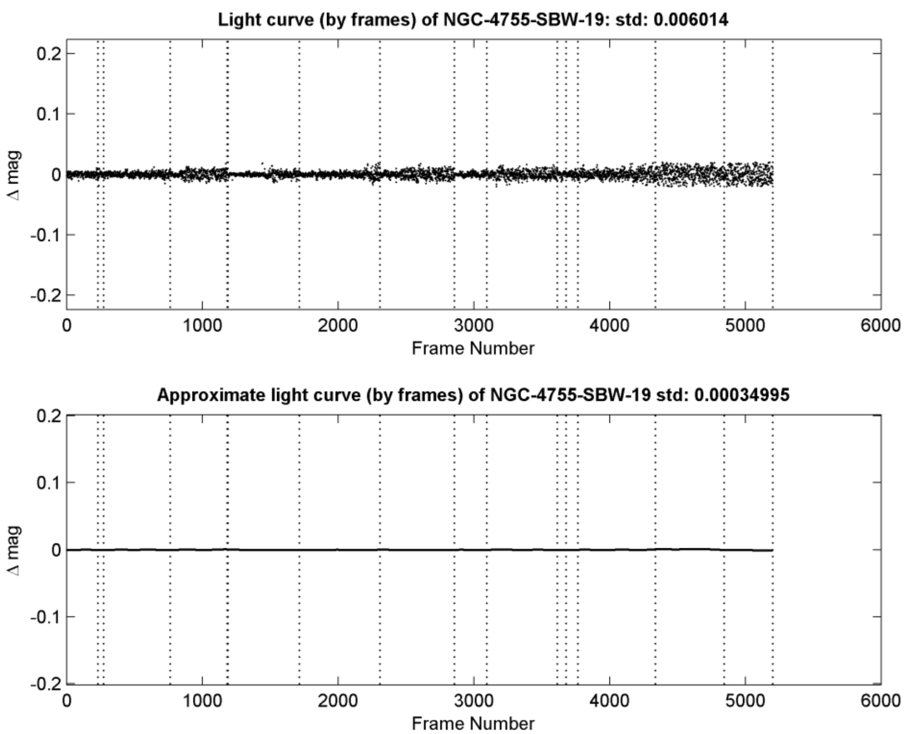

Figure C.2.4 Reference Star (frame base) NGC 4755 SBW 19

Figure C.2 Light curves of reference stars NGC 4755 (frames)

Appendix D

Summary of the photometry results

Star # Webda Data base	Star name Sanner et al (2001) or Evans et al (2005) or SIMBAD preference	RA (ICRS 2000)	Dec (ICRS 2000)	Spectral type	R mag	Std dev.	15pt Std Dev	Comments
226	NGC 4755 SBW 197	12 53 50.51	-60 19 07.56		12.32	0.030	0.010	
225	NGC 4755 SBW 218	12 53 51.92	-60 19 31.25		13.74	0.100	0.044	
137	NGC 4755 SBW 111	12 53 37.52	-60 19 26.6	B6.5III	9.29	0.040	0.020	
1	NGC 4755 ESL 1	12 53 21.9	-60 19 42.56	B9IA	6.47	0.050	0.022	V
138	NGC 4755 SBW 38	12 53 25.4	-60 19 11.32	B2V	11.06	0.030	0.008	
139	NGC 4755 SBW 58	12 53 26.50	-60 19 00.1	B3Vn	11.16	0.030	0.008	
140	NGC 4755 SBW 179	12 53 23.76	-60 19 01.25		12.19	0.070	0.021	
145	NGC 4755 SBW 251	12 53 30.00	-60 19 08.50		13.74	0.100	0.035	
146	NGC 4755 SBW 304	12 53 29.16	-60 18 47.94			----		
233	NGC 4755 SBW 272	12 53 49.19	-60 18 21.25		13.28	0.080	0.031	
232	NGC 4755 SBW 207	12 53 51.18	-60 18 13.75		12.73	0.083	0.042	
231	NGC 4755 SBW 225	12 53 57.16	-60 18 53.06		13.73	0.010	0.030	
5033	NGC 4755 SBW 8438	12 53 41.3	-60 20 57.9	M2Iab	6.61	0.040	0.017	V,I,DU Cru
214	NGC 4755 SBW 37	12 53 43.2	-60 20 47.1	B2.5Vn	8.33	0.088	0.031	
213	NGC 4755 SBW 57	12 53 44.05	-60 20 57.8	B3V	9.97	0.100	0.036	
207	NGC 4755 SBW 77	12 53 45.4	-60 21 07.7	B3Vn	11.60	0.040	0.013	
216	NGC 4755 SBW 102	12 53 48.72	-60 20 39.2	B5V	12.62	0.040	0.017	
215	NGC 4755 SBW 56	12 53 49.4	-60 20 57.2	B3V	12.01	0.020	0.009	V,P,EH Cru
212	NGC 4755 SBW 146	12 53 50.7	-60 21 21.8	B8III	12.22	0.040	0.017	
211	NGC 4755 SBW 96	12 53 51.4	-60 21 17.2		11.91	0.060	0.020	
210	NGC 4755 SBW 20	12 53 53.02	-60 21 30.5	B2Vn	10.54	0.010	0.003	CZ Cru
712	NGC 4755 ESL 102	12 53 53.17	-60 21 24.9			---		
208	NGC 4755 SBW 76	12 53 56.44	-60 21 40.19		12.27	0.030	0.010	
217	NGC 4755 SBW 72	12 53 57.9	-60 21 22.56		12.24	0.030	0.009	
222	NGC 4755 SBW 184	12 54 04.68	-60 20 54.88		13.87	0.100	0.046	
219	NGC 4755 SBW 120	12 54 08.67	-60 21 45.62		11.37	0.015	0.005	
218	NGC 4755 SBW 89	12 54 09.06	-60 22 09.9	B3V	12.60	0.030	0.011	
14	NGC 4755 SBW 138	12 54 11.43	-60 20 34.25		12.69	0.040	0.013	
203	NGC 4755 SBW 23	12 53 48.20	-60 21 54.19	O+	10.01	0.221	0.131	CPD 59-4556
202	NGC 4755 SBW 15	12 53 51.8	-60 21 58.3	B1V	10.17	0.030	0.010	V,BC,CX Cru
201	NGC 4755 SBW 4	12 53 52.03	-60 22 15.4	B1V	9.17	0.010	0.003	V,BC,EI Cru
307	NGC 4755 SBW 7	12 53 52.3	-60 22 27.5	B1.5V	9.21	0.017	0.005	V,BC,CY Cru
308	NGC 4755 SBW 194	12 53 56.87	-60 22 25.2		12.80	0.050	0.020	
309	NGC 4755 SBW 135	12 53 57.06	-60 22 29.8		12.77	0.040	0.020	
310	NGC 4755 SBW 180	12 53 54.1	-60 22 45.9		12.87	0.084	0.046	
311	NGC 4755 SBW 30	12 53 58.31	-60 23 22.62	B2	11.16	0.010	0.004	
726	NGC 4755 ESL 46	12 54 07.16	-60 23 13.4	B3Vn	11.69	0.017	0.006	
320	NGC 4755 SBW 150	12 54 03.27	-60 24 00.81		12.57	0.039	0.012	

Star # Webda Data base	Star name Sanner et al (2001) or Evans et al (2005) or SIMBAD preference	RA (ICRS 2000)	Dec (ICRS 2000)	Spectral type	R mag	Std dev.	15pt Std Dev	Comments
321	NGC 4755 SBW 200	12 54 02.37	-60 24 06.44		12.61	0.037	0.012	
322	NGC 4755 SBW 219	12 54 04.98	-60 24 22.19		13.45	0.081	0.027	
312	NGC 4755 SBW 75	12 53 52.70	-60 23 57.88		11.48	0.012	0.004	
313	NGC 4755 SBW 53	12 53 51.9	-60 23 54.3	B3Ve	11.48	0.011	0.005	
308	NGC 4755 SBW 194	12 53 56.8	-60 22 25.19		12.79	0.040	0.020	
323	NGC 4755 SBW 220	12 53 57.35	-60 25 12.62		10.49	0.098	0.031	
344	NGC 4755 ESL 51	12 53 53.1	-60 23 07.4	B3Vn	10.59	0.043	0.011	
306	NGC 4755 SBW 13	12 53 51.61	-60 23 16.6	B2IVne	10.12	0.012	0.004	
	CCDM J1 2538-6023B	12 53 48.97	-60 23 02.5		8.04	0.085	0.045	FS, Double system
2	NGC 4755 ESL 2	12 53 48.9	-60 22 34.4	B3Ia	6.57	0.040	0.017	Kappa Cru
19	NGC 4755 SBW 6	12 53 47.28	-60 22 20.2	B1.5Vnpe	7.52	0.060	0.043	
18	NGC 4755 SBW 5	12 53 46.57	-60 22 18.5	B1.5V	8.84	0.100	0.031	CU Cru
204	NGC 4755 SBW 149	12 53 45.11	-60 22 06.50		10.98	0.080	0.025	
5	NGC 4755 SBW 8349	12 53 46.47	-60 24 12.33	B1III	8.71	0.006	0.003	
317	NGC 4755 SBW 277	12 53 47.77	-60 25 04.81		12.08	0.060	0.016	
318	NGC 4755 SBW 50	12 53 47.0	-60 25 17.9	B2.5V	11.41	0.013	0.005	
301	NGC 4755 SBW 11	12 53 43.9	-60 22 29.3	B1.5V	10.09	0.010	0.004	V,BC,CT Cru
302	NGC 4755 ESL 93	12 53 44.65	-60 22 32.4	B8II-V		----		
401	NGC 4755 SBW 151	12 53 41.77	-60 22 43.9	B8III	11.47	0.020	0.008	
402	NGC 4755 SBW 47	12 53 41.8	-60 22 50.6		11.49	0.013	0.007	
411	NGC 4755 ESL 33	12 53 39.95	-60 23 27.1	B3V	11.41	0.044	0.016	
10010	NGC 4755 SBW 10	12 53 38.99	-60 23 43.63	B2IVne	9.91	0.007	0.003	V,Em,CS Cru
315	NGC 4755 SBW 80	12 53 43.1	-60 23 51.38		11.22	0.012	0.005	
316	NGC 4755 SBW 49	12 53 43.36	-60 24 01.88	B3Vn	11.28	0.012	0.006	V,P,EG Cru
415	NGC 4755 SBW 209	12 53 41.64	-60 23 59.2		11.33	0.025	0.004	
416	NGC 4755 SBW 121	12 53 40.61	-60 24 12.5		12.82	0.049	0.026	
427	NGC 4755 SBW 67	12 53 41.84	-60 24 37.9	B3Vn	12.17	0.021	0.010	
428	NGC 4755 SBW 169	12 53 42.44	-60 25 12.19		13.49	0.067	0.027	
435	NGC 4755 SBW 134	12 53 38.11	-60 25 59.12		12.42	0.030	0.011	
433	NGC 4755 SBW 78	12 53 36.93	-60 25 26.8	B5V	12.51	0.027	0.009	
434	NGC 4755 SBW 259	12 53 33.19	-60 25 39.44		12.51	0.027	0.013	
8	NGC 4755 SBW 25	12 53 33.27	-60 24 32.9	B5.1V	10.31	0.007	0.007	CPD-59 4540
430	NGC 4755 SBW 87	12 53 33.49	-60 24 20.0	B5V	10.48	0.028	0.008	
418	NGC 4755 SBW 8	12 53 35.5	-60 23 46.4	B1.5V	10.01	0.005	0.003	V,BT Cru
419	NGC 4755 SBW 95	12 53 37.20	-60 23 41.2		9.83	0.027	0.008	
421	NGC 4755 SBW 144	12 53 34.16	-60 23 44.88		10.09	0.008	0.003	
	NGC 4755 ESL 26	12 53 39.41	-60 22 40.0	B2.5V	10.09	0.008	0.003	
	NGC 4755 SBW 19	12 53 38.07	-60 22 39.31	B2	10.19	0.010	0.003	EF Cru
	NGC 4755 ESL 52	12 53 37.1	-60 22 54.8		11.61	0.044	0.018	
407	NGC 4755 SBW 129	12 53 33.9	-60 22 41	B8III	11.73	0.020	0.010	
	NGC 4755 SBW 61	12 53 32.48	-60 22 38.8	B3V	11.70	0.010	0.007	
412	NGC 4755 SBW 187	12 53 31.22	-60 23 07.75		13.38	0.060	0.028	
423	NGC 4755 SBW 240	12 53 28.94	-60 23 10.7		13.85	0.090	0.038	

Star # Webda Data base	**Star name Sanner et al (2001) or Evans et al (2005) or SIMBAD preference**	**RA (ICRS 2000)**	**Dec (ICRS 2000)**	**Spectral type**	**R mag**	**Std dev.**	**15pt Std Dev**	**Comments**
422	NGC 4755 SBW 191	12 53 31.16	-60 23 39.31		13.07	0.052	0.022	
444	NGC 4755 SBW 147	12 53 22.05	-60 25 00.6	B8IIIn	13.41	0.059	0.022	
11	NGC 4755 SBW 45	12 53 22.62	-60 23 47.4	B3V	11.74	0.019	0.007	
431	NGC 4755 SBW 83	12 53 17.94	-60 23 25.9	B6.5III-V	12.31	0.029	0.015	
7	NGC 4755 SBW 9	12 53 20.70	-60 23 16.7	B1V	10.13	0.006	0.003	V,BC,BS Cru
424	NGC 4755 SBW 159	12 53 23.59	-60 23 12.1	B8III-V	12.95	0.067	0.028	
	NGC 4755 SBW 22	12 53 24.00	-60 23 00.0	B1V	10.38	0.003	0.001	
413	NGC 4755 SBW 62	12 53 26.23	-60 22 52.0	B3V	10.35	0.010	0.002	
732	NGC 4755 ESL 81	12 53 27.77	-60 22 37.7	B6.5IIIn	12.14	0.030	0.017	
410	NGC 4755 SBW 29	12 53 25.62	-60 22 27.62	B3	10.91	0.010	0.005	CPD-59-4533
425	NGC 4755 SBW 115	12 53 17.27	-60 22 51.8	B8III-V	13.00	0.050	0.024	
432	NGC 4755 SBW 170	12 53 12.27	-60 23 14.62		13.37	0.080	0.030	
426	NGC 4755 SBW 44	12 53 09.91	-60 22 27.1	B2.5V	11.76	0.021	0.008	
120	NGC 4755 SBW 104	12 53 18.42	-60 22 07.6	B5III-V	12.71	0.040	0.013	CQ Cru
111	NGC 4755 SBW 105	12 53 25.88	-60 22 14.5	B5III-V	10.54	0.240	0.010	
113	NGC 4755 SBW 18	12 53 25.73	-60 21 59.8	B1V	10.49	0.010	0.003	
307	NGC 4755 SBW 113	12 53 52.3	-60 22 27.5		12.00	0.020	0.008	
109	NGC 4755 SBW 85	12 53 32.3	-60 22 19.4	B6.5V	11.95	0.021	0.008	
342	HD 312082	12 54 33.04	-60 25 13.25	B+				FS
108	NGC 4755 SBW 112	12 53 35.63	-60 21 47.8	B5V	12.02	0.040	0.019	
107	NGC 4755 SBW 46	12 53 38.21	-60 21 44.8	B5V	9.20	0.150	0.123	
101	NGC 4755 SBW 92	12 53 40.77	-60 21 39.8	B3Vn	11.47	0.070	0.397	
103	NGC 4755 SBW 171	12 53 42.49	-60 21 28.88		9.16	0.290	0.220	
205	NGC 4755 SBW 175	12 53 43.92	-60 21 45.31		13.10	0.090	0.060	
104	NGC 4755 SBW 106	12 53 41.35	-60 21 13.7	K3III	7.26	0.070	0.029	
106	NGC 4755 SBW 8354	12 53 37.61	-60 21 25.4	B1.5Ib	7.23	0.012	0.004	V,CR Cru
114	NGC 4755 SBW 86	12 53 34.4	-60 21 12.6		11.73	0.020	0.008	
	NGC 4755 SBW 27	12 53 34.1	-60 20 59.75	B1V	10.46	0.010	0.004	
718	NGC 4755 ESL 71	12 53 33.78	-60 20 54.3		10.56	0.030	0.009	
117	NGC 4755 SBW 31	12 53 24.3	-60 21 30.6	B2.5Vn	11.27	0.010	0.003	
119	NGC 4755 SBW 174	12 53 22.77	-60 21 51.19		12.95	0.050	0.019	
118	NGC 4755 SBW 114	12 53 19.58	-60 21 30.7	B5V	12.76	0.040	0.013	
156	NGC 4755 SBW 237	12 53 20.95	-60 21 43.00		12.81	0.040	0.015	
6	NGC 4755 SBW 3	12 53 57.54	-60 24 58.1		9.44	0.006	0.002	BW Cru
132	NGC 4755 SBW 253	12 53 18.77	-60 20 56.50		14.13	0.130	0.048	
134	NGC 4755 SBW 128	12 53 17.07	-60 20 30.69		12.46	0.030	0.012	
133	NGC 4755 SBW 148	12 53 18.21	-60 20 30.81		12.45	0.030	0.013	
135	NGC 4755 SBW 243	12 53 23.15	-60 20 23.62		10.00	1.004	0.534	
136	NGC 4755 SBW 93	12 53 25.37	-60 20 21.0	B5V	12.29	0.030	0.012	
10	NGC 4755 SBW 33	12 53 25.97	-60 20 47.7	B2V	11.38	0.010	0.004	
130	NGC 4755 SBW 119	12 53 25.85	-60 21 08.88		12.99	0.040	0.017	
151	NGC 4755 SBW 193	12 53 32.93	-60 20 37.3		13.16	0.060	0.030	
116	NGC 4755 SBW 103	12 53 36.15	-60 20 32.2	B2V	11.89	0.020	0.010	V,P,EE Cru

Star # Webda Data base	Star name Sanner et al (2001) or Evans et al (2005) or SIMBAD preference	RA (ICRS 2000)	Dec (ICRS 2000)	Spectral type	R mag	Std dev.	15pt Std Dev	Comments
122	NGC 4755 SBW 82	12 53 08.97	-60 21 22.3	B5V	12.52	0.030	0.011	
125	NGC 4755 SBW 261	12 53 09.22	-60 20 58.62		12.92	0.070	0.022	
121	NGC 4755 SBW 165	12 53 09.23	-60 22 02.4	B8III-V	13.23	0.070	0.025	
126	NGC 4755 SBW 222	12 53 09.79	-60 20 44.81		13.33	0.090	0.030	
128	NGC 4755 SBW 154	12 52 56.58	-60 20 28.75		13.28	0.070	0.022	
123	NGC 4755 SBW 98	12 52 55.45	-60 21 50.50			---		
449	NGC 4755 SBW 36	12 53 01.06	-60 23 09.44		11.54	0.020	0.012	
	NGC 4755 SBW 205	12 53 01.06	-60 23 43.75		13.87	0.095	0.042	
326	NGC 4755 SBW 59	12 54 03.63	-60 25 20.7	B3V	11.91	0.027	0.010	
446	NGC 4755 SBW 66	12 53 14.05	-60 24 12.9	B3V	12.18	0.023	0.009	CPD-59 4525
448	NGC 4755 SBW 211	12 53 12.35	-60 24 34.00		13.79	0.093	0.032	
452	NGC 4755 SBW 16	12 53 10.19	-60 25 59.3	B1.5V	10.38	0.008	0.003	HD312079
445	NGC 4755 SBW 139	12 53 20.33	-60 25 34.4	B8III	13.08	0.052	0.018	
436	NGC 4755 SBW 110	12 53 38.18	-60 26 10.62		12.41	0.031	0.011	
442	NGC 4755 SBW 65	12 53 33.94	-60 26 21.7	B3V	12.09	0.023	0.008	
443	NGC 4755 SBW 81	12 53 29.47	-60 26 14.81		12.26	0.024	0.009	
326	NGC 4755 SBW 35	12 54 03.63	-60 25 20.7	B2.5V	11.40	0.013	0.004	
331	NGC 4755 SBW 12	12 53 59.81	-60 26 20.0		9.67	0.007	0.003	HD 312081
332	NGC 4755 SBW 34	12 53 56.67	-60 26 32.38		11.27	0.015	0.006	
327	NGC 4755 SBW 68	12 54 14.77	-60 24 25.75		11.59	0.016	0.005	
328	NGC 4755 SBW 221	12 54 12.48	-60 24 52.75		13.66	0.067	0.027	
227	NGC 4755 SBW 234	12 54 14.87	-60 22 16.44		13.90	0.110	0.037	
228	NGC 4755 SBW 32	12 54 14.54	-60 21 47.4	B8	11.32	0.010	0.004	
15	NGC 4755 SBW 166	12 54 14.46	-60 20 30.06		13.38	0.070	0.020	
17	NGC 4755 SBW 173	12 54 12.13	-60 19 44.19		13.26	0.060	0.023	
230	NGC 4755 SBW 275	12 54 09.02	-60 19 06.38		13.83	0.100	0.035	
229	NGC 4755 SBW 196	12 54 04.60	-60 19 02.31		13.24	0.050	0.017	
12	NGC 4755 SBW 71	12 53 23.16	-60 18 35.94	B8:V	11.69	0.020	0.007	
13	NGC 4755 SBW 116	12 53 18.21	-60 18 50.0	B8III-V	12.59	0.040	0.013	
141	NGC 4755 SBW 216	12 53 10.77	-60 19 00.50		13.18	0.060	0.024	
142	NGC 4755 SBW 229	12 53 10.66	-60 18 52.81		13.18	0.060	0.022	
129	NGC 4755 SBW 94	12 52 56.77	-60 19 21.5	B8V	12.56	0.030	0.013	
	NGC 4755 SBW 8343	12 54 20.81	-60 18 23.19		13.99	0.130	0.044	
333	NGC 4755 SBW 142	12 53 55.11	-60 26 49.8	B8III	13.16	0.061	0.020	
334	NGC 4755 SBW 84	12 53 55.21	-60 27 09.8	B3V	12.66	0.032	0.010	
453	NGC 4755 SBW 63	12 53 16.59	-60 26 11.00		11.89	0.019	0.008	
220	NGC 4755 SBW 41	12 54 08.63	-60 21 40.3	B9		----		HD 312083
	HD 312073	12 52 57	-60 15.2					FS
	CPC-20.13735	12 53 39.15	-60 21 13.16					FS
	NGC 4755 SBW 123	12 53 23.5	-60 22 18.81		12.49	0.080	0.026	
221	NGC 4755 SBW 264	12 54 05.49	-60 21 15.3		12.81	0.048	0.016	
154	NGC 4755 SBW 286	12 53 32.84	-60 21 43.88		12.76	0.044	0.020	
303	NGC 4755 SBW 278	12 53 44.87	-60 22 44.88					

Star # Webda Data base	Star name Sanner et al (2001) or Evans et al (2005) or SIMBAD preference	RA (ICRS 2000)	Dec (ICRS 2000)	Spectral type	R mag	Std dev.	15pt Std Dev	Comments
330	NGC 4755 SBW 263	12 54 15.71	-60 25 43.00		13.81	0.091	0.027	
438	NGC 4755 SBW 226	12 53 35.4	-60 26 50.2		13.94	0.097	0.034	
437	NGC 4755 SBW 201	12 53 38.43	-60 26 58.5		13.80	0.086	0.026	
336	NGC 4755 SBW 100	12 54 14.56	-60 26 54.2		12.70	0.042	0.014	
454	NGC 4755 SBW 17	12 53 14.26	-60 27 38		10.59	0.038	0.012	

Table D.1 Results of brighter stars of the cluster NGC 4755

BC - Beta Cepheid, FS- Field Star, E - Elliptical, D- Double, V -Variable, I - Irregular, P - Pulsating, EB - Eclipsing Binary, Em - Emission Line, FS -Field Stars

Jcu Star #	Webda Db #	RA	Dec	Rmag	Std Dev	15ptStd Dev
1		12 54 6.27	-60 17 18.84	16.57	0.38	0.27
2		12 53 35.79	-60 17 43.49	14.33	0.48	0.33
3		12 53 28.14	-60 17 49.14	15.48	0.35	0.36
4		12 54 7.08	-60 17 20.39	16.71	0.72	0.36
5		12 53 29.50	-60 17 48.29	16.22	1.61	0.55
6		12 52 56.60	-60 18 16.92	15.61	0.74	0.25
7		12 52 51.59	-60 18 19.54	17.03	0.87	0.33
8		12 53 52.77	-60 17 32.59	15.90	1.22	0.45
9		12 53 52.17	-60 17 33.68	15.91	1.02	0.40
10		12 54 5.09	-60 17 25.62	15.87	0.34	0.35
11		12 53 37.00	-60 17 47.83	14.91	0.36	0.30
12	15636	12 53 7.14	-60 18 11.68	17.38	1.93	0.71
13		12 52 54.47	-60 18 22.33	18.17	1.86	0.65
14		12 53 16.15	-60 18 5.65	14.82	0.56	0.38
15	1515	12 53 5.87	-60 18 14.23	15.98	0.59	0.47
16		12 53 49.39	-60 17 40.74	14.10	1.05	0.52
17		12 53 43.29	-60 17 45.49	15.77	0.31	0.29
18		12 53 15.36	-60 18 8.23	16.04	1.56	0.64
19		12 53 4.88	-60 18 16.65	16.09	0.46	0.25
20		12 53 21.85	-60 18 7.04	16.60	1.54	0.53
21		12 53 9.24	-60 18 13.84	16.69	1.43	0.53
22	11073	12 53 0.58	-60 18 19.08	16.21	0.38	0.23
23		12 53 14.77	-60 18 10.49	16.65	0.52	0.31
24		12 53 12.90	-60 18 9.96	18.16	1.79	0.52
25	11324	12 54 7.52	-60 17 29.86	17.66	1.64	0.57
26	23155	12 53 8.02	-60 18 17.53	15.72	1.24	0.54
27	11846	12 54 2.20	-60 17 33.98	16.59	1.19	0.41
28	11846	12 54 1.77	-60 17 37.95	16.75	1.38	0.45
29		12 54 0.06	-60 17 35.47	16.80	2.00	0.83
30		12 53 58.18	-60 17 38.46	14.31	0.46	0.28
31		12 53 31.03	-60 18 3.72	17.34	0.64	0.28

Jcu Star #	Webda Db #	RA	Dec	Rmag	Std Dev	15ptStd Dev
32	14721	12 52 54.17	-60 18 32.93	17.76	1.66	0.63
33		12 54 14.28	-60 17 30.27	15.50	0.25	0.27
34		12 53 40.39	-60 17 56.66	15.21	0.45	0.34
35	1516	12 53 5.11	-60 18 24.33	16.11	0.41	0.27
36		12 53 19.27	-60 18 14.20	12.79	1.62	0.71
37		12 53 18.67	-60 18 15.83	14.06	1.57	0.65
38	1517	12 53 8.36	-60 18 24.72	15.32	0.28	0.28
39		12 53 57.10	-60 17 48.78	16.23	0.56	0.35
40		12 53 54.22	-60 17 49.94	14.66	0.39	0.26
41	14463	12 54 2.78	-60 17 44.03	16.38	0.80	0.47
42		12 53 54.62	-60 17 51.46	14.63	0.27	0.26
43		12 53 17.70	-60 18 20.93	15.57	0.23	0.20
44		12 53 16.51	-60 18 22.19	16.44	0.39	0.26
45	15663	12 53 25.27	-60 18 15.27	14.35	0.37	0.41
46		12 54 7.95	-60 17 46.77	17.38	1.95	0.78
47	14092	12 53 34.17	-60 18 13.94	15.97	0.44	0.37
48		12 53 24.90	-60 18 23.44	14.52	0.31	0.29
49	17526	12 53 59.15	-60 17 58.04	16.32	0.35	0.28
50		12 53 45.40	-60 18 6.92	17.17	0.60	0.36
51		12 53 46.29	-60 18 9.85	14.38	0.98	0.34
52	11965	12 53 30.57	-60 18 20.37	16.80	0.81	0.33
53		12 53 1.25	-60 18 46.81	17.23	0.84	0.32
54		12 53 50.99	-60 18 6.36	13.99	0.31	0.35
55		12 52 50.97	-60 18 56.53	15.80	0.36	0.27
56	11099	12 53 12.68	-60 18 40.06	16.43	0.40	0.32
57	16571	12 54 8.56	-60 17 56.34	15.37	0.15	0.24
58	15045	12 53 49.90	-60 18 11.06	14.56	0.39	0.40
59		12 53 28.97	-60 18 27.54	15.87	0.27	0.31
60	1521	12 53 4.22	-60 18 48.37	14.88	0.24	0.25
61		12 53 25.10	-60 18 31.43	12.16	0.61	0.33
62	1522	12 52 55.76	-60 18 56.00	15.16	0.34	0.28
63		12 53 48.98	-60 18 14.42	14.57	0.57	0.36
64		12 54 13.44	-60 17 56.83	15.74	1.54	0.52
65		12 53 50.77	-60 18 15.12	13.41	0.75	0.40
66		12 53 26.29	-60 18 34.89	15.36	0.66	0.34
67		12 53 22.53	-60 18 36.96	11.07	0.62	0.34
68	16342	12 54 11.92	-60 17 59.20	14.78	0.53	0.37
69		12 53 58.15	-60 18 10.86	17.33	0.74	0.34
70	15954	12 53 54.79	-60 18 13.10	16.02	0.35	0.33
71		12 54 1.93	-60 18 9.70	16.38	0.31	0.21
72		12 53 42.69	-60 18 26.36	18.68	1.76	0.59
73		12 53 10.55	-60 18 50.00	14.40	0.35	0.33
74	10438	12 54 8.94	-60 18 6.26	16.62	1.11	0.53
75		12 53 37.93	-60 18 29.74	15.69	0.34	0.28

Jcu Star #	Webda Db #	RA	Dec	Rmag	Std Dev	15ptStd Dev
76		12 54 10.20	-60 18 6.33	17.38	0.63	0.26
77	10804	12 53 0.51	-60 19 1.61	15.82	0.32	0.26
78		12 54 14.39	-60 18 4.60	16.74	0.28	0.23
79		12 53 39.66	-60 18 32.05	17.09	0.61	0.32
80		12 53 31.59	-60 18 37.53	14.70	0.27	0.30
81		12 54 7.89	-60 18 11.93	16.37	0.56	0.24
82		12 54 4.25	-60 18 13.15	17.29	1.82	0.64
83		12 54 2.47	-60 18 15.39	16.41	0.33	0.26
84		12 53 47.97	-60 18 27.31	11.24	0.40	0.35
85	14923	12 52 58.89	-60 19 5.98	17.78	1.61	0.58
86		12 52 54.57	-60 19 10.26	18.05	1.94	0.57
87		12 53 59.15	-60 18 20.18	16.67	0.39	0.25
88		12 53 43.60	-60 18 31.66	17.37	0.97	0.50
89		12 53 29.05	-60 18 43.04	14.50	0.55	0.34
90		12 53 20.21	-60 18 50.08	11.24	0.68	0.32
91	141	12 53 10.67	-60 18 58.37	14.32	0.56	0.35
92	13665	12 54 5.69	-60 18 12.95	18.19	1.65	0.55
93	14648	12 54 12.20	-60 18 13.77	15.70	0.16	0.23
94		12 53 12.28	-60 19 3.10	15.85	1.50	0.58
95		12 53 37.54	-60 18 41.66	17.07	1.97	0.60
96		12 54 9.98	-60 18 17.55	16.50	0.28	0.27
97		12 53 53.55	-60 18 29.94	14.58	0.32	0.31
98		12 53 50.67	-60 18 32.94	13.61	1.76	0.67
99		12 53 41.46	-60 18 39.52	16.29	0.41	0.34
100		12 54 0.78	-60 18 24.90	15.88	0.36	0.26
101	15341	12 53 14.57	-60 19 3.81	16.68	0.78	0.34
102	10981	12 53 5.31	-60 19 9.66	15.34	0.31	0.26
103		12 53 44.78	-60 18 40.01	13.69	0.42	0.30
104		12 53 15.03	-60 19 5.05	16.78	0.71	0.35
105	1211	12 52 59.80	-60 19 16.76	15.10	0.21	0.19
106		12 53 13.77	-60 19 6.10	17.09	1.70	0.54
107		12 53 46.29	-60 18 42.77	13.58	0.32	0.32
108	10456	12 53 22.00	-60 19 3.06	11.12	1.32	1.06
109		12 53 10.10	-60 19 14.75	17.79	1.98	0.61
110		12 52 51.98	-60 19 26.49	18.72	1.89	0.54
111		12 53 45.35	-60 18 46.05	13.69	0.29	0.23
112		12 53 38.80	-60 18 50.12	14.98	0.30	0.23
113	11551	12 53 18.26	-60 19 6.56	12.77	0.59	0.38
114	1205	12 53 7.44	-60 19 14.73	16.36	0.25	0.25
115	1209	12 53 4.00	-60 19 18.61	15.85	0.48	0.27
116	14934	12 54 3.28	-60 18 31.90	15.68	0.37	0.34
117		12 54 0.63	-60 18 34.73	16.20	0.33	0.34
118	11463	12 53 2.96	-60 19 21.80	17.10	0.91	0.36
119		12 53 55.72	-60 18 40.28	17.16	0.76	0.37

Jcu Star #	Webda Db #	RA	Dec	Rmag	Std Dev	15ptStd Dev
120		12 53 43.29	-60 18 49.80	14.98	0.19	0.30
121	12267	12 53 15.98	-60 19 12.07	17.04	0.72	0.33
122	11400	12 53 1.86	-60 19 23.52	15.59	0.87	0.36
123	11394	12 52 54.27	-60 19 30.64	16.19	1.10	0.37
124		12 53 40.44	-60 18 54.74	15.65	0.52	0.31
125		12 53 31.75	-60 19 2.39	16.85	0.34	0.33
126		12 53 27.58	-60 19 4.53	15.30	0.61	0.27
127	11258	12 52 54.97	-60 19 30.75	15.86	0.46	0.24
128		12 53 58.09	-60 18 41.03	14.38	1.57	0.64
129		12 53 29.87	-60 19 4.44	13.89	0.17	0.35
130		12 53 35.27	-60 19 1.76	15.22	0.24	0.22
131		12 54 2.94	-60 18 40.84	15.41	0.30	0.27
132		12 53 55.28	-60 18 47.29	17.11	1.51	0.54
133	1210	12 53 1.14	-60 19 29.89	15.28	0.29	0.22
134		12 53 56.98	-60 18 46.41	14.36	0.41	0.33
135	10782	12 53 24.26	-60 19 12.74	11.39	1.49	0.99
136	11059	12 53 18.13	-60 19 17.36	15.56	0.31	0.35
137	12173	12 53 15.87	-60 19 20.92	16.58	0.49	0.26
138	1208	12 53 5.71	-60 19 29.19	16.29	0.31	0.24
139		12 52 58.32	-60 19 35.99	17.80	1.61	0.47
140		12 53 56.66	-60 18 48.13	14.38	0.59	0.30
141		12 53 32.96	-60 19 8.91	14.59	0.24	0.33
142	11845	12 53 10.87	-60 19 27.53	17.41	0.65	0.29
143		12 52 55.06	-60 19 39.68	16.25	1.63	0.50
144		12 53 58.32	-60 18 50.91	11.91	0.83	0.39
145		12 53 22.82	-60 19 19.07	13.18	0.22	0.31
146	16960	12 54 2.03	-60 18 48.23	13.82	0.29	0.33
147	13226	12 53 17.04	-60 19 25.00	15.39	0.22	0.22
148	1206	12 53 6.74	-60 19 33.46	16.55	0.35	0.27
149	1204	12 53 9.48	-60 19 31.90	15.10	0.25	0.36
150		12 52 55.91	-60 19 42.65	16.04	1.60	0.49
151		12 53 39.90	-60 19 8.75	15.98	0.42	0.29
152		12 53 31.45	-60 19 16.09	13.90	0.34	0.30
153		12 53 50.33	-60 19 1.70	14.20	0.27	0.15
154		12 53 40.65	-60 19 13.82	15.82	0.50	0.29
155	1207	12 53 5.33	-60 19 42.18	15.91	0.25	0.23
156	1213	12 52 58.60	-60 19 47.26	15.68	0.21	0.20
157		12 54 8.27	-60 18 52.54	15.50	0.19	0.27
158		12 54 4.38	-60 18 55.33	13.62	0.34	0.29
159		12 53 30.71	-60 19 22.12	13.40	0.24	0.22
160	11891	12 53 16.36	-60 19 35.35	15.18	0.44	0.44
161		12 54 11.19	-60 18 51.81	16.52	1.81	0.54
162		12 52 55.83	-60 19 53.12	16.23	0.84	0.32
163		12 52 52.67	-60 19 55.95	16.11	0.80	0.25

Jcu Star #	Webda Db #	RA	Dec	Rmag	Std Dev	15ptStd Dev
164		12 53 50.57	-60 19 10.64	13.27	0.42	0.35
165	13599	12 53 39.66	-60 19 20.29	16.18	0.78	0.51
166		12 53 24.14	-60 19 34.04	8.40	0.29	0.30
167		12 54 8.85	-60 18 59.18	14.39	0.19	0.14
168	16129	12 53 54.98	-60 19 9.78	14.97	0.29	0.29
169	1203	12 53 10.95	-60 19 44.17	15.22	0.27	0.31
170		12 53 58.74	-60 19 7.43	11.32	0.28	0.29
171	11063	12 53 14.07	-60 19 43.42	15.93	0.53	0.31
172	11597	12 53 7.92	-60 19 48.64	17.37	0.73	0.35
173	11991	12 52 53.28	-60 20 0.64	16.29	1.10	0.34
174	11194	12 52 52.58	-60 20 1.30	16.51	0.67	0.28
175		12 53 35.39	-60 19 27.23	15.27	0.21	0.15
176		12 53 24.17	-60 19 35.06	8.40	0.29	0.28
177		12 53 44.03	-60 19 22.14	17.46	0.55	0.26
178	1202	12 53 12.45	-60 19 46.59	14.65	0.26	0.32
179		12 53 45.10	-60 19 24.28	16.14	0.72	0.42
180		12 53 42.19	-60 19 26.66	15.49	0.28	0.19
181	10653	12 53 29.88	-60 19 35.93	11.54	0.28	0.24
182	10590	12 53 14.62	-60 19 46.91	15.62	0.23	0.30
183	16272	12 54 2.00	-60 19 12.01	11.53	1.70	0.54
184	10528	12 53 29.44	-60 19 37.58	11.29	0.29	0.22
185	11083	12 53 9.63	-60 19 53.13	15.72	0.26	0.23
186	11387	12 53 3.45	-60 19 57.95	17.21	0.78	0.33
187	1214	12 52 56.04	-60 20 4.64	15.10	0.21	0.28
188		12 52 52.25	-60 20 5.68	15.75	0.53	0.25
189		12 53 19.80	-60 19 46.34	8.47	0.57	0.32
190	10992	12 53 0.63	-60 20 1.70	15.88	0.32	0.28
191		12 53 57.36	-60 19 17.46	11.33	0.38	0.31
192		12 54 13.41	-60 19 5.95	15.51	0.32	0.24
193		12 52 57.74	-60 20 8.44	16.63	0.82	0.32
194		12 54 14.84	-60 19 7.07	16.77	0.29	0.25
195		12 54 5.43	-60 19 14.68	18.01	2.00	0.69
196		12 54 4.00	-60 19 16.73	16.40	0.28	0.26
197		12 53 51.80	-60 19 25.96	13.09	0.47	0.31
198		12 53 38.80	-60 19 38.86	16.44	0.43	0.38
199		12 53 29.21	-60 19 45.90	12.32	0.58	0.49
200		12 52 57.00	-60 20 11.03	16.78	1.59	0.58
201	10485	12 53 30.08	-60 19 45.83	13.04	0.44	0.42
202		12 54 10.81	-60 19 14.93	17.05	0.66	0.28
203		12 54 0.03	-60 19 22.39	11.33	0.73	0.36
204		12 53 53.37	-60 19 28.55	13.20	1.32	0.47
205	16908	12 53 14.33	-60 19 59.65	15.56	0.40	0.25
206	1215	12 52 58.37	-60 20 11.65	16.41	0.36	0.28
207		12 53 42.95	-60 19 38.60	15.70	0.38	0.35

Jcu Star #	Webda Db #	RA	Dec	Rmag	Std Dev	15ptStd Dev
208	11210	12 53 34.40	-60 19 44.85	16.16	0.49	0.26
209		12 53 19.70	-60 19 56.55	9.73	1.75	1.18
210		12 54 2.17	-60 19 24.37	12.31	0.71	0.35
211		12 53 49.54	-60 19 35.71	12.90	0.98	0.65
212		12 53 39.83	-60 19 42.72	11.58	0.35	0.31
213		12 53 36.04	-60 19 45.32	13.94	0.23	0.36
214		12 53 24.93	-60 19 51.62	9.76	1.69	0.99
215	719	12 53 14.98	-60 20 1.77	15.40	0.17	0.24
216	11154	12 53 29.42	-60 19 50.91	14.14	0.52	0.45
217	11179	12 53 27.79	-60 19 52.15	11.44	0.35	0.45
218		12 53 8.27	-60 20 11.36	17.42	1.63	0.56
219	10892	12 53 16.85	-60 20 1.44	16.30	0.28	0.27
220	11497	12 54 11.09	-60 19 22.11	16.27	0.41	0.31
221		12 53 57.54	-60 19 34.06	12.05	0.69	0.34
222	10430	12 53 36.79	-60 19 51.71	14.94	0.34	0.38
223	13305	12 53 14.68	-60 20 9.81	16.64	0.89	0.40
224	10686	12 52 57.52	-60 20 23.79	15.08	0.97	0.44
225		12 54 14.03	-60 19 25.49	16.60	0.34	0.29
226	13030	12 53 15.43	-60 20 11.55	16.74	0.42	0.31
227	11756	12 53 12.84	-60 20 12.62	17.50	0.64	0.32
228		12 54 4.06	-60 19 35.29	12.30	1.44	0.42
229		12 53 49.76	-60 19 46.13	13.62	0.34	0.33
230		12 53 7.35	-60 20 20.60	17.01	1.77	0.54
231	128	12 52 56.57	-60 20 29.92	13.87	0.40	0.29
232		12 53 24.33	-60 20 9.25	13.90	0.24	0.40
233		12 53 52.59	-60 19 48.72	11.49	0.20	0.22
234	10991	12 53 28.31	-60 20 9.67	14.73	0.36	0.31
235		12 53 25.33	-60 20 10.89	13.18	0.72	0.58
236	10612	12 53 5.29	-60 20 27.08	14.92	0.36	0.31
237		12 54 7.81	-60 19 39.16	16.55	0.94	0.60
238	10963	12 53 29.49	-60 20 8.98	14.82	0.19	0.27
239	1128	12 53 27.79	-60 20 12.14	14.61	0.23	0.27
240	15227	12 53 14.46	-60 20 22.19	16.87	0.60	0.38
241	10506	12 53 10.03	-60 20 26.40	14.87	0.23	0.30
242	11806	12 53 2.66	-60 20 32.51	14.51	1.45	0.83
243		12 54 11.93	-60 19 37.91	13.81	0.24	0.26
244		12 54 5.78	-60 19 42.98	12.96	0.38	0.27
245		12 53 57.58	-60 19 48.89	14.52	0.26	0.39
246		12 52 58.90	-60 20 36.42	17.35	1.04	0.31
247		12 54 10.06	-60 19 41.11	15.61	0.25	0.19
248	673	12 53 12.90	-60 20 24.82	16.78	0.47	0.33
249		12 54 1.54	-60 19 49.19	9.92	1.55	0.97
250		12 53 50.86	-60 19 57.45	11.56	0.26	0.31
251		12 53 34.28	-60 20 9.87	13.98	0.37	0.31

Jcu Star #	Webda Db #	RA	Dec	Rmag	Std Dev	15ptStd Dev
252	12613	12 53 11.37	-60 20 30.10	17.38	0.77	0.38
253		12 52 55.38	-60 20 40.47	16.44	1.62	0.47
254	23090	12 53 44.70	-60 20 5.14	14.82	0.67	0.32
255	674	12 53 23.14	-60 20 22.41	13.82	0.24	0.17
256	672	12 53 14.84	-60 20 26.98	17.22	0.90	0.34
257	11338	12 52 59.55	-60 20 41.32	17.04	0.79	0.33
258		12 54 2.81	-60 19 51.05	9.81	1.44	0.64
259		12 52 52.11	-60 20 47.70	16.01	0.29	0.28
260		12 54 11.77	-60 19 43.68	13.82	0.31	0.18
261		12 54 4.86	-60 19 49.94	11.30	0.26	0.24
262	134	12 53 17.00	-60 20 29.86	13.47	0.30	0.28
263		12 54 9.75	-60 19 49.16	17.03	1.26	0.42
264	133	12 53 18.18	-60 20 29.97	13.80	0.27	0.33
265	11150	12 53 7.72	-60 20 37.91	14.90	0.33	0.24
266	11440	12 53 32.29	-60 20 19.49	15.28	0.56	0.37
267		12 54 11.44	-60 19 49.47	14.65	1.36	0.58
268		12 53 57.78	-60 20 1.14	9.73	1.77	1.22
269	11911	12 53 6.45	-60 20 41.08	15.06	0.97	0.33
270		12 52 59.56	-60 20 47.17	15.90	1.06	0.45
271		12 54 2.57	-60 19 58.24	8.83	0.91	0.45
272	12105	12 53 43.73	-60 20 13.67	14.69	0.55	0.44
273	11318	12 53 35.81	-60 20 19.83	11.31	0.35	0.35
274		12 53 25.56	-60 20 29.71	13.48	1.24	0.47
275		12 53 21.94	-60 20 33.85	14.35	0.54	0.29
276	1217	12 52 58.79	-60 20 50.49	15.48	0.34	0.26
277		12 54 12.50	-60 19 54.77	15.58	1.33	0.69
278		12 54 6.85	-60 19 58.52	11.46	0.53	0.33
279		12 53 48.39	-60 20 12.93	15.05	0.19	0.24
280	11018	12 53 30.13	-60 20 27.99	14.17	0.44	0.33
281		12 52 53.64	-60 20 56.99	15.75	1.66	0.49
282	10520	12 53 42.09	-60 20 19.80	11.57	0.26	0.29
283		12 53 37.34	-60 20 23.57	11.23	0.27	0.28
284		12 53 32.20	-60 20 28.42	14.45	0.78	0.34
285	126	12 53 9.77	-60 20 44.99	14.37	0.21	0.29
286	11108	12 53 46.83	-60 20 16.86	15.21	0.36	0.39
287	14150	12 53 43.65	-60 20 19.10	14.57	0.51	0.36
288	12740	12 53 35.27	-60 20 26.51	11.22	0.28	0.25
289	668	12 53 21.51	-60 20 36.58	14.40	0.30	0.29
290	11602	12 53 8.84	-60 20 46.92	15.04	1.47	0.71
291		12 53 48.93	-60 20 15.93	15.79	0.50	0.37
292		12 53 53.42	-60 20 14.03	16.46	0.38	0.27
293		12 53 20.42	-60 20 40.87	15.62	0.46	0.36
294		12 54 12.21	-60 20 0.31	14.74	0.23	0.34
295	12997	12 54 7.76	-60 20 3.84	12.90	0.55	0.34

Jcu Star #	Webda Db #	RA	Dec	Rmag	Std Dev	15ptStd Dev
296	661	12 53 10.34	-60 20 49.19	14.56	0.83	0.42
297	1220	12 53 7.87	-60 20 51.22	15.50	0.30	0.23
298		12 53 47.18	-60 20 23.00	14.75	0.31	0.24
299	15669	12 53 30.40	-60 20 36.55	14.52	1.63	0.55
300	11809	12 53 20.71	-60 20 43.46	15.96	0.47	0.27
301		12 52 58.01	-60 21 2.38	17.81	1.01	0.38
302	151	12 53 32.86	-60 20 35.33	14.13	0.42	0.33
303		12 53 23.56	-60 20 43.28	13.99	1.88	0.84
304	660	12 53 12.63	-60 20 52.63	16.08	0.76	0.35
305		12 54 15.28	-60 20 4.01	17.16	0.47	0.24
306	17273	12 53 44.10	-60 20 28.54	12.47	1.50	0.62
307	10852	12 53 31.50	-60 20 38.77	14.53	0.39	0.27
308	14291	12 54 5.81	-60 20 12.33	11.39	0.24	0.26
309		12 53 48.78	-60 20 27.36	14.83	0.53	0.35
310	12892	12 53 37.30	-60 20 36.45	11.35	0.23	0.23
311	1219	12 53 6.48	-60 21 0.44	15.70	0.31	0.28
312		12 54 11.51	-60 20 9.89	15.53	0.30	0.29
313		12 53 53.15	-60 20 25.16	13.69	0.22	0.17
314	11042	12 53 39.17	-60 20 35.13	11.28	0.22	0.29
315	12902	12 53 32.05	-60 20 40.70	14.66	1.00	0.46
316	125	12 53 9.14	-60 20 59.43	13.94	0.37	0.26
317		12 54 10.25	-60 20 12.70	14.56	0.12	0.20
318	13439	12 53 3.50	-60 21 4.42	17.07	0.70	0.32
319		12 53 56.11	-60 20 24.94	13.71	1.73	1.02
320	10550	12 53 42.78	-60 20 35.71	13.22	1.71	1.07
321	1119	12 53 30.00	-60 20 45.25	14.41	0.20	0.21
322	1121	12 53 36.26	-60 20 41.22	11.23	0.44	0.41
323		12 53 22.29	-60 20 52.58	16.60	1.50	0.56
324	657	12 53 20.04	-60 20 55.49	16.62	1.02	0.47
325	132	12 53 18.75	-60 20 56.23	14.64	0.39	0.27
326	12257	12 54 8.91	-60 20 18.36	16.71	0.51	0.25
327	10872	12 53 46.70	-60 20 34.95	14.64	0.32	0.31
328	1224	12 53 8.38	-60 21 6.16	14.91	0.41	0.24
329		12 54 8.39	-60 20 19.94	16.40	0.52	0.34
330	11017	12 53 5.87	-60 21 9.60	15.72	0.26	0.31
331		12 52 56.52	-60 21 17.18	17.90	1.72	0.57
332		12 54 6.78	-60 20 22.82	14.11	1.84	0.68
333	659	12 53 26.31	-60 20 54.22	12.13	0.48	0.32
334	653	12 53 10.61	-60 21 6.81	16.46	0.35	0.28
335		12 54 11.03	-60 20 20.54	15.51	0.26	0.26
336	17451	12 54 7.19	-60 20 23.51	15.55	1.86	0.59
337	11180	12 53 38.67	-60 20 46.98	8.52	0.47	0.33
338	1118	12 53 29.01	-60 20 54.16	14.60	0.40	0.31
339	20186	12 54 15.11	-60 20 17.92	16.02	0.16	0.18

Jcu Star #	Webda Db #	RA	Dec	Rmag	Std Dev	15ptStd Dev
340		12 54 2.04	-60 20 30.46	14.74	0.56	0.42
341		12 53 39.95	-60 20 50.30	8.49	0.49	0.39
342		12 52 58.25	-60 21 22.60	17.43	0.73	0.24
343	14147	12 53 53.14	-60 20 39.69	13.75	1.63	0.75
344		12 53 46.24	-60 20 44.82	11.17	0.34	0.32
345	644	12 53 12.12	-60 21 11.48	15.42	0.33	0.27
346		12 53 3.52	-60 21 19.25	17.15	0.53	0.27
347		12 53 1.32	-60 21 20.85	17.46	1.73	0.58
348		12 54 14.28	-60 20 24.59	13.88	0.08	0.21
349		12 54 9.59	-60 20 28.17	15.06	0.42	0.33
350	15694	12 53 52.66	-60 20 42.84	13.63	1.70	0.73
351	1116	12 53 22.10	-60 21 6.62	15.81	0.26	0.23
352		12 54 11.25	-60 20 29.56	13.43	0.17	0.26
353	14955	12 52 59.13	-60 21 26.46	16.87	0.44	0.27
354	642	12 53 16.44	-60 21 13.99	16.27	0.42	0.29
355		12 53 10.17	-60 21 22.19	13.51	1.36	0.72
356		12 53 3.78	-60 21 22.86	17.13	0.71	0.29
357		12 53 2.46	-60 21 25.54	16.79	0.50	0.25
358		12 54 12.93	-60 20 30.87	16.99	0.42	0.26
359		12 54 8.58	-60 20 32.31	16.42	1.20	0.57
360	10807	12 53 38.49	-60 20 59.39	9.72	0.21	0.27
361		12 53 26.92	-60 21 8.78	13.43	0.74	0.50
362	14429	12 53 5.14	-60 21 25.39	19.11	1.65	0.47
363		12 52 56.75	-60 21 31.99	15.13	0.25	0.25
364		12 53 51.56	-60 20 49.89	13.19	0.25	0.28
365	13921	12 53 47.82	-60 20 52.79	13.03	1.51	0.62
366		12 53 59.19	-60 20 45.17	14.75	0.21	0.37
367		12 53 56.92	-60 20 46.63	15.17	0.36	0.34
368	639	12 53 18.58	-60 21 18.48	15.61	0.44	0.34
369		12 53 40.40	-60 21 2.17	8.43	0.53	0.32
370	131	12 53 23.11	-60 21 16.75	14.29	0.32	0.32
371	13403	12 53 6.89	-60 21 29.26	16.71	1.65	0.53
372	14060	12 53 3.78	-60 21 30.38	18.14	1.34	0.45
373		12 53 1.05	-60 21 34.44	16.79	1.76	0.57
374		12 54 13.45	-60 20 37.58	16.85	0.41	0.29
375	152	12 53 30.76	-60 21 12.42	14.30	0.42	0.38
376	637	12 53 22.46	-60 21 19.56	14.66	0.40	0.27
377	20689	12 54 0.76	-60 20 49.61	16.35	0.30	0.31
378		12 53 43.60	-60 21 3.33	11.85	0.38	0.40
379		12 53 36.85	-60 21 9.46	8.68	0.52	0.43
380	634	12 53 18.22	-60 21 23.57	15.59	0.82	0.42
381	17175	12 53 2.55	-60 21 36.65	15.46	0.28	0.25
382		12 53 56.49	-60 20 55.12	14.47	0.32	0.21
383		12 52 56.45	-60 21 44.24	15.00	0.34	0.28

Jcu Star #	Webda Db #	RA	Dec	Rmag	Std Dev	15ptStd Dev
384		12 54 7.22	-60 20 48.67	14.72	0.51	0.44
385		12 54 4.57	-60 20 50.72	14.17	0.29	0.26
386		12 53 22.08	-60 21 22.49	15.08	1.48	0.66
387	10935	12 53 53.04	-60 21 0.68	14.83	0.38	0.31
388	11300	12 53 11.01	-60 21 34.87	15.52	0.41	0.32
389	10821	12 53 33.62	-60 21 17.78	13.42	1.32	0.84
390		12 53 27.62	-60 21 22.84	13.05	1.61	0.70
391		12 54 1.62	-60 20 56.85	15.94	0.66	0.32
392		12 53 31.28	-60 21 20.25	13.40	1.52	0.50
393		12 54 0.13	-60 20 59.04	16.00	0.44	0.28
394		12 53 44.52	-60 21 13.54	11.26	1.44	0.72
395		12 54 3.71	-60 20 57.20	15.18	1.36	0.63
396	12220	12 53 20.64	-60 21 32.10	14.15	1.19	0.68
397		12 53 5.89	-60 21 44.04	18.65	1.75	0.51
398	10400	12 53 34.36	-60 21 22.25	14.56	0.64	0.47
399		12 53 52.51	-60 21 9.01	13.53	1.25	0.70
400	10729	12 53 29.74	-60 21 26.40	12.96	1.61	1.13
401		12 53 59.78	-60 21 4.76	15.49	0.48	0.30
402	12778	12 53 54.39	-60 21 8.30	15.50	1.54	0.60
403		12 52 59.37	-60 21 51.70	15.29	0.69	0.30
404		12 52 56.76	-60 21 55.71	13.63	1.36	0.47
405	2107	12 53 48.51	-60 21 16.13	11.56	0.37	0.31
406	10638	12 53 31.03	-60 21 31.80	15.01	0.21	0.15
407	14529	12 53 2.59	-60 21 53.26	16.48	0.39	0.26
408	10645	12 53 32.31	-60 21 32.61	14.58	0.28	0.25
409	6420	12 53 55.91	-60 21 14.61	14.14	0.27	0.36
410	619	12 53 12.70	-60 21 48.36	16.72	0.65	0.45
411		12 53 5.33	-60 21 53.65	18.00	0.95	0.35
412	212	12 53 50.64	-60 21 19.33	12.57	0.43	0.32
413	156	12 53 20.90	-60 21 43.49	14.37	0.23	0.26
414		12 53 10.98	-60 21 50.97	16.47	0.51	0.44
415		12 53 4.05	-60 21 56.33	18.54	1.98	0.58
416		12 54 14.80	-60 21 0.24	14.51	0.60	0.31
417	10927	12 53 45.23	-60 21 25.98	13.00	0.31	0.36
418	103	12 53 42.46	-60 21 27.33	11.15	0.25	0.24
419		12 53 36.20	-60 21 31.83	8.95	0.54	0.32
420		12 54 0.49	-60 21 14.53	14.88	0.24	0.31
421		12 52 57.24	-60 22 3.39	15.58	0.37	0.22
422		12 54 11.72	-60 21 6.03	15.38	0.28	0.32
423		12 54 5.39	-60 21 11.53	14.62	0.27	0.23
424	712	12 53 53.04	-60 21 24.11	10.97	0.66	0.42
425	711	12 53 34.51	-60 21 34.97	13.42	0.63	0.34
426	153	12 53 32.15	-60 21 37.74	14.53	0.32	0.28
427		12 53 8.78	-60 21 57.30	15.09	1.30	0.69

Jcu Star #	Webda Db #	RA	Dec	Rmag	Std Dev	15ptStd Dev
428		12 53 55.32	-60 21 20.35	14.42	0.29	0.32
429	155	12 53 21.52	-60 21 46.91	14.53	0.25	0.19
430		12 54 6.63	-60 21 11.64	16.61	0.41	0.30
431	10865	12 53 42.04	-60 21 31.97	11.06	1.43	0.93
432	102	12 53 40.71	-60 21 33.74	11.19	0.23	0.30
433	10627	12 53 33.76	-60 21 39.83	13.91	0.92	0.53
434	10575	12 54 0.26	-60 21 20.54	14.31	0.20	0.25
435	617	12 53 24.64	-60 21 49.96	13.66	1.54	1.22
436	17073	12 54 4.58	-60 21 19.06	14.59	1.32	0.59
437	154	12 53 32.79	-60 21 43.73	14.25	0.22	0.26
438	119	12 53 22.73	-60 21 51.90	13.95	0.34	0.30
439		12 52 54.01	-60 22 14.12	13.16	0.13	0.08
440	12001	12 53 49.32	-60 21 31.78	11.21	1.00	0.43
441	11361	12 53 29.88	-60 21 47.49	13.76	0.33	0.25
442	10575	12 54 0.10	-60 21 23.59	14.22	0.46	0.34
443	11037	12 53 33.38	-60 21 43.85	14.48	0.46	0.36
444	121	12 53 9.31	-60 22 4.73	14.01	0.28	0.33
445	210	12 53 52.71	-60 21 31.36	10.93	0.37	0.35
446	5134	12 53 30.66	-60 21 49.52	13.68	0.35	0.24
447	10855	12 53 42.12	-60 21 41.79	13.18	0.43	0.40
448	6335	12 54 5.49	-60 21 23.54	13.52	0.22	0.26
449		12 53 58.22	-60 21 30.74	13.73	0.66	0.48
450		12 53 10.53	-60 22 8.75	15.81	0.32	0.36
451	612	12 53 23.45	-60 21 58.08	14.52	0.52	0.37
452		12 53 4.95	-60 22 14.32	17.63	0.78	0.32
453		12 54 10.47	-60 21 22.18	14.49	0.20	0.13
454	205	12 53 43.87	-60 21 43.93	12.90	0.23	0.25
455		12 54 8.16	-60 21 25.64	14.62	0.42	0.33
456	11114	12 53 50.67	-60 21 39.37	13.00	0.58	0.45
457		12 53 31.20	-60 21 55.58	13.68	1.24	0.46
458	15476	12 53 16.49	-60 22 6.72	15.22	0.33	0.38
459	11522	12 53 45.40	-60 21 46.82	11.86	1.05	0.48
460	5030	12 53 41.70	-60 21 50.09	14.38	0.29	0.29
461	12734	12 52 59.23	-60 22 24.03	14.65	1.13	0.41
462		12 54 3.91	-60 21 34.27	16.31	0.23	0.26
463		12 54 14.76	-60 21 27.60	14.62	0.23	0.16
464		12 54 2.21	-60 21 35.31	17.72	2.06	0.80
465	1103	12 53 34.32	-60 21 59.64	15.59	0.24	0.29
466		12 53 50.12	-60 21 48.71	11.42	1.20	0.59
467	5004	12 53 44.19	-60 21 52.30	14.87	0.33	0.31
468	5054	12 53 39.49	-60 21 56.09	14.47	0.33	0.33
469	1109	12 53 28.84	-60 22 4.09	13.78	0.44	0.31
470	12010	12 54 5.67	-60 21 36.52	16.46	0.58	0.33
471	6429	12 53 54.94	-60 21 44.56	13.47	0.25	0.26

Jcu Star #	Webda Db #	RA	Dec	Rmag	Std Dev	15ptStd Dev
472	22887	12 53 44.93	-60 21 53.36	15.36	0.50	0.17
473	13198	12 53 36.98	-60 21 58.81	14.67	1.44	0.84
474		12 53 2.76	-60 22 29.50	16.63	0.87	0.34
475	6399	12 53 59.74	-60 21 41.69	14.98	0.32	0.36
476		12 53 16.03	-60 22 17.71	15.89	1.75	0.72
477		12 53 15.01	-60 22 18.36	15.00	0.68	0.29
478	5005	12 53 44.16	-60 21 59.32	15.15	0.21	0.27
479		12 53 19.14	-60 22 19.16	13.21	1.68	0.75
480		12 52 58.22	-60 22 35.99	13.53	0.24	0.27
481	11711	12 53 54.47	-60 21 51.89	13.64	1.15	0.56
482	5042	12 53 40.13	-60 22 3.88	14.87	0.34	0.33
483	12518	12 53 31.65	-60 22 11.13	13.48	0.40	0.28
484	6375	12 54 1.53	-60 21 47.58	17.13	0.88	0.41
485		12 53 6.48	-60 22 31.49	16.23	0.26	0.26
486	6398	12 53 59.34	-60 21 51.48	16.25	1.61	0.54
487	10239	12 53 53.00	-60 21 55.42	12.85	0.25	0.24
488	1102	12 53 36.98	-60 22 7.63	14.57	0.24	0.17
489	15283	12 53 20.70	-60 22 21.37	13.37	0.43	0.27
490		12 53 23.22	-60 22 20.84	13.49	0.43	0.38
491	20420	12 54 11.41	-60 21 43.15	15.46	0.35	0.25
492	6405	12 53 59.03	-60 21 51.89	16.56	1.21	0.42
493	5011	12 53 43.57	-60 22 5.76	16.09	0.80	0.38
494		12 53 16.70	-60 22 27.45	14.47	0.54	0.36
495		12 53 0.42	-60 22 39.52	14.90	0.32	0.29
496		12 52 58.75	-60 22 41.18	13.71	1.09	0.43
497		12 52 57.56	-60 22 42.49	13.74	1.26	0.51
498	6385	12 54 0.86	-60 21 53.10	17.06	0.73	0.40
499	204	12 53 45.08	-60 22 5.76	13.76	0.30	0.14
500	23124	12 53 38.61	-60 22 10.98	16.52	0.42	0.33
501	10392	12 53 46.11	-60 22 7.10	11.57	1.01	0.61
502	5017	12 53 42.74	-60 22 9.68	16.05	0.22	0.24
503	591	12 53 24.38	-60 22 24.69	12.77	1.63	0.78
504	12219	12 54 9.48	-60 21 49.86	13.99	0.92	0.39
505		12 54 5.24	-60 21 52.81	16.42	0.26	0.28
506	6402	12 53 59.12	-60 21 57.95	16.70	0.35	0.28
507	12343	12 54 7.08	-60 21 53.22	14.95	0.21	0.26
508	5137	12 53 30.52	-60 22 21.69	13.42	1.13	0.60
509		12 53 20.15	-60 22 30.75	13.34	1.14	0.48
510		12 52 56.70	-60 22 49.39	13.82	1.56	0.53
511	6428	12 53 54.99	-60 22 3.98	13.07	0.46	0.32
512	5087	12 53 35.57	-60 22 19.94	15.87	1.19	0.48
513		12 53 15.99	-60 22 35.32	15.70	1.19	0.58
514		12 53 54.30	-60 22 5.94	12.03	1.19	0.56
515	5070	12 53 37.59	-60 22 19.96	16.36	0.59	0.36

Jcu Star #	Webda Db #	RA	Dec	Rmag	Std Dev	15ptStd Dev
516	5099	12 53 34.23	-60 22 21.56	14.94	0.36	0.29
517	5114	12 53 33.20	-60 22 23.97	14.73	1.21	0.67
518	16982	12 53 14.99	-60 22 39.16	16.79	0.77	0.40
519		12 53 6.92	-60 22 45.66	16.80	0.66	0.33
520		12 53 0.62	-60 22 50.75	16.86	1.04	0.39
521	13811	12 54 3.99	-60 22 2.71	18.34	1.66	0.56
522		12 54 12.92	-60 21 57.04	13.30	1.62	0.55
523	6424	12 53 55.36	-60 22 9.05	13.02	0.21	0.21
524	409	12 53 28.31	-60 22 30.98	13.77	0.40	0.36
525	573	12 53 12.47	-60 22 43.03	15.77	0.29	0.25
526	582	12 53 21.94	-60 22 36.35	15.34	0.48	0.32
527		12 53 16.55	-60 22 41.25	15.08	1.44	0.58
528		12 53 15.92	-60 22 38.82	16.24	0.86	0.44
529	12129	12 54 6.38	-60 22 3.48	16.94	0.82	0.41
530	5058	12 53 39.21	-60 22 27.26	13.99	0.35	0.30
531		12 52 57.44	-60 23 0.51	17.46	1.65	0.62
532		12 53 49.64	-60 22 22.17	8.49	0.34	0.24
533	5149	12 53 29.34	-60 22 35.78	15.33	0.53	0.32
534		12 53 24.16	-60 22 39.63	12.68	1.32	0.61
535	12756	12 53 3.62	-60 22 56.27	15.91	0.42	0.43
536	577	12 53 25.64	-60 22 42.46	13.91	1.60	1.05
537		12 52 57.87	-60 23 4.23	18.20	1.69	0.63
538	6257	12 54 12.48	-60 22 5.99	15.68	0.69	0.29
539	576	12 53 26.86	-60 22 43.51	13.91	1.52	0.94
540	23056	12 53 10.46	-60 22 57.78	15.91	0.19	0.23
541	3125	12 54 0.24	-60 22 18.41	14.48	0.40	0.30
542	4132	12 53 20.68	-60 22 50.89	14.07	0.37	0.38
543		12 53 40.71	-60 22 36.04	13.68	1.62	1.07
544		12 53 19.17	-60 22 53.14	17.70	0.76	0.35
545		12 53 12.11	-60 22 59.04	15.84	0.22	0.31
546	6300	12 54 8.52	-60 22 15.31	13.58	0.22	0.26
547	308	12 53 56.82	-60 22 23.96	12.74	0.22	0.24
548	407	12 53 33.97	-60 22 42.11	13.32	0.29	0.31
549	5081	12 53 36.18	-60 22 42.44	14.45	0.33	0.28
550	16753	12 53 10.22	-60 23 3.10	16.07	0.47	0.27
551		12 52 56.93	-60 23 14.46	15.71	0.22	0.11
552		12 54 14.78	-60 22 13.52	14.44	0.16	0.21
553		12 53 21.65	-60 22 55.68	14.11	0.73	0.38
554		12 53 17.92	-60 22 58.76	13.51	0.19	0.22
555	6383	12 54 1.07	-60 22 25.90	15.41	0.38	0.27
556	5122	12 53 31.54	-60 22 49.72	14.29	0.85	0.42
557	5143	12 53 29.80	-60 22 50.81	13.85	0.65	0.36
558		12 53 47.15	-60 22 37.99	8.50	0.49	0.38
559	6332	12 54 6.06	-60 22 23.61	14.90	0.58	0.39

Jcu Star #	Webda Db #	RA	Dec	Rmag	Std Dev	15ptStd Dev
560	401	12 53 41.78	-60 22 43.88	13.08	0.33	0.15
561		12 53 12.58	-60 23 7.14	15.94	0.24	0.26
562	4122	12 53 27.86	-60 22 56.18	13.89	0.35	0.30
563		12 53 22.57	-60 23 0.50	14.66	0.61	0.39
564	12898	12 53 30.98	-60 22 56.18	13.68	0.97	0.45
565		12 53 14.13	-60 23 8.80	15.38	0.38	0.31
566	3126	12 54 0.55	-60 22 32.95	15.05	0.24	0.31
567	20748	12 53 55.19	-60 22 37.32	13.31	0.28	0.36
568	10538	12 53 45.97	-60 22 44.76	12.58	0.25	0.29
569	10490	12 53 44.84	-60 22 45.51	13.90	0.29	0.31
570	4117	12 53 34.98	-60 22 52.15	13.30	0.17	0.11
571	6215	12 54 16.07	-60 22 21.83	17.50	0.60	0.37
572	6337	12 54 5.62	-60 22 30.17	15.20	0.39	0.24
573	3201	12 54 7.51	-60 22 29.72	15.35	0.44	0.36
574	20116	12 54 2.41	-60 22 33.55	16.41	0.55	0.30
575		12 53 15.77	-60 23 13.85	16.64	1.58	0.61
576		12 53 9.05	-60 23 15.66	15.45	0.21	0.26
577	6346	12 54 4.54	-60 22 33.46	15.85	0.24	0.25
578	14862	12 52 59.04	-60 23 24.66	17.37	0.84	0.29
579		12 53 56.07	-60 22 41.78	13.26	0.89	0.39
580	5009	12 53 43.76	-60 22 50.41	14.50	0.38	0.31
581		12 53 30.64	-60 23 1.81	13.54	0.26	0.22
582		12 53 4.78	-60 23 21.63	16.74	0.73	0.33
583	11182	12 53 54.93	-60 22 43.76	13.46	1.37	0.71
584	15399	12 52 54.30	-60 23 29.96	16.13	1.12	0.37
585	10557	12 54 1.24	-60 22 39.76	15.64	0.32	0.27
586		12 53 56.05	-60 22 43.78	13.64	1.42	0.52
587	310	12 53 54.08	-60 22 45.55	13.14	0.29	0.31
588		12 53 12.38	-60 23 18.45	13.89	0.22	0.20
589		12 53 4.19	-60 23 23.64	17.51	1.53	0.51
590	15584	12 54 16.20	-60 22 29.06	17.56	1.37	0.51
591	4116	12 53 35.44	-60 23 1.63	13.30	0.25	0.15
592	5345	12 53 7.03	-60 23 25.73	14.59	0.23	0.28
593	15584	12 54 16.67	-60 22 31.16	18.47	1.98	0.60
594	704	12 53 45.70	-60 22 55.42	14.31	0.55	0.38
595	5035	12 53 41.32	-60 22 59.63	13.36	1.06	0.63
596	5106	12 53 33.64	-60 23 5.95	13.45	0.79	0.40
597		12 53 23.66	-60 23 14.71	12.97	0.43	0.35
598		12 54 16.01	-60 22 34.07	18.34	1.59	0.49
599	412	12 53 31.31	-60 23 9.96	14.03	0.25	0.32
600		12 52 55.28	-60 23 38.79	16.78	0.45	0.25
601	20450	12 54 13.63	-60 22 37.64	18.52	1.12	0.36
602	423	12 53 29.01	-60 23 12.90	14.30	0.58	0.32
603	15772	12 53 7.86	-60 23 29.90	14.80	0.32	0.27

Jcu Star #	Webda Db #	RA	Dec	Rmag	Std Dev	15ptStd Dev
604		12 53 7.38	-60 23 29.90	14.86	0.33	0.25
605		12 53 6.40	-60 23 30.97	15.27	0.35	0.26
606	5092	12 53 35.01	-60 23 10.57	15.20	0.31	0.19
607		12 54 17.91	-60 22 36.22	17.59	0.69	0.25
608	6212	12 54 16.34	-60 22 36.97	18.29	1.26	0.40
609	3128	12 54 3.47	-60 22 47.58	14.88	0.27	0.24
610	5078	12 53 36.68	-60 23 9.93	15.03	0.34	0.29
611	5016	12 53 43.12	-60 23 4.97	14.91	0.47	0.39
612	5022	12 53 42.50	-60 23 5.90	14.72	0.42	0.37
613	14555	12 53 39.61	-60 23 10.15	14.64	0.40	0.30
614	15566	12 53 13.48	-60 23 30.96	15.32	0.86	0.46
615		12 53 22.48	-60 23 23.98	14.62	0.26	0.32
616		12 53 13.68	-60 23 31.23	15.29	0.93	0.49
617	6359	12 54 3.22	-60 22 52.89	14.92	0.26	0.27
618		12 53 51.39	-60 23 1.95	10.31	1.82	1.16
619	12681	12 53 44.46	-60 23 8.20	13.00	0.62	0.31
620	5071	12 53 37.42	-60 23 13.46	15.50	1.24	0.51
621		12 53 19.69	-60 23 27.72	12.56	0.82	0.59
622	5037	12 53 40.76	-60 23 12.81	16.23	0.54	0.43
623		12 53 25.95	-60 23 24.81	13.33	0.32	0.25
624		12 53 20.80	-60 23 27.36	10.73	0.26	0.30
625		12 53 5.17	-60 23 40.92	18.02	2.00	0.58
626		12 53 4.03	-60 23 42.68	14.98	1.07	0.40
627	6291	12 54 9.46	-60 22 51.00	17.80	0.73	0.32
628	6427	12 53 55.02	-60 23 2.68	11.92	0.31	0.34
629		12 52 57.01	-60 23 48.21	15.33	0.33	0.26
630	6370	12 54 1.92	-60 22 55.61	17.37	0.91	0.37
631	411	12 53 38.21	-60 23 18.31	14.84	0.12	0.23
632	16336	12 53 34.18	-60 23 22.07	16.50	1.78	0.72
633	22896	12 53 30.35	-60 23 24.79	16.90	0.72	0.37
634		12 53 19.40	-60 23 33.53	14.14	0.90	0.50
635	6423	12 53 55.51	-60 23 5.13	13.21	0.25	0.29
636	10943	12 53 45.99	-60 23 13.24	11.88	0.40	0.36
637	304	12 53 48.36	-60 23 12.64	11.04	0.84	0.66
638		12 53 3.20	-60 23 49.30	14.36	0.35	0.25
639	10678	12 53 45.79	-60 23 14.75	11.92	0.36	0.32
640	3101	12 53 43.99	-60 23 17.40	12.69	0.50	0.26
641		12 53 32.34	-60 23 26.87	14.44	0.24	0.23
642		12 53 13.49	-60 23 41.26	18.17	1.45	0.53
643		12 52 56.33	-60 23 56.91	16.53	0.85	0.30
644	6197	12 54 17.69	-60 22 52.82	16.37	0.22	0.18
645	6355	12 54 3.38	-60 23 5.24	16.85	0.97	0.45
646		12 53 52.86	-60 23 13.87	12.47	0.33	0.31
647	16732	12 53 28.46	-60 23 34.54	15.81	0.24	0.17

Jcu Star #	Webda Db #	RA	Dec	Rmag	Std Dev	15ptStd Dev
648	6263	12 54 11.75	-60 22 59.79	15.04	0.72	0.31
649	5059	12 53 38.84	-60 23 26.10	13.27	1.62	0.98
650		12 53 23.10	-60 23 38.98	13.92	1.45	0.69
651	6238	12 54 13.91	-60 22 59.42	17.00	0.55	0.25
652	12350	12 53 1.11	-60 23 58.66	15.47	0.30	0.19
653		12 52 55.98	-60 24 1.54	16.39	0.40	0.19
654	6377	12 54 1.30	-60 23 12.19	14.30	0.67	0.37
655	5003	12 53 44.56	-60 23 24.66	11.90	0.53	0.40
656		12 53 14.20	-60 23 48.83	17.57	1.79	0.53
657		12 53 7.02	-60 23 56.93	18.62	1.68	0.53
658		12 53 27.06	-60 23 41.28	15.04	1.85	0.65
659	3202	12 54 11.33	-60 23 6.67	14.58	0.14	0.19
660	6288	12 54 9.71	-60 23 7.94	15.36	1.25	0.50
661	3123	12 53 54.39	-60 23 19.98	14.88	0.19	0.24
662	11013	12 53 48.87	-60 23 24.90	14.68	0.31	0.30
663	10736	12 53 50.02	-60 23 24.56	13.70	0.87	0.56
664	5024	12 53 42.01	-60 23 32.30	15.07	0.22	0.27
665	22831	12 53 38.19	-60 23 34.38	13.95	0.27	0.28
666	22832	12 53 31.22	-60 23 41.57	13.57	0.48	0.29
667		12 53 55.79	-60 23 23.60	13.50	1.54	0.61
668		12 53 3.68	-60 24 4.97	18.82	1.45	0.46
669	6367	12 54 1.97	-60 23 20.48	14.29	0.78	0.38
670	10505	12 53 39.84	-60 23 39.26	10.63	0.62	0.42
671		12 53 32.77	-60 23 45.19	13.12	1.04	0.55
672	701	12 53 31.41	-60 23 45.58	13.15	0.40	0.32
673	16034	12 53 20.95	-60 23 55.62	14.67	0.21	0.23
674		12 53 10.04	-60 24 4.47	14.24	0.29	0.25
675	11339	12 53 51.59	-60 23 31.46	12.32	1.41	0.92
676	5029	12 53 41.68	-60 23 40.25	14.49	0.28	0.32
677		12 53 13.10	-60 24 4.06	14.65	1.59	0.56
678		12 53 12.57	-60 24 5.48	15.70	0.99	0.45
679		12 53 2.63	-60 24 14.37	16.68	0.78	0.29
680	6213	12 54 16.21	-60 23 16.51	16.09	0.17	0.24
681	6259	12 54 12.23	-60 23 20.59	15.80	0.15	0.19
682	6325	12 54 6.50	-60 23 24.67	14.87	0.29	0.27
683	16190	12 53 17.13	-60 24 4.06	15.51	0.50	0.29
684	20740	12 54 7.90	-60 23 25.28	16.29	0.68	0.23
685	5015	12 53 43.13	-60 23 44.76	13.13	0.65	0.44
686		12 53 18.30	-60 24 4.12	15.29	1.69	0.51
687		12 53 16.51	-60 24 8.32	15.79	0.77	0.42
688	16986	12 53 6.56	-60 24 16.26	18.36	1.20	0.39
689		12 53 41.64	-60 23 49.89	12.98	0.53	0.36
690		12 53 27.32	-60 24 1.34	16.14	0.22	0.23
691	507	12 53 23.36	-60 24 5.44	15.30	0.21	0.29

Jcu Star #	Webda Db #	RA	Dec	Rmag	Std Dev	15ptStd Dev
692		12 53 18.93	-60 24 10.41	15.34	1.81	0.56
693	3104	12 53 48.99	-60 23 47.45	14.60	0.34	0.27
694		12 53 26.55	-60 24 6.41	16.44	0.40	0.28
695		12 53 13.07	-60 24 16.59	12.71	0.31	0.27
696	10813	12 53 51.55	-60 23 48.36	12.57	0.35	0.31
697		12 53 42.18	-60 23 53.66	12.90	0.98	0.41
698	22999	12 53 20.23	-60 24 11.76	16.44	0.65	0.37
699		12 53 4.66	-60 24 24.45	16.74	0.69	0.31
700		12 53 39.71	-60 23 57.81	11.53	1.61	1.04
701		12 53 28.38	-60 24 6.53	15.70	0.18	0.21
702	6387	12 54 0.48	-60 23 42.54	15.14	0.28	0.21
703	6393	12 53 59.96	-60 23 42.93	14.99	0.18	0.19
704	6361	12 54 2.76	-60 23 41.15	17.00	0.83	0.40
705		12 53 30.59	-60 24 6.79	15.94	0.31	0.30
706		12 53 29.40	-60 24 9.84	17.10	0.81	0.33
707	23103	12 53 24.95	-60 24 14.79	15.48	0.23	0.24
708		12 53 16.81	-60 24 21.27	16.30	1.47	0.44
709	3122	12 53 55.70	-60 23 51.42	14.33	0.21	0.24
710		12 53 41.68	-60 24 1.84	14.26	0.24	0.24
711		12 53 33.66	-60 24 8.22	16.21	0.46	0.23
712		12 53 36.06	-60 24 7.59	14.49	0.25	0.23
713	6371	12 54 1.83	-60 23 48.58	17.85	0.98	0.32
714		12 53 0.94	-60 24 37.63	17.74	1.04	0.33
715	20639	12 54 11.64	-60 23 41.91	16.78	0.54	0.28
716	13924	12 53 49.61	-60 24 0.11	11.97	1.52	0.86
717		12 53 25.44	-60 24 16.97	15.55	0.31	0.22
718	6345	12 54 4.84	-60 23 48.41	16.51	0.44	0.26
719	6357	12 54 3.43	-60 23 49.48	16.52	0.52	0.33
720	14534	12 53 39.46	-60 24 6.79	13.96	1.47	0.52
721	23060	12 53 38.06	-60 24 11.66	14.58	0.44	0.31
722	6302	12 54 8.47	-60 23 48.40	17.16	0.49	0.32
723		12 53 32.57	-60 24 17.46	13.16	0.16	0.23
724		12 54 0.58	-60 23 57.29	17.90	1.61	0.51
725	314	12 53 48.01	-60 24 6.59	13.50	0.27	0.27
726		12 53 36.27	-60 24 14.89	14.59	0.73	0.45
727		12 53 34.01	-60 24 17.40	13.47	0.85	0.45
728	17454	12 53 18.19	-60 24 29.98	17.67	1.78	0.60
729	3207	12 54 11.36	-60 23 49.11	15.71	0.19	0.24
730		12 53 9.36	-60 24 39.31	16.30	0.33	0.23
731		12 52 58.50	-60 24 47.03	16.34	0.53	0.26
732	6331	12 54 6.10	-60 23 53.61	16.52	0.85	0.43
733		12 53 57.22	-60 24 1.49	12.68	0.27	0.23
734		12 53 2.95	-60 24 44.82	17.29	0.96	0.31
735		12 54 15.95	-60 23 48.66	18.06	1.73	0.49

Jcu Star #	Webda Db #	RA	Dec	Rmag	Std Dev	15ptStd Dev
736		12 53 29.00	-60 24 25.23	16.53	0.32	0.25
737		12 53 24.19	-60 24 30.83	18.80	1.97	0.59
738		12 53 39.93	-60 24 17.49	13.69	0.42	0.32
739	5254	12 53 16.34	-60 24 36.78	15.78	0.22	0.31
740		12 53 14.17	-60 24 38.01	16.84	0.64	0.30
741	23107	12 53 12.54	-60 24 40.01	14.34	0.28	0.35
742	20502	12 53 53.62	-60 24 8.21	13.99	1.52	0.70
743		12 53 39.45	-60 24 19.45	14.40	1.63	0.92
744	320	12 54 3.25	-60 24 1.70	13.83	0.43	0.33
745	11041	12 54 5.77	-60 24 1.01	16.14	0.57	0.41
746		12 53 36.89	-60 24 23.81	14.49	1.42	0.52
747		12 53 55.01	-60 24 10.94	13.39	1.93	0.66
748		12 53 31.32	-60 24 29.58	15.54	0.32	0.27
749		12 53 1.80	-60 24 52.78	16.10	0.39	0.30
750	14030	12 53 38.84	-60 24 22.75	14.45	1.66	0.86
751		12 52 57.23	-60 24 58.15	15.87	0.25	0.19
752	12701	12 54 9.29	-60 24 1.80	18.10	0.83	0.29
753	321	12 54 2.36	-60 24 7.39	14.07	0.15	0.23
754		12 53 5.51	-60 24 52.17	15.59	0.23	0.25
755		12 52 55.40	-60 25 0.57	16.48	0.62	0.23
756	17807	12 53 24.32	-60 24 39.20	17.30	1.85	0.67
757		12 53 4.01	-60 24 56.50	17.51	1.69	0.59
758		12 52 58.46	-60 25 0.90	18.21	1.67	0.54
759	22824	12 53 19.68	-60 24 45.20	15.14	0.50	0.45
760	23062	12 53 1.62	-60 25 0.64	16.81	0.66	0.30
761	16297	12 54 6.26	-60 24 9.61	16.59	0.80	0.36
762	11077	12 53 53.23	-60 24 19.50	15.93	0.33	0.24
763	3105	12 53 50.03	-60 24 22.36	11.93	0.24	0.33
764	20731	12 53 25.77	-60 24 41.84	16.51	0.43	0.29
765		12 53 22.94	-60 24 43.36	15.09	0.26	0.34
766		12 53 0.65	-60 25 1.89	17.35	1.07	0.30
767		12 52 56.92	-60 25 3.78	15.46	0.26	0.16
768	3118	12 54 3.41	-60 24 13.06	14.81	0.16	0.27
769		12 53 42.45	-60 24 31.57	14.32	1.59	0.67
770		12 53 39.91	-60 24 32.19	15.17	0.21	0.30
771		12 53 29.84	-60 24 41.64	16.79	0.47	0.30
772		12 53 24.39	-60 24 44.74	17.03	1.84	0.61
773		12 53 14.28	-60 24 55.27	18.84	1.96	0.63
774	10834	12 53 53.11	-60 24 24.06	14.27	0.21	0.21
775		12 53 31.33	-60 24 40.94	11.73	1.64	0.68
776		12 53 17.30	-60 24 51.22	16.55	0.46	0.24
777		12 53 11.40	-60 24 56.42	17.12	0.88	0.38
778		12 54 0.01	-60 24 19.39	16.03	1.79	0.54
779	12737	12 53 56.70	-60 24 21.91	15.44	0.81	0.43

Jcu Star #	Webda Db #	RA	Dec	Rmag	Std Dev	15ptStd Dev
780	5010	12 53 43.25	-60 24 32.74	16.58	0.86	0.51
781		12 53 30.46	-60 24 43.21	16.75	0.48	0.34
782	12572	12 53 19.70	-60 24 51.71	14.80	0.43	0.39
783		12 53 43.88	-60 24 33.28	16.24	0.50	0.41
784	23010	12 53 9.12	-60 25 1.89	14.64	0.49	0.34
785	14596	12 53 26.36	-60 24 49.58	16.96	0.84	0.32
786		12 52 55.91	-60 25 15.67	16.57	1.25	0.35
787	10564	12 53 53.34	-60 24 31.08	15.73	0.31	0.27
788		12 53 39.18	-60 24 41.99	14.38	0.45	0.29
789		12 53 31.88	-60 24 48.62	14.65	0.72	0.38
790	322	12 54 5.03	-60 24 23.00	14.49	0.17	0.30
791	325	12 54 11.82	-60 24 18.53	14.55	0.19	0.22
792		12 53 9.74	-60 25 8.26	13.65	1.50	0.55
793	11286	12 54 3.13	-60 24 27.17	14.59	0.53	0.31
794	16597	12 53 19.24	-60 25 1.45	15.88	0.17	0.29
795	10407	12 54 14.92	-60 24 22.28	12.15	0.34	0.35
796	14198	12 53 50.09	-60 24 39.22	16.96	1.90	0.64
797		12 54 17.05	-60 24 19.88	15.40	1.84	0.75
798	14622	12 53 49.24	-60 24 42.14	16.41	0.85	0.39
799		12 53 44.87	-60 24 45.53	15.26	1.75	0.73
800		12 53 38.01	-60 24 50.20	14.23	0.21	0.32
801		12 53 31.32	-60 24 56.47	16.22	0.34	0.30
802	17583	12 53 25.38	-60 25 0.90	16.39	1.59	0.56
803	10893	12 53 51.23	-60 24 41.33	16.28	0.29	0.28
804		12 53 41.32	-60 24 48.65	12.90	0.30	0.28
805		12 53 23.12	-60 25 4.37	14.37	1.14	0.43
806	5245	12 53 17.66	-60 25 8.39	15.85	0.45	0.32
807		12 52 58.97	-60 25 23.61	14.71	0.22	0.26
808	10739	12 54 12.16	-60 24 25.41	15.51	0.29	0.22
809	10763	12 53 56.42	-60 24 39.15	15.90	0.39	0.25
810	20267	12 53 43.76	-60 24 48.62	17.83	0.84	0.40
811		12 53 32.73	-60 24 57.98	16.56	0.84	0.42
812		12 53 13.83	-60 25 12.33	18.89	1.62	0.56
813		12 52 56.27	-60 25 23.63	16.89	1.62	0.43
814	3116	12 54 4.36	-60 24 33.03	14.65	0.36	0.33
815	12013	12 53 58.59	-60 24 38.57	16.44	0.84	0.46
816		12 53 27.07	-60 25 3.83	16.20	0.58	0.38
817	14834	12 53 53.55	-60 24 44.69	17.68	0.68	0.33
818		12 53 47.21	-60 24 49.15	14.74	0.35	0.25
819		12 53 38.10	-60 24 56.90	15.05	1.07	0.47
820	5085	12 53 35.00	-60 24 59.51	16.54	1.64	0.78
821		12 53 23.23	-60 25 9.48	14.88	1.58	0.63
822	10533	12 53 2.43	-60 25 25.51	15.61	0.61	0.30
823		12 53 36.12	-60 25 0.39	15.39	0.36	0.27

Jcu Star #	Webda Db #	RA	Dec	Rmag	Std Dev	15ptStd Dev
824		12 53 0.48	-60 25 28.47	17.42	0.82	0.33
825	12222	12 53 46.17	-60 24 54.27	15.64	1.07	0.47
826		12 53 42.54	-60 24 56.72	16.24	0.34	0.29
827		12 53 48.08	-60 24 54.63	15.77	1.39	0.69
828		12 53 40.40	-60 24 59.41	16.14	0.29	0.25
829	15762	12 53 16.99	-60 25 19.63	14.58	0.47	0.26
830		12 53 1.23	-60 25 31.45	17.40	0.89	0.32
831	3209	12 54 17.35	-60 24 31.35	14.56	0.55	0.33
832		12 53 30.45	-60 25 9.74	17.21	0.88	0.31
833		12 53 16.79	-60 25 20.06	14.51	0.43	0.27
834	12383	12 53 9.77	-60 25 26.03	13.98	0.79	0.30
835	12562	12 54 12.99	-60 24 37.22	14.26	1.79	0.82
836		12 53 2.96	-60 25 32.90	15.08	0.39	0.25
837		12 53 0.20	-60 25 34.50	17.11	0.57	0.26
838	10468	12 53 58.49	-60 24 50.08	12.84	1.34	0.81
839	11345	12 53 55.95	-60 24 52.65	11.36	1.69	1.14
840		12 53 45.33	-60 25 0.33	15.16	0.39	0.29
841	11748	12 54 0.26	-60 24 49.09	13.03	0.39	0.29
842	10977	12 54 7.09	-60 24 45.57	16.06	0.35	0.26
843	3115	12 54 4.17	-60 24 47.85	14.88	0.16	0.22
844	13188	12 53 54.22	-60 24 54.42	15.21	1.67	0.86
845		12 53 42.47	-60 25 6.46	16.08	0.66	0.37
846		12 52 58.48	-60 25 40.68	16.52	1.25	0.47
847		12 52 56.79	-60 25 43.19	16.10	0.61	0.25
848	10790	12 54 6.52	-60 24 47.62	16.07	0.20	0.26
849	20738	12 53 47.01	-60 25 3.73	15.03	0.44	0.27
850		12 53 3.01	-60 25 38.53	15.28	0.55	0.30
851	11379	12 54 13.36	-60 24 43.82	16.74	0.36	0.29
852		12 53 36.98	-60 25 12.31	15.82	0.43	0.38
853		12 53 13.67	-60 25 32.82	16.19	0.47	0.32
854		12 53 19.42	-60 25 29.60	15.44	0.22	0.26
855		12 53 47.83	-60 25 8.33	14.57	0.43	0.28
856	16950	12 53 5.64	-60 25 41.86	17.07	1.26	0.39
857		12 52 58.08	-60 25 48.17	15.64	0.17	0.14
858		12 53 40.67	-60 25 15.70	16.57	0.88	0.34
859	14423	12 53 33.70	-60 25 20.74	16.49	0.39	0.26
860	11118	12 53 17.77	-60 25 33.19	16.14	0.43	0.25
861	16177	12 54 6.89	-60 24 55.94	16.29	1.12	0.42
862	17156	12 53 23.77	-60 25 30.30	16.14	1.47	0.58
863		12 53 1.75	-60 25 47.74	16.37	0.47	0.25
864	13753	12 52 57.58	-60 25 50.39	15.63	0.22	0.20
865		12 52 56.62	-60 25 52.21	15.87	0.66	0.31
866	12021	12 54 8.97	-60 24 56.77	17.99	1.11	0.45
867	3114	12 54 1.85	-60 25 0.95	12.56	0.16	0.27

Jcu Star #	Webda Db #	RA	Dec	Rmag	Std Dev	15ptStd Dev
868		12 53 56.02	-60 25 5.16	10.39	0.42	0.29
869		12 53 42.57	-60 25 16.66	14.03	0.27	0.30
870		12 53 25.91	-60 25 29.40	15.83	0.31	0.31
871		12 53 16.78	-60 25 36.65	16.57	1.42	0.53
872	328	12 54 12.32	-60 24 54.41	14.21	0.36	0.29
873		12 53 18.12	-60 25 37.19	16.54	0.43	0.30
874	10314	12 53 58.70	-60 25 5.82	10.66	0.51	0.32
875	11149	12 54 14.33	-60 24 54.42	16.43	0.80	0.34
876	10810	12 54 6.27	-60 25 1.43	15.72	0.42	0.31
877		12 53 59.62	-60 25 6.25	10.90	1.36	0.59
878	15858	12 53 35.47	-60 25 25.50	13.92	1.50	0.54
879		12 53 21.73	-60 25 36.74	14.83	1.59	0.59
880		12 53 13.62	-60 25 43.79	15.34	1.67	0.61
881		12 54 18.52	-60 24 51.27	17.85	1.65	0.54
882		12 52 57.85	-60 25 55.32	16.08	1.40	0.44
883		12 53 50.51	-60 25 16.45	14.51	0.18	0.27
884	11668	12 54 14.92	-60 24 58.46	16.43	0.95	0.44
885		12 53 56.13	-60 25 13.21	10.26	0.61	0.34
886		12 53 51.92	-60 25 16.19	15.18	0.34	0.26
887		12 53 28.35	-60 25 35.39	15.11	0.74	0.35
888	15236	12 53 23.26	-60 25 39.15	15.10	0.24	0.26
889	11561	12 54 5.00	-60 25 8.16	16.46	1.01	0.37
890	15899	12 53 12.50	-60 25 48.82	14.93	0.41	0.33
891		12 53 30.80	-60 25 36.33	16.11	0.33	0.26
892		12 53 29.26	-60 25 36.49	15.02	0.46	0.35
893		12 54 12.60	-60 25 4.65	15.10	0.88	0.44
894		12 53 57.39	-60 25 15.97	13.95	0.31	0.34
895		12 53 25.17	-60 25 42.45	16.38	1.70	0.65
896	16371	12 53 20.88	-60 25 43.91	13.74	0.17	0.26
897		12 53 9.21	-60 25 54.54	12.50	1.69	1.01
898		12 53 55.07	-60 25 19.35	15.05	0.32	0.32
899		12 53 38.59	-60 25 32.38	13.96	1.55	0.60
900		12 53 15.60	-60 25 49.67	15.34	0.86	0.32
901		12 53 1.24	-60 26 1.96	17.50	1.21	0.36
902		12 53 0.12	-60 26 3.09	16.03	0.42	0.24
903		12 52 56.96	-60 26 4.99	18.35	1.61	0.52
904		12 53 42.56	-60 25 32.43	15.92	0.65	0.29
905		12 53 29.06	-60 25 43.24	15.77	1.11	0.46
906	14256	12 53 1.81	-60 26 5.50	17.86	1.38	0.44
907		12 53 0.03	-60 26 7.42	16.02	0.45	0.26
908	12863	12 54 0.67	-60 25 20.33	14.65	0.26	0.33
909		12 53 35.78	-60 25 40.20	13.93	1.42	0.61
910		12 53 53.73	-60 25 27.54	15.45	0.28	0.30
911		12 53 50.33	-60 25 30.92	15.89	0.43	0.33

Jcu Star #	Webda Db #	RA	Dec	Rmag	Std Dev	15ptStd Dev
912		12 53 32.72	-60 25 44.37	14.61	0.32	0.29
913		12 52 59.45	-60 26 11.03	16.23	0.88	0.37
914	10274	12 54 15.72	-60 25 11.47	13.92	0.22	0.23
915		12 53 47.58	-60 25 33.80	13.24	0.31	0.28
916	12857	12 53 33.44	-60 25 45.38	14.19	0.20	0.20
917	11575	12 53 35.22	-60 25 43.61	16.90	0.75	0.38
918		12 53 57.81	-60 25 28.47	12.95	0.30	0.23
919		12 53 47.25	-60 25 36.73	14.54	1.29	0.69
920		12 53 26.66	-60 25 52.14	15.15	0.30	0.30
921		12 53 16.42	-60 26 1.00	14.86	1.33	0.55
922		12 53 59.58	-60 25 28.18	12.95	1.12	0.57
923	10662	12 53 8.66	-60 26 8.72	11.98	1.42	0.85
924		12 53 58.47	-60 25 30.70	12.87	0.30	0.34
925		12 53 29.11	-60 25 54.05	15.36	0.23	0.28
926		12 53 17.79	-60 26 2.80	16.80	0.66	0.31
927		12 53 9.50	-60 26 8.43	11.35	0.55	0.34
928		12 53 35.50	-60 25 50.01	17.01	1.55	0.54
929	12302	12 53 23.78	-60 25 58.22	17.61	1.07	0.39
930	3211	12 54 7.68	-60 25 25.34	14.24	0.14	0.19
931		12 53 45.46	-60 25 44.21	16.87	0.62	0.35
932		12 53 29.94	-60 25 56.10	16.01	0.59	0.32
933		12 52 59.29	-60 26 20.07	16.73	0.84	0.29
934		12 53 50.89	-60 25 42.54	14.80	0.29	0.28
935		12 53 49.68	-60 25 43.02	16.05	0.27	0.28
936		12 53 34.80	-60 25 54.78	15.96	0.21	0.27
937		12 53 30.63	-60 25 58.13	15.34	0.49	0.27
938		12 53 8.81	-60 26 16.20	14.90	0.22	0.23
939		12 52 57.59	-60 26 24.00	17.77	1.37	0.46
940		12 53 55.25	-60 25 39.80	14.61	0.64	0.31
941	12602	12 53 41.60	-60 25 50.96	15.94	0.38	0.31
942		12 54 2.97	-60 25 35.46	13.39	0.91	0.60
943		12 53 59.75	-60 25 38.15	12.63	0.36	0.36
944		12 53 19.57	-60 26 11.10	15.09	0.64	0.32
945		12 53 17.47	-60 26 12.12	12.70	0.66	0.30
946	11360	12 52 58.63	-60 26 28.14	16.83	0.78	0.29
947		12 53 52.24	-60 25 46.10	17.64	1.90	0.65
948		12 53 44.28	-60 25 56.14	17.84	0.75	0.32
949	15486	12 53 23.57	-60 26 9.70	18.15	1.21	0.45
950	3213	12 54 19.31	-60 25 27.31	14.05	0.18	0.27
951	12462	12 54 16.71	-60 25 28.53	17.33	0.62	0.23
952	11496	12 53 57.67	-60 25 42.67	13.35	1.37	0.50
953		12 53 58.76	-60 25 44.54	12.83	1.36	0.81
954		12 53 46.16	-60 25 54.93	17.73	1.27	0.45
955	23132	12 53 7.38	-60 26 26.69	15.84	0.36	0.25

Jcu Star #	Webda Db #	RA	Dec	Rmag	Std Dev	15ptStd Dev
956		12 54 18.09	-60 25 33.59	15.16	1.40	0.50
957		12 53 51.20	-60 25 53.31	17.08	1.77	0.72
958		12 53 47.32	-60 25 54.09	17.58	0.66	0.34
959	14026	12 53 45.53	-60 25 57.84	17.27	0.94	0.44
960		12 53 20.91	-60 26 17.18	15.05	0.61	0.29
961		12 53 31.47	-60 26 10.48	15.19	0.64	0.37
962	14454	12 53 5.79	-60 26 30.28	14.38	0.21	0.25
963		12 53 36.19	-60 26 8.84	16.62	0.48	0.28
964		12 53 9.71	-60 26 29.66	16.29	0.53	0.24
965		12 53 36.65	-60 26 8.77	16.26	1.03	0.49
966		12 53 18.42	-60 26 23.38	14.24	1.62	0.64
967		12 52 59.04	-60 26 38.55	15.99	0.25	0.18
968	16634	12 53 15.12	-60 26 27.12	15.94	0.94	0.39
969		12 53 7.12	-60 26 34.12	15.56	0.39	0.27
970		12 52 57.52	-60 26 41.14	17.31	1.12	0.40
971		12 54 6.89	-60 25 47.50	16.64	0.38	0.25
972		12 53 56.11	-60 25 55.53	14.31	1.56	0.60
973		12 53 48.90	-60 26 2.07	17.70	0.82	0.31
974	13250	12 53 7.89	-60 26 33.66	15.29	0.29	0.23
975	10788	12 54 16.92	-60 25 40.23	15.90	0.26	0.16
976		12 53 35.24	-60 26 13.67	16.73	1.02	0.41
977		12 54 12.25	-60 25 46.74	14.29	0.24	0.26
978		12 53 55.48	-60 26 0.21	14.49	0.42	0.30
979		12 54 15.67	-60 25 45.63	14.33	0.10	0.24
980		12 53 32.31	-60 26 20.49	14.99	0.85	0.47
981		12 53 13.51	-60 26 35.01	17.61	1.44	0.49
982		12 54 0.01	-60 25 58.83	16.70	0.65	0.30
983	13514	12 53 17.97	-60 26 33.25	17.13	0.72	0.33
984		12 53 7.08	-60 26 41.14	16.39	1.69	0.57
985	12940	12 53 46.69	-60 26 8.10	17.30	1.43	0.47
986		12 53 16.82	-60 26 35.95	17.69	1.30	0.45
987	12772	12 53 16.09	-60 26 37.14	17.77	1.14	0.41
988	12137	12 54 7.87	-60 25 57.05	17.20	0.56	0.28
989		12 54 6.55	-60 25 58.30	17.07	0.56	0.28
990	11917	12 54 3.41	-60 26 0.82	15.54	0.65	0.36
991	17651	12 53 42.48	-60 26 16.72	15.64	0.42	0.28
992	11920	12 54 11.95	-60 25 54.11	14.67	0.19	0.19
993		12 53 54.86	-60 26 8.15	14.69	0.54	0.40
994		12 53 44.49	-60 26 16.05	16.24	0.57	0.33

Table D.2 Results of fainter stars of the cluster NGC 4755

Appendix E

Summary of PSD graphs
- Stars suspected as variables

JCU star #	Arp Star #	B	V	R calc	Appx Spectral type	Peaks @Freq 1/days	Comments
155	1207	15.50	14.58	15.91	K2	19,31,42	FFP=0.09 days
121	11714	17.18	16.01	16.68	K5	23,33,45	FFP=0.09 days
12	15636	19.38	16.99	17.37	M8+	23,42,52,62	FFP=0.09 days

Table E.1 Summary of the frequencies in PSD graphs, possible variable stars

Note: FFP-Fundamental frequency period

Star No.	Name	Period (in Days)	Spec. Type
1	BS Cru	0.275	B0.5V
2	BT Cru	0.133	B2:V
3	BU Cru		B1.5Ib
4	BV Cru	0.16	B0.5III(n)
5	BW Cru	0.203	B2III
6	CC Cru		
7	CN Cru		
8	CQ Cru		
9	CR Cru		
10	CS Cru		
11	CT Cru		B
12	CU Cru		
13	CV Cru		B
14	CW Cru		B
15	CX Cru		B
16	CY Cru		B
17	CZ Cru		B
18	DS Cru		
20	DU Cru		
21	EI Cru		
22	EH Cru		
23	EG Cru		
24	EE Cru		

Table E.2 Summary of the frequencies of the known variable stars

Appendix F

Wavelets - Approximate calculations for finding the level of decomposition

These calculations are based on Figure 3.1. Assuming cadence as T seconds, the given light curve has a bandwidth of W (in Hz), where W = 1/T.

In level 1, approximate signal has a bandwidth of W/2 and detailed signal has a bandwidth of W/2.

Similarly,

Level	Bandwidth of Approximate and Detailed signals	Bandwidth range of Approximate Signal	Bandwidth range of Detailed Signal	If T = 30 seconds, minimum orbital time of the approximate signal in seconds
1	W/2	0 - W/2	W/2 - W	2 * 30
2	W/4	0 - W/4	W/4 - W/2	4 * 30
3	W/8	0 - W/8	W/8 - W/4	8 * 30
4	W/16	0 - W/16	W/16 - W/8	16 * 30
5	W/32	0 - W/32	W/32 - W/16	32 * 30
6	W/64	0 - W/64	W/64 - W/32	64 * 30
7	W/128	0 - W/128	W/128 - W/64	128 * 30
n	$W/2^n$	$0 - W/2^n$	$W/2^n - W/2^{n-1}$	$2^n *30$

Table F.1 Summary of the of frequency and time relations of sub-band coding.

Appendix G

Statistical averages of Noise

Assuming ideal white noise conditions,

Number of data points used for the average	Noise reduced by
2	1.414
4	2
8	2.828
16	4
32	5

Table G.1 Statistical averages of noise

Appendix H

MATLAB default setting and routines for calculations

MATLAB wavelet toolbox functions were used for FWTs

1. wavedec

[C,L] = wavedec(X,N,'wname') returns the wavelet decomposition of the signal X at level N, using 'wname' the wavelet. N must be a strictly positive integer. The output decomposition structure contains the wavelet decomposition vector C and the bookkeeping vector L.

2. wrcoef

X = wrcoef('type',C,L,'wname',N) computes the vector of reconstructed coefficients, based on the wavelet decomposition structure [C,L, at level N. 'wname' is a string containing the wavelet name.

Argument 'type' determines whether approximation ('type' = 'a') or detail ('type' = 'd') coefficients are reconstructed. When 'type' = 'a', N is allowed to be 0; otherwise, a strictly positive number N is required. Level N must be an integer such that N length (L)-2.

3. wden

[XD,CXD,LXD] = wden(X,TPTR,SORH,SCAL,N,'wname') returns a de-noised version XD of input signal X obtained by thresholding the wavelet coefficients. This performs an automatic de-noising process of a one-dimensional signal using wavelets.

Additional output arguments [CXD,LXD] are the wavelet decomposition structure of the de-noised signal XD.

TPTR string contains the threshold selection rule:

'rigrsure' uses the principle of Stein's Unbiased Risk.

'heursure' is an heuristic variant of the first option.

'sqtwolog' for universal threshold

'minimaxi' for minimax thresholding

SORH ('s' or 'h') is for soft or hard thresholding

SCAL defines multiplicative threshold rescaling:

'one' for no rescaling

'sln' for rescaling using a single estimation of level noise based on first-level coefficients
'mln' for rescaling done using level-dependent estimation of level noise
Wavelet decomposition is performed at level N and 'wname' is a string containing the name of the desired orthogonal wavelet.

General functions used:

4. detrend

MATLAB detrend computes the least-squares fit of a straight line (or composite line for piecewise linear trends) to the data and subtracts the resulting function from the data. It removes the mean value or linear trend from a vector or matrix, usually for FFT. y = detrend(x) removes the best straight-line fit from vector x and returns it in y. If x is a matrix, detrend removes the trend from each column.

5. polyfit

P = polyfit(X,Y,N) finds the coefficients of a polynomial P(x) of degree that fits the data Y best in a least square sense. P is a row vector of length N+1 containing the polynomial coefficients in descending powers, $P(1)*X^N + P(2)X^{(N-1)}) + \ldots + P(N)*X + P(N+1)$

6. polyval

Y=polyval(P,X) returns the value of a polynomial P evaluated at X. P is a vector of length N+1 whose elements are the coefficients of the polynomial in descending order.
$Y = P(1)*X^N + P(2)X^{(N-1)}) + \ldots + P(N)*X + P(N+1)$

7. lomb

[f,P,prob] = lomb(t,h,ofac,hifac)

LOMB (T,H,OFAC,HIFAC) computes the Lomb normalized periodogram (spectral power as a function of frequency) of a sequence of N data points H, sampled at times T, which are not necessarily evenly spaced. T and H must be vectors of equal size. The routine will calculate the spectral power for an increasing sequence of frequencies (in reciprocal units of the time array T) up to HIFAC times the average Nyquist frequency, with an oversampling factor of OFAC (typically >= 4).

The returned values are arrays of frequencies considered (f), the associated spectral power (P) and estimated significance of the power values (probability). Note: the significance returned is the false alarm probability of the null hypothesis, i.e. that the data is composed of independent Gaussian random variables. Low probability values indicate a high degree of significance in the associated periodic signal.

Although this implementation is based on that described in Press et al. Numerical Recipes In C, section 13.8, rather than using trigonometric recurrences, this takes advantage of MATALB's array operators to calculate the exact spectral power as defined in equation 13.8.4 on page 577. This may cause memory issues for large data sets and frequency ranges.
Written by Dmitry Savransky 21 May 2008

Appendix I

Notch filter description

This filter is based on the pages of "Cookbook formulae for audio EQ biquad filter coefficients" by Roberts Bristow-Johnson listed in cookbook webpage[31].

By Robert Bristow-Johnson <rbj@audioimagination.com>.

All filter transfer functions were derived from analogue prototypes (that are shown next for each EQ filter type) and had been digitized using the Bilinear Transform. BLT frequency warping has been taken into account for both significant frequency relocation (this is the normal "prewarping" that is necessary when using the BLT) and for bandwidth readjustment.

First, given a biquad transfer function defined as:

```
           b0 + b1*z^-1 + b2*z^-2
H(z) = -------------------------------
           a0 + a1*z^-1 + a2*z^-2
```

This shows 6 coefficients instead of 5 so, depending on your architecture, you will likely normalize a0 to be 1 and perhaps also b0 to 1 (and collect that into an overall gain coefficient). Then your transfer function would look like:

The most straight forward implementation would be the "Direct Form 1"

```
y[n] = (b0/a0)*x[n] + (b1/a0)*x[n-1] + (b2/a0)*x[n-2]
              - (a1/a0)*y[n-1] - (a2/a0)*y[n-2]
```

Begin with these user defined parameters:

Fs - The sampling frequency

f0 - Centre Frequency or Corner Frequency, or shelf midpoint frequency, depending on which filter type.

dBgain - Used only for peaking and shelving filters

Q - The EE kind of definition, except for peaking EQ in which A*Q is the classic EE Q. That adjustment in definition was made so that a boost of N dB followed by a cut of N dB for identical Q and f0/Fs results in a precisely flat unity gain filter or "wire".

[31] http://musicdsp.org/files/Audio-EQ-Cookbook.txt

BW- The bandwidth in octaves (between -3 dB frequencies for BPF and notch or between midpoint (dBgain/2) gain frequencies for peaking EQ

S- A "shelf slope" parameter (for shelving EQ only). When S = 1, the shelf slope is as steep as it can be and remain monotonically increasing or decreasing gain with frequency. The shelf slope, in dB/octave, remains proportional to S for all other values for a fixed f0/Fs and dBgain.

Then compute a few intermediate variables:

A = sqrt(10^(dBgain/20))

= 10^(dBgain/40) (for peaking and shelving EQ filters only)

w0 = 2*pi*f0/Fs

alpha = sin(w0)/(2*Q) (case: Q)

= sin(w0)*sinh(ln(2)/2 * BW * w0/sin(w0)) (case: BW)

= sin(w0)/2 * sqrt((A + 1/A)*(1/S - 1) + 2) (case: S)

The relationship between bandwidth and Q is

1/Q = 2*sinh(ln(2)/2*BW*w0/sin(w0)) (digital filter w BLT)

or 1/Q = 2*sinh(ln(2)/2*BW) (analogue filter prototype)

The relationship between shelf slope and Q is

1/Q = sqrt((A + 1/A)*(1/S - 1) + 2)

2*sqrt(A)*alpha = sin(w0) * sqrt((A^2 + 1)*(1/S - 1) + 2*A)

is a handy intermediate variable for shelving EQ filters.

Finally, compute the coefficients for whichever filter type you want:

(The analogue prototypes, H(s), are shown for each filter (type for normalized frequency.)

Notch: H(s) = (s^2 + 1) / (s^2 + s/Q + 1)

b0 = 1

b1 = -2*cos(w0)

b2 = 1

a0 = 1 + alpha

a1 = -2*cos(w0)

a2 = 1 - alpha

As transfer function is known it can be used directly in MALTAB.

Appendix J

Kepler 4b light curve (relative flux based) has very high SNR (over 100) and transit is clearly visible. When magnitudes are taken (log scale) , it gives SNR of 4.55, which is still a high SNR for transit search. Practically, there is no need to do any de-noising for Kepler 4b. However, Kepler 32b and 70b have lower SNR and transit is not clear. Kepler data had a 30 minutes cadence while simulations had 30 seconds. That means, Kepler represents a typical 3 hour transit by just 6 data points.

ESP parameters	Kepler 4b	Kepler 32b	Kepler 70b
Orbital Period	3.21346 days	5.9012 days	0.2401 days
Orbital Inclination	89.76	87.660	~65
Metallcity [Fe/H]	+0.17	-0.01	-
Mass M_p (M_j)	1.223	0.54	0.496
Radius R_p (R_j)	1.487	0.53	0.203

Table J.1 Characteristics of known Kepler ESPs

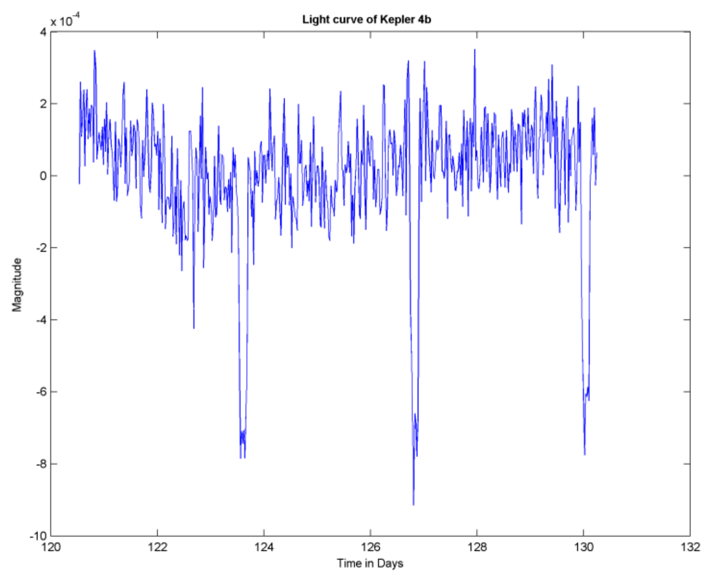

Figure J.1 Light curve of Kepler 4b (From MJD 54833+)

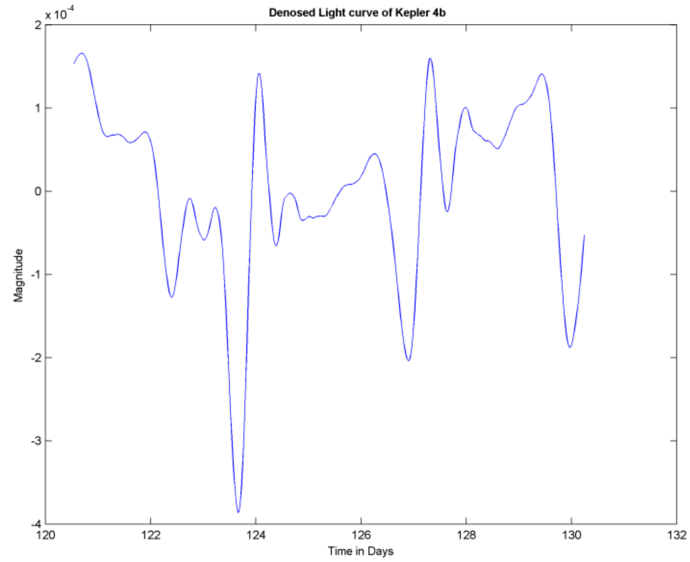

Figure J.2 De-noised Light curve of Kepler 4b

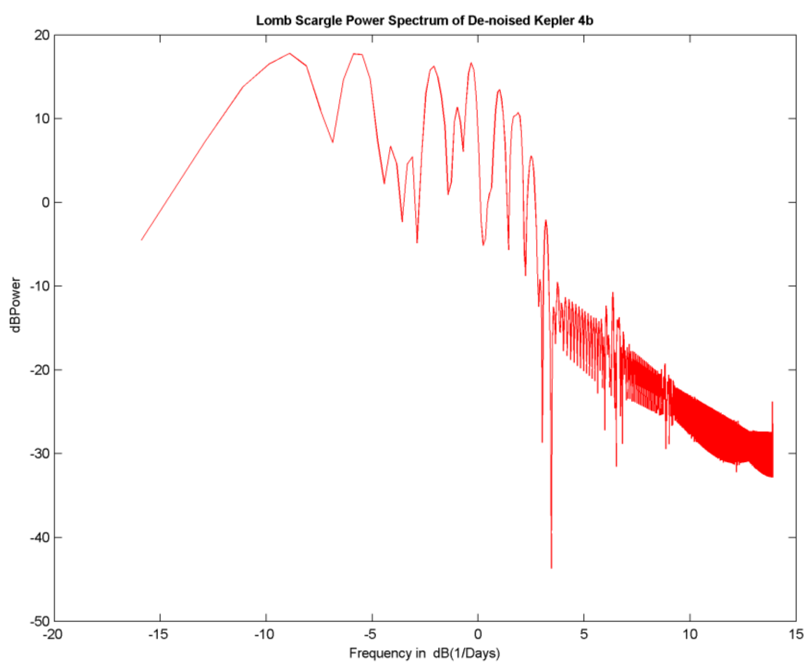

Figure J.3 Lomb Scargle Periodogram of Kepler 4b

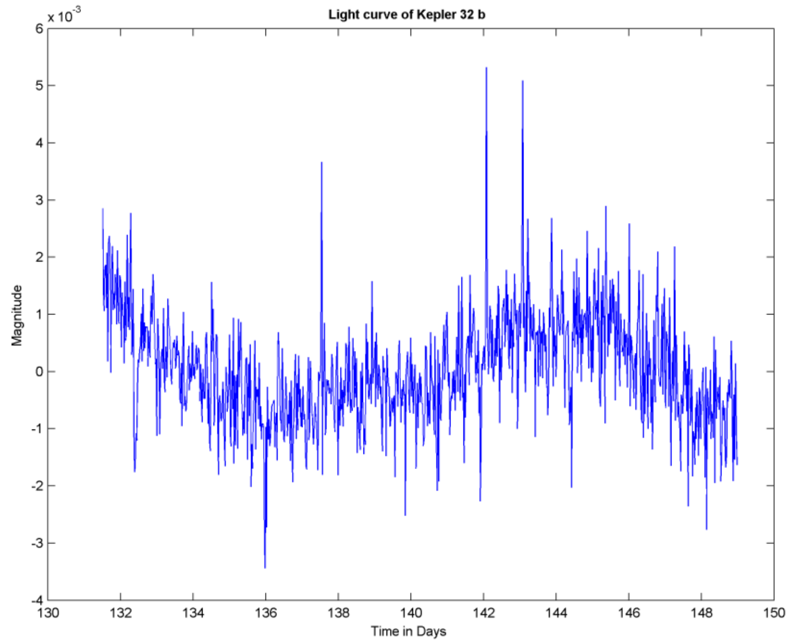

Figure J.4 Light curve of Kepler 32b (From MJD 54834+)

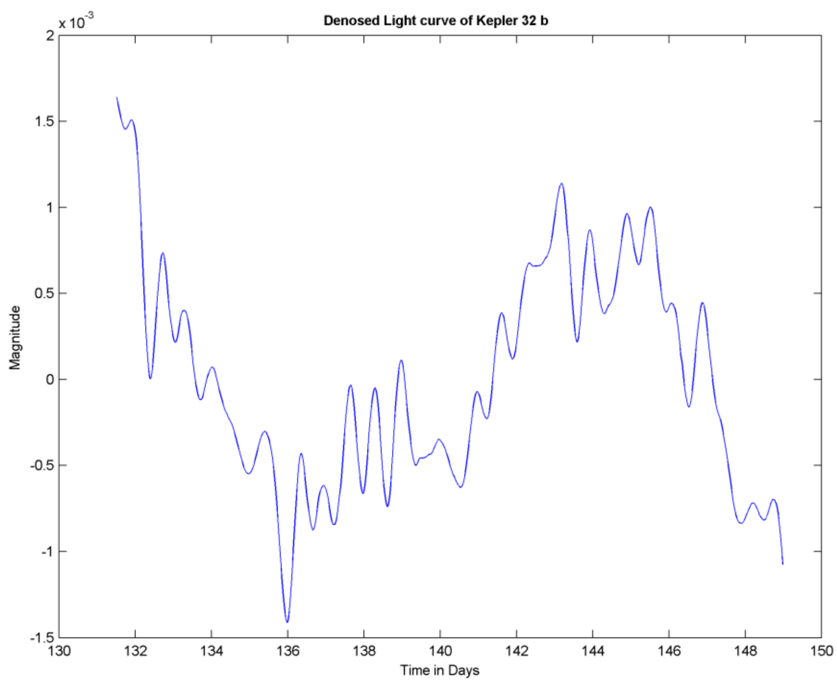

Figure J.5 De-noised Light curve of Kepler 32b

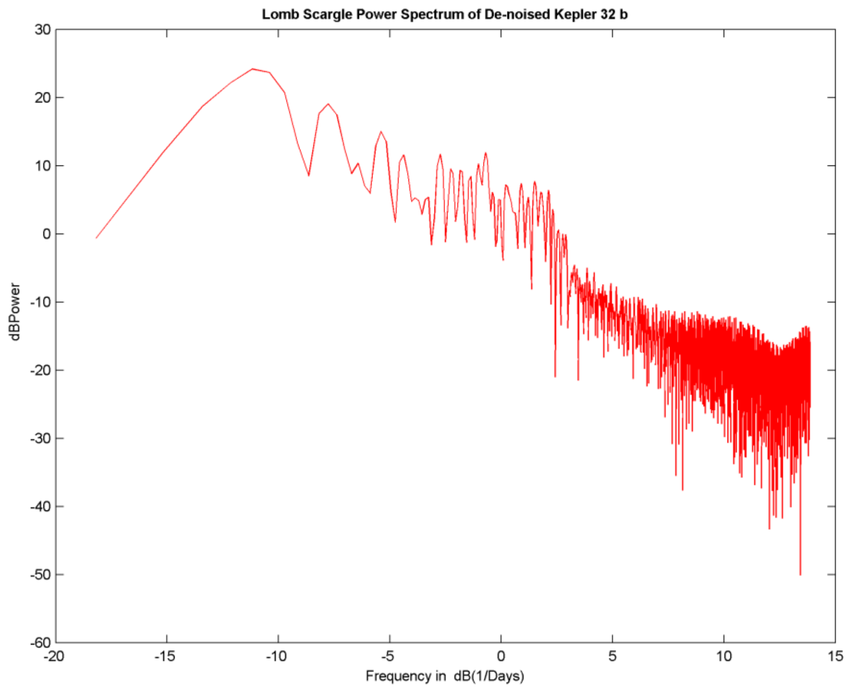

Figure J.6 Lomb Scargle Periodogram of Kepler 32b

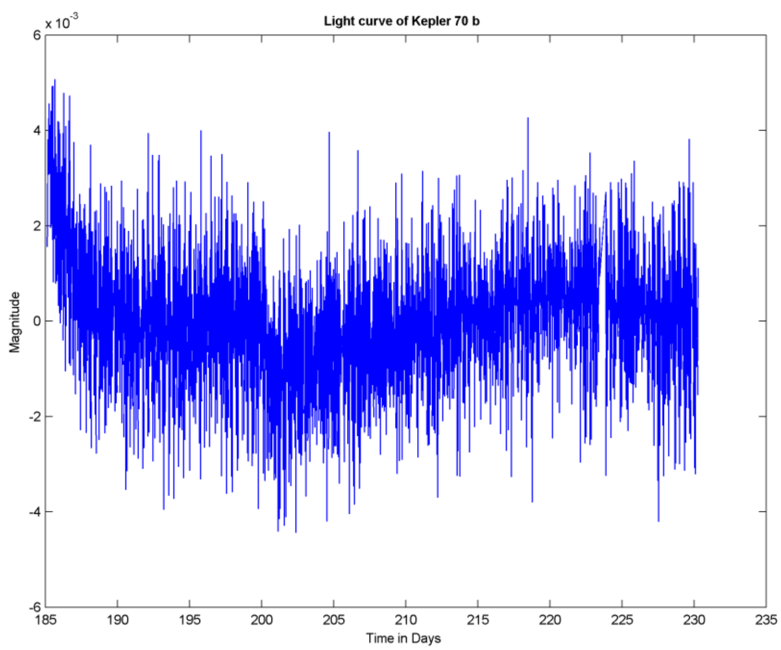

Figure J.7 Light curve of Kepler 70b (from MJD 55832+)

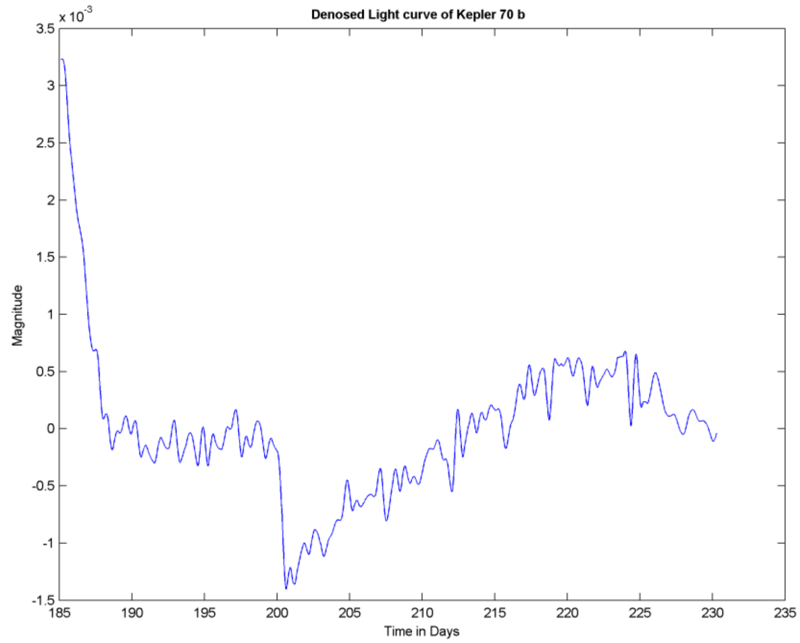

Figure J.8 De-noised Light curve of Kepler 70b

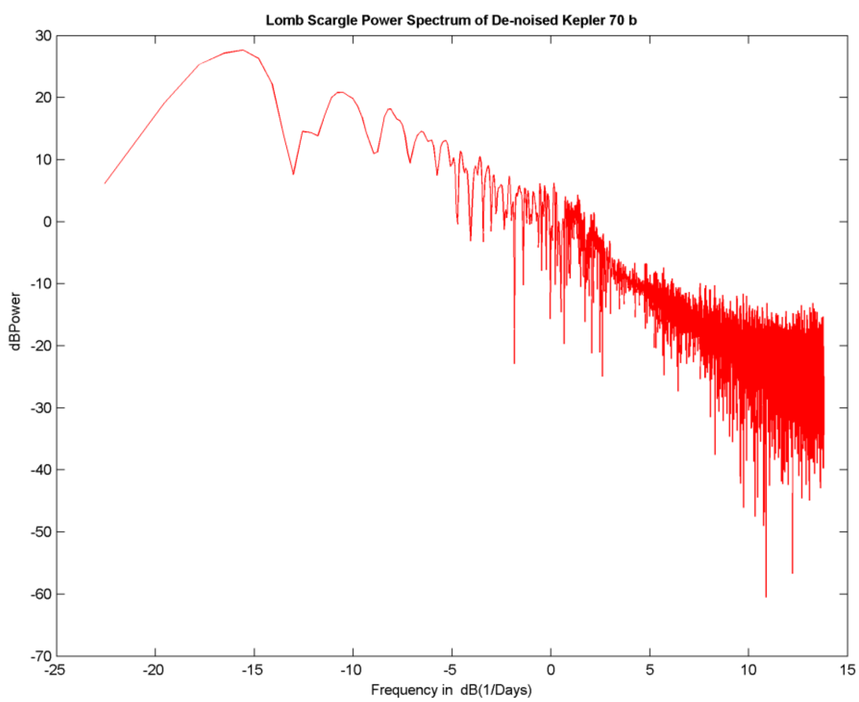

Figure J.9 Lomb Scargle Periodogram of Kepler 70b

	Kepler 4b	Kepler 32b	Kepler 70b
Orbital Period (De-noised with LS method)	3.41 (1st Har)	6.1 (2^{nd} Har)	
Standard Deviation (Original)	$1.879 * 10^{-4}$	$9.704*10^{-4}$	0.0016
Standard Deviation (De-noised)	$1.054 * 10^{-4}$	$6.254*10^{-4}$	$6.545*10^{-4}$
SNR (in Magnitudes)	4.55	3.4	2.75

Table J.2 Comparison of results with published values of ESPs

Kepler data has very high flux level anomalies, sampling rate is sixty times lesser than the simulations; hence there are not enough samples between successive transits to put into de-noising. A big transit depth (e.g. Kepler 4b) pushes denoising to its limits. There are no flat baseline segments for Kepler 32b and 70b to put into de-noising algorithm. Due to these anomalies, these light curves cannot be denoised successfully as a full unit; however it still can be denoised as segments. As the sampling rate is lesser (once in every 30 minutes) the number of levels in de-noising have to be reduced from 7 to 4 to match the sampling rate (Appendix F) to give reasonable denoised curve. Denoising, still gives good results for Kepler 4b and Kepler 32b. Kepler 32b and Kepler 70b de-noising curves show many transits like signatures and LS periodogram shows many possible frequencies (and harmonics), with one of them being the one for the transiting planet "b". These could be real transits (the fundamental) or aliased of a real. The 3^{rd} harmonic of Kepler 32 (3.1 days) seems to be Kepler 32e (with 2.89 days orbital time) and its 1^{st} harmonic gives the signal for 12 days orbital time, which is the half of the orbital time of Kepler 32d. Not all of those peaks in LS periodogram are smooth and this makes an error on the selection of peak points (done by eye estimation) of log frequency scale on the LS periodogram; thus making an error in calculated orbital frequency.

De-noising and LS method work well if the orbital period is in the range of many days, as there are enough samples for the calculations. For very short orbital period, e.g. Kepler 72b with 5.76 hours; even level 4 de-noising with 30 minutes cadence, 8 hours of minimum orbital period is necessary (See Appendix F). Hence, there is no fundamental peak frequency for Kepler 72b in the LS periodogram.

This validation shows the limitations of light curves used for de-noising. De-noising assumes that

1. The transit is hidden in the noise; i.e. it is not visible to the naked eye and flux based SNR is less than 3. Kepler 4b has SNR more than 100, hence definitely not for de-noising.
2. Light curves do not have huge flux level anomalies, and
3. There are sufficient data points between transits.

Kepler data does not satisfy conditions 2 and 3 and Kepler 4 doesn't satisfy condition 1. For Kepler 4b, transit is clearly visible and there is no need to think about de-noising.

Appendix K

The light curves of variable stars of published periods were checked by NASA Exoplanet Archive Periodogram Service[32]. This service uses LS and BLS methods for generated periodograms and provides x-axis in time domain instead of frequency domain. The periodograms for BSCru are given in Figures K.1 and K.2. The cyclic time of first 4 ranks of the peaks are given in Table K.1.

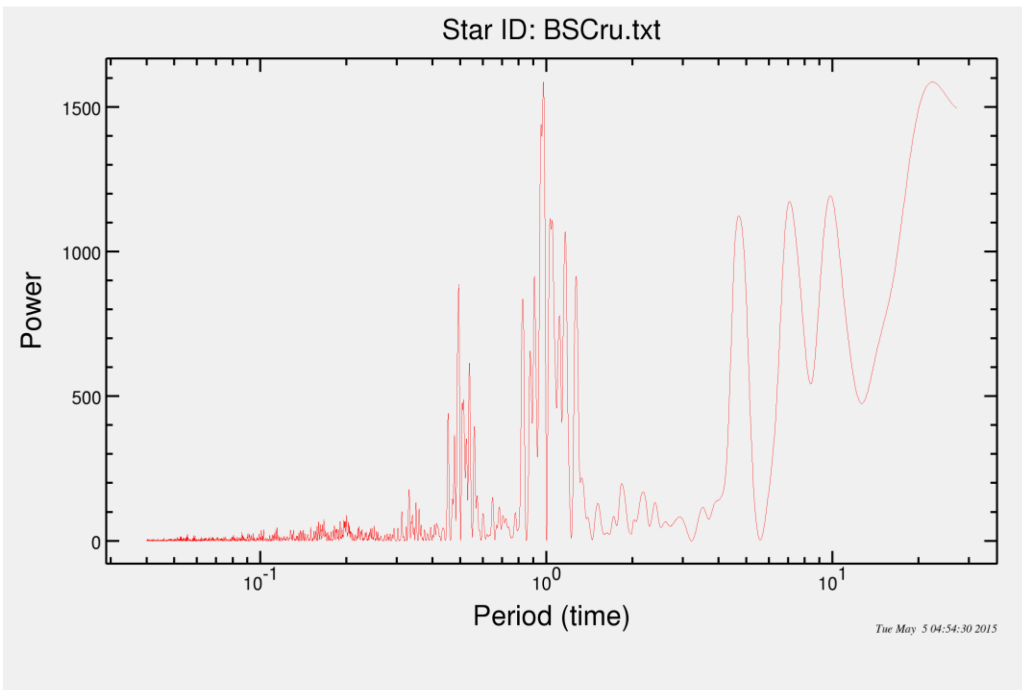

Figure K.1 Periodogram of BSCru using LS method

The values of two period grams are not matching except time over 22 days, which is obviously incorrect as it is beyond expected cyclic times. Periodograms show low frequency components contain most of the energy. In LS periodograms, all stars have a peak around 0.95 days, which could be the common noise component in all stars. For LS method, other top ranked period values are not closer to the expected. For BLS periodograms, there are peaks of cyclic times which seem to be the variable star cyclic time but there is no way to determine which one matches the actual period unless light curve shows the point of variability. On the other hand, those published values

[32] http://exoplanetarchive.ipac.caltech.edu./cgi-bin/Periodogram/nph-simpleupload

were from a search done in many decades ago, hence there is a question on the accuracy of the published cyclic times.

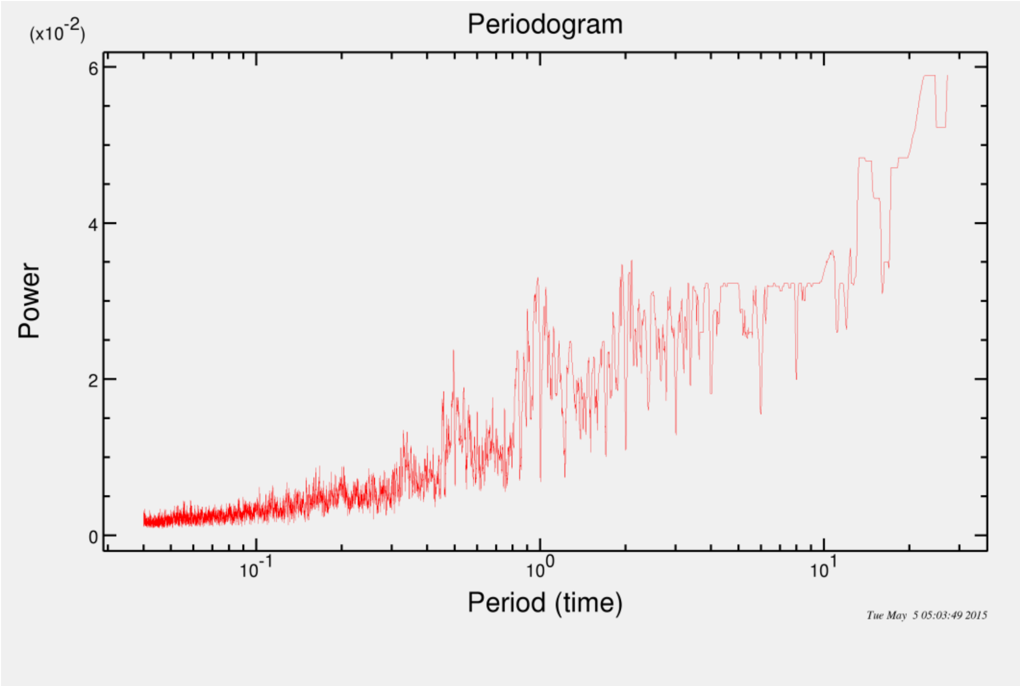

Figure K.2 Periodogram of BSCru using BLS method

Variable Star	Published Period (in Days)	Top 4 ranked periods (in Days) by LS method	Top 4 ranked periods (in Days) by BLS method
BS Cru	0.275	0.975506	24.61603
		22.48329	0.329101
		4.70429	0.399821
		1.029692	0.311523
BT Cru	0.133	22.84449	27.19427
		1.024648	0.338439/
		0.954353	0.307142
		4.80578	0.294314
BV Cru	0.16	22.6339	24.70604
		0.956049	0.338436
		1.027967	0.307365
		4.689758	0.39294
BW Cru	0.203	23.92455	24.51417
		1.026385	0.334546
		0.955401	0.249495
		1.254953	0.314053

Table K.1 Results of the Periodograms from NASA periodogram utility

Acronyms

2MASS	Two Micron All Sky Survey
AAT	Anglo-Australian Telescope
AAVSO	American Amateur Variable Star Observers
ADU	Analogue to Digital Unit
AU	Astronomical Unit
BCEP	Beta Cepheid
BLS	Box-fitting Least Squares
CCD	Charge Coupled Devices
COROT	COnvection ROtation and planetary Transits
DC	Direct Current
ESA	European Space Agency
ESP	Extra Solar planets
FT	Fourier Transform
FFT	Fast Fourier Transform
FITS	Flexible Image Transport System
FOV	Field of View
FWHM	Full Width at Half Maximum
FWT	Fast Wavelet Transform
HST	Hubble Space Telescope
IRAF	Image Reduction and Analysis Facility
LS	Lomb Scargle
LOS	Line of Sight
MC	Monte Carlo
MFA	Matched Filter Algorithm
NIR	Near Infra-Red
PSD	Power Spectral Density
PSF	Point Spread Function
RV	Radial Velocity
SD	Standard Deviation
SNR	Signal to Noise ratio
STARE	STellar Astrophysics & Research in Exo-planets

STEPSS	Survey for Transiting Extra-solar Planets in Stellar Systems
TIA	Transit Identification Algorithm
WGN	White Gaussian Noise

References

1. Abry, P., and Sellan, F., Applied and Computational Harmonic Analysis, 3(4), 377-383, (1996).
2. Aigrain, S., PhD Thesis, University of St Andrews UK (2002)
3. Aigrain, S., Favata, S., A&A 395, 625-636 (2002)
4. Aigrain, S., Irwin M., Astron Soc 350, 331-345 (2004)
5. Aigrain, S., Pont F., MNRAS 378, 741 (2007)
6. Alard, C., Lupton, R., ApJ 503,325 (1998)
7. Alonso, R., Brown, T., Torres, G., Latham, D., Sozzetti, A., Mandushev, G., Belmonte, J., Charbonneau, D., Deeg, H., Dunham, E., O'Donovan, F., Stefanik, R., ApJ 613L, 153 (2004)
8. Archinal, B., Hynes, S., Star Clusters, Willmann-Bell, Inc (2003)
9. Arp, H., Van Sant, C, Astron 63, 341-346 (1958)
10. Arzoumanian, Z., Joshi, K., Rasio, F., Thorsett, S., Proceedings of the 160th colloquium of the IAU, 105, 525 (1999).
11. Bakos, G., Shporer, A., Pál, A., Torres, G., Kovács G, Latham. D, Mazeh, T., Ofir, A., Noyes, R., Sasselov, D., Bouchy, D., Pont. F., Queloz, D., Udry, S., Esquerdo. G., Sipőcz, G., Kovács, G., Lazar, J., Papp, I., and Sári. P., ApJ 671, L173 (2007)
12. Baraffe, I., Chabrier, G., Barman, T., Allard, F., Hauschildt. P., A&A 402, 701-702 (2003)
13. Barnes, J., PASP 119(85), 986-993 (2007)
14. Bayliss, D., Sackett, P., Weldrake, D., Proc IAU 4, 333-335 (2008)
15. Bedelman, W., PASP 66, 249 (1954)
16. Bennet, D., Anderson, J., Gaudi, B., ApJ 660, 781 (2007)
17. Berta, Z., Irwin, J., Charbonneau, D., AJ, 775, Issue 2, 91 (2013)
18. Bissinger, R., Detection of Possible Anomalies in the Transit Light curves of Exoplanet TrEs-1b Using a Distributed Observer Network (2004) http://kepler.nasa.gov/ed/pdf/200410TrES-1b.pdf
19. Blank, D., Jayawardene, B., et al, For MNRAS in prep. (2015)
20. Bodenheimer, P., Laughlin, G., Lin, D., ApJ 592(1), 555-563 (2003)
21. Bonfils, X., Lo Curto, G., Correia, A., Laskar, J., Udry, S., Delfosse, X,, Forveille, T., Astudillo-Defru, N., Benz, W., Bouchy, F., Gillon, M., Hébrard, G., Lovis, C., Mayor, M., Moutou, C., Naef, D., Neves, V. Pepe, F., Perrier, C., Queloz, D., Santos, N., Ségransan, D., A&A 556, A110_1-A110_16 (2013)

22. Borucki, W., Caldwell, D., Koch, D., Webster, L., Jenkins, J., Ninkov, Z., Showen, R., PASP 113, 439-451 (2001)
23. Borucki, W., Koch, D., Basri, G., et al. ApJ 736(1), 19,22 (2011)
24. Borucki, W., Summers, A., Icarus 58, 121-134 (1984)
25. Boss, A., ApJ 503, 923 (1998)
26. Boss, A., ApJLett 536, L101 (2000)
27. Brown, T., ASP Conf Ser 219 (2000)
28. Brown, T., Charbonneau, D., 195th AAS Meeting (2000)
29. Brucalassi, A., Pasquini, L., Saglia, R., Ruiz, M., Bonifacio,P., Bedin, L., Biazzo, K., Melo, C., Lovis, C., Randich, S., A&A, 61, p. L9 (2104)
30. Bryan, M., Alsubai, K., Latham, D., Parley, N., Cameron, A., Quinn, S., Carter, J., Fulton, B., Berlind, P., Brown, W., Buchhave, L., Calkins, M., Esquerdo, G., Fűrész, G., Jørgensen, G., Horne, K., Stefanik, R., Street, R., Torres, G., West, G., Dominik, M., Harpsøe, K., Liebig, C., Novati, S., Ricci, D., Skottfelt, J., ApJ 750, 84 (2012)
31. Burke, C., Gaudi, B., DePoy, D., Pogge, R., Pinsonneault, M., AJ 127, 2382 (2004)
32. Burrows, A., Ibgui, L., Hubeny, I., ApJ 682, 1277-1282 (2008)
33. Burrows, A., Sudarsky, D., Hubbard, W., ApJ 594, 545-551 (2003)
34. Cabrera, J., Csizmadia, S., Erikson, A., Rauer, H., Kirste, S., A&A 548, 44 (2012)
35. Cabrera, J., Csizmadia, S., Montagnier, G., Fridlund, M., Ammler-von Eiff, M., Chaintreuil, S., Damiani, C., Deleuil, M., Ferraz-Mello, S., Ferrigno, A., Gandolfi, D., Guillot, T., Guenther, E., Hatzes, A., Hébrard, G., Klagyivik, P., Parviainen, H., Pasternacki, T., Pätzold, M., Sebastian, D., Tadeu dos Santos, M., Wuchterl, G., Aigrain, S., Alonso, R., Almenara, J., Armstrong, J., Auvergne, M., Baglin, A., Barge, B., Barros, S., Bonomo, A., Bordé, P., Bouchy, F., Carpano, S., Chaffey, C., Deeg, H., Díaz, R., Dvorak, R., Erikson, A., Grziwa, S., Korth, J., Lammer, H., Lindsay, C., Mazeh, T., Moutou, C., Ofir, A., Ollivier, M., Pallé E., Rauer, H., Rouan, D., Samuel, B., Santerne, A., Schneider, A., arXiv:1504.01532 (2015)
36. Carpano, S., Aigrain, S., Favata, F., A&A 401, 743-753 (2003)
37. Cassen, P., Guillot, T., Quirrenbach, A., Extra solar Planets, Saas-Fee Advanced Course 31, Berlin, Springer, (2006)
38. Castellano, T., Laughlin, G., Terry, S., Kaufmann, M., Hubert, S., Schelbert, G., Bohler, D., Rhodes, R., The Journal of the AAVSO, 33(1), 1-21 (2004)
39. Castellano, T., Laughlin, G., The discovery of Extra-solar planets by backyard astronomers, (2001), www.transitsearch.org

40. Chabrier, G., Baraffe, I., Selsis, F., Barman, T., Hennebelle, P., Alibert, Y., Protostar & Planets V, Edited by B. Reipurth & D. Jewitt, K Keil, Univ Of Arizona Press, Tucson (2006)
41. Chabrier, G., Baraffe, I., Leconte, J., Gallardo, J., Barman, T., AIP Conf Proc 1094, 102-111 (2009)
42. Charbonneau, D., Brown, D., Latham, D., Mayor, M., ApJ 529, L45-L48 (2000)
43. Charbonneau, D., Current challenges facing planet transit survey, Space Science Reviews, ISSI Workshop on Planetary Systems and Planets in Systems (2003)
44. Charbonneau, D., Winn, J., Latham, D., Bakos, G., Falco, E., Holman, M., Noyes, R., Csak, B., ApJ 636, 445 (2006)
45. Charbonneau, D., Brown, T., Burrows, A., Laughlin, G., Reipurth, B., Jewitt, D., Keil, K., (Eds.). Protostars and Planets V (701-716). University of Arizona Press (2007)
46. Chauvin, G., Lagrange, A., Dumas. C., Zuckerman, B., Mouillet, D., Song, J., Beuzit; P, A&A 425, L29 – L32 (2004)
47. Chochran, W., Hatzes, A., ApJ 483, 457-463 (1997)
48. Coifman, R., Donoho, D. L., Translation-invariant de-noising. p 125--150 of: Antoniadis, A., & Oppenheim, G. (eds), Wavelets and Statistics, Lecture Notes in Statistics 103. New-York: Springer-Verlag (1995)
49. Collier Cameron, A., Pollack, D., Street, R., Lister, T., West, R., Wilson, D., Pont, F., Christian, D., Clarkson, W., Enoch, B., Evens, A., Fitzsimmons, A., Haskell, C., Hellier, C., MNRAS 373, 799 (2006)
50. Cooley, J., Tukey, J., Mathematics of Computation, 19, 297-301 (1965)
51. Crossfield, I., Petigura, E., Schlieder, J., Howard, A., Fulton, B., Aller, K., Ciardi, D., Lepine, S., Barclay, T., de Pater, I., de Kleer, K., Quintana, E., Christiansen, J., Schlafly, E., Kaltenegger, L., Crepp, J., Henning, T., Obermeier, C., Deacon, N., Weiss, L., Isaacson, H., Hansen, B., Liu, M., Greene, T., Howell, S., Barman, T., Mordasini, C., ApJ, 804, 10 (2015)
52. Daubechies, I., IEEE Tans. Inform Theory 36, 961-1004 (1990).
53. Da Silva, R., Udry, S, Bouchy, F., Mayor, M., Moutou, C., Pont, F., Queloz, D., Santos, N., Ségransan, D., Zucker, S., A&A 446, 717-722 (2006)
54. Deeg, H., Doyle, L., Kozhevnikov, V., Martin, E., Oetiker, B., Palaiologou, E., Schneider, J., Afonso, C., Dunham, E., Jenkins, J., Ninkov, Z., Stone, R., Zakharova, P., A&A 338, 479 (1998)
55. Defay, C., Deleuil, M., Barge, P., A&A 365, 330 (2001)
56. Deleuil, M., Deeg, H., Alonso, R, Bouchy F., Rouen, D, et al, " Transiting exo-planets from the COROT space mission IV", A&A 491(3), 889-897 (2008)

57. Deming, D., Harrington, J., Laughlin, G., Seager, S., Navarro, S., Bowman, W., Horning, K., ApJ 667(2), L199-L202 (2007)
58. Donoho, D., IEEE, Trans. on Inf. Theory 41(3), 613-627 (1995).
59. Donoho, D., Johnstone, I., Kerkyacharian, G., Picard, D., Journal. Roy. Stat. Soc., series B, 57(2), 301-369 (1995).
60. Eggenberger, A., Udry, S., Maseh, T., Segal. Y., Mayaor, M., A&A 466 (3): 1179–1183 (2008)
61. Evans, C., Smartt, S., Lee, J., Lennon D., Kaufer, A., Dufton, P., Trundle, C., Herrero, A., Simon-Diaz, S., De Koter, A., Hamann, W., Hendry, M., Hunter, I., Irwin, M., Korn, A., Kudritzki, R., Langer, N., Mokeim, M., Najarro, F., Pauldrach, A., Przybilla, N., Puls, J., Ryans, R., Urbaneja, M., Venn, K., Villamariz, M., A&A 437, 467-482 (2005)
62. Fadavi, M., Verveer, A., Aymon, J., Merlin, D., Situ. K., Pennypackker, C., Biggs, J., White, G., Gould, A., Greenberg, G., Hoette, V., McCarron, K., Archer, K., Pino, F., Hibbs, M., Ford, M., Wetsch, J., Astron, Nachr, 327,811 (2006)
63. Fischer, D.A., & Valenti, J. ApJ 622, 1102 (2005)
64. Fortney, J., Sudarsky, D., Hubeny, I., Cooper, C., Hubbard, W., Burrows, A., Lunine, J., AJ, 589, 615-622 (2003)
65. Freedman, R., Kaufman, W., Universe, Freeman, New York (2002)
66. Freedman, W., Madore, B., Gibson, B., Ferrarese, L., Kelson, D., Sakai, S., Mould, J., Kennicutt, R., Jr., Ford, H., Graham, J., Huchra, J., Hughes, S., Illingworth, G., Macri, L., Stetson, P., ApJ 553(1), 47-72 (2001)
67. Fressin, F., Torres G., Charbonneau D., Bryson, S., Christiansen J., Dressing, C., Jenkins, J., Walkowicz, L., Batalha, N., ApJ 766 81 (2013)
68. Gillon, M., Deming, D., Demory, B., Lovis, C., Seager, S., Mayor, M., Pepe, F., Queloz, D., Segransan, D., Udry, S., Delmelle, S., Magain, P., A&A, 518, A25 (2010)
69. Gillon, M., Demory, B., Benneke, B., Valencia, D., Deming, D., Seager, S., Lovis, C., Mayor, M., Pepe, F., Queloz, D., Ségransan, D., Udry, S., A&A, 539, A28, 7 pp. (2012)
70. Goldreich, P., and Tremaine, S., AJ 233, 857 (1979)
71. Grillmair, C, Burrows, A., Charbonneau[3], D., Armus, L,., Stauffer, J., Meadows, V., Cleve, Jefffry Nature 456 (7223), 767-769 (2008),
72. Guillot, T., Showman, A., A&A 385, 166 (2002)
73. Harrington, R., Kallarakal, V., Dahn, C., AJ 88, 1038, 103 (1983)
74. Hartman, J., Bayliss, D., Brahm, R., Bakos, G., Mancini, L., Jordán, A., Penev, K., Rabus, M., Zhou, G., Butler, R., Espinoza, N., De Val-Borro. M., Bhatti, W., Csubry, Z., Ciceri, S.,

Henning, T., Schmidt, B., Arriagada, P., Shectman, S., Crane, J., Thompson, I., Suc, V., Csák, B., Tan, T., Noyes, R., Lázár J., Papp, I., Sári, P Astron. J., 149, 166(2015)

75. Hartman, J., Gaudi, S., Holman, N., McLeod, B., Stanek, K., Barranco, J., Pinsonneault, M., Meibom, S., Kalirai, J., ApJ 695, 336 (2009)
76. Hatzes, A., A&A, 568, A86 (2014)
77. Hebb, L., Petro, L., Ford, H., Ardial, D., Toledo, I., Minniti, D., Golimowski, D., Clampin, M, MNRAS 379, 63 (2007)
78. Holman, M., Murray N., Science 307, 1288-1291 (2005)
79. Horne, K., Hot Jupiters Galore, ASP conference series, 294 (2003)
80. Howell, S., Handbook of CCD Astronomy, 1st Edition, Cambridge University Press, UK (2000)
81. Howell, S., Everett, M., Some considerations for ultra-High precision CCD Photometry, Third Workshop on Improvements to Photometry (2000)
82. Howell, S., Everett, M., Esquerdo, G., Davis, D., Weidenschilling, S., Lew, T., Foxley, A., Photometric Search For Extra-Solar Planets ASP Conference Series no. 189, 170 (2000)
83. IEEE Signal Processing magazine, p 13-14 Volume 31, Number 4, July 2014
84. Jarret, T., Chester, T., Cutri, R., Schneider, S., Skrutskie, M., Huchra, J., AJ 119, 2498 (2000)
85. Jayawardene, B., White, G., Blank, D., Hons, A., Verveer, A., Biggs, J., Mercury, 36(2), 26-31 (2007)
86. Jenkins, J., Cullers, K., Doyle, L., Icarus 119, 244-260 (1996)
87. Jenkins, J., Caldwell, D., Borucki, W., ApJ 564. 495-507 (2002)
88. Kalas, P., Graham, J., Chiang, E., Fitzgerald, M, P., Clampin, M., Kite, E, Stapelfeldt, K, Marois, C., Krist J., Science 322, 1345 (2008)
89. Kirkpatrick, D., Reid, I., Liebert, J., Curti, R., Nelson, B., Beichman, C., Dahn, C., Monet, D., Gizis, J., Skurutskie, M., ApJ 519, 802 (1999)
90. Kirkpatrick, D., Reid, I., Liebert, J., Gizis, J., Burgasser, A., Monet, D., Dahn, C., Nelson, B., Williams, R., AJ 120, 447-472 (2000)
91. Konacki, M., Nature 436, 230-233 (2005)
92. Kovacs, G., Zucker, S., Mazeh, T., A&A 391, 369-377 (2002)
93. Kovacs, G., Bakos, G., Noyes, R., MNRAS 356, 557-567 (2005)
94. Lawler, S., Greenstreet, S., Gladman, B., ApJ, 802, L20 (2015)
95. Laughlin, G., Wolf, A., Vanmunster, T., Bodenheimer, P., Fischer, D., Marcy, G., Butler, P., Vogt, S., ApJ 621, 1072 (2004)

96. Lafreniere, D., Doyon, R., Marios, C., Nadeau, D., Oppenheimer, B., Roche, P., Rigaut, F., Graham., J., Jayawardhana, R., Johnstone, D., Kalas, P., McIntosh, B., Racine, R., ApJ 670, 1367-1390 (2007)
97. Lin, D., Papaloizou, J. MNRAS 186, 799 (1979)
98. Lister, T., West, R., Wilson, S., Collier Cameron, A., Clarkson, W., Street, R., Enoch, B., Parley, N., Christian, D., Kane, S., Evans, A., Fitzsimmons, A., Haswell, C., Hellier, C., Hodgkin, S., Horne, K., Irwin, J., Keenan, F., Norton, A., Osborne, J., Pollacco, D., Ryans, R., Skillen, I., Wheatley, P., Barnes, J., MNRAS 379(2), 647-662 (2007)
99. Loeb, A, New Astronomy, 14, 363 (2009)
100. Mallat, S., IEEE Pattern Analysis and Machine Intelligence, 11(7), 674-693 (1989)
101. Mallen-Ornelas, G., Seager, S., Yee, H., Minniti, D., Gladders, M., Mallen-Fulerton, G., Brown, T., ApJ 582, 1123-1140 (2003)
102. Mandel, K., Agol, E., ApJ 580, L171–L175 (2002)
103. Marcy, G., Butler, R., AAS Abstract 187:70.04 (1995)
104. Marcy, G., Butler, R., Fischer, D., Vogt, S., Lissauer, J., Rivera, E., ApJ 556, 296-301 (2001)
105. Marios, C., Macintosh, B., Barman, T., Zuckerman, B., Song, I., Patience, J., Lafrenière, D., Doyon, R., Science 322, 1348 (2008)
106. Marios, C., Zuckerman, B., Konopacky, McIntosh, M., Barmen, Nature, 468, 1080-1083 (2010)
107. Mayor, M., Queloz D, Mandel, K., Agol, E., Nature 378, 355 (1995)
108. Mazeh, T., Tamuz, O., Zucker, S., PASP proceedings of “Transiting Extrasolar planets workshop”, Germany (2006)
109. Meibom, S., Torres, G., Fressin, F., Latham, D., Rowe, J., Ciardi, D., Bryson, S., Rogers, L., Henze, C., Janes, K., Barnes, S., Marcy, G., Isaacson, H., Fischer, D., Howell, S., Horch, E., Jenkins, J., Schuler, S., Crepp, J., Nature, 10.1038/nature12279 (2013)
110. Mochejeska, B., Stanek, K., Sasselov, D., Szentgyorgi, A., ApJ 123, 3460 (2002)
111. Montalto, M., Piotto, G., Desidera, S., De Marchi, F., Bruntt, H., Stetson, P., Arellano Ferro, A., Momany, Y., Gratton, R., Poretti, E., Aparicio, A., Bebieri, M., Claudi, R., Grundahl, F., Rosenberg, A., A&A 470(3), 1137-1156 (2007)
112. Moutou, C., Pont, F., Barge, P., Aigrain, S., Auvergne, M., Blouin. D., Cautain, R., Erikson, A., Guis, V., Guterman, P., Irwin, M., Lanza, A., Queloz, D., Rauer, H., Voss, H., Zucker, S., A&A 437, 355-368 (2005)

113. Muirhead, P., Johnson, J., Apps, K., Carter, J., Morton, T., Fabrycky, D., Pineda, J., Bottom, M., Rojas-Ayala, B., Schlawin, E., Hamren, K., Covey, K., Crepp, J. R., Stassun, K. G., Pepper, J., Hebb, L., Kirby, E. N., Howard, A., Isaacson, H., Marcy, G., Levitan, D., Diaz-Santos, T., Armus, L., Lloyd, J., 2012, ApJ, 747, 144 (2012)

114. Neugebauer, G., Leighton, R., Two Micron Sky Survey, NASA SP-3047 (1969).

115. Palmer, J., Davenhall, A., The CCD Photometric Calibration Cookbook, Starlink Project (2001)

116. Paunzen ,E., Heiter, U., Netopil, M., Soubiran, C., A&A 517:A32 (2010)

117. Pepper, J., Gould, A., DePoy, D., Acta Astronomica, 53, 213-228 (2003)

118. Pepper, J., Stanek, K., Pogge, R., Latham, D., DePoy, D., Siverd, R., Pointdexter, S., Sivakoff, G., AJ 135, 907-921 (2008)

119. Pollack, J., Hubuckyj, O., Bodenheimer, P., Lissauer, J., Podalak, M., Greenzweig, Y., Icarus 124, 62 (1996)

120. Pont, F., Potential of Photometric Searches for Transiting Planet, ASP Conference Series, Volume366 transiting Extra solar Planets W/S (2006)

121. Pont, F., Zucker, S., Queloz, D., R.Astron. Soc. 373, 231-242 (2006).

122. Pravado, S., Shaklan, S., ApJ 700, 623-632 (2009)

123. Press, W., Teukolsky, S., Flannery, B., Vetterling, W., “Numerical recipes in C”, Cambridge university Press. (1992)

124. Price, F., ‘Planet Observer’s Handbook ‘ 2nd Edition, Cambridge University Press (2000)

125. Quinn, S., White, R., Latham, D., Buchhave, L., Cantrell. J., Dahm, S., Fürész, G., Szentgyorgyi. A., Geary, J., Torres, G., Bieryla, A., Berlind, P., Calkins, M., Esquerdo, G., Stefanik, R., ApJL, 756, 33 (2012)

126. Regulo, C., Almenara, J., Alonso, R., Deeg, H., Rocs Cortes, T., A&A 467(3), 1345-1352 (2007)

127. Rosenblatt, F., Icarus 14, 71-93 (1971)

128. Sagar, R., Cannon. R., A&A Supplement series III 75-84 (1995)

129. Sanner, J., Brunzendorf, J., Will, J., Geffert, M., A&A 369, 511-526 (2001)

130. Santos, N., Israelian, G., Mayor, M., Rebolo, R., Udry, S., A&A 398, 363 (2003)

131. Seager, S., Kuchner, M., Hier-Majumder, C., Meltzer, B., ApJ 669, 1279 (2007)

132. Seagroves, S., Harker, J., Laughlin, G., Lacy, J., Castellano, T., PASP 115, 355 (2003)

133. Schmitt. J., Wang, J., Fischer, D., Jek, J., Moriarty, J., Boyajian, T., Schwamb, M., Lintott, C., Smith, A., Parrish, M., Schawinski, K., Lynn, S., Simpson, R., Omohundro, M., Winarski, T., Goodman, S., Jebson, A., Lacourse. D., AJ148,28 (2013)

134. Shu, F., Najita, J., Ostriker, E., Wilkin, F., Ruden, S., Lizano, S., ApJ 429, 797 (1994)

135. Skrutskie, M., Cutri, R., Stiening, R., Weinberg, M., Schneider, S., Carpenter, J., Beichman, C., Capps, R., Chester, T., Elias, J., Huchra, J., Liebert, J., Lonsdale, C., Monet, D., Price, S., Seitzer, P., Jarrett, T., Kirkpatrick, J., Gizis, J., Howard, E., Evans, T., Fowler, J., Fullmer, F., Hurt, R., Light, R., Kopan, E., Marsh, K., McCallon, H., Tam, T., Van Dyk, S., Wheelock, S., The Two Micron All Sky Survey (2MASS) , AJ 131, 1163 (2006)

136. Smith, R. Observational Astrophysics Cambridge University Press, Cambridge, UK, (1995)

137. Starck, J., Murtagh, F., "Astronomical Image and data analysis" 2nd Ed, Springer, Berlin (2006)

138. Struve, O., The Observatory 72, 199-200 (1952)

139. Sudarsky, D., Burrows, A., Pinto. P., ApJ 538, 885-903 (2000)

140. Szulagyi, J., Kovacs, G., Welch, D., A&A 500, 917 (2009)

141. Tamuz, O, Mazeh, T., North MNRS 367,1521 (2006)

142. Taswell, C., IEEE Computational Science and Engineering, 3(2), 12-19 (2000)

143. Templeton, M., AVVSO 32, 41-54 (2004)

144. Tingley, B.(a), A&A 403, 329-337 (2003)

145. Tingley, B.(b), A&A 408, L5-L7 (2003)

146. Trilling, D., Benz, W., Gulliot, T., Lunine, J., Hubbard, W., Burrows, A., ApJ 500, 428 (1998)

147. Udalaski, A., Paczynski, B., Zebrun, K., Szymaski, M., Kubiak, M., Soszynski, I, Szewczyk, O., Wyrzykowski, L., Pietrzynski, G., Acta Astron., 52, 1 (2002)

148. Valenti J. A., Fischer D., ApJ 159, 141 (2005)

149. Vauclair, S., Laymand, M., Bouchy, F., Vauclair, G., Hui Bon Hoa, A., Charpinet, S., Bazot, M. A&A 482, L5-L8 (2008)

150. Vidal-Madjar, A., Desert, J., Lecavelier des Etangs, A., Hebrard, G., Ballester, G., Ehrenreich, D., Ferlet, R., McConnell, J., Mayor., M., Parkinson, C., ApJ 604, L69 (2004)

151. Von Braun, K., Lee, B., Seager, S., Yee, H., Mallen-Ornelas, G., Gladders, M., PASP, 11,141-159, (2005)

152. Von Braun, K., Boyajian, T., Kane, S., van Belle, G., Ciardi, D., López-Morales, M., McAlister, H., Henry, T., Jao, W., Riedel, A., Subasavage, J., Schaefer, G., ten Brummelaar, T., Ridgway, S., Sturmann, L., Sturmann, J., Mazingue, J., Turner, N., Farrington, C., Goldfinger, P., Boden, A., ApJL, 729, L26 (2011)

153. Wall, J., Jenkins, C., "Practical Statistics for Astronomers" 1st Edition, Cambridge University Press, Cambridge, UK (2003)

154. Winn, J., Noyes, R., Holman, M., Charbonneau, D., Ohta, Y., Taruya, A., Suto, Y., Narita, N., Turner, E., Johnson, J., Marcy, G., Butler, P., Vogt, S., ApJ 631, 1215-1226 (2005)

155. Wolszczan, A., Science, 264, 538. (1994)

156. Wolszczan, A., Frail, D., Nature 355, 145-147, (1992)

157. Zombeck, M, Handbook of Space Astronomy and Astrophysics, 2nd Ed, Cambridge University Press, New York (1990)

158. Zuluaga, J., Kipping, D., Sucerqu, M., Alvarado, J. ApJ, 803 L14 (2015)

Reference Web sites.

1. AAVSO CCD Observing Manual, http://www.avvso.org/observing/programs/ccd/manual
2. Boss, http://www.dtm.ciw.edu/boss/IAU/div3/wgesp/planets.shtml
3. Canadian Space Agency, http://www.space.gc.ca/asc/eng/satellites/most.asp
4. ESA, http://www.esa.int/esaCP/SEMCKNU681F_index_0.html
5. ESA, http://www.esa.int/esaSC/120382_index_0_m.html
6. ETD - Exo-planet Transit Database, Czech Astronomical Union, http://var2.astro.cz/ETD/protocol.php,
7. EXOPLANET, http://exoplanet.org
8. Exo-planet News, http://exoplanet.open.ac.uk
9. Help pages of MATLAB Wavelet Tool Box, www.mathworks.com
10. Interactive Extra-solar Planets Catalog, http://exoplanet.eu/catalog.php
11. Kepler, http://kepler.nasa.gov/about/news.html
12. Kepler Supplementary information, http://www.nature.com/nature/journal/v480/n7378/full/nature10631.html#supplementary-information
13. Planetary Science Institute, http://www.psi.edu/esp/process.html
14. SIMBAD, http://simbad.u-strasbg.fr/
15. Terrestrial Planet Finder, http://planetquest.jpl.nasa.gov/TPF/tpf_index.cfm
16. The Extra solar Planets Encyclopedia, http://www.obspm.fr/encycl/encycl.html
17. Transiting circum-binary planets Kepler-34b and Kepler-35b, Welsh et al, http://www.nature.com/nature/journal/v481/n7382/full/nature10768.html

18. Vartools, http://www.astro.princeton.edu/~jhartmon/vartools..html
19. WEBDA, http://www.univie.ac.at/webda/